The role of ADAM10 and mucin-like molecules in modulating cell-cell interactions

Linnea Zoé Drexhage



A thesis presented for the degree of

Doctor of Philosophy

Sir William Dunn School of Pathology

Christ Church

University of Oxford

Michaelmas 2023

”The business of life is the acquisition of memories.”

- Charles Carson

Abstract

To preserve the non-inflammatory nature of apoptotic cell death, a rapid removal of apoptotic cells, known as efferocytosis, is required to maintain tissue homeostasis. Uptake of apoptotic corpses by phagocytes is facilitated by the molecular expression and secretion of find-me and eat-me signals by apoptotic cells, balanced with negative efferocytic don't eat-me signals and don't-come-close-to-me barriers. Transmembrane mucins, which are traditionally associated with mucosal tissues, are heavily glycosylated proteins and major components of the cell glycocalyx. Their extensive ectodomains protrude far from the cell surface, thereby influencing adhesion and forming a protective barrier. Several mucins are excluded from the immunological synapse, and some have been reported to undergo removal from the cell surface of activated or apoptotic cells. This suggests that the mucin shield necessitates active regulation to permit cell-cell interactions. The mechanism underlying mucin regulation during efferocytic clearance and T cell activation remain unclear. The main theme of this study explores a novel efferocytic pathway centered around the cleavage of specific mucins on apoptotic T cells, which otherwise function as a don't eat-me barrier for macrophages. Data presented in this thesis show that the mucins CD43, MUC1 and PSGL-1 are selectively cleaved off the membrane of apoptotic T cells by the metalloprotease ADAM10, and further analysis into the pathway revealed that this process requires activity of the apoptosis-induced phosphatidylserine (PS) scramblase XKR8. When mucin cleavage is prevented, efferocytic uptake by macrophages is reduced in an in vitro assay, and if mucins are removed by a pan-mucinase enzyme, uptake is increased. A related theme of my work is the regulation of mucin expression on activated T cells. In summary, transmembrane mucins have broad impacts on modulating immune cell interactions, and my thesis contributes to our understanding of mucin expression and regulation on T cells under steady-state conditions, activation, and apoptosis.

Acknowledgements

First and foremost, I would like to thank my supervisor, Professor Quentin Sattentau, for his unending guidance, patience and support throughout the past three years. You ignited my passion for T cell interactions and apoptosis. I am immensely grateful for your enthusiasm, encouragement, and optimism throughout this journey.

This work would not have been possible without the help of my fellow Sattentau lab members, Dr Becky Moore, Dr Maeva DuPont, Dr Lu Li, Dr Kate Dicker, Dr Lachlan Deimel and Dr Scarlett Harris, and the hive mind of the Dunn School DPhil students, postdocs and lab managers. Similarly, this thesis couldn't have been completed without the help of the Dunn School facility managers, mainly Dr Robert Hedley and Vasiliki Tsioligka for support with all things flow cytometry, Dr Alan Wainman the imaging facility manager, Dr Phil Cobden the safety and cell bank manager, as well as all workshop and stores staff for supporting me with orders, reagents and shipping.

Without the inspiration of Prof Louise Boyle, Dr Tudor Ilca, Dr Andreas Neerincx and Dr Ida Hafstrand, and them urging me to apply to the IITM programme in Oxford; without you, I would not be writing this section and your encouragement and belief was truly inspiring. I feel incredibly honoured having been accepted into the Wellcome Trust IITM programme. Big thank you to Prof Chris Tang, Prof Jan Rehwinkel, Prof Nicole Zitzman and Dawn Gibbons for running an incredible programme and providing me with the opportunity to read at Oxford, participate in great science, and meet fantastic people.

Additionally, I would also like to thank figures at my college, Christ Church, mainly Pauline Linières-Hartley, Prof Dirk Aarts, Dr Anna Clark, my college advisor Prof Sarah Rowland-Jones, and the The Very Reverend Prof Sarah Foot, Dean of Christ Church, for supporting me during one of the most enriching personal developments I experienced during my time at Oxford. I value your support, input and trust incredibly.

Oxford has been an incredible time of my life, largely due to the great experiences and friendships I have made along the way. A big thank you goes out to my first rotation supervisors and trusted "Beer o'clock" members, Philipp and Hossain. Thank you for always offering your brains to be picked on for all things science, and for cheers-ing to my experiments; whether they were successful or failed for the 100^{th} time. Your camaraderie has made this journey truly enjoyable and inspiring. I also could not be more grateful for all the friends I have made along the way outside the lab; Oliver, Cyril, Luna, Suzi, Amanda, Alaa, Emilė and Alex, Mark, Milena, Fede and the rowing crowd. I am extremely lucky to have met Helene in Oxford, you

have grown to be one of my best friends and I am so grateful for all your support, good cheer, and the culinary enrichment that your presence inevitably brings!

I would like to extend a massive thank you from the bottom of my heart to my parents. To my dad for nourishing my scientific interest from day one, spending countless hours patiently explaining the world to me, and for continually supporting me in whichever journey I set my mind to embarking on. And to Mama, thank you for introducing me to the world of biology and of the creative mind. Without your open-mindedness, support and touching inspiration, I wouldn't be the person I am today. Nothing could have equipped me with more optimism and resilience than growing up with my siblings Joëlle, Finn and Kian; thank you for always having my back and keeping things real!

And finally, to Del: your boundless ability to ground me, brighten things up with unexpected jokes, prepare great food, offer invaluable scientific ideas, and to provide loving advice on all things in life, all serve to show that the world, and dissertations, are, in fact, quite manageable with you by my side.

Abbreviations

Table 1: Abbreviations

Abbreviations used in this thesis	
Abbreviation	Definition
ACAMPs	Apoptotic Cell-Associated Molecular Pattern
ACD	Accidental Cell Death
ACID	Activation-Induced Cell Death
ADAM	A Disintegrin and Metalloproteinase domain-containing protein
AF	Alexa Fluor
AML	Acute Myeloid Leukemia
ANOVA	Analysis of Variation
APAF1	Apoptotic Protease-Activating Factor 1
APC	Allophycocyanin
APC	Antigen Presenting Cell
APP	Amyloid Precursor Protein
ATP	Adenosinetriphosphate
B-ALL	Acute B cell Lymphoid Leukemia
Bak	Bcl-2 antagonist or killer
Bax	Bcl-2-associated X protein
BH3-only	B-cell lymphoma-2 (Bcl-2) homology 3-only
Bid	Bcl-2 family member BH3 interacting-domain death agonist
BSG	Basigin
CAD	Caspase-Activated Dnase
CAR	Chimeric Antigen Receptor
Casp3	Caspase 3
Casp	Caspase
CD	Cluster of Differentiation
cDNA	complementary DNA
CRISPR	Clustered Regularly Interspaced Short Palindromic Repeats
cryo-EM	Cryogenic Electron Microscopy
cSMAC	Central Supramolecular Activation Cluster
CTCL	Cutaneous T-Cell Lymphoma
D10	Complete Dulbecco's Modified Eagle's Medium
DC	Dendritic cCell
DMEM	Dulbecco's Modified Eagle's Medium

DMSO	Dimethyl Sulphoxide
DN	Double nNegative
DNA	Deoxyribonucleic Acid
DP	Double Positive
EDTA	Ethylenediaminetetraacetic Acid
epPCR	Error-prone PCR
FADD	Fas-Associated Death Domain
FCS	Fetal Calf Serum
FITC	Fluorescein Isothiocyanate
FSC	Forward Scatter
GFP	Green Fluorescent Protein
GI	GI254023X
GI	GI254023X
gMFI	Geometric Mean Fluorescence Intensity
GPVI	Glycoprotein VI
GW	GW280264X
GW	GW280264X
hHSPCs	Human Hematopoietic Stem and Progenitor Cells
HLA	Human Leukocyte Antigen
HRP	Horse Radish Peroxidase
ICAM	Intercellular Adhesion Molecule
IL	Interleukin
IS	Immunological Synapse
ITAM	Immunoreceptor Tyrosine Activating Motif
ITIM	Immunoreceptor Tyrosine Inhibitory motif
KO	Knock-Out
l/d	Live/dead stain
LAG3	Lymphocyte Activation Gene-3
LAP	LC3-Associated Phagocytosis
m	Milli
M-CSF	Macrophage Colony-Stimulating Factor
mAb	Monoclonal Antibody
MDM	Monocyte-Derived Macrophage
MESF	Molecules of Equivalent Soluble Fluorochrome
MFG-8	Milk Fat Globule Protein
MGL	Macrophage Galactose-type Lectin

MHC	Major hHistocompatibility Complex
MOMP	Mitochondrial Outer Membrane Permeabilisation
MR	Mannose Receptor
NEM	Alkylating agent N-Ethylmaleimide
NLS	Nuclear Localisation Signal
NOX2	NADPH Oxidase 2
NPTN	Neuroplastin
PBMC	Peripheral Blood Mononuclear Cells
PBS	Phosphate Buffered Saline
PC7	Prohormone Convertase 7
PCR	Polymerase Chain Reaction
PI	Protease Inhibitor
PI3K	Phosphoinositide 3-Kinase
PILR	Paired Immunoglobulinelike type 2 Receptor
PIP_3	Phosphatidylinositol 3,4,5-trisphosphate
PPARα	Peroxisome Proliferator-Activated Receptor alpha
PPARδ	Peroxisome Proliferator-Activated Receptor-δ
PS	Phosphatidylserine
PTPase	Protein Tyrosine Phosphatase
PTS	Proline, Threonine and Serine
R10	Complete Roswell Park Memorial Institute medium
RAR/RXR	Nuclear Retinoic Acid Receptor
RBC	Red Blood Cell
RCD	Regulated Cell Death
RIP	Regulated iIntramembrane Proteolysis
RNA	Ribonucleic Acid
ROS	Reactive Oxygen Species
RPMI	Roswell Park Memorial Institute medium
RT	Room Temperature
SD	Standard Deviation
SEA	Sea urchin sperm protein, enterokinase and agrin
SH3	Src Homology 3-binding domain
SLe^X	Sialic acid and sialyl Lewis x tetrasaccharide
SSC	Side Scatter
ssDNA	Single stranded DNA
T-ALL	Acute T cell Lymphoid Leukemia

tBid	Truncated Bid
TCR	T Cell Receptor
TNFR1	Tumor Necrosis Factor Receptor 1
TRAIL	Tumour necrosis factor-Related Apoptosis-Inducing Ligand
Tspan	Tetraspanin
UTP	Uridine 5' Triphosphate
UV	Ultra Violet
VEGF	Vascular Endothelial Growth Factor
VEGF2	Vascular Endothelial Growth Factor Receptor 2
VISTA	V-type Immunoglobulin domain-containing Suppressor of T cell Activation
VNTR	Variable Number Tandem Repeat
WT	Wild Tpe
µ	Micro

Table of contents

Contents

Abstract **2**

Acknowledgements **3**

Abbreviations **5**

Table of contents **9**

1 Introduction **14**

1.1 Mucin-like molecules 14

1.1.1 Mucin family 14

1.1.2 CD43 16

1.1.3 PSGL-1 17

1.1.4 MUC1 18

1.1.5 MUC24 19

1.1.6 CD45 20

1.1.7 Expression of mucins on T cells 21

1.1.8 Mucin ligands – selectins and siglecs and their tissue expression and functions 23

1.2 T cell apoptosis 25

1.2.1 Apoptotic cell death 25

1.2.2 T cell apoptosis in physiological settings 28

1.3 Efferocytosis 30

1.3.1 Overview 30

1.3.2 Efferocytic signals and barriers, and apoptotic cell recognition 30

1.3.3 Apoptotic cell internalisation by phagocytes 32

1.3.4 Implications of dysregulated efferocytosis 33

1.4 ADAM10 36

1.4.1 Classification of ADAM metalloproteases 36

1.4.2 ADAM10 expression, structure and function 37
1.4.3 ADAM10 substrates 38
1.4.4 Regulation of ADAM10 activity 39
1.4.5 ADAM10 as a regulator of development and its role in T lymphocytes . 41
1.5 Scramblases and Phosphatidylserine 43
1.5.1 Overview 43
1.5.2 TMEM16F 44
1.5.3 XKR8 44
1.6 Context, hypotheses and specific aims 47

2 Chapter 2: Materials and Methods 49

2.1 Tissue culture of cell lines 49
2.2 CRISPR/Cas9 gene editing 49
2.2.1 PSGL-1, MUC1 and XKR8 knockout in CEM 49
2.2.2 CD43 knockout in primary $CD4^{+}$ cells 50
2.3 Cloning of double-tagged CD43 51
2.4 Lentiviral transduction of $CD43^{-/-}$ CEM with Halo and SNAP-tagged forms of CD43 52
2.5 Peripheral blood mononuclear cell isolation 52
2.6 Monocyte-derived macrophage preparation and differentiation 53
2.7 Apoptosis induction in cell lines and primary T cells 53
2.7.1 Staurosporine-induced apoptosis 53
2.7.2 UV-C radiation-induced apoptosis 54
2.7.3 Dexamethasone-induced apoptosis 54
2.8 Metalloprotease inhibitors 54
2.9 StcE mucinase 54
2.10 Flow cytometry analysis 55
2.10.1 Analysis of apoptosis induction in cell lines and primary T cells 55
2.10.2 Activated Jurkats 56
2.10.3 Activated primary T cells 56
2.11 Molecules of Equivalent Soluble Fluorochrome (MESF) Quantification 57

2.12 T cell surface biotinylation 57
2.13 Western blot 58
2.14 Mass spectrometry 58
2.15 Multispectral flow cytometry (ImageStream) assay of efferocytosis 59
2.16 T cell activation assays 60
2.16.1 PMA/Ionomycin stimulation 60
2.16.2 TCR-mediated stimulation of primary $CD4^+$ and $CD8^+$ T cells 60
2.17 Statistical analysis 61
2.18 Illustration software 61

3 Downregulation of mucin labelling in apoptotic immune cells 62

3.1 Introduction 62
3.1.1 Hypothesis 63
3.1.2 Specific aims 63
3.2 Results 64
3.2.1 Mucin expression on the CEM T cell line 64
3.2.2 Mucin labelling of apoptotic CEM 67
3.2.3 Mucin labelling of CEM with UV light-induced apoptosis 73
3.2.4 Mucin labelling of apoptotic Jurkat cells 74
3.2.5 Mucin labelling of apoptotic primary $CD4^+$ cells 75
3.2.6 Mucin labelling of other apoptotic immune cell types 77
3.2.7 Mucin labelling of CEM, Jurkat and primary $CD4^+$ cells with dexamethasone-induced apoptosis 78
3.3 Discussion 79

4 The mechanism of mucin downregulation in apoptosis 83

4.1 Introduction 83
4.1.1 Hypothesis 85
4.1.2 Specific aims 86
4.2 Results 87
4.2.1 Intracellular mucin labelling of healthy and apoptotic CEM 87
4.2.2 Creation of a C and N-terminally tagged CD43 CEM cell line 88

4.2.3 $CD43_{Halo/SNAP}$CEM labelling during apoptosis 90
4.2.4 ADAM10 inhibition in apoptotic CEM and primary T cells 91
4.2.5 ADAM10 inhibition in dexamethasone-treated T cells 95
4.2.6 ADAM10 knockout in CEM 96
4.2.7 Surface biotinylation and pull-down of WT and $ADAM10^{-/-}$ CEM lysates and supernatants during apoptosis 98
4.2.8 Mass spectrometric analysis of WT and $ADAM10^{-/-}$ CEM during apoptosis 99
4.2.9 XKR8 function in apoptotic CEM 106
4.3 Discussion 110

5 Efferocytic uptake of apoptotic T cells by MDMs 116
5.1 Introduction 116
5.1.1 Hypothesis 117
5.1.2 Specific aims 117
5.2 Results 118
5.2.1 Establishment of an MDM-apoptotic T cell co-culture assay 118
5.2.2 Efferocytic clearance of apoptotic $MUC1^{-/-}$ and $PSGL\text{-}1^{-/-}$ CEM 121
5.2.3 Influence of modified ADAM10 activity and mucinase treatment on efferocytosis 123
5.2.4 Efferocytic clearance of apoptotic primary $CD4^{+}$ $CD43^{-/-}$ CEM 126
5.3 Discussion 127

6 Downregulation of Mucin-like Molecules in Activated T cells 132
6.1 Introduction 132
6.1.1 Hypothesis 134
6.1.2 Specific aims 134
6.2 Results 135
6.2.1 Mucin expression on ionophore-activated Jurkat cells 135
6.2.2 Mucin expression on primary T cells activated by TCR engagement . . 137
6.2.3 Discussion 142

7 Conclusion and future directions 146

7.1 Suggestions for future studies 147
7.1.1 Mucin cleavage and ADAM10 specificity 147
7.1.2 The efferocytosis assay 148
7.1.3 The role of ADAM10 in efferocytosis 149
7.1.4 Immune cell activation and mucin expression 149

1 Introduction

1.1 Mucin-like molecules

1.1.1 Mucin family

Mucus is a dilute, viscous secretion mainly consisting of water, electrolytes, lipids and protein [1]. It is prevalent in epithelial tissues in the respiratory, gastrointestinal and reproductive tracts, pancreas, liver, eyes, kidney, gallbladder and the lacrimal and salivary glands [2, 3]. 1-5% of mucus consists of mucins and mucus function varies with the specific mucin composition [1, 4, 5]. Mucins were named in the order of their discovery and to date, 22 genes (MUC1-MUC22) have been discovered in humans, which can further be classified into transmembrane and secreted mucins [3]. Secreted mucins include non-gel forming MUC7 and gel forming MUC2, MUC5, MUC6 and MUC19. MUC1, MUC3, MUC4, MUC11-18, MUC20-22 and MUC24 are tethered mucins [6–8], while MUC9, MUC14 (endomucin) and MUC22 remain unclassified [9]. Mucins are characterised by their proline, threonine and serine-rich tandem repeat domains (PTS domains), and by cysteine-rich regions that are located at the carboxy (C) and amino (N) termini within the PTS domains [1]. In humans, mucins contain variable number tandem repeat regions (VNTR), also termed mucin domain, which are enriched with PTS domains and are heavily glycosylated [1, 9], and some mucins exhibit a Sea Urchin Sperm Protein Enterokinase and Agrin (SEA) domain or an Epidermal Growth Factor-like (EGF) domain [2, 10]. Transmembrane mucins are class I transmembrane proteins with a stop-transfer anchor sequence and a single membrane-spanning domain close to their C-terminus [11] (Figure 1A). In the case of some transmembrane mucins, the C-terminus can contain phosphorylation sites with downstream signalling functions. Mucins and mucin-like molecules are characterised by the structural feature of densely arranged O-linked oligosaccharides attached to serine or threonine residues of the ectodomain. These glycans are generally sialic acid-terminated which introduces a negative charge to the proteins and, in conjunction with the substantial size of mucins, are proposed to create a protective shield around the cell within the context of the cell glycocalyx [3, 12]. This mucin-created barrier serves to protect mucosal membranes and regulates cellular differentiation, signalling, regeneration, adhesion, immune response and tumour progression [13, 14].

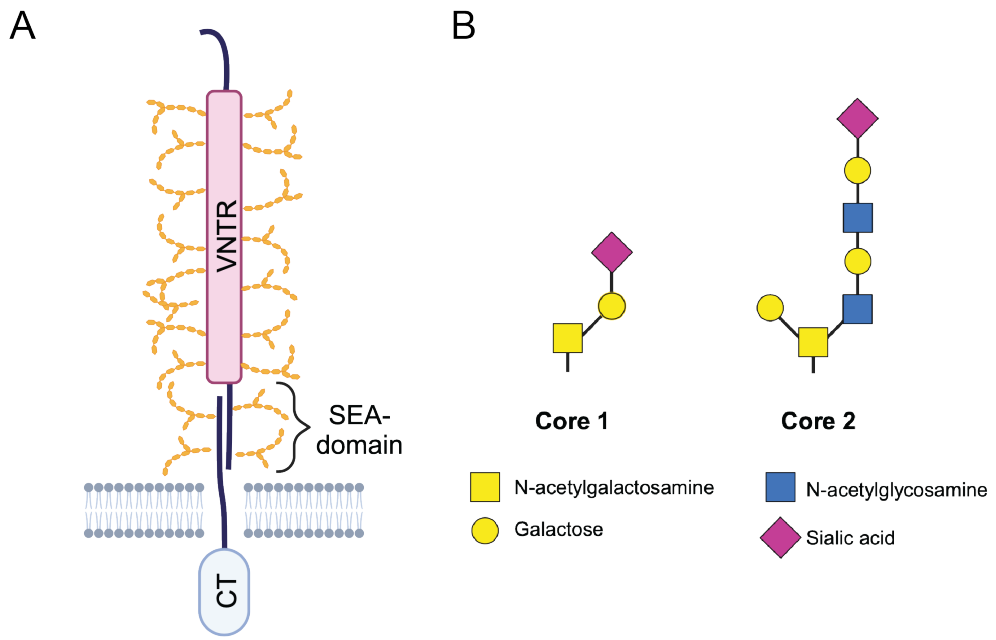


Figure 1: A) Schematic representation of a transmembrane mucin on the cell surface depicting the C-terminus (CT), transmembrane region, SEA domain, VNTR domain and the N-terminus. The SEA domain and VNTR domain are decorated with N- and O-glycans (orange). B) Core 1 or core 2 glycans comprised of N-acetylglycosamine, galactose, N-acetylglycosamine and sialic acid.

The molecular weight of mucins often exceeds 200 kDa, and O-linked glycans can account for 50-90% of the molecular mass of the mature glycoprotein. O-linked glycans are primarily made up of simple core sugars with, as mentioned above, a large proportion of terminal sialyl groups [3, 12, 15, 16]. The specific composition of O-glycans depend on the type of mucin and the glycosyltransferases expressed in the specific cell type [17]. The substantial quantity of carbohydrate side chains, in conjunction with the considerable size of the VNTR domains results in transmembrane mucins that reach far beyond the cell glycocalyx, which varies with cell type, but has been estimated to be 12-40 nm thick on most cells [18–21]. MUC16 has been described as the largest transmembrane mucin, extending as far as 1500 nm from the cell surface [22]. Shurer and colleagues recently demonstrated that the composition and density of mucins on the cell surface have the capacity to influence membrane structure, generating forces capable of bending the membrane. Thus, mucins can shape cellular architecture from a flat phenotype to blebs, tubes and pearls-on-a-string with increasing mucin density [23]. In addition to the MUC proteins, other molecules with similar properties have been categorised as so called mucin-like molecules. Similar to mucins, mucin-like molecules have mucin domains containing repeating proline, threonine and serine residues. As with proteins of the

MUC family, the mucin domains are densely decorated with O-linked glycans providing them with similar biochemical and physical properties. My study primarily revolves around transmembrane molecules that are either mucins or mucin-like molecules. They will henceforth be referred to collectively as ”mucins”. Since the focus of my work relates to the regulation of transmembrane mucin expression on immune cells and particularly T cells, mucin expression will primarily be considered on these cell types.

1.1.2 CD43

CD43, also known as sialophorin (SPN) or leukosialin, is highly expressed on most leukocytes except resting B cells [24], where it extends 45 nm from the cell membrane [25]. The CD43 ectodomain has one N-glycan site and is decorated with approximately 80 O-linked glycans of sialylated core 1 or core 2 type, which accounts for 60% of its weight [25]. On T cells, two glycoforms of 112 kDa (core 1 O-glycans) and 130 kDa (core 2 O-glycans) have been identified by Western blot [26] (Figure 1B). Whereas 112 kDa is the predominant glycoform on most T cell subsets, the 130 kDa glycoform is upregulated on immature double positive thymocytes as well as on activated peripheral T cells [26]. Aberrant expression and changes in glycosylation patterns are associated with Wiskott-Aldrich Syndrome, which is also the context in which CD43 was first discovered [27]. T cells which are deficient in CD43 show enhanced adhesion and decreased activation thresholds, indicating a suppressive role of CD43 in T cell receptor (TCR) signalling [28–30]. During activation and adhesion, CD43 re-localises to the uropod and is excluded from immunological synapses, most likely due to its size and charge [28]. This functionality is achieved through interactions of its cytoplasmic domain with ezrin, radixin, and moesin, which are members of the cytoskeleton linker protein family. This interaction not only regulates T cell activation but also has broader implications for processes like cell migration and survival [31–34]. On neutrophils and lymphocytes, CD43 is downregulated upon activation and apoptosis, and is proposed to be cleaved by the serine protease Cathepsin G [32, 35]. Interestingly, soluble CD43 has been detected in human serum [36]. CD43 downregulation on apoptotic neutrophils has also been reported to occur by shedding of microparticles, unrelated to membrane blebbing [37]. Capping CD43 on Jurkat, an immortalised $CD4^+$ T cell line, is reported to be sufficient to initiate phagocytosis by

macrophages and macrophage uptake is reversible by neuraminidase treatment [38]. Kim and colleagues showed that crosslinking of CD43 on Jurkats accelerated Fas-mediated apoptosis and was reversed by blocking caspase activation [39]. After cleavage of the ectodomain, γ-secretase mediates regulated intramembrane proteolysis (RIP) release of the cytoplasmic domain [32, 33]. The CD43 cytoplasmic tail contains a functional nuclear localisation signal (NLS), which enables it to translocate into the nucleus where it has been shown to bind and enhance expression of the β-catenin target genes c-MYC and CyclinD1, thus contributing to cell proliferation regulation [40]. *In vivo*, CD43 knock-out mice have increased apoptosis of $CD4^+$ and $CD8^+$ central memory cells, as well as decreased T_{reg} and elevated Th_2 counts, resulting in an increased mortality during sepsis [41]. Downmodulation of immune responses is delayed in $CD43^{-/-}$ mice. CD43 glycosylation patterns are altered in a variety of cancer types, which promotes tumourigenesis [42–44], which is attributed at least in part to CD43-induced activation of β-catenin and NF-κB [45, 46]. This highlights that CD43 is an important immune-regulatory molecule with particular importance in T cells, that negatively regulates cell-cell interaction and plays a role in mitigating inflammation.

1.1.3 PSGL-1

P-Selectin Glycoprotein Ligand 1 (PSGL-1, or SELPLG and CD162) is a transmembrane protein of 120 kDa that is expressed as a homo-dimer connected by a disulfide bond [47] and extends approximately 50 nm from the cell surface [48]. PSGL-1 contains circa 40 potential O-glycosylation sites [49] and three N-linked glycosylation sites [50] in its ectodomain and is expressed on haematopoietic cells such as neutrophils, lymphocytes, monocytes and macrophages [51–54]. During inflammatory conditions, PSGL-1 is upregulated to mediate leukocyte tethering and rolling on the surface of endothelium for migration into inflamed tissue, facilitated by binding to its ligands P-, L- and E-selectins [54–56]. Interestingly, ligand binding depends on O- and N-linked glycosylation patterns [57, 58]. PSGL-1 expression increases the suppressive capacity of T_{reg} cells [59, 60] and antibody-mediated PSGL-1 ligation paired with TCR signalling can extinguish downstream signalling events of the TCR [61]. When repeated on exhausted $CD8^+$ T cells, these events elicit increased expression of PD-1, LAG3 and TIM-3, further promoting the exhaustion phenotype [62]. These implications exhibit

similarities with the dynamics of molecules like PD-1. Based on these findings, PSGL-1 has been proposed as an immune checkpoint regulator [61]. In macrophages, Nowakowska and colleagues demonstrated that targeting PSGL-1 using an antagonistic antibody resulted in the polarisation from an M2 to an M1-like state on macrophages. This shift was associated with alterations in the production of pro-inflammatory cytokines and chemokines and leading to a favorable clinical outcome in a tumour model [63]. PSGL-1 is overexpressed in a multitude of cancers and several groups suggest that overexpression facilitates extravasation and metastasis [64–66]. *In vivo*, PSGL-1–deficient mice exhibited elevated blood leukocytes, and binding capacity of PSGL-1 to E-selectin on neutrophils was approximately 70% reduced, indicating impaired tethering [67]. T_{reg} numbers were 30% reduced in the thymus [68], as were peripheral, naive $CD4^+$ and $CD8^+$ T cells [69]. This implies a role of PSGL-1 in limiting T cell responses and positively regulating adhesion. Although PSGL-1 was initially identified in its role as an adhesion receptor molecule, its function as a potential checkpoint molecule on T cells endows it with growing immunological relevance.

1.1.4 MUC1

MUC1, initially known as Human Polymorphic Epithelial Mucin, was the first protein of the mucin family to be described in 1982, when it was isolated from breast milk [70]. The name MUC1 was later coined by Peat and colleagues in 1992 [71]. MUC1 is a large transmembrane mucin with a molecular weight of 250 - 500 kDa, depending on its glycosylation pattern [72], and extends 200–500 nm from the plasma membrane [73]. It is expressed on epithelial cells [74], T cells [75], B cells [15] and macrophages [76]. MUC1 is involved in a plethora of signalling pathways. For example, MUC1 acts as a regulator of ERBB2-4, fibroblast growth factor receptor 3 (FGFR3), platelet-derived growth factor-β (PDGFRβ), and MET, influencing their downstream signalling pathways [14]. The MUC1 ectodomain contains all domains typical for mucins as outlined above, including a SEA motif in its extracellular domain [77]. MUC1 is reported to be shed from the surface of cells either via shear force-mediated release of the non-covalent SEA linker domain, or via the action of the metalloproteases A Disintegrin And Metalloprotease domain containing protein 17 (ADAM17, or TACE) and MT1-MMP30 [78]. After cleavage, the MUC1 cytoplasmic tail is released from the membrane through RIP medi-

ated by γ-secretase [79], after which the MUC1 C-terminus can translocate into the nucleus. Nuclear transport of the MUC1 C-terminus is dependent on a CQC motif, which is required for its dimerisation and direct interaction with importin-β and nucleoporin [80]. In the nucleus, the MUC1 C-terminus associates with and stabilises β-catenin, which activates Wnt target genes, genes that are involved in tumour progression and metastasis [14, 81]. Furthermore it is hypothesised that association with β-catenin sequesters the MUC1 C-terminus from adherens junctions, thereby leading to decreased adhesion [81]. Lillehoy and colleagues demonstrated that once the MUC1 ectodomain has been dissociated from the membrane through protease-mediated shedding or release through its SEA domain, it can serve as a decoy receptor, effectively binding to *P. aeruginosa* and fully obstructing its adhesion to cells [82]. Upon stimulation with the migratory chemokine CCL5, T cells undergo surface molecule polarisation, with MUC1 and other mucins accumulating on the leading edge. This spatial separation has implications for endothelial-T cell interactions during migration to inflammatory tissues [83]. Vasir et al. observed a reversal of this process during the formation of the T cell synapse. Specifically, they found that MUC1 is translocated to the opposite side of the T cell upon dendritic cell (DC)-T cell synapse formation [84], implying exclusion from the synapse most probably because of its large size. Various tumours show overexpression and aberrant glycosylation of MUC1 [6] which has motivated novel therapeutic targets such as MUC1 targeting chimeric antigen receptor (CAR) T cells and bispecific antibodies [85, 86]. This highlights the extensive involvement of MUC1 in cellular pathways and underscores its significance in immunological and oncogenic processes.

1.1.5 MUC24

MUC24, also known as CD164 or endolyn, is a type 1 transmembrane mucin with a molecular weight ranging from 80 to 90 kDa [87]. It has the capacity to form homodimers, resulting in larger complexes with a molecular weight of 160 to 180 kDa [87]. Initially, it was identified on the surface of $CD34^+$ hematopoietic cells [88] and was later characterised as a specific marker of human hematopoietic stem and progenitor cells (hHSPCs) [89, 90]. The length of its extracellular domain is currently unknown however it comprises two mucin domains with 32 O-linked and nine N-linked glycans, with a cysteine-rich domain located between the mucin

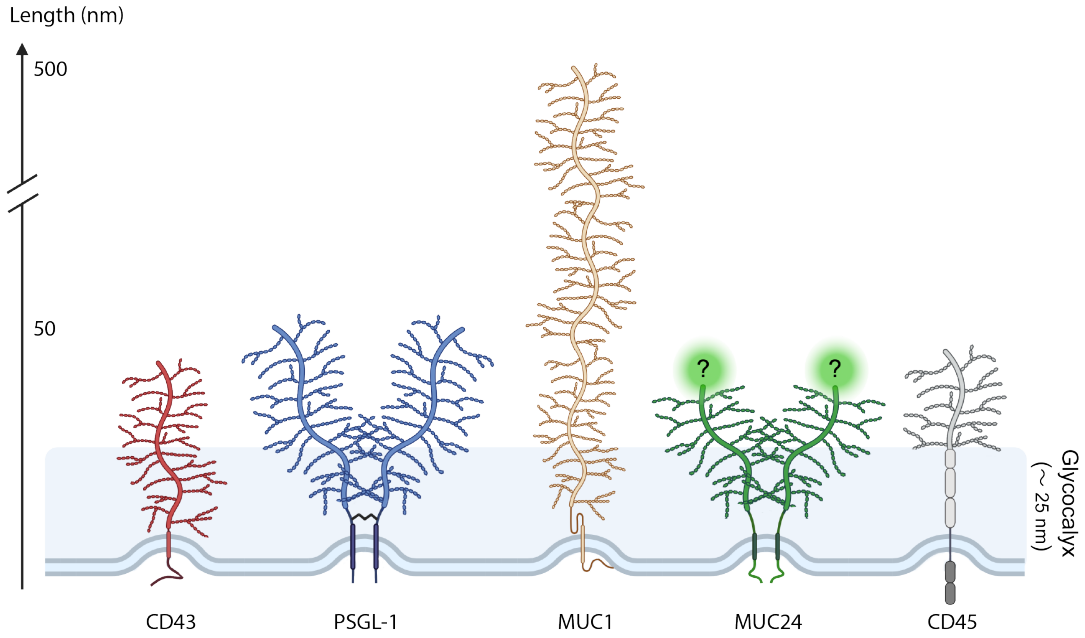


Figure 2: Schematic representation of transmembrane mucins on the cell surface. X-axis shows approximate length (nm) of mucins apart from MUC24, the size of which is unknown. PSGL-1 and MUC24 form homodimers.

domains [90]. Within MUC24 as a homodimer, four cysteine residues putatively establish a disulfide bond. [91, 92]. The cytoplasmic tail comprises the endocytosis motif YHTL, indicating intracellular functions [93]. MUC24 exhibits heightened expression levels in various cancer types, including colon cancer, where it has been shown to drive cell proliferation, migration, and metastasis [94, 95]. In contexts not involving cancer, MUC24 has been attributed key roles in adhesion of hHSPCs to bone marrow stromal cells and in regulating cell proliferation [87, 88, 90]. More recently, high expression of MUC24 on $CD4^+$ T cells was shown in patients with Sézary syndrome, a type of a cutaneous T-cell lymphoma (CTCL), in which expression correlated with tumour burden [96, 97]. MUC24 remains an area of limited study, and many of its functions in adhesion and its relevance in immunological contexts remains to elucidated.

1.1.6 CD45

CD45 (or Ly-5) is a receptor protein tyrosine phosphatase which varies between 180–220 kDa in molecular weight and extends 28-50 nm from the plasma membrane, depending on its isoform [98, 99]. All nucleated haematopoietic cells and their precursors, excluding mature erythrocytes and platelets, strongly express CD45 thus making it a widely used pan-leukocyte

marker [100]. The CD45 molecule consists of an extracellular domain, a transmembrane domain, and a long, conserved cytoplasmic tail [101]. Six CD45 isoforms have been described which are generated by differential splicing and differ in the composition of their ectodomain, which varies in length and O-linked glycans [102, 103]. The cytoplasmic tail comprises two protein tyrosine phosphatase (PTPase) domains and a putative, inhibitory wedge-like domain [104]. While both PTPase domains play an important role in cell physiology, one is enzymatically active, whereas the other serves as a phosphorylation site for Src kinase [99]. During the formation of the immunological synapse, CD45 and Lck are initially recruited to the central supramolecular activation cluster (cSMAC) and CD45 is later excluded from the cSMAC [105–107]. This exclusion is consistent with the kinetic segregation model, which describes the removal of phosphatases from the MHC-TCR space [108, 109]. However a more recent paper describes pre-exclusion of CD45 at the tips of micro villi prior to immunological synapse formation, resulting in more CD45-free TCR-MHC complexes. CD45 deletion in mice led to impaired thymocyte maturation, reduced numbers of peripheral T cells, and hindered B cell proliferation [110], highlighting its central role in hematopoietic cell development and function.

1.1.7 Expression of mucins on T cells

While many mucins are ubiquitously expressed on epithelial cells such as on the ocular surface and the epithelium of the ear, digestive, urogenital and respiratory tracts, some mucins are expressed on leukocytes [5, 111–113]. A general overview of the most well-characterised mucins on immune cells is presented in Table 2.

Table 2: Mucins on immune cells

Mucin family member	**Other names**	**Expression on epithelial tissues**	**Expression on immunological tissues**
MUC1	EMA, MCD, PEM, PUM, KL-6, MAM6, CD227	Stomach, breast, gall bladder, cervix, pancreas, respiratory tract, colon, duodenum, oesophagus, kidney, eye, middle ear epithelium [111]	T cells, macrophages, monocytes [111]
MUC14	Endomucin	Heart, kidney, lungs [111]	Basophils and NK cells [114]

MUC15	Cell surface associated	Prostate, testis, ovary, small intestine, colon, breast, fetal liver, lungs, middle ear epithelium [111]	Spleen, thymus, peripheral blood leukocytes, bone marrow, lymph node, appendix and tonsils [115]
MUC18	MCAM, MelCAM, CD146	All types of epithelial cells, hair follicular cells [116]	T cells, B cells, trace amounts on NK cells [117]
MUC21	Epiglycanin	Respiratory tract [118]	Thymus [118]
MUC24	CD164, Endolyn	Bone marrow stromal cells [24]	Monocytes and malignant T cells [24, 97]
CD43	Sialophorin (SPN), Leukosialin, Galgp	-	All hematopoietic progenitors and in most leukocytes, except resting B cells [24, 119]
CD45	Leukocyte common antigen, Ly-5	-	All hematopoietic cells except erythrocytes and platelets [100, 120]
CD68	Macrosialin	Fibroblasts and endothelial cells [121]	Macrophages, monocytes [121]
PSGL1	SELPLG, CD162	-	All myeloid and lymphoid lineages [122]

CD43 is sometimes considered a T cell marker due to its expression by over 95% of thymocytes and circulating T cells [123] and signalling through its cytoplasmic tail regulates T cell proliferation, migration and activation [124, 125]. While signals are primarily conveyed through its cytoplasmic tail, Mody and colleagues demonstrated that the CD43 ectodomain plays a crucial role in transmitting extracellular signals essential for effective T cell trafficking [31]. As outlined above, PSGL-1 plays a central role in T cell activation as an inhibitory receptor, however PSGL-1 further functions as a negative regulator in T cell responses of effector and memory T cells during infection [126]. While MUC1 is not expressed on resting T cells, activated T cells express MUC1 uniformly [75]. Even though expression is still comparatively low on activated T cells, MUC1 can serve as an immunoregulatory molecule through its immunoreceptor tyrosine activating motif (ITAM) and immunoreceptor tyrosine inhibitory motif (ITIM) [127], the molecular interactions of which are yet to be elucidated [128]. MUC24 thus far has only been described on malignant $CD4^+$ T cells from patients with Sézary syndrome and expression was confirmed in this study on the $CD4^+$ acute lymphoblastic leukemia (ALL) cell

line CEM [91]. CD45 is a well-characterised molecule on T cells, and its distinct isoforms can serve as a T cell differentiation and memory markers. Naive T cells express CD45RA, while memory and activated T cells express the shortest isoform of CD45, CD45RO [129].

1.1.8 Mucin ligands – selectins and siglecs and their tissue expression and functions

In addition to their suggested barrier function attributed to their substantial size and charge, the above mucins have also been noted for their specific ligand interactions, often involving lectins, a family of carbohydrate binding proteins. In this context, CD43 has been identified as a co-receptor for the adhesion molecule E-selectin [130]. Specifically, E-selectin binds to the 130 kDa glycoform of CD43 which contains sialyl-Lewis X tetrasaccharides on activated peripheral T cells, as several groups have shown [131–133]. CD43 has further reported functions as a ligand for various immune adhesion receptors, including siglec-1 (sialoadhesin) on macrophages [134], siglec-7 on natural killer (NK) cells and monocytes [132, 135], E-selectin on endothelial cells [132] and galectin-1 on epithelial cells [136]. In most cases ligand binding is specific to the CD43 glycoform expressed, for instance siglec-1 and E-selectin bind CD43 glycoforms containing α-2,3–linked sialic acid and sialyl Lewis × tetrasaccharide (sLe^X), respectively. Conflicting evidence was reported on intercellular adhesion molecule 1 (ICAM1) serving as a ligand to CD43 [137, 138].

Contrary to its name, PSGL-1 is capable of binding to all three selectins (P-, E-, and L-selectin) with varying avidity [139–141]. Its binding specificity has, similar to CD43, been shown to depend on specific carbohydrate moieties on the PSGL-1 N-terminus such as sialylated fucosylated O-linked glycan or sLe^X [142, 143]. While the above ligands share their function in adhesion and cell-cell interactions, PSGL-1 has also been reported to bind to lymphoid tissue chemokines such as CCL19 and CCL21 regulating T cell entry and migration [144]. Recently, V-type immunoglobulin domain-containing suppressor of T cell activation (VISTA) was identified as a ligand and negative regulator for PSGL-1 on T cells [145]. VISTA is expressed on granulocytes and myeloid cells and binds to PSGL-1 under low pH, depending on tyrosine sulfation but not sLe^X [146].

MUC1 engages with a range of molecules on DCs and macrophages, for example DC-SIGN (CD209), macrophage galactose-type lectin (MGL), mannose receptor [147] and siglec-1 [148]. MUC1 can also bind ICAM1 and E-selectin expressed on endothelial cells and immune cells, highlighting its function in adherence and cell migration [149]. Furthermore, binding of Galectin-3 to oncofetal Thomsen-Friedenreich carbohydrate (Galβ1) of the MUC1 ectodomain on T cells was reported [127, 150, 151].

Further studies are required to fully characterise the MUC24 ligandome, however Watt et al. have found that MUC24 lacks sLe^X moieties that are required for binding by E-selectin or P-selectin. They predict that due to its ectodomain sialylation and absence of fucosylation, siglecs might constitute novel ligands for MUC24. Preliminary data from Jorgensen-Tye and colleagues show that biotinylated recombinant MUC24 binds to siglec-5 however more studies are needed to confirm these findings [152].

Few specific ligands have been reported for CD45. MGL has been reported to interact with CD45 on T cells through N-acetylgalactosamine (GalNAc) binding on its ectodomain, resulting in decreased proliferation of effector T cells, the secretion of proinflammatory cytokines, and potential induction of apoptosis [153]. Further to the above, CD45 was shown to bind to galectin-1 [154], galectin-3 [155], and other lectins such as CD22 [156]. Clear parallels can be observed between mucins and their respective binding partners. These interactions have broad implications in cell signalling pathways, highlighting a role of mucins that extends beyond their electrostatic properties.

1.2 T cell apoptosis

1.2.1 Apoptotic cell death

Cell death can be categorised into two principal groups: regulated cell death (RCD) and accidental cell death (ACD) [157]. RCD occurs during development or tissue turnover [158, 159] or as a response to high or prolonged stresses of intracellular or extracellular origin [160]. Examples of RCD include apoptosis, autophagy-dependent cell death, entotic cell death, mitotic catastrophe, ferroptosis, pyroptosis and necroptosis [157]. While RCD is a tightly regulated and controlled process, ACD results from exposure to severe insults of chemical, physical or mechanical nature and includes ischemic cell death and necrosis [160–162]. Apoptotic cell death, first described in 1842 by Carl Vogt [163], is a programmed and controlled form of cell death. The term ”apoptosis” has its roots in Greek, where it translates to ”falling off” and refers to the shedding of leaves from a tree [164]. Apoptosis is a conserved process which is crucial for development [165, 166], tissue homeostasis [167, 168] and cancer prevention [169]. Key characteristics of apoptotic cells include cell shrinkage, membrane blebbing, nuclear fragmentation, DNA fragmentation, chromatin condensation and mRNA decay [170, 171]. It is in contrast to necrosis, a type of cell death resulting from acute trauma and which is an unregulated process [157]. Apoptotic cell death is a conserved process that can be initiated via two main pathways: the extrinsic, or death receptor pathway, and the intrinsic, or mitochondrial pathway (Figure 3). Additionally, immune cells with killing effector functions such as NK cells and $CD8^+$ are capable of directly inducing apoptosis in their target cells via the perforin/granzyme A/B pathway [172]. Both pathways are driven by proteins of the cysteine aspartate-specific proteases called (caspase) family [173]. Caspases are produced as an inactive proenzyme, also called procaspases, that require dimerisation and cleavage to gain function [174]. Upon activation, caspases induce a cascade of events during which they undergo auto-activation or lead to the activation of other caspases [175]. To date, 14 caspases have been identified, out of which caspases 1-10 are included in further classifications: initiator caspases (Casp2, 8, 9, 10), inflammatory caspases (Casp1, 4, 5) and effector caspases (Casp3, 6, 7) [176]. All cases of apoptosis induction result in activation of Casp3 and subsequent DNA degradation [175] with the exception of granzyme A, which induces an apoptotic pathway independent of caspases [177].

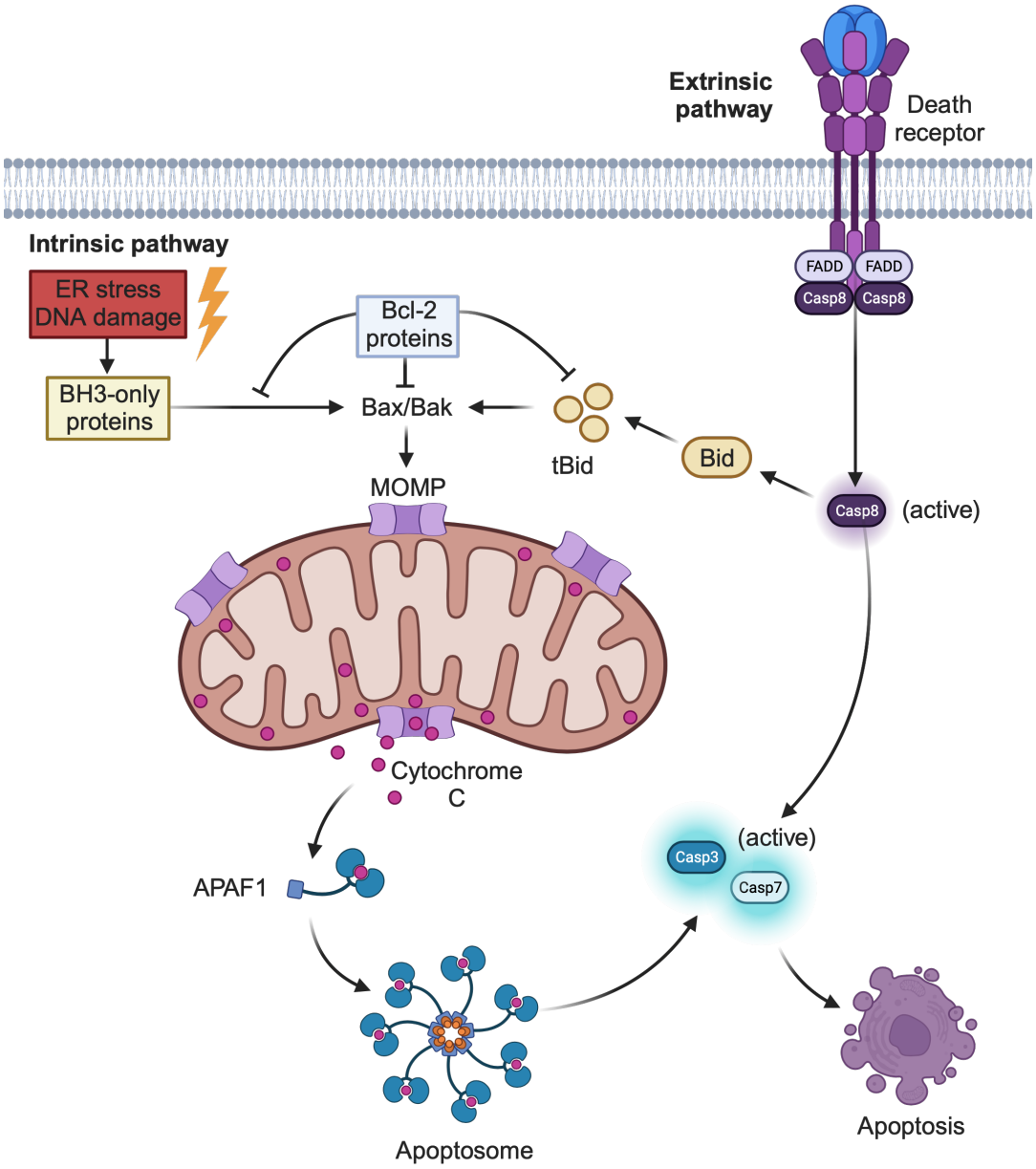


Figure 3: Schematic representation of the extrinsic and intrinsic pathway during apoptosis. Both pathways ultimately trigger the release of cytochrome c from the mitochondria, which leads to the assembly of the apoptosome and the activation of effector Casp3 and Casp7.

Various intracellular signals can initiate the intrinsic apoptotic pathway. Examples are physiochemical stressors such as DNA damage-inducing agents, free radicals and chemotherapeutic agents. Lack of oxygen, growth factors, nutrients, pro-inflammatory cytokines, as well as changes in temperature and osmolarity are triggers of the intrinsic pathway [178–181]. These signals activate BH3-only proteins (B-cell lymphoma-2 (Bcl-2) homology 3-only proteins) [182], which in turn trigger the Bcl-2-associated X protein (Bax) and Bcl-2 antagonist or killer (Bak) [183, 184] (Figure 3). Once Bax and Bak have been activated, they undergo conformational changes leading to their homo-oligerisation enabling formation of pores within the outer membrane of the mitochondria [185, 186]. This is referred to as mitochondrial outer membrane permeabilisation (MOMP) and causes the release of mitochondrial proteins into the cytosol such as cyochrome c [187, 188]. Once released, cytochrome c binds the apoptotic protease-activating factor 1 (APAF1), which thereby multimerises, forming the apoptosome (Figure 3). Initiator Casp9 is recruited to the apoptosome and activated, subsequently cleaving and further activating the effector Casp3 and Casp7 [189], which in turn initiate the final phase of the apoptotic cascade. Caspase-activated DNase (CAD) and other endonucleases are activated and nuclear and plasma membrane cytoskeletal proteins and cytokeratins are cleaved, ultimately leading to the hallmark features of apoptosis as described above [190, 191].

The extrinsic signalling pathway is initiated by formation of the death-inducing signalling complex (DISC) on the cell surface [192]. For DISC formation, death ligands such as CD95L (or FasL and Apo-1L), TNF-related apoptosis inducing ligand (TRAIL) and tumor necrosis factor (TNF) bind to their receptors, which leads to their activation. As a result, the adaptor protein Fas-associated protein with death domain (FADD) is recruited to the complex [193]. Binding of Casp8 to FADD via its death effector domains [194] causes its activation and subsequently leads to the activation of the executioner caspases Casp3 and Casp7 [195] (Figure 3). The crosstalk between the intrinsic and the extrinsic pathway is mediated by pro-apoptotic Bcl-2 family member BH3 interacting-domain death agonist (Bid) [196]. Bid is activated through cleavage by Casp8, thereby forming truncated Bid (tBid). tBid induces Bax, which forms MOMP, triggering release of cytochrome c and its downstream effects [197].

1.2.2 T cell apoptosis in physiological settings

T cells die from apoptosis under two distinct conditions: as immature thymocytes during thymic education, and as mature effector T cells after antigen encounter and activation. During development, T cells derive from hematopoietic stem cells (HSCs) which originate from the fetal liver or bone marrow [198, 199]. Progenitor cells then migrate and home to the thymic cortex and expand to become immature thymocytes ($CD4^-CD8^-$, also termed double-negative (DN)). In the majority of cases they then develop into double-positive (DP) thymocytes. TCRs are generated by genetic recombination and subsequently positively selected in the cortex, based on their capacity to recognise and interact with major histocompatibility complex (MHC) molecules expressed by cortical thymic epithelial cells [198]. Upon successful binding, DP thymocytes receive critical survival signals such as DDL4 and IL-7 from the cortical thymic epithelial cells, and differentiation signals for their development into single positive cells (cathepsin L and TSSP for $CD4^+$ differentiation or PSB11 for $CD8^+$ differentiation [200–203]). Thymocytes that fail to show affinity for MHC do not receive survival signals and undergo apoptosis, a process referred to as ”death by neglect”. The intrinsic apoptotic pathway was found to be of major importance in this context. As early as 1980, glucocorticoid hormones were identified that mediate death by neglect [204]. Dexamethasone is a synthetic glucocorticoid hormone that is widely used for the induction of apoptosis *in vitro* [205]. Veis and colleagues demonstrated that disrupting BCL-2 in murine thymocytes enhances dexamethasone-mediated apoptosis [206], which can be prevented by lack of BAX and BAK [207], confirming the connection between glucocorticoid hormones and the intrinsic apoptosis pathway. Interaction of paired immunoglobulin-like type 2 receptor (PILR) on thymic epithelial cells with D4 on thymocytes was proposed as another mechanism to regulate Casp8-dependent death by neglect [208, 209]. Once $CD4^+$ or $CD8^+$ T cells have been positively selected they up-regulate expression of the chemokine receptor CCR7 and migrate into the medulla, where the CCR7 ligands CCL19 and CCL21 are secreted [210]. In the medulla, T cells interact with medullary thymic epithelial cells and thymic dendritic cells (DCs) which present self-antigens, resulting in the elimination of auto-reactive cells [211, 212]. If single positive T cells bind to self-MHC with a high affinity apoptosis is induced (negative selection). Negative selection is mediated via TCR signalling and MAPK pathways and depends on the duration of MHC-binding determining cell

fate [213–218]. While most auto-reactive $CD4^+$ T cells undergo apoptosis in the medulla, a proportion of them differentiate and become T_{reg} cells, specialising in mediating peripheral immune tolerance [219]. There is remaining controversy in the field as some studies suggest that Casp3 and Casp8 are not required for negative selection [220, 221] and that caspase-independent pathways alone are sufficient to induce negative selection [222, 223].

The primary role of T cells is to protect the host from pathogen challenge, during which T cells are activated by encounter of their TCR with cognate ligand presented by an antigen presenting cell. After the successful clearance of the pathogen or other inflammatory source, immune memory is generated and the T cell response is switched off to return to a steady state. To achieve this, a subset of T cells differentiates into memory T cells, while the majority of T cells undergo a process known as Activation-Induced Cell Death (AICD) [224, 225]. AICD is mediated via the extrinsic apoptotic pathway through binding of FasL with the death receptor Fas [226] (Figure 3). Additionally, cytokines and co-stimulatory signals have also been reported to regulate T cell AICD. CD28 signalling contributes to effector function and expansion of T cells, resulting in an increased sensitivity to AICD [227]. Under normal conditions, IL-2 is required for T cell proliferation, serves as a survival signal and ensures effector function [228]. Murine knockout models have shown that IL-2 and IL-2Rα are required to sensitise T cells to AICD [229]. Rafaeli and colleagues showed similar effects in a IFN-γ knockout mouse and found that IFN-γ regulates Casp8 expression. The addition of exogenous IFN-γ restored sensitivity to AICD in their model, highlighting IFN-γ, alongside IL-2 and IL-2Rα as important regulators of AICD [230]. The transcription factors NFκB and NFAT are key regulators of T cell activation and differentiation and their dysregulation causes aberrant expression of FasL, thereby influencing susceptibility to AICD [231, 232]. This suggests that classical T cell activation signals can under circumstances of over-stimulation, transition into signals triggering AICD.

1.3 Efferocytosis

1.3.1 Overview

In any multicellular organism, dead cells arise during development, normal tissue function [233], infection and inflammation [234]. However even within tissues with a high apoptotic burden such as the thymus, the number of apoptotic cells that are detectable is comparatively low, which indicates a high rate of removal [235–237]. In human adults, approximately 10^6 cells per second are estimated to undergo apoptosis [238]. To maintain tissue homeostasis, efficient clearance is therefore of upmost importance. Phagocytosis is characterised by the engulfment of particles larger than 0.5–1 μm [239, 240] and is carried out by both professional and non-professional phagocytes. Professional phagocytes primarily include immature DCs, macrophages, tissue-infiltrating monocytes, eosinophils and neutrophils. Astrocytes in the brain [241], epithelial cells of mammary epithelium [242], smooth muscle cells [243, 244], renal cells [245] and hepatocytes [246] are considered non-professional phagocytes and are able to capture and internalise nearby material such as apoptotic cells, but unlike professional phagocytes are static and so cannot migrate towards their targets. The engulfment of dying and dead cells and their debris by phagocytes is termed efferocytosis [247, 248]. This process exhibits features from both classical phagocytosis and macropinocytosis, a fluid-phase uptake mechanism, resulting in the formation of large phagosomes [249–251].

1.3.2 Efferocytic signals and barriers, and apoptotic cell recognition

Recognition of apoptotic cells by phagocytes is mediated by apoptotic cell-associated molecular patterns (ACAMPs) [252] that facilitate efferocytosis in four distinct stages [253, 254]: 1) Apoptotic cells release so-called ”find-me” signals [255, 256] such as lysophosphatidylcholine, the nucleotides adenosinetriphosphate (ATP) and uridine 5’ triphosphate (UTP), sphingosine 1-phosphate and CX3CL1 (fractalkine), which create a gradient for phagocytes, leading to detection of the dying cells [253, 254]. 2) Expression of ”eat-me” signals on the cell surface [257, 258] (Figure 4). Phosphatidylserine (PS) is the best characterised eat-me signal, which, with the help of scramblases (see section 1.5 below), is exposed to the outer leaflet of the membrane during apoptosis. During pyroptosis and necrosis, PS also becomes exposed, however in a less controlled manner through membrane permeabilisation [254, 255]. Other

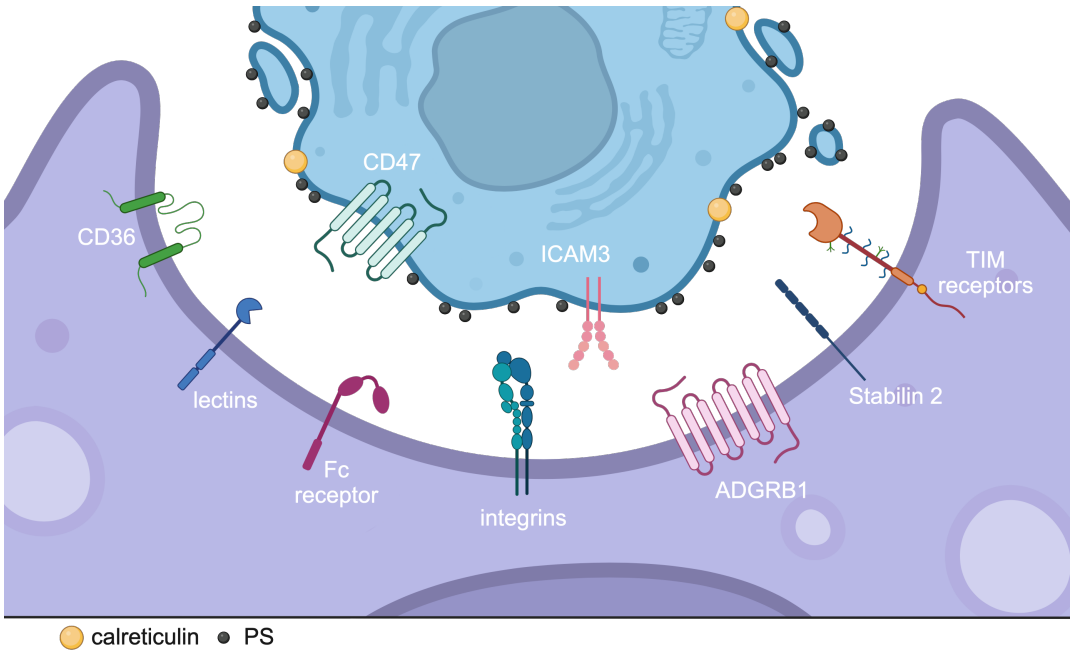


Figure 4: Schematic representation of eat-me and don't eat-me signals and their receptors. Apoptotic T cell (blue) and macrophage (purple). Eat-me signals include PS, ICAM3 and calreticulin, CD47 is a don't eat-me signal. Receptors of eat-me signals on macrophage include CD36, lectins, Fc receptors, integrins, ADGRB1, stabilin 2 and TIM receptors. The molecules illustrated in this figure are not exhaustive, as numerous others have been reported in the literature.

eat-me signals are calreticulin, complement factors and ICAM3 [259, 260]. On apoptotic cells, pro-phagocytic signals are counter-balanced with "don't eat-me" signals on apoptotic cells such as CD47 [261, 262]. 3) Several eat-me signals are then recognised by phagocyte receptors e.g. complement receptors CR3 and CR4, mannose receptor (MR), scavenger receptors SRA and CD36, stabilin 2, integrins αVβ3 and αVβ5, adhesion G protein-coupled receptor B1 (ADGRB1) and members of the T-cell immunoglobulin domain and mucin domain (TIM) family TIM1, TIM3, and TIM4 [259, 260] (Figure 4). Others require recognition by binding bridging molecules such as C1qR, collectins, mannose binding lectin (MBL), ficolins, pentraxin3, milk fat globule protein (MFG-8) and thrombospondin [258, 263–265]. Following recognition, some receptors such as TIM-4 function by tethering the apoptotic cell, while others such as complement [266] and Fc receptors [266] lead to immediate phagocytosis. On phagocytes, don't-eat-me molecules can bind to "don't-eat" receptors on phagocytes such as SIRPα [267], thus contributing to negative regulation of phagocytosis. On top of specific receptor-ligand interactions, a nonspecific, a so-called "don't-come-close-to-me" barrier further contributes to negative regulation of phagocytosis [268]. Efferocytosis receptors are typically short (approximately 5 nm) and require close proximity to their ligands for successful binding [269].

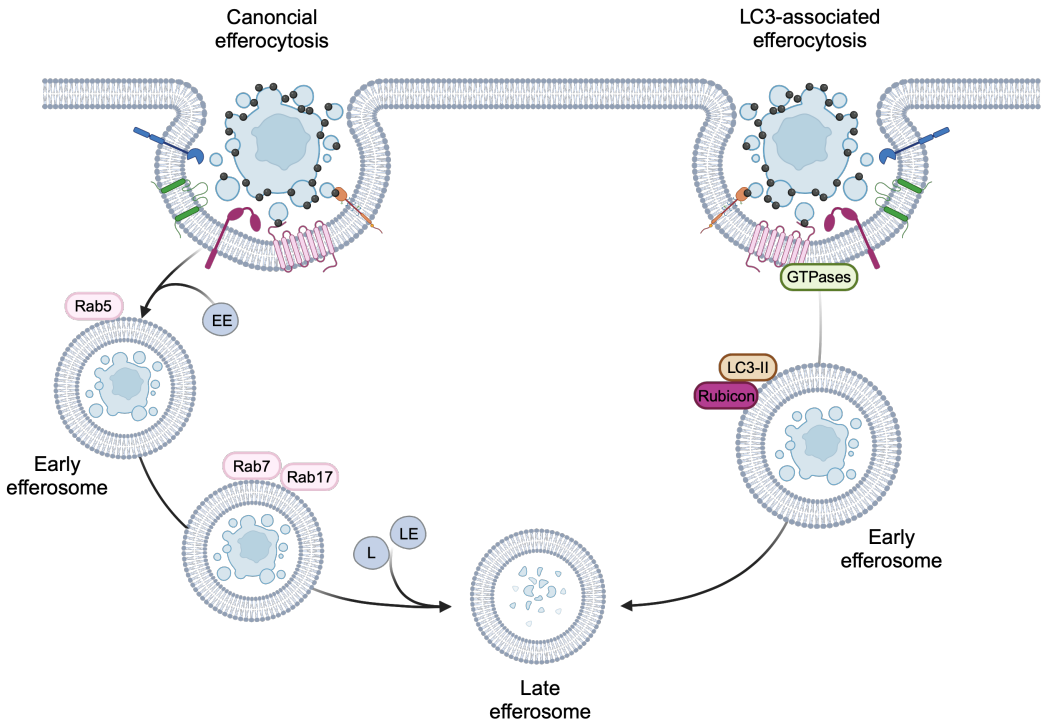


Figure 5: Schematic representation of the canonical and LC3-associated efferocytosis pathway. Adapted from Yin et al. [272]. Canonical efferocytosis involves Rab5, 7 and 17 which mediate fusion with early endosomes (EE), late endosomes (LE) and lysosomes (L) to achieve apoptotic content degradation. LC3-associated efferocytosis involves the binding of LC3 and rubicon to the early efferosome, leading to rapid maturation of the efferosome and the degradation of its apoptotic contents.

However, molecules like mucins, which constitute the cell glycocalyx, serve as a biophysical barrier that hinders uptake. They do so by virtue of their size, creating steric hindrance, and form an electrical barrier due to their extensive glycosylation [270]. Consequently, glycocalyx molecules like MUC1 are regarded as ”don’t-come-close-to-me” signals [268]. The balance and integration of all types of signals leads to the decision whether or not the target cell will be engulfed [247, 254, 271]. If a cell has been selected for phagocytosis this leads to the final step: 4) Internalisation of the target cell via cytoskeletal rearrangement [236, 253, 254].

1.3.3 Apoptotic cell internalisation by phagocytes

Direct or indirect engagement of receptors on phagocytes leads to the engulfment of the apoptotic cell, enclosing it within a vacuole derived from the plasma membrane, termed efferosome [273]. PS interaction with receptors on the phagocyte leads to the activation of small GTPases such as RAC1 and RhoA, which mediate actin polymerisation, assembly of the phagocytic cup

and subsequent internalisation [274, 275]. In the canonical endosomal-lysosomal maturation pathway, Rab5 is recruited to efferosomes and remains bound to the early efferosome for several minutes [276, 277] (Figure 4). Once associated with the efferosome, Rab5 mediates fusion with early endosomes [278]. Rab5 is subsequently exchanged for Rab7, which regulates fusion with lysosomes and late endosomes. This results in the creation of a highly hydrolytic environment, leading to full degradation of the apoptotic body through activation of lysosomal proteases [276, 279]. By contrast with phagocytosis, the canonical efferocytosis pathway involves Rab17-directed movement of the efferosome to the recycling endosome, preventing the deposition of apoptotic material within antigen-loading compartments [276, 280]. Alternatively, apoptotic cells can undergo LC3-associated phagocytosis (LAP) (Figure 4). During LAP, mitochondrial fission triggers a spike in cytoplasmic Ca^{2+}, necessary for phagosome sealing and assembly of the phosphoinositide 3-kinase (PI3K) complex, which consists of the autophagy-related proteins ATG5 and ATG7 [281–283]. Increased Ca^{2+} also stabilises the NADPH oxidase 2 (NOX2) complex with rubicon, which leads to the production of reactive oxygen species (ROS) [281, 284]. Both ROS and PIP_3 are required for binding LC3-II to lipids of the efferosomal membrane, leading to rapid maturation of the efferosome and the degradation of its apoptotic contents. Similar to the canonical pathway, antigens are not forwarded to the antigen processing compartments and the LAP pathway was shown to polarise macrophages towards an anti-inflammatory state [285]. Additional research is required to comprehensively understand the distinctions in signalling pathways between phagocytosis and efferocytosis. However, a notable difference lies in the absence of apoptotic cargo trafficking to antigen-processing compartments in both pathways [272, 276, 285]. This distinction serves to ensure that the degradation of apoptotic cells occurs in an immunologically silent manner.

1.3.4 Implications of dysregulated efferocytosis

Considering efferocytosis is a process that is highly regulated, dysregulated macrophage efferocytosis can lead to the development and progression of various diseases. MFG-E8 serves as a bridging molecule for $\alpha V\beta 3/\alpha V\beta 5$ integrin on phagocytes and knockout mice develop the autoimmune disease glomerulonephritis, likely caused by impaired efferocytic recogni-

tion [286]. Knockout of the efferocytosis receptor MERTK [235] or impairing transcription of the bridging molecule C1q by targeting the transcription factor peroxisome proliferator-activated receptor-δ (PPARδ) [287, 288] impaired efferocytosis and led to the production of auto-antibodies, SLE-like symptoms and splenomegaly [235]. In atherosclerosis, ADAM17-mediated cleavage of MERTK results in the release of soluble MER into the supernatant [289–292]. This has a dual impact, reducing efferocytic uptake by both eliminating surface-bound MERTK and by sequestering GAS6, which is the bridge molecule required for MERTK-mediated efferocytic recognition [290, 293]. In lesional atherosclerosis, expression of the don't eat-me signal CD47 is disproportionally increased, thus suppressing uptake by efferocytes [294]. In mice recovering from ischaemia–reperfusion injury or myocardial infarction, both overexpression of CD47 [295] and MERTK cleavage [296–298] occur on apoptotic cardiomyocytes and cardiac macrophages, contributing to impaired resolution after myocardial infarction. In a murine diet-induced obesity model and in leptin-deficient mice, efferocytic uptake was impaired [299, 300]. MERTK cleavage contributed to decreased efferocytosis, however even though ADAM17 is considered the major metalloprotease responsible for MERTK cleavage, in this instance ADAM9 levels were elevated [301]. While further research is required to confirm a direct interaction between ADAM9 and MERTK in this context, it is likely that tetraspanins may play a role in modulating the activity of different ADAM proteins involved in this process. Erythropoietin signalling is also disrupted in macrophages of obese mice, which regulates expression of pro-efferocytic proteins such as MERTK, GAS6, CD36 and MFG-E8 [299]. Recent efforts have explored enhancing efferocytosis as a strategy to enhance tumour cell uptake in clinical studies. For instance, the use of monoclonal antibodies to block the don't eat-me signal CD24 and its interaction with siglec-10 showed increased clearance of tumor cells [302]. Additionally, ongoing phase I/II clinical trials are exploring inhibitors and antibodies targeting MERTK, TIM3 and TIM4 [303–307]. In contexts outside of disease and cancer, ageing has been associated with accumulation of cellular debris, apoptotic and senescent cells, which can exacerbate inflammation due to the presence of misplaced self-antigen [308, 309]. Interestingly, conditioned media from senescent cells induced MERTK cleavage and suppressed macrophage efferocytosis. Administration of the lipid Resolvin D1 rescued uptake through a mechanism that requires further investigation [310, 311]. Increasing efferocytosis and inducing apoptosis in senescent cells could serve as potent strategies for

extending the healthspan of patients. These examples highlight the far-reaching implications of impaired efferocytosis and the multitude of therapeutic and clinical opportunities available for exploration.

1.4 ADAM10

1.4.1 Classification of ADAM metalloproteases

Proteolysis is a fundamental cellular process defined as a breakdown of protein substrates by proteolytic degradation within or on the surface of the cell, for example in the proteasome and in the lysosome. Proteases recognise specific substrates and site-specifically hydrolyse peptide bonds to break down proteins partially into peptides or fully into amino acids, through which proteases not only degrade proteins but can exert regulatory function. As such, enzymatic proteases are involved in regulating key physiological processes such as development, cell differentiation, hormone activation, neurodegeneration, cancer and apoptosis [312]. Approximately 600 genes encode for human proteases, giving rise to thousands of proteases that have been discovered to date [313]. If proteases are capable of cleaving inside peptide bonds they are referred to as endopeptidases (or proteinases), whereas exopeptidases are capable of recognising, and cleaving terminal amino acids. Endopeptidases are the largest gene family for enzymes in vertebrates. Metalloproteases are a group of approximately 200 endopeptidases, which make up the largest group within the proteolytic enzyme family [314]. Some of the most prominent members within the metalloproteases are the A Disintegrin And Metalloproteinase (ADAM) proteins. There are 22 human ADAM members with multiple domains, 13 of which have been attributed catalytic function (ADAMs: 1, 8, 9, 10, 12, 15, 17, 19, 20, 21, 28, 30, 33) [315, 316]. ADAMs are involved in a host of biological processes for example receptor-ligand signalling, development modulation, differentiation, migration, and regulation of cell–cell and cell-matrix interactions [317, 318]. As type-1 transmembrane proteins, ADAMs are membrane-anchored zinc-dependent proteases [319, 320] and their catalytic domain acts on substrates in close proximity to the membrane, actively ”shedding” their ectodomains [316]. Circa 2-4% of cell surface proteins are assumed to be targets of ectodomain shedding [321, 322], however it is likely that the number of possible substrates is larger than predicted, depending on the cell type and its physiological state. Ectodomain shedding holds particular significance in the context of RIP, which generates membrane remnants that can undergo proteolytic modification by intramembrane proteases such as by the γ-secretase complex [323]. ADAM proteins are capable of cleaving Notch which triggers RIP and a release of its C-terminus into the cytoplasm, where it can translocate into the nucleus

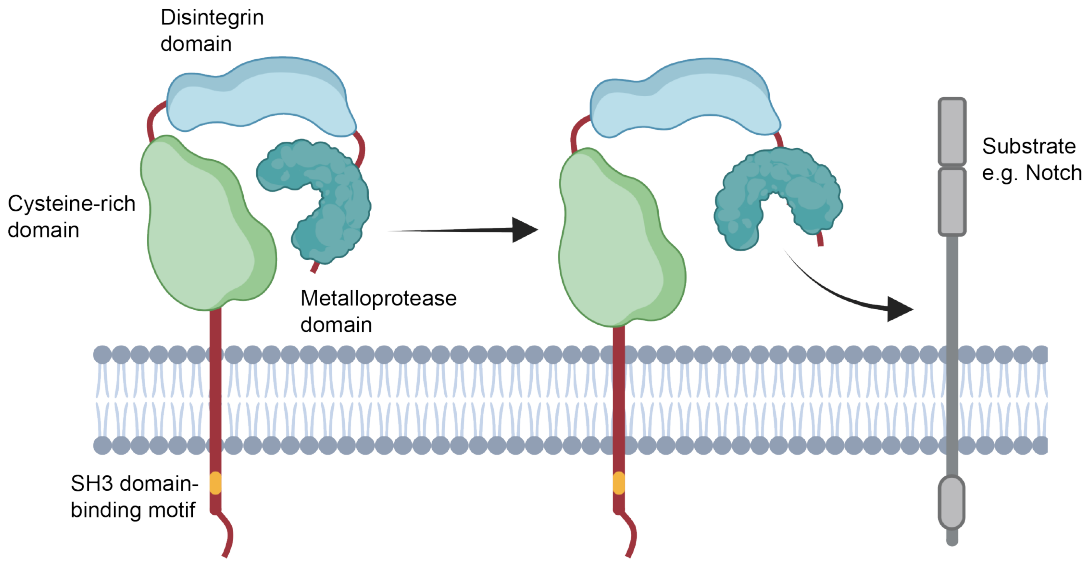


Figure 6: Schematic representation of the ADAM10 domain organisation. The mature ADAM10 protein is comprised of a SH3 domain-binding motif, transmembrane domain, cysteine-rich domain, disintegrin domain, metalloprotease domain. ADAM10 activation triggers a conformational change, leading to the exposure of the enzymatically active site and leading to substrate cleavage (e.g. Notch).

and regulate target gene transcription [324, 325]. ADAM10 is one of the best characterised members of the ADAM family and has close structural resemblance with ADAM17 (or TACE). ADAM10 and ADAM17 are promiscuous sheddases, and their substrate pool is described to include over 100 target proteins. Most of those substrates are uniquely cleaved by one or the other enzyme, whereas some are shared substrates [326]. Some of the most prominent members of the ADAM17 substrate pool include interleukin (IL)-6, epidermal growth factor receptor, and TNFα signalling, which are involved in immune system regulation and cancer development [327]. Although the expression of certain ADAMs is specific to particular tissues, such as ADAM22 in the brain, ADAM23 in both the brain and the heart, and ADAM12 and 19 in muscle tissues, ADAM10, as well as ADAM9, 15, and 17, are ubiquitously expressed in the human body, highlighting their conserved functions [315, 328].

1.4.2 ADAM10 expression, structure and function

Several transcription factors have been described to bind to specific motifs within the ADAM10 promotor region, altering its transcription, for example peroxisome proliferator-activated receptor alpha (PPARα) and nuclear retinoic acid receptor (RAR/RXR), which are positive regulators of ADAM10 mRNA synthesis [329, 330]. Further to that, microRNAs are capable of

binding to the 3' untranslated region of ADAM10, inhibiting translation [331, 332]. The human ADAM10 gene is evolutionary conserved and contains 16 exons for which 17 isoforms have been predicted derived from alternative splicing. During translation in the ER, its 748 amino acids make up a 85 kDa pro-enzyme [333]. At this stage, ADAM10 is expressed as an inactive zymogen, auto-inhibited by its pro-peptide, which is cleaved off by prohormone convertase 7 (PC7) and furin in the Golgi, leading to its maturation [334, 335]. Following its transporting to the cell surface, ADAM10 is comprised of several functional domains as confirmed by x-ray crystallography and cryogenic electron microscopy (cryo-EM) [336, 337]. The N-terminal signal peptide is followed by a pro-domain after which there is the metalloprotease domain (Figure 6). The metalloprotease domain contains a Zn^{2+} binding consensus motif HExGHxxGxxHD, which encompasses the active site responsible for the proteolytic properties of ADAM10 [315]. The disintegrin domain and cysteine-rich region that follow the metalloprotease domain contribute to its catalytic activity and substrate recognition and the disintegrin domain constitutes the 11G2 antibody binding site [338, 339], which is the antibody used in most ADAM10-related studies incuding my own. Next, there is a transmembrane domain, after which the protein ends in its cytoplasmic tail. The intracellular C-terminus contains a Src homology 3 domain-binding motif (SH3), and SH3-binding proteins have been proposed to play a role in proteolytic activity, signalling processes, and its surface localisation [340–342]. In steady-state conditions, the metalloprotease domain is wrapped by the disintegrin and the cystein-rich domain, thereby restricting access and inhibiting the enzymatic activity of mature ADAM10. ADAM10 activation triggers a conformational change, leading to the exposure of the enzymatically active site and triggering substrate cleavage. This mechanism is further explained in the sections below.

1.4.3 ADAM10 substrates

ADAM10 is the major sheddase of over 40 substrates, many of which are involved in health and disease. Known substrates include the cell fate regulator Notch [343], the transmembrane chemokines CXCL16 and CX3CL1 [344], amyloid precursor protein (APP) [345], adhesion molecule VE-cadherin [346], glycoprotein VI (GPVI) [347, 348], cellular prion protein [349], the EGF receptor ligands EGF and betacellulin [321, 350–352], Fas ligand (FasL) [353], cadherin

and CD44 [346, 354, 355], vascular endothelial growth factor receptor 2 (VEGFR2) [356] and the immunoglobulin E receptor CD23 [357] to name only a few. The broad expression and the large substrate pool of ADAM10 contribute to a plethora of biological processes such as adhesion, chemotaxis, proliferation, migration, vascular permeability, receptor-ligand signalling, immnunity and cell fate and differentation [358, 359]. Considering the biological significance of ADAM10's cleaved substrates, various pathologies have been associated with dysregulation of ADAM activity including cardiovascular diseases, neurodegenerative conditions, inflammatory disorders, and cancer. Therefore, targeting ADAM10 function is considered to have great therapeutic potential [360].

1.4.4 Regulation of ADAM10 activity

ADAM10 is involved in a wide range of cellular function making its regulation of pivotal importance. ADAM10's protease activity can generally be altered by gene expression and transcriptional regulation, post-translational modifications, trafficking to the plasma membrane, compartmentalisation at the plasma membrane and protein-protein interactions [361]. The ADAM10 cytoplasmic tail can bind to AP2 and synapse-associated protein 97 (SAP97), which control internalisation and transport to the plasma membrane from the Golgi [362, 363]. ADAM10 trafficking and localisation to the surface can further be promoted by Rab14 and its exchange factor FAM116 [364]. Once at the cell membrane, ADAM10 itself can be shed by ADAM9 and ADAM15, which results in a membrane-bound C-terminal fragment (10 kDa), a remaining cytoplasmic fragment (7 kDa) and the release of the soluble ectodomain (55 kDa), thus regulating its activity. ADAM10 cleavage further triggers γ-secretase activity and the release of its cytoplasmic tail [365–367]. Additionally, ADAM10 activity can be regulated by the composition of the plasma membrane. Association of ADAM10 with cholesterol-rich regions can cause a downregulation in its catalytic activity [368, 369]. Sathya et al. found that high levels of cholesterol led to reduced expression and circulation of ADAM10 to the surface, whereas high levels of isoprenoids resulted in increased ADAM10 activity [370].

Several inhibitors and stimuli have been shown to modulate ADAM10 function. The ADAM10 pro-domain [371] and the endogenous tissue inhibitor of metalloproteases (TIMP) TIMP-1

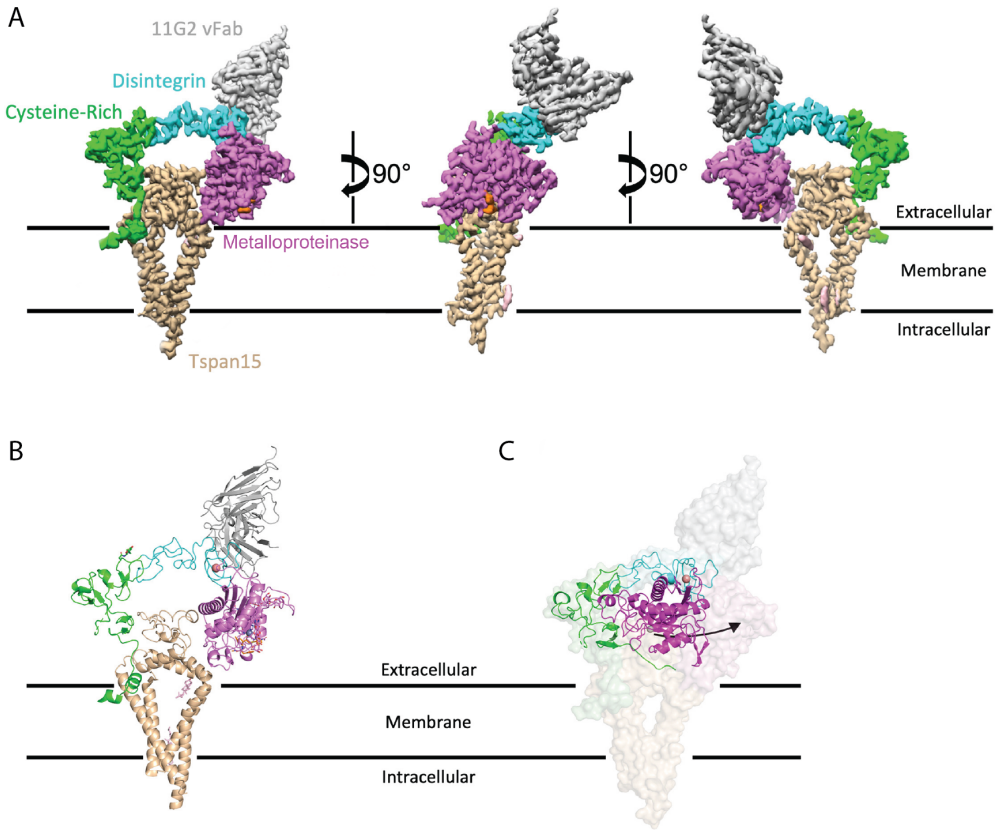


Figure 7: Schematic representation of the ADAM10-Tspan15 complex, adapted from Lipper et al. [339]. A) Cryo-EM electron density map of the vFab-ADAM10-Tspan15 complex. Tspan15 (beige), 11G2 vFab (gray), and the catalytic (pink), disintegrin (cyan), and cysteine-rich domains (green) of ADAM10. B) Cartoon of the complex. Zinc ion at the active site (grey sphere), Ca^{2+} in the disintegrin domain (orange). C) Comparison of ADAM10 in the vFab-ADAM10-Tspan15 complex (surface) with free ADAM10 ectodomain (ribbon)

and TIMP-3 are naturally occurring ADAM10-specific inhibitors [372, 373]. The synthetic inhibitors GI254023X (GI) and GW280264X (GW) are used in this study and inhibit ADAM10 and both ADAM10 and ADAM17, respectively, by binding the Zn^{2+} ion in the active site of the metalloprotease domain, thereby inhibiting substrate cleavage [336]. ADAM10 activity can further be enhanced by growth factors like vascular endothelial growth factor (VEGF) [356], or the alkylating agent N-ethylmaleimide (NEM) [374]. Previously, it had been shown that Ca^{2+} ionophores promote ADAM10 function [352, 375]. Other labs have shown that both Ca^{2+} and cleaved Caspase3 (Casp3) can activate the scramblases TMEM16F(ANO6) and XKR8. These scramblases facilitate the translocation of the phospholipid phosphatidylserine (PS) from the inner membrane leaflet to the outer membrane during cell activation and apoptosis, respectively [257, 376]. More recently, Bleibaum et al. reported that once on the outer leaflet, PS binds to the basic patch in the membrane-proximal domain of ADAM10 and ADAM17, causing its activation and subsequent substrate shedding [377].

Tetraspanins (Tspan) are a superfamily of conserved membrane-embedded proteins that consist of four transmembrane domains. Tspan5, Tspan10, Tspan14, Tspan15, Tspan17, and Tspan33 can interact with ADAM10 and regulate its maturation, trafficking, stability and enzymatic function [378–381]. To date, the best studied interaction of Tspans is the ADAM10-Tspan15 complex, the structure of which was first solved in 2022 [337]. Some studies report that Tspan15 associates with ADAM10 already whilst in the ER, after which the complex is trafficked to the cell surface [382]. The cryo-EM structure of the vFAb-ADAM10-Tspan15 complex has unveiled that the interaction site is situated within a conserved region within the variable portion of the large extracellular loop of Tspan15 [337] (Figure 7). Lipper and colleagues further describe that it is through binding of Tspan15 with ADAM10 that its auto-inhibition is relieved, moving the catalytic site to approximately 20 Å from the cell membrane [339]. They further found that ADAM10 cleavage efficiency is optimal when the site of processing is between eight and 14 residues from the plasma membrane and that different Tspans yield different cleavage products [339].

In a more clinical context, conditions including asthma, inflammation, skin disorders, and cancer may benefit from the modulation of ADAM10 activity [320]. Some breast cancers exhibit increased activity of ADAM10, which correlates with poor prognosis and cancer progression in patients. Inactivation of ADAM10 reduces cancer cell migration and invasion in an *in vitro* study. Therefore the authors concluded that ADAM10 downregulation on such cancers could provide a therapeutic benefit [383]. Conversely, other disorders have been described that could benefit from an increased ADAM10 activity such as Alzheimer's disease, stroke caused by thrombosis and heart attack [320, 384]. In a mouse model for Alzheimer's disease, increased ADAM10 activity was associated with a reduction of the pathologies caused by amyloid plaque formation and hippocampal defects [345].

1.4.5 ADAM10 as a regulator of development and its role in T lymphocytes

In vivo models such as ADAM10 knockout in mice led to embryonic lethality due to major developmental defects at approximately 9.5 days of embryogenesis. Defects included disturbed formation of somites, nervous system abnormalities and severe vascular defects, which are

attributed to the role of ADAM10 in the Notch signalling pathway [385]. Several conditional knockouts have since aimed to circumvent embryonic lethality, which allowed researchers to uncover ADAM10-mediated ectodomain cleavage in the central nervous system, the cardiovascular system, endothelium, immune system, intestine and kidney, contributing to the exploration of the ADAM10 substrate pool [317, 320, 386]. ADAM10-mediated shedding of Notch1 has also been shown on T cells, and mutations surrounding the cleavage site of Notch1 cause excessive activation of Notch1 and ligand-independent proteolysis, ultimately leading to T cell acute lymphocytic leukemia (T-ALL). This type of mutation is responsible for approximately 50% of all T-ALL cases [387]. The overexpression of a dominant negative form of ADAM10 under the T-cell-specific *lck* promotor in a mouse model led to a partial block in thymocyte development, specifically from the double negative (DN) to the double positive (DP) stage. This resulted in a premature downregulation of CD25 and a decrease in TCR expression [388]. ADAM10 sheds Lymphocyte activation gene-3 (LAG3) on intra-tumour T-cells which plays a crucial role in the anti-tumour immune response and impacts sensitivity to immune therapy [389, 390]. ADAM10-mediated FasL cleavage on T cells modulates FasL-induced cytotoxicity and activation-induced cell death (AICD). This highlights the wide-ranging effects of ADAM10-mediated substrate interactions on T cells.

1.5 Scramblases and Phosphatidylserine

1.5.1 Overview

The plasma membrane serves as a protective barrier, separating cellular contents from the external environment. Membranes surrounding cellular components like mitochondria, the Golgi apparatus, the endoplasmic reticulum (ER), lysosomes and the nucleus create a partition between organelles and the cytoplasm, thereby establishing cellular compartmentalisation. Cellular membranes are composed of lipid bilayers containing sphingolipids, glycerophospholipids, and cholesterol. The composition of these varies across different lipid bilayers. Sphingomyelin is considered the predominant sphingolipid present in cellular membranes, whereas phosphatidylethanolamine, phosphatidylcholine, phosphatidylinositol, and PS are the primary glycerophospholipids [391, 392]. PS is the most asymmetrically distributed phospholipid, which almost exclusively localises to the inner membrane leaflet on healthy cells and its exposure on the cell surface serves various biological functions. Besides its role as an eat-me signal for phagocytes during apoptosis (see section 1.3), PS is exposed on necroptotic cell membranes [393] and PS-exposing vesicles are released during pyroptosis [394]. PS is further externalised on senescent erythrocytes and platelets, facilitating clearance by macrophages [395, 396]. Neuronal pruning, a developmental process involving the re-connection and elimination of synapses within neuronal networks, also requires the exposure of PS [397] and in the context of cancer, PS is externalised on tumours with poor treatment efficacy [398]. Evidently, PS is a key player in a multitude of cellular processes, and the necessity of its tight regulation make it a prominent substrate for membrane flippases and scramblases. Flippases translocate PS and phatidylethanolamine specifically from the outer to the inner leaflet in an ATP-dependent manner, while scramblases work in a bi-directional, unspecific manner and are capable of neutralising membrane asymmetry without the use of ATP [399, 400]. Human PS-scramblases are made up of two families (TMEM16 and XKR) that are localised in the plasma membrane and consist of 10 transmembrane regions. The following sections will elaborate on TMEM16F and XKR8, both of which have been verified to be expressed on human T cells [401, 402].

1.5.2 TMEM16F

The TMEM16 (or ANO) family comprises 10 human members [403], five of which (16C, 16D, 16F, 16G and 16J) are located at the plasma membrane and carry conserved charged residues in their transmembrane regions [404]. Two members, TMEM16E and 16K, are expressed within the ER, where they potentially execute Ca^{2+}-dependent functions [405]. TMEM15F and TMEM16K are ubiquitously expressed across various tissues while TMEM16F is the only isoform expressed in the plasma membrane of platelets [406]. On the plasma membrane, TMEM16F forms a homodimer with a cavity in its subunits which contains polar residues and leads to thinning of the lipid bilayer at a specific area. Ca^{2+} binding to TMEM16F triggers a reversible conformational change, which opens this cavity to allow phospholipids to pass, causing PS scrambling to the outer leaflet. This model is sometimes referred to as the credit card or stepping stone model, drawing a parallel with the movement of phospholipids as they move through the scramblase [376, 407, 408] (Figure 8A, B). While the main activity of TMEM16F (ANO6) is considered to be lipid scrambling, a secondary activity as a Cl^- channel was reported [409–412]. Brunner et al. have solved the crystal structure of fungal TMEM16 in which they show the exposure of a hydrophilic groove, which could potentially serve as a channel for lipids and ions [413]. Bricogne showed selective shedding of PD-1 in vesicles on Jurkats after activation of TMEM16F [401]. Another group demonstrated that TMEM16F-mediated PS scrambling led to activation of ADAM10 and 17 on the cell surface and subsequent substrate cleavage [377, 414]. The clinical significance of TMEM16F is highlighted in patients with Scott syndrome, a mild bleeding disorder, in which a loss-of-function mutation of *tmem16f* causes defective PS exposure on platelets [376, 415–417]. This suggests that Ca^{2+}-activated TMEM16F causes PS externalisation which in turn activates membrane sheddase function.

1.5.3 XKR8

The ten XKR family genes found in humans seem to be generated via co-duplicating adjacent genes [419]. With the exception of XKR2, all members localise to the cell plasma membrane, with XKR8 being the best described XKR protein to date [402]. The type I membrane proteins Basigin (BSG) or Neuroplastin (NPTN) function as chaperones to localise XKR8

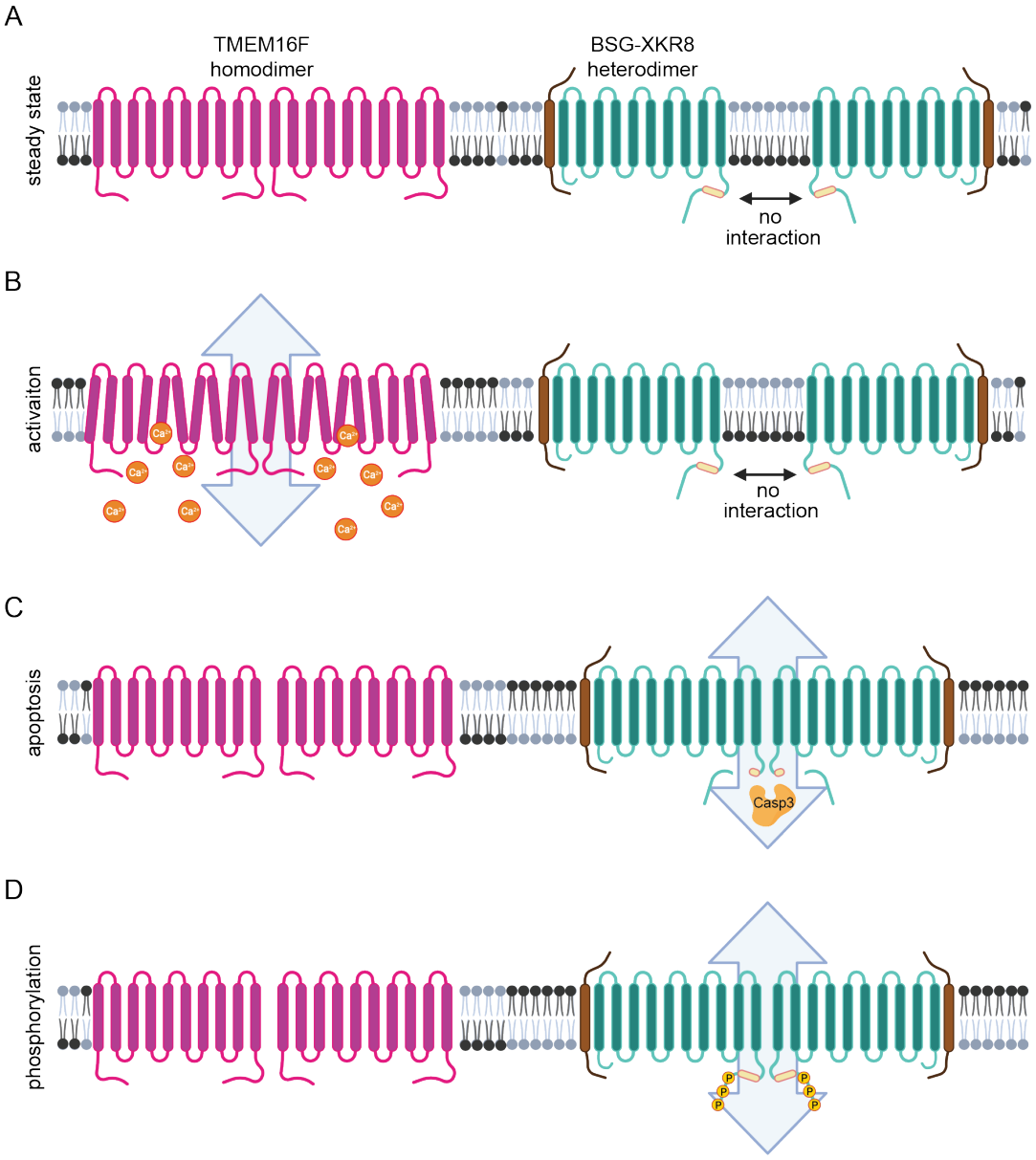


Figure 8: Schematic representation of TMEM16F and XKR8 mechanism. Bottom of bilayer represents cytosol. PS (black), TMEM16F (pink), BSG (brown), XKR8 (teal), Casp3 cleavage motif (yellow). A) steady state B) activation C) apoptosis D) phosphorylation. Schematic adapted from Nagata et al. [418]

to plasma membranes, creating a heterodimer [420] (Figure 8A). In human XKR8, the C-terminal domain, located downstream of the Casp3 recognition site, appears to engage with the cytoplasmic region of the transmembrane helices, thus inhibiting scrambling activity. It is proposed that phosphorylation of these residues blocks this interaction, releasing auto-inhibition and triggering PS scrambling [412]. During apoptosis-mediated Casp3 activation, the XKR8 Casp3 recognition site is cleaved, causing multimerisation of BSG-XKR8 and leading to an irreversible activation of XKR8 PS scrambling activity [353] (Figure 8A, C). In the IL-3-dependent mouse Ba/F3 cell line, XKR8 is constitutively active due to phosphorylation of all three serine/threonine residues downstream of its Casp3 recognition site [421] (Figure 8D). This highlights two potential mechanisms through which XKR8 activity can be induced, either reversibly or irreversibly. XKR4, XKR8, and XKR9 carry a Casp3 recognition site in their cytoplasmic tail [402]. While XKR8 is presumed to be ubiquitously expressed, XKR4 and XKR9 expression is restricted to the brain and intestines, respectively [402]. Notably, the exposure of PS during apoptosis is not dependent on TMEM16F [376]. Therefore, it is assumed that XKR8 serves as the primary PS scramblase in the majority of cell types undergoing apoptosis [422]. *In vivo*, models of XKR8$^{-/-}$ mice showed blocked PS exposure on apoptotic cells, subsequently leading to male infertility due to accumulation of dead cells in the testis [423]. In female mice, XKR8 deficiency leads to acceleration of SLE-like autoimmune diseases [422]. This highlights a central role for XKR8 in apoptosis-mediated PS exposure and its dysregulation leading to inflammatory disease.

1.6 Context, hypotheses and specific aims

The research for my DPhil project was motivated by a study conducted by previous members of the Sattentau laboratory, Drs. Niloofar Karaji and Rebecca Russell. Their work illuminated the ADAM10-mediated shedding of CD43 on apoptotic and HIV-1-infected $CD4^+$ T cells, introducing the intriguing possibility of CD43 serving as a novel ”don't eat-me” barrier. My initial aim encompassed the characterisation of several other transmembrane mucins on human T cells, with the hypothesis that other mucins might be modulated during apoptosis. Having confirmed expression of CD43, PSGL-1, MUC1, MUC24 and CD45 on several T cell lines, their expression during chemical- and radiation-induced apoptosis was investigated. Labelling of CD43, PSGL-1 and MUC1, but not MUC24 and CD45 was downmodulated during apoptosis. These results make up the majority of results chapter 1.

In my next chapter I hypothesised that the observed downregulation of mucins might mechanistically result from reduced antibody binding due to changes in mucin antigenicity, mucin internalisation, or enzymatic cleavage. A major aim was therefore to engineer T cells to expressed a C- and N-terminally tagged form of CD43, with which the loss of CD43 ectodomain from the cell surface of apoptotic T cells but retention of the cytoplasmic domain was confirmed. I hypothesised, based on the results by previous lab members that downmodulation of CD43 is mediated by ADAM10, that other mucins might be cleaved by ADAM10 on apoptotic cells. This was confirmed for CD43, PSGL-1 and MUC1 using ADAM10-specific pharmacological inhibitors and an ADAM10 knockout cell line. Since Bleibaum et al. [377] demonstrated that ADAM10 is activated by apoptosis-induced PS flipping, I hypothesised that the apoptosis-activated PS scramblase XKR8 might be required for this pathway. A major aim was therefore to knock out XKR8 in a T cell line. Using this approach confirmed that XKR8-mediated PS flipping activates ADAM10 sheddase activity, causing the loss of CD43, PSGL-1 and MUC1 ectodomain from the surface of apoptotic T cells. This work makes up the majority of results chapter 2.

Based on the large size and charge of mucins, and their removal during apoptosis, I then hypothesised that CD43, PSGL-1 and MUC1 may function as a don't eat-me barrier. A co-culture assay developed in the Sattentau lab provided a robust method to quantify the en-

gulfment of apoptotic T cells by monocyte-derived macrophages (MDM). A major aim was therefore to knock out other mucins (PSGL-1 and MUC1) in a T cell line, which was then used to confirm that lack of CD43, PSGL-1 and MUC1 contributed to enhanced efferocytic uptake during apoptosis. ADAM10 knockout revealed that the persistence of mucins on the surface of apoptotic cells hinders efferocytic uptake. This hindrance could be alleviated by the StcE mucinase, an enzyme known to cleave CD43, PSGL-1, MUC1, MUC24, and CD45. These findings confirmed that mucin expression on apoptotic T cells holds a pivotal regulatory role in the efferocytic uptake process. This work is explored in results chapter 3.

Based on the reported exclusion of several mucins from the T cell synapse [62, 424, 425], I hypothesised that mucins might require downmodulation during T cell activation to allow enhanced interaction between APCs and target T cells. A major aim was therefore to investigate the regulation of mucins during T cell activation. Using ionophore-based and TCR-mediated activation models showed that PSGL-1 antibody labelling is reduced in both models. During TCR-mediated activation, loss of PSGL-1 was prevented by ADAM10 inhibitors, implying ADAM10 cleavage of PSGL-1 during T cell activation. Whilst the work of this thesis was initiated in the context of apoptosis, the results unveiled within this study extend their relevance beyond cell death. The findings uncovered in this work offer a promising pathway towards comprehending the broader implications of how ADAM10 impacts mucin expression and its role in modulating T cell-antigen presenting cell interactions.

2 Chapter 2: Materials and Methods

2.1 Tissue culture of cell lines

The Ardman lab kindly provided WT CEM and CD43$^{-/-}$ CEM. ADAM10$^{-/-}$ CEM were kindly generated and provided by Dr. Rebecca Russell. Acute T cell lymphoid leukemia Jurkat (T-ALL), NALM6 (B-ALL) and U937 (acute myeloid leukaemia, AML) lines were grown in complete RPMI (R10: 10% FCS, 1% penicillin/streptomycin) at 37℃/5% CO_2. Adherent cell line HEK293T was grown in complete DMEM (10% FCS, 1% penicillin/streptomycin, 1% HEPES) at 37℃/5% CO_2.

2.2 CRISPR/Cas9 gene editing

2.2.1 PSGL-1, MUC1 and XKR8 knockout in CEM

ThermoFisher's Neon transfection system was used for knockout of functional gene expression in CEM. The following guide RNA (gRNA) sequences were used: PSGL-1: ACCACGGAGCUGGCC, GACCACUCAACCAGU, CACUCAACCUGUGCC. MUC1: GCUACGAUCGGUACU, GCAACAGUUGUUACG, GGUCAUGCAAGCUCU, CAUGCAAGCUCUACC. Sequences for XKR8: CCTACGCCGACTTCCTCGCCCTG, CCTTGCGCACCTGCCTCCCCTCC, CCTCCGTGATCTACTTCCTGTGG. Each gRNA (4.4 μL of 100 pmol/μL, IDT) was incubated with 4.4 μL tracrRNA and 1.2 μL Duplex buffer and boiled at 95℃ for 5 min. Ribonucleoproteins (RNPs) were formed by incubating 0.6 μL RNA mix, 0.6 μL Cas9 (Alt-R® S.p. HiFi Cas9 Nuclease V3, 100 μg, IDT) for 20 min at RT. WT CEM T cells were resuspended at 2 x 10^7/mL in buffer R (Thermo Fisher). This step was done last as buffer R reduces cell viability if left too long, thus decreasing CRISPR efficiency. 10 μL of cells, 2 μL transfection enhancer (10.8 μM Alt-R^{TM} Cas9 Elec Enhancer, IDT) and 1 μL RNPs were mixed and immediately added into a Neon Transfection System pipette tip. The pipette was inserted into the Neon Transfection Machine (Thermo Fisher), containing 3 mL buffer E (Thermo Fisher). Transfection conditions were adjusted for CEM at 1230 V, 40 ms pulse width, 1 pulse. Post transfection, cells were resuspended in R10 without antibiotics. After 48 h, antibiotics were added and knockout efficiencies for PSGL-1 and MUC1 assessed by flow cytometry. Cell sorting was carried out on the single, live and PSGL-1-negative or MUC1-negative popula-

tion of each clone using the Aria III cell sorter (BD). Single cells sorts were done for PSGL-1 and MUC1. Subsequent PSGL-1$^{-/-}$, MUC1$^{-/-}$ and double knockout cell lines were confirmed by Western blot. Due to failed validation of commercially available XKR8 antibodies for flow cytometry, selection of knockout clones was done by single cell sorting of single, live and annexin-V-negative cells, followed by expansion and analysis of clones for lack of PS flipping to the outer membrane of staurosporine-treated cells that were positive for intracellular Casp3 labelling. Cells from clones that showed negative annexin-V, but positive caspase-3 staining were subsequently expanded for further analysis. Due to lack of validated antibodies for Western blot, protein content was not able to be confirmed by Western blotting. Instead, the knockout was characterised by sequencing the XKR8 gene PCR product from individual clonal lines using primers targeting Exon 3. GDNA was purified from pre-screened clones using the Monarch® Genomic DNA Purification Kit (New England Biolabs) and Exon 3 amplified using Q5® High-Fidelity DNA Polymerase (New England Biolabs). The following primers were used: 5'-3' ACCTGTGACCGCTGGGGAGT, 3'-5' TGGGTCTCTACAAGTGACAGATGTGTTG. Subsequent 1% agarose gel analysis of the PCR product with SYBR^{TM}Safe DNA Gel Stain (Invitrogen) was performed. The products were gel-purified using the QIAquick® Gel Extraction Kit (Qiagen) and sequenced in Cambridge by Source BioScience. Sequence analysis was done using software from SnapGene and alignment visualised using Jalview.

2.2.2 CD43 knockout in primary CD4^{+} cells

Using the RosetteSep™ Human CD4^{+} T Cell Enrichment Cocktail (STEMCELL Technologies), primary human CD4^{+} T cells were isolated from leukocyte cones. T cells were cultured in complete RPMI supplemented with 50 U/mL IL-2 (GM). Every 48 h, media was changed and cells resuspened at a density of 10^6/mL. Cas9 ribonucleoproteins (RNPs) were prepared by mixing 8.5 μg of TruCut Cas9 protein v2 (ThermoFisher) with 150 pmol of sgRNA mix (Truguide synthetic grna, ThermoFisher) and Opti-MEM (Gibco) to a final volume of 5 μL. The RNPs were incubated for 15 min at RT. Three different sgRNA were used (GCAGTGCAGACACCCACCTCCGG, TTGGTCTCTACTAGCGAGCC ,CCTCATGCAACCAGTCATCCTGC). 1 x 10^6 freshly isolated CD4^{+}T cells were washed three times with Opti-MEM (Gibco) and resuspended at a density of 2 x 10^7/mL. RNPs and T cells were mixed and transferred into a

BTX Cuvette Plus electroporation cuvette (2 mm gap, Harvard Bioscience). Electroporation was conducted using a BTX ECM 830 Square Wave Electroporation System (Harvard Bioscience) at 300 V, 2 ms, 1 pulse. Cells were transferred immediately to complete RPMI media supplemented with IL-2 (50 U/mL, PeproTech). Dynabeads® Human T-Activator CD3/CD28 (ThermoFisher) were added 24 h after electroporation. 3 and 5 days post activation, 1 mL of medium was exchanged with fresh IL-2 supplemented media. The magnetic beads were removed 5 days after electroporation and cells were re-suspended at 1 x 10^6 cells/mL with fresh IL-2 every 48 h. T cells were maintained until 16 days after electroporation. The knock-out efficiency of CD43 was very high (90%). For depletion of residual CD43-expressing T cells, cells were re-suspended in MACS buffer (PBS, 0.5% BSA, 2 mM EDTA) at a density of 1x10^7/mL. Cells were stained with 5 μL of APC-labelled anti-CD43 antibody per 1 x 10^6 cells for 20 min at 4℃, washed with MACS buffer and re-suspended at a density of 1x10^8/mL. 1 μL of anti-APC nanospheres (StemCell) were added per 1x10^6 cells and incubated for 15 min on ice. After an additional washing step using MACS buffer, magnetic beads were added to the samples and incubated for 10 min. After washing, beads were pulled down magnetically using a StemCell magnet. The negatively selected cells contained in the flow-through were collected and analysed for surface expression of CD43 by flow cytometry.

2.3 Cloning of double-tagged CD43

Plasmids encoding CD43 with an N-terminal Halo-tag or a C-terminal SNAP tag respectively, kindly provided by Prof Simon Davis, were resuspended in CutSmart buffer (New England Biosciences) and digested with NotI-HF and BstXI (New England Biosciences) at 37ºC for 60 min. Running the products on a 1% agarose gel allowed me to cut out the Halo-CD43 backbone (10,252 bp) and the CD43-SNAP fragment (1046 bp). After purifying the DNA fragments with a DNA Gel Extraction kit (Quiagen), DNA concentration was measured using a Nanodrop machine. T4 ligase (ThermoFisher) and T4 ligase buffer was used to ligate the Halo-CD43 backbone with the CD43-SNAP fragment for at 16ºC overnight. NEB® Stable Competent *E. coli* (High Efficiency) (New England Biosciences) were thawed on ice. 1 μL of the ligation mix was mixed with the *E. coli* and heat shocked for 60 s at 42ºC. After a 30 min incubation on ice, 500 μL of S.O.C. medium (ThermoFisher) was added and incubated

at 37ºC at 180 rpm for 1 h. Cells were centrifuged at 1,000 g for 1 min and resuspended in 100 μL LB broth. 10 μL *E. coli* was plated on ampicillin agar plates (100 μg/mL ampicillin) and colonies grown at 37ºC overnight. The next day colonies were picked and expanded in 1 L selection media (LB broth with 100 μg/mL ampicillin). Plasmids were purified using the Plasmid Maxi Kit (Qiuagen) and frozen at -20ºC for further use.

2.4 Lentiviral transduction of CD43$^{-/-}$ CEM with Halo and SNAP-tagged forms of CD43

After sub-cloning to obtain a double-tagged CD43$_{Halo/SNAP}$ construct (see above), 2 μg p8.91, 2 μg pMD-G and 2 μg CD43$_{Halo/SNAP}$ were gently mixed with 520 μL plain DMEM and 30ul PEI (1 mg/mL PEI stock) and incubated for 10 min at RT. The mix was added dropwise to 70% confluent HEK293L and incubated for 4 h. Media was replaced with complete DMEM. Cell culture supernatant was harvested 48 h and 72 h post transfection. Lentiviral particles were mixed with Lenti-X concentrator at a 1:3 ratio, incubated for 4 h and centrifuged at 4ºC for 45 min at 1500 g. The viral pellet was resuspended in 500 μL complete DMEM and added to CD43$^{-/-}$ CEM and CD43$^{-/-}$/ADAM10$^{-/-}$ CEM with polybrene at 2–10 μg/mL for increased transduction efficiency. Transduced cells were flow-sorted using a BD FACSAria^{TM} III for double-positive CD43$_{Halo/SNAP}$ and ADAM10$^{-/-}$CD43$_{Halo/SNAP}$ and further characterized by flow cytometry.

2.5 Peripheral blood mononuclear cell isolation

Leukocyte cones from healthy donors were obtained from the NHS Blood and Transplant services (Oxford, UK) under contract 17/WM/0333. Each donor gave consent before blood collection. Each cone was topped up to 50 mL with 1x PBS. In a 50 mL falcon tube, 25 mL of the mix was added to 15 mL Ficoll-HistoPaque 1077 (Sigma-Aldrich). Density centrifugation was performed at 400 g for 25 min at RT with no brake. The PBMC layer of each donor was transferred to a separate 50 mL tube, which was then topped up to 50 mL with 1x PBS. PBMCs were washed at 400 g for 10 min at room temperature. After repeating the washing step two additional times, the pellet was resuspended in 5 mL ACK lysis buffer (Gibco) for 3-5

min. The falcon tube was topped up to 50 mL with 1x PBS and centrifuged at 400 g for 5 min. Cells were counted and processed depending to further applications.

2.6 Monocyte-derived macrophage preparation and differentiation

After PBMC isolation cells were plated on 10 cm^2 tissue culture petri-dishes (Corning) at 150×10^6 cells/dish for 2 h at 37℃/5% CO_2 in RPMI-1640 (Gibco). For successful adhesion of the monocyte fraction contained in the PBMC population, medium was FCS-free. Plates were washed once to remove non-adherent cells with warm PBS before replacing the media with complete DMEM (10% FCS, 1% Penicillin/Streptavidin, 1% HEPES) supplemented with recombinant human M-CSF (10 ng/mL, Life Technologies) for 7-10 days to differentiate monocyte-derived macrophages (MDM). The washed off cells, hereon termed "$PBMC^+$" were either frozen in freezing media (10% DMSO, 90% FCS) or immediately stimulated with PHA (1 μg/mL, Sigma) or CD3/CD28 Dynabead activator beads and cultured in recombinant human IL-2 (10 U/mL, NIBSC) in complete RPMI and used between days 4-7. After 7-10 days MDM differentiation, cells were detached with TrypLE (ThermoFisher) and gentle scraping and replated at 5 x 10^6 cells per 6 cm petri dish (Corning) at least 24 h prior to co-culture with CEM or primary T cells.

2.7 Apoptosis induction in cell lines and primary T cells

2.7.1 Staurosporine-induced apoptosis

Cell lines and $PBMC^+$ were counted and resuspended at a concentration of 2-3 x 10^6 cells/mL in complete RPMI. Staurosporine (Cambridge Bioscience) was resuspended in DMSO to make up a stock solution at 10 mM and added at 1:1000 for a final concentration of 10 μM. Incubation duration was 3 h, with the exception of 0-6 h in timecourse experiments at 37℃. A vehicle-only control was performed for all new experiments, for which cells were treated with DMSO at 1:1000. After incubation, cells were washed in PBS and further processed according to the individual protocol.

2.7.2 UV-C radiation-induced apoptosis

Cell lines and PBMC$^+$ were counted and resuspended at a concentration of 2-3 x 10^6 cells/mL in complete RPMI. Exposure to UV-C light was used to induce apoptosis in CEM at 50 J/m^2/s for 2 min. If required, UV-sensitive metalloprotease inhibitor GW was added again at 10 μM after irradiation (see section 2.7). Post radiation, CEM were incubated for 24 h, which allowed the cells to recognise any damage caused by the radiation and enter the apoptotic programme. Cells were washed in PBS and further processed according to the individual protocol.

2.7.3 Dexamethasone-induced apoptosis

Cell lines and PBMC$^+$ were counted and resuspended at a concentration of 2-3 x 10^6 cells/mL in complete RPMI. The synthetic glucocorticoid hormone dexamethasone (Fisher Scientific) was resuspended in DMSO at 10 mM and frozen in aliquots. CEM, Jurkat or primary CD4$^+$ were treated with dexamethasone at 1:1000 for a final concentration of 10 μM for 48 h. Cells were washed in PBS and further processed according to the individual protocol.

2.8 Metalloprotease inhibitors

The broad-spectrum metalloprotease-specific inhibitors GM6001 (R&D) and Marimastat (R&D) and the ADAM10 inhibitors GI254023X (”GI”, Aobious) and ADAM10/17 inhibitor GW280264X (”GW”, Aobious) were resuspended in DMSO at 10 mM and cells treated at 1:1000 for a final concentration of 10 μM for 45 min prior to any other treatment. When cell death was induced by staurosporine or dexamethasone, cells were incubated with inhibitors as described above followed by addition of staurosporine or dexamethasone. In the case of UV-C induced apoptosis, cells were incubated with GI and GW prior to irradiation as described above and UV-sensitive GW was added again at a final concentration of 10 μM after irradiation.

2.9 StcE mucinase

The Bertozzi lab (Stanford) kindly provided secreted protease of C1 esterase inhibitor (StcE) mucinase. For flow cytometric analyses, CEM were treated with StcE for 1 h at 37°C at 1:1000 (2 mg/mL stock, endotoxin tested). For efferocytosis assays, CEM were pre-treated with StcE

for 1 h at 37℃ at 1:1000 prior to staurosporine/DMSO treatment, keeping StcE in the culture supernatant for the duration of apoptosis induction and removing it through washing with PBS prior to co-culture.

2.10 Flow cytometry analysis

Specific surface and intracellular staining was conducted as specified in the subsections below. Antibody clones, working concentrations and manufacturers are outlined in the antibody table. After fluorescent labelling, all cells were analysed by flow cytometry using the Cytoflex LX flow cytometer (Beckman Coulter) or an LSRFortessa (BD Biosciences) and data processed using the FlowJo-V10 software (FlowJo, LLC). Isotype controls, Fluorescence Minus One (FMO) controls and unstained controls were performed for all colours, antibodies, cell lines and primary cell donors to gate on positive and negative populations. Compensation matrices were generated using UltraComp eBeads^{TM} compensation beads (Invitrogen). Lymphocytes were gated based on forward scatter (FSC) and side scatter (SSC) before doublet and live/dead cell dye to allow exclusion of dead cells with dye-permeable membranes. Subsequent gating was carried out on Annexin-V and/or cleaved caspase-3 labelling to differentiate apoptotic from non-apoptotic cells within the same population.

2.10.1 Analysis of apoptosis induction in cell lines and primary T cells

CEM, Jurkat, U937, NALM6 or primary $CD4^+$/$CD8^+$ T cells were centrifuged for 2 min at 400 g in U-bottom plates and resuspended in PBS or annexin-V binding buffer (BD Pharmingen), which is a calcium-rich buffer which was used if the staining mix contained annexin-V. Surface markers were stained for 20 min at RT in the dark using annexin-V conjugated with FITC, APC, or Pacific Blue (Biolegend), near-IR fixable viability dye (Invitrogen) and fluorophore-conjugated primary antibodies depending on the experiment. After labelling, cells were washed with annexin-V binding buffer, centrifuged for 2 min at 400 g at 4℃, and fixed with Fixation Buffer (Biolegend) for 10 min at RT. Cells were washed with PBS and intracellular staining was carried out using anti-human activated Casp3 antibody conjugated with FITC or BV421 (BD Biosciences) in perm buffer (Biolegend) for 20 min at RT in the dark.

2.10.2 Activated Jurkats

Activated Jurkats (see section 2.16.2) were centrifuged for 2 min at 400 g in U-bottom plates and resuspended in cold annexin-V binding buffer (BD Pharmingen). For surface staining, cells were stained in annexin-V binding buffer containing annexin-V (BV421), anti-CD69 (BV711), anti-CD45 (FITC), anti-CD43 (PE), PSGL-1 (APC) and near-IR fixable viability dye (near-IR). Staining was done at 4ºC to limit cellular activity for 30 min in the dark as set out in the experiment. After labelling, cells were washed, centrifuged for 2 min at 400 g at 4℃, fixed with Fixation Buffer (Biolegend) for 10 min at RT and washed with PBS. Cells were washed with PBS and intracellular staining was carried out using anti-human cleaved Casp3 antibody conjugated with FITC or BV421 (BD Biosciences) in perm buffer (Biolegend) for 20 min at RT in the dark.

2.10.3 Activated primary T cells

Primary $CD4^+$ and $CD8^+$ T cells (see section 2.16.2) were centrifuged for 2 min at 400 g in U-bottom plates and resuspended in cold annexin-V binding buffer (BD Pharmingen). For surface staining, half the wells received master mix A, the other half was incubated with master mix B. Master mix A contained FcX (Biolegend), annexin-V (BV421), anti-CD3 (AF700), anti-CD43 (PE), anti-PSGL-1 (APC) and near-IR fixable viability dye (near-IR). Master mix B contained FcX (Biolegend), annexin-V (BV421), anti-CD45 (FITC), anti-CD3 (AF700), anti-MUC24 (PE), anti-MUC1 (APC) and near-IR fixable viability dye (near-IR). Staining was done at 4ºC for 30 min in the dark. After labelling, cells were washed, centrifuged for 2 min at 400 g at 4℃, fixed with Fixation Buffer (Biolegend) for 10 min at RT and washed with PBS. Cells were washed with PBS and intracellular staining was carried out using anti-human cleaved Casp3 antibody conjugated with FITC or BV421 (BD Biosciences) in perm buffer (Biolegend) for 20 min at RT in the dark.

2.11 Molecules of Equivalent Soluble Fluorochrome (MESF) Quantification

1 x 10^6 healthy cells were seeded in a 96-well U-bottom plate and stained with Near-IR live/dead dye and 1 μg PE-labelled antibody specific for CD43, PSGL-1, MUC1, MUC24 or CD45 for 30 min at 4℃ in the dark. The inclusion of live/dead dye in the staining mix was necessary as mucin expression levels can vary depending on cell viability. Samples were centrifuged for 2 min at 400 g at 4℃ and resuspended in PBS. One drop per standard of PE-standard beads (Quantum™ R-PE MESF, Bangs Laboratories Inc.) was used. The beads were washed and all samples run immediately on a Cytoflex LX. Data were analysed using the manufacturer's software QuickCal v 3.0.

2.12 T cell surface biotinylation

WT CEM and ADAM10$^{-/-}$ cells were biotinylated using the Pierce™ Cell Surface Biotinylation and Isolation Kit (ThermoFisher). Post biotinylation, apoptosis was induced in half of the samples by incubating with 10 μM staurosporine, the other control half with vehicle (10 μM DMSO) for 3 h at 37℃. Samples were immediately put on ice and cOmplete™ Protease Inhibitor Cocktail (Roche) added for a 1x final concentration. Samples were centrifuged for 1 min at 10,000 g to separate cell fraction from the supernatant fraction. An additional 10 min centrifugation step at 13,000 g served to pellet cells in the cell fraction and apoptotic vesicles in the supernatant fraction. Cells were lysed by incubation with lysis buffer (1% Triton-X, 10 nM NEM, 1 mM PMSF, 1x Protease Inhibitor Cocktail) for 30 min at 4℃ with rotation. After removal of cellular debris by centrifugation, biotinylated molecules were pulled down using the Pierce™ Cell Surface Biotinylation and Isolation Kit (ThermoFisher) for 2 h with rotation at 4ºC. Beads were washed 5 times with the kit's wash buffer. Proteins were not removed from the beads as per the kit's instructions, and NuPAGE™ LDS Sample Buffer (4X) (Thermo Fisher) was added immediately and the samples boiled at 95℃ for 10 min and analysed by Western blot as below.

2.13 Western blot

NuPAGE™ LDS Sample Buffer (4X) (Thermo Fisher) was added to samples and boiled at 95ºC for 10 min. To prevent condensated water at the top of the lids which would alter protein concentration across samples, samples were centrifuged for 10 seconds and loaded onto a 4-12% gradient gel (Thermo Fisher) with a SeeBlue™ Plus2 Pre-stained Protein Standard (ThermoFisher) and run at 120 V for 90 min. Gels were immediately transferred using the Trans-Blot Turbo DNA Midi 0.2 μm Nitrocellulose Transfer kit (BioRad), using the high molecular weight programme for 10 min. Membranes were blocked with 5% milk in PBS-Tween at RT for 1 h with rotation. Anti-CD43 (SP55, Invitrogen), anti-PSGL-1 (108, Thermo Fisher), anti-MUC1 (MH1-CT2, ThermoFisher), anti-CD45 (EP322Y, Abcam) or anti-ADAM10 (11G2, Cell Signaling Technology) were used at 1:1000 in 5% milk in PBS-Tween for 2 h at RT with rotation. After washing 3 times with PBS-Tween, HRP-conjugated secondary antibodies were used at 1:1000 at RT with rotation for 1 h (Anti-rabbit-HRP, Invitrogen, anti-Armenian Hamster-HRP, ThermoFisher). The housekeeping protein β-actin was used as a loading control and stained using an HRP-conjugated anti-β-actin antibody (BA3R, ThermoFisher) at 1:10,000 in 5% milk in PBS-Tween at RT for 2 h. Pierce™ ECL Western blotting Substrate (ThermoFisher) was used for lysate samples and SuperSignal™ West Femto Maximum Sensitivity Substrate (ThermoFisher) for supernatant samples. Imaging was done using an Amersham Imager 600, and band density quantified with ImageStudio software.

2.14 Mass spectrometry

Surface biotinylated lysate and supernatant samples were prepared as above, however PBS was used instead of the kit's unspecified wash buffer to prevent interference with downstream processing and to increase sample purity. After washing, the beads were resuspended in PBS and frozen at -80ºC. Three independent repeats were collected this way and sent to Berlin, Germany, for mass spectrometric analysis. Samples were shipped to Kerstin Fentker, who processed the samples from hereon based on methods described in [426, 427] with the following modifications. 20 μL of 4x Urea buffer (8 M Urea/Thiourea in 40 mM HEPES, pH 8) were added to the samples, proteins were reduced and alkylated using DTT (12 mM final concentration) and CAA (40 mM final concentration). 1 μg LysC and 1 μg Trypsin were added

to the samples and incubated overnight. The supernatant was harvested and transferred to a clean tube. The beads underwent a 50 μl ABC buffer wash, and the resulting supernatant added to the initial harvest. Formic acid was added for a final concentration of 1% formic acid, and the peptides desalted using stage tips. Peptides elution was performed in 90% acetonitrile (0.1% formic acid), dried and resuspended in 15 μL 3% acetonitrile. 5 μL peptide was separated on a 98 min gradient and run on a Thermo Q Exactive Plus instrument. Analysis of raw files was performed using MaxQuant (Version 2.0.3.1). Spectra were searched against a human UniProt database (2023-02). N-terminal acetylation, deamidation (N,Q) and Methionine oxidation were taken into consideration for variable modification and carbamidomethyl cysteine was included for fixed modification. Missed cleavage cutoff was set to s maximum of 2. Data were further analysed with R (Version 4.0.4). Following $\log_2$ transformation, protein groups were filtered on a minimum of 50% valid values and missing values were imputed by taking values from a log normal distribution with 0.25x the standard deviation of the log-transformed values, and shifted down by 1.8 standard deviations. The Limma package was used for statistical testing of differential protein abundance [428].

2.15 Multispectral flow cytometry (ImageStream) assay of efferocytosis

MDM were plated at 5 x 10^6 cells per 6 cm petri dish (Corning) and given 24 h to adhere. T cell lines were labelled with 0.5 μM Cell Tracker Green CMFDA (Invitrogen) and MDM stained with 1 μM Cell Tracker Orange CMRA (Invitrogen) for 30 min at 37℃. After washing with PBS to remove unbound dye, depending on the experiment, CEM were pre-treated with 10 μM GI, 10 μM GW or StcE at 1:1000 for 1 h. Without an additional washing step, 10 μM staurosporine was added to half the samples for 3 h at 37℃ to induce apoptosis in about 50% of cells. After washing with PBS, all samples were stained with near-IR fixable viability dye, counted and added to MDM at a 1:1 ratio for 1 h. After collection unattached CEM, MDM were lifted with cold 10 mM EDTA in PBS for 10 min on ice, gently scraped off and all cells collected with an additional PBS wash. All cells were pelleted by centrifugation and fixed in 200 μL fixation buffer for 10 min at RT. Intracellular staining was performed for Casp3 as described above. Data were acquired on an ImageStream® MK II (Amnis) machine using INSPIRE

software and data analysed with IDEAS software. Cells in focus and doublet exclusion were gated on prior to fluorescence analysis. The Cell Tracker Green and Orange double-positive population was split into engulfed, attached and unattached T cells based on the delta-centroid function, which calculates the distance between the centre of CEM and MDMs within each image. Subsequent gating was performed on Casp3 staining to differentiate apoptotic from non-apoptotic cells within the engulfed gate. The engulfed CEM fraction of non-apoptotic compared to apoptotic cells was used to create an uptake index, which is calculated as [% MDM-engulfed apoptotic T cells/% apoptotic T cells prior to co-culture] x 100. The index was calculated for non-apoptotic cells as [ratio of % MDM-engulfed non-apoptotic cells/% non-apoptotic T cells prior to co-culture] x 100.

2.16 T cell activation assays

2.16.1 PMA/Ionomycin stimulation

Healthy Jurkat cells were plated at 400 x 10^5 per well in a U-bottom plate and stimulated with 25 μg/mL PMA and Ionomycin or carrier only (DMSO) for 0, 15, 30 or 60 min at 37ºC. Samples were put to 4ºC immediately following the stimulation, and the subsequent surface staining was also carried out as described in section 2.10.2

2.16.2 TCR-mediated stimulation of primary CD4$^+$ and CD8$^+$ T cells

This method is adapted from Pettmann and colleagues as established in the Dushek laboratory [429]. CD4$^+$ and CD8$^+$ T cells were isolated from leukocyte cones using the RosetteSep Human CD4$^+$/CD8$^+$ enrichment cocktail (STEMCELL) at 150 μL/mL according to the kit's instructions. The CD4$^+$ or CD8$^+$ containing fractions were collected, washed in PBS and counted. Cells were resuspended at 1x10^6/mL in cRPMI with CD3/CD28 Human T-activator Dynabeads (Thermo Fisher) at a 1:1 bead:cell ratio and 50 U/mL IL-2 (PeproTech) and left to expand overnight. The next day, cells were transduced with VSV-pseudotyped lentivirus encoding for the 1G4 TCR [429, 430]. Two days post transduction, 1 mL of medium was exchanged and IL-2 added as before at 50 U/mL. Dynabeads were magnetically removed 5 days post-transduction, and cells resuspended at 1x10^6/mL with added IL-2 at 50 U/ml every

other day after. Based on donor-dependent expansion, T cells were used 10-16 days after transduction. On the day before co-culture, $3x10^4$ U-87 MG cells were seeded in a 96-flat bottom plate and left to adhere overnight. On the next day, NY-ESO-1 peptide, which is the cognate antigen for 1G4 TCR, was added to half the U-87 MG-containing wells at 1:10,000 dilution (100 nM final) and incubated for 2 h at 37ºC, while the other half remained without peptide. Peptide was subsequently washed off and $6x10^4$ T cells were added per well and spun for 2 min at 50 g. Co-culture proceeded for 4-20 h after which T cells were harvested for flow cytometric analysis as described in section 2.10.3.

2.17 Statistical analysis

All data sets were tested for normal distribution using the Kolmogorov-Smirnov test. In the case of a normal distribution, student's *t*-test for two-way comparisons or ANOVA for multiple comparisons were applied with Dunnett's post-test correction. Where data was not normally distributed, they were either subjected to log-transformation and subjected to ANOVA for multiple comparisons with Dunnett's post-test correction, or a Mann-Whitney U for two-way comparisons or Kruskal Wallis for multiple comparisons with Dunn's post-hoc test was performed. Unpaired analysis was performed for cell line data and paired analyses were applied to data derived from individual donor primary cell samples. Unless otherwise stated, results are plotted as mean ± standard deviation (SD).

2.18 Illustration software

For schematic and workflow overviews Biorender and Adobe Photoshop (24.5.0) were used. Graphs were created using Prism (10.0.2) and Adobe Illustrator (27.5) was used to compile figures.

3 Downregulation of mucin labelling in apoptotic immune cells

3.1 Introduction

While members of the transmembrane mucin family have been well characterised on mucosal and epithelial tissues, scant knowledge is available about the expression or regulation of mucins on immune cells. Expression of MUC1, MUC15, MUC18 (CD146, MCAM) and MUC24 (CD164) has previously been reported within the glycocalyx of leukocytes [115], T cells [83, 97, 117], B cells and NK cells [117], and monocytes [24]. In addition to canonical transmembrane mucins, the glycoproteins CD43, CD44, CD45 and TIM1 have one or more mucin-like domains in their extracellular portion and carry heavy O-linked glycosylation [431–434]. I have termed these mucin-like molecules “mucins” for the purpose of this study. In the context of cancer, aberrant glycosylation patterns of mucin ectodomains such as in CD43, PSGL-1 and MUC1 has been reported, some being used as cancer biomarkers and being considered checkpoint molecules [127, 144, 435]. CD43, CD44, PSGL-1, MUC1, MUC24 and CD45 are often overexpressed on cancers and correlate with worse disease progression and survival [436–438]. The selection pressure for over-expression of mucins on transformed cells is not fully established, but might in part be due to their anti-adhesive properties which appear to reduce their elimination by immune cells such as cytotoxic T cells, NK cells and macrophages [439]. In this chapter immune cell lines are screened for expression of mucins under steady-state and apoptotic conditions. The predominantly used cell line is CEM, a $CD4^+$ lymphoblastic cell line, originally derived from a young child with acute T cell lymphoblastic leukemia (T-ALL) in 1963 [440]. Jurkat are used, which is another T-ALL cell line isolated from a 14-year-old boy [441]. In addition NALM6 are used which is a transformed human pre-B cell line and U937 which is a transformed monocyte/macrophage-like cell line [442, 443].

Manjunath et al. found that CD43 knockout showed enhanced adhesion in CEM and increased proliferation in primary T cell activation assays in mice [124, 444]. The same CEM knockout cells were used by Walker et al. to show that the CD43 cytoplasmic tail is necessary to mediate the anti-adhesive effects described above, implying signalling properties [125]. In keeping

with their anti-adhesive role in intercellular interactions, it has also been shown that some mucins can reduce pathogen infection, presumably by a similar anti-adhesive mechanism reducing pathogen engagement with the target cell. Thus PSGL-1 and CD43 overexpression on CEM led to reduction of HIV-1 virion infectivity [445, 446]. Similarly, HIV-1 and Human T Cell Leukemia Virus Type 1 (HTLV-1) infectivity was reduced in a knock-down model of CD43 and PSGL-1 in CEM and Jurkat [447, 448]. Previous lab members have shown that when staining CD43 on apoptotic T cells, antibody binding was reduced compared to the non-apoptotic counterpart. Because of the anti-adhesive properties of CD43, this finding implied that these properties might be negatively regulated during apoptosis, with consequences for dying cell recognition and uptake by phagocytes. This observation therefore led me to consider that this might be a wider phenomenon shared amongst multiple transmembrane mucins expressed on immune cells. Thus characterising the expression of mucins on healthy and apoptotic immune cells could help further our understanding of immune cell activation and clearance.

3.1.1 Hypothesis

Based on the previous observations outlined above, I hypothesised that transmembrane mucins additional to CD43 may be expressed on T cells and perhaps other immune cells, and that their cell surface expression may be modulated during apoptosis influencing cell adhesion and intercellular interactions.

3.1.2 Specific aims

1. To screen transmembrane mucin expression on T cell and other immune cell lines
2. To extend this analysis to primary T cells
3. To establish and optimise apoptosis induction systems and analyse mucin expression

3.2 Results

3.2.1 Mucin expression on the CEM T cell line

Since mucins are primarily associated with mucosal surfaces and expression on epithelial cells, expression of mucins on T cells has previously only been sporadically characterised and limited literature is published in regards to T cell lines and primary cells. The Human Protein Atlas was consulted for a brief screening of expression on immune cells [449]. MUC1, MUC15, MUC18 (CD146, MCAM) and MUC24 (CD164) are members of the transmembrane mucin family. CD43, CD45 and TIM1 have a mucin-like domain in their extracellular portion and carry heavy glycosylation. An expression screening was conducted on CEM T cells by flow cytometry. Target molecules were chosen based on their characteristics of either being members of the sialomucin family with heavy glycosylation and large size, or as in the case of CD47, because they have previously been described to have inhibitory effects on cell-cell interactions such as phagocytosis via negative intercellular signalling pathways [450].

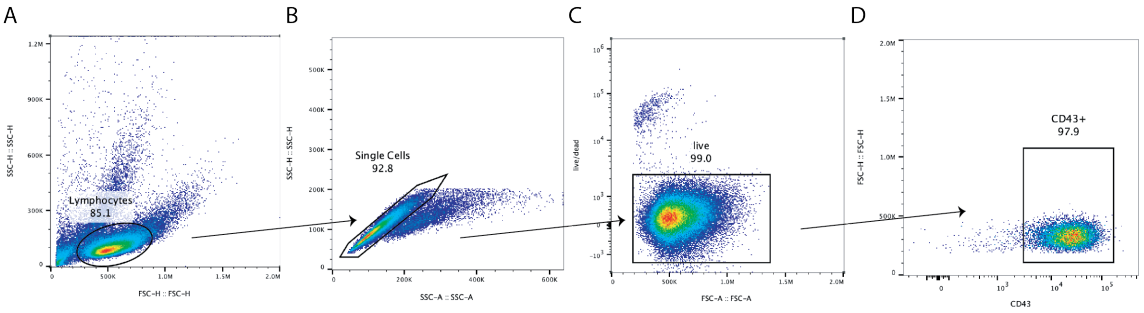


Figure 9: Representative gating strategy for CEM T cells. Gating on: A) lymphocytes; B) single cells; C) live cells followed by; D) gating on the relevant marker, here CD43.

Healthy CEM T cells were stained for surface markers (see Material and Methods on page 55) and gated on lymphocytes, single cells and live cells (Figure 9A-C).

Expression analyses were plotted as an overlay of the marker of interest and the respective isotype control (Figure 10). All antibodies were purchased directly conjugated either with phycoerythrin (PE) or allophycocyanin (APC). PE was chosen as a fluorochrome for the majority of my antibodies of interest, as it is one of the brightest and best-characterised fluorophores available [451], and has the advantage of little spectral overlap when used in panels with many other fluorescent dyes. If a suitable antibody clone was unavailable conjugated with PE, APC was chosen as an alternative. APC is a bright fluorochrome [451], but compared with PE, has

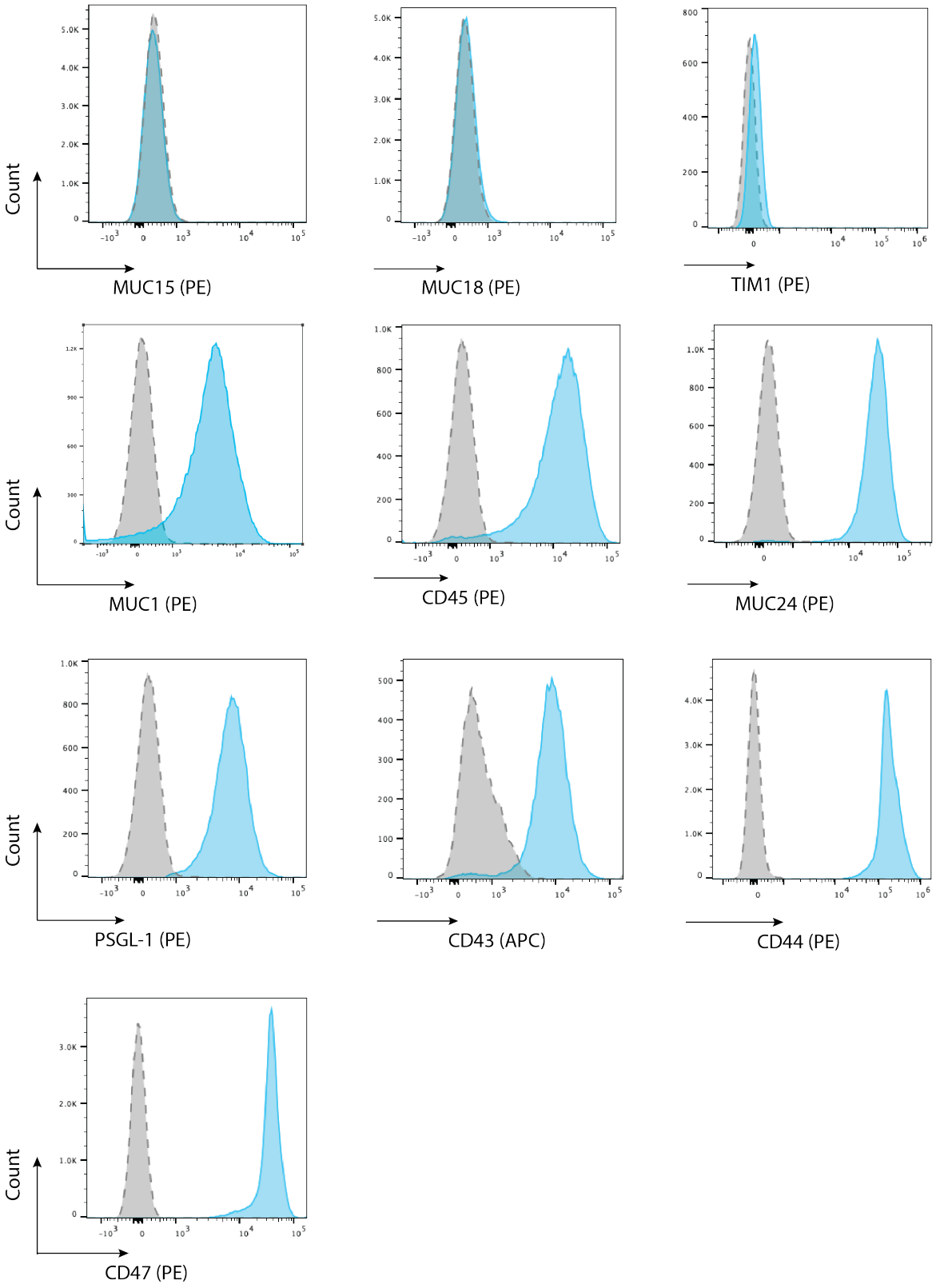


Figure 10: Histogram overlays of mucin-like targets (blue) and their respective IgG_1 H+L isotype control (grey, dashed) on CEM T cells. Staining was performed for MUC15, MUC18, TIM1, MUC1, CD45, MUC24, PSGL-1, CD43, CD44 and CD47. Gating on lymphocytes, single cells and live cells.

slightly more spectral overlap with other commonly used fluorescent dyes. MUC15, MUC18 and TIM1 staining was negative and these mucins were excluded from further study. CD47 was excluded because it lacks a mucin domain and as mentioned above acts as a negative signalling molecule. CD44 was excluded because its N-terminus has a more complex tertiary structure in contrast to the relatively simple ectodomains typically found in mucins [452]. MUC1 staining gave a low to intermediate signal, while the CD45, MUC24, PSGL-1 and CD43 signal was high, and therefore a focus was put on these molecules for the rest of my studies. Flow cytometry does not yield a fluorescence intensity signal that is proportional to the number of labelled molecules on the cell. Therefore to compare expression of these mucins on CEM in a quantitative manner, the Molecules of Equivalent Soluble Fluorochrome (MESF) values were acquired for each of the markers.

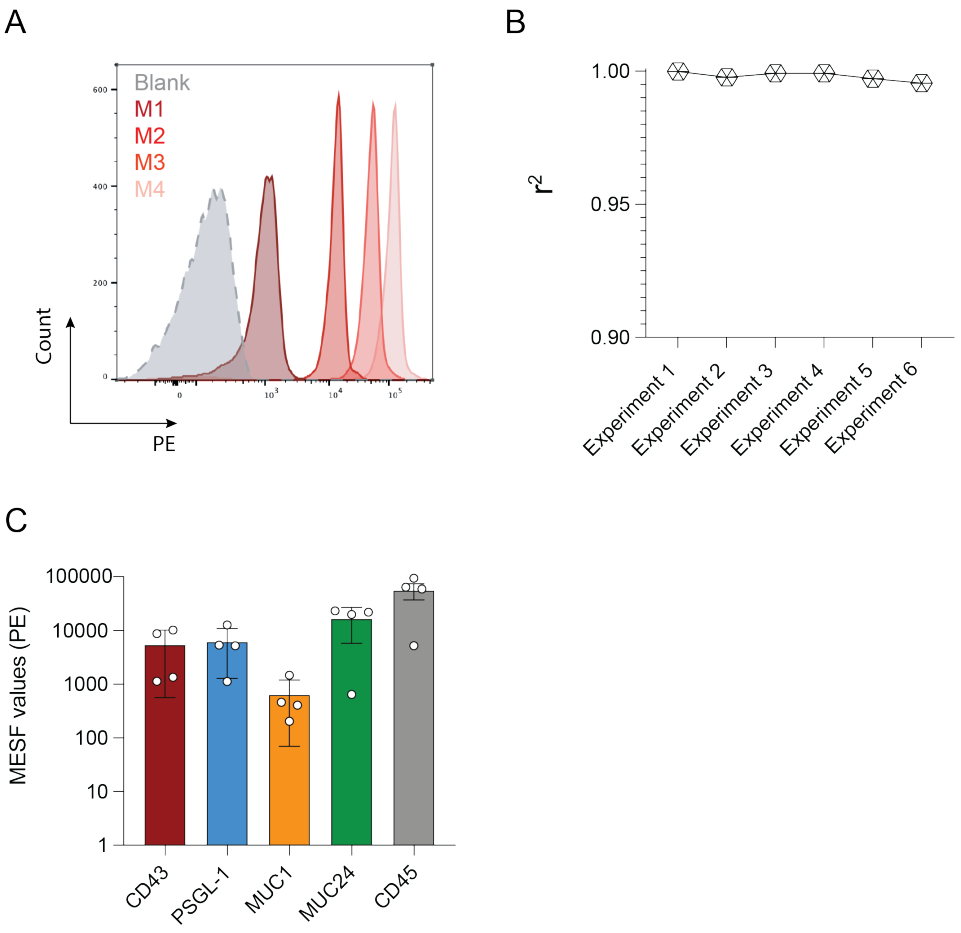


Figure 11: Quantitative MESF acquisition for the mucins CD43, PSGL-1, MUC1, MUC24 and CD45. A) Histogram of pre-stained beads blank, M1-M4 in PE. B) R^2 values of the individual repeats. C) Calculated MESF values for each marker.

The Quantum™ MESF kit uses five populations of PE pre-stained beads with a defined MESF value, which together form a standard curve (Figure 11A), allowing calibration of the flow

data. The MESF value corresponds to the antibody-bound PE molecules detected on each cell. Each of my experiments had an r^2 of at least 0.995 (Figure 11B). The freshness of the beads and stained samples is of essence which is why a new standard curve was required for each experimental repeat. As anticipated from the initial analysis, MUC1 gave the weakest MESF value (mean = 636.8), followed by CD43 (mean = 5381.3) and PSGL-1 (mean = 6131), and the strongest signals were recorded for MUC24 (mean = 16506.3) and CD45 (mean = 56076.5).

3.2.2 Mucin labelling of apoptotic CEM

Previous work in the Sattentau lab has shown that CD43, but not CD45 surface expression is reduced on apoptotic CEM (unpublished). Having screened and established expression of CD43, PSGL-1, MUC1, MUC24 and CD45 on CEM, this chapter serves to shed light on their dynamics on healthy and apoptotic T cells, in an effort to establish whether downregulation during apoptosis is a wider phenomenon of the transmembrane mucin family.

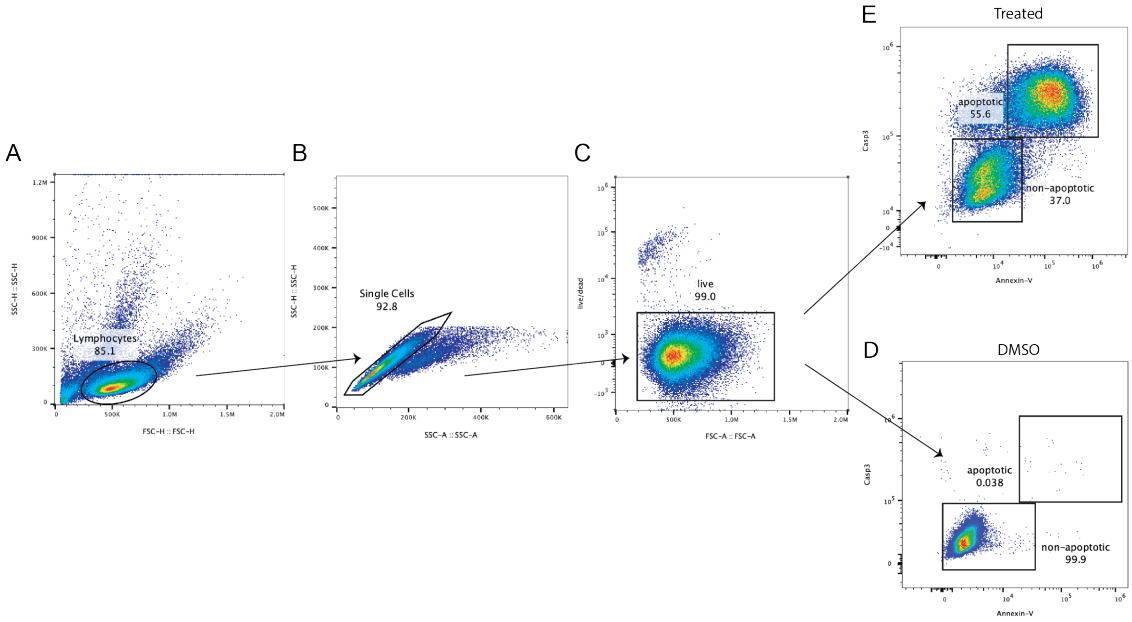


Figure 12: Representative gating strategy for analysis of non-apoptotic (DMSO) and apoptotic (treated) samples. Cells were gated on A) lymphocytes; B) single cells; C) live cells; D) non-apoptotic samples or E) apoptotic samples.

Having confirmed CEM surface expression of CD43, PSGL-1, MUC1, MUC24 and CD45, their expression profiles was tested under apoptotic conditions. An apoptosis induction assay was previously established in the Sattentau lab by Dr Niloofar Karaji. Staurosporine is an alkaloid isolated from *Streptomyces staurosporeus* and first described in 1977 [453] and is an ATP-

competitive kinase inhibitor, which leads to rapid apoptosis induction and downstream DNA fragmentation [454]. Alongside UV-radiation it is popular in its use for apoptosis induction due to its rapid and well-characterised application. Unless otherwise stated all further flow cytometry data were gated on lymphocytes, single cells, live cells and on apoptotic or non-apoptotic cells as shown in Figure 12.

Incubating healthy CEM with 10 μM staurosporine for 3 h led to approximately 70% cells positive for cleaved caspase3 (Casp3), while retaining membrane integrity as determined by LIVE/DEAD™ Fixable Near-IR dye used in the staining master mix (Figure 13A). Samples referred to as untreated from hereon have received 10 μM Dimethyl sulfoxide (DMSO) as vehicle control.

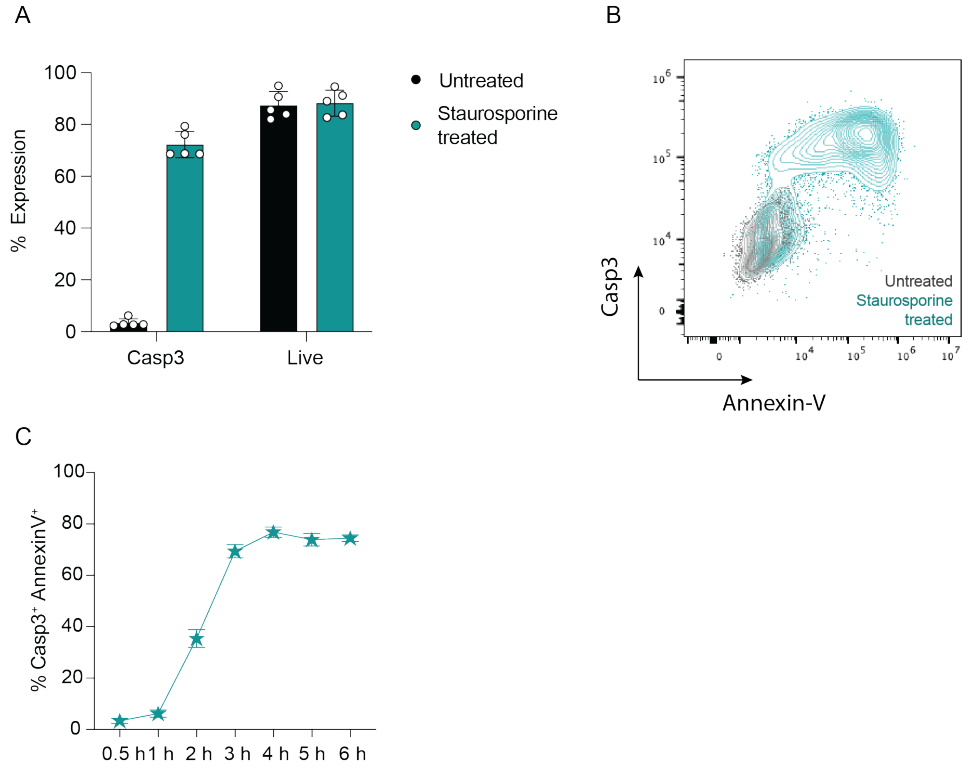


Figure 13: Staurosporine induces apoptosis without negatively impacting cell viability. CEM incubated with 10 μM staurosporine for 3 h show increased Casp3 expression with similar live/dead staining (A). Staurosporine treated cells (teal) show increased Casp3 and annexin-V expression compared to carrier-only control (grey) (B). C) Casp3 and annexin-V expression for cells exposed to 10 μM staurosporine treatment over time.

Annexin-V is a protein which selectively binds to phosphatidylserine (PS) and when used on non-permeabilised cells serves as an early apoptosis marker since PS is flipped to the outer leaflet of the plasma membrane in early stages of apoptosis. Cells that received staurosporine treatment strongly expressed both Casp3 and annexin-V (Figure 13E), and the labelling of

both markers was largely overlapping. To investigate the kinetics of apoptosis, a timecourse was carried out after staurosporine treatment. This revealed a gradual increase of Casp3 and annexin-V expression on CEM over 6 h (Figure 13C). These plots show that staurosporine at 10 μM staurosporine for 3 h reliably induces approximately 50% apoptosis without impacting cell viability as defined by membrane permeability to the live/dead dye. In this, and in all further experiments, Casp3 and annexin-V were co-stained using the same fluorochrome. As mentioned above, PS expression on the cell surface occurs early during apoptosis and remains high throughout apoptosis, while cleaved Caspase3 is a marker of mid to late stage apoptotic cells. Using both markers alongside each other allows for a better resolution of mucin labelling across healthy, early apoptotic and fully apoptotic cells by flow cytometry. Besides providing the opportunity to gate on the specific stages of apoptosis, without annexin-V staining, cells that have entered the apoptotic programme but are not yet positive for Casp3 would fall into the non-apoptotic gate, which would distort results if there are any changes in mucin labelling of apoptotic cells. Staining for them using the same fluorophore made an additional channel available for other markers such as the mucins, facilitating the distinction and exclusion of cells shifting from a healthy to a fully apoptotic state.

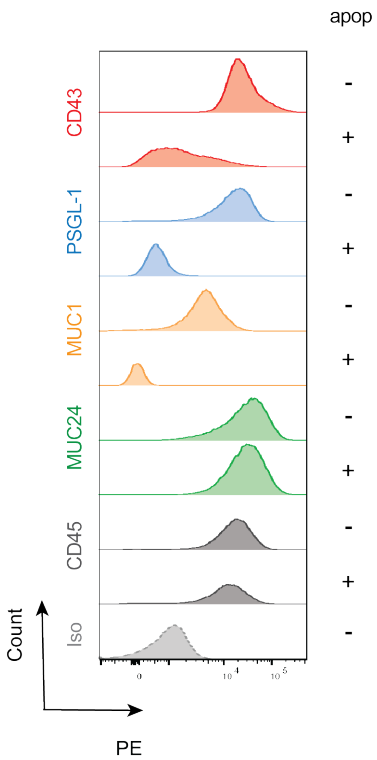


Figure 14: CD43, PSGL-1 and MUC1 show reduced labelling of staurosporine-treated CEM. Overlay of expression histograms of the individual mucins CD43 (red), PSGL-1 (blue), MUC1 (yellow), MUC24 (green), CD45 (dark grey) and an appropriate isotype control (Iso, light grey). Staurosporine treatment is indicated as + for treatment and - for DMSO addition only.

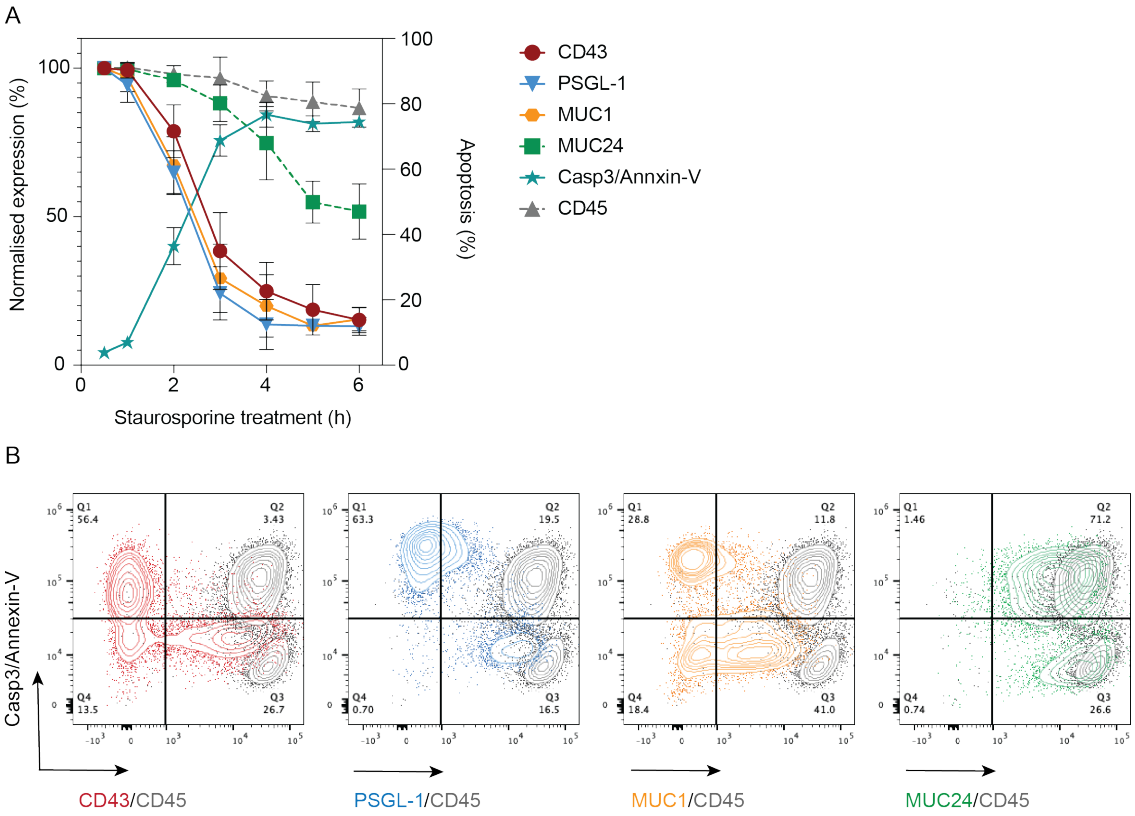


Figure 15: Mucin labelling is selectively downregulated on apoptotic CEM. A) timecourse of normalised mucin labelling between 0 and 6 h. Absolute Casp3/annexin-V labelling over time (teal). n = 5, error bars are SD. B) Contour plots of Casp3 and mucins. CD43 (red), PSGL-1 (blue), MUC1 (yellow), MUC24 (green), CD45 (dark grey).

Next, the mucin markers CD43, PSGL-1, MUC1, MUC24 and CD45 were stained on untreated and staurosporine-treated CEM. When comparing signals with the included isotype control, CD43, PSGL-1 and MUC1 labelling was downregulated on treated cells (Figure 14), whereas MUC24 and CD45 labelling appeared comparable to the respective untreated sample. All antibodies used are IgG_1, which is why a PE-conjugated IgG_1 H+L isotype control was used in this experiment.

To investigate mucin labelling of CEM over time after apoptosis induction, a timecourse experiment was conducted. Cells were treated with staurosporine as before with the incubation stopped at 30 min, 1, 2, 3, 4, 5 and 6 h (Figure 15A). An untreated control (0 h) was included to record baseline levels. All mucin values were normalised to baseline labelling of untreated cells, and Casp3 levels are plotted as absolute % expression. gMFI should not be used when analysing bimodal distributions such as the ones the apoptosis experiments yield, as taking an average only holds true for normal distributions, while bi-modal populations are by definition not normally distributed. To truly compare gMFI between experiments, changes

between experiments such as antibody binding, machine performance and laser fluctuations would have to be compensated for by using a standard curve in each experiment (i.e. Figure 11). Therefore, % expression was instead used to compare signals between experiments. Interestingly, CD43, PSGL-1 and MUC1 labelling strongly decreased as Casp3/annexin-V expression increased. Loss of mucin labelling may arise for different reasons, including loss of antibody binding to the target protein due, for example, due to conformational changes without actual changes in protein expression at the membrane, internalisation of the target molecule, or cleavage of the target molecule from the cell surface. Since the mechanism of loss of mucin signal in apoptotic cells is unclear, the term "labelling" is used to describe the change in signal throughout this chapter. The signal for all three mucins was reduced to 20-30% of labelling of healthy cells at 3 h incubation and seemingly plateauing around 15% between 5 and 6 h. MUC24 labelling was moderately downregulated from 4 h onward, although approximately 50% of its expression was retained even at 6 h. The CD45 signal was not reduced for the first 3 h, after which it slightly decreased to about 80% of its starting value. Even though both MUC24 and CD45 showed similar labelling compared to untreated levels, CD45 retained the highest labelling and hence was used as a negative control for loss of mucin labelling going forward. Since the trend for reduced mucin labelling was clear and robust by 3 h post-staurosporine treatment, this together with high level of Casp3 cleavage led me to choose this time point for all further experiments, unless otherwise specified.

Figure 15B shows representative contour plot overlays of staurosporine-treated samples at 3 h. CD43, PSGL-1 and MUC1 lost most mucin labelling of Casp3/annexin-V-positive cells compared to the signal on Casp3/annexin-V-negative cells. Both MUC24 and CD45 showed a modest shift in labelling of the Casp3/annexin-V-positive population but retained a strong signal overall. Gates were set using an appropriate isotype control.

To quantify the potential differences in labelling observed in Figure 15, multiple independent biological repeats were performed with 3 h staurosporine incubation, and displayed as absolute expression on non-apoptotic cells (Casp3-negative, annexin-V-negative) or apoptotic cells (Casp3-positive, annexin-V-positive) within the same sample. CD43 and PSGL-1 expression on healthy cells was around 85% and decreased to approximately 20% (Figure 16). MUC1 was expressed at around 65% on healthy cells and similarly decreased to 20% of its

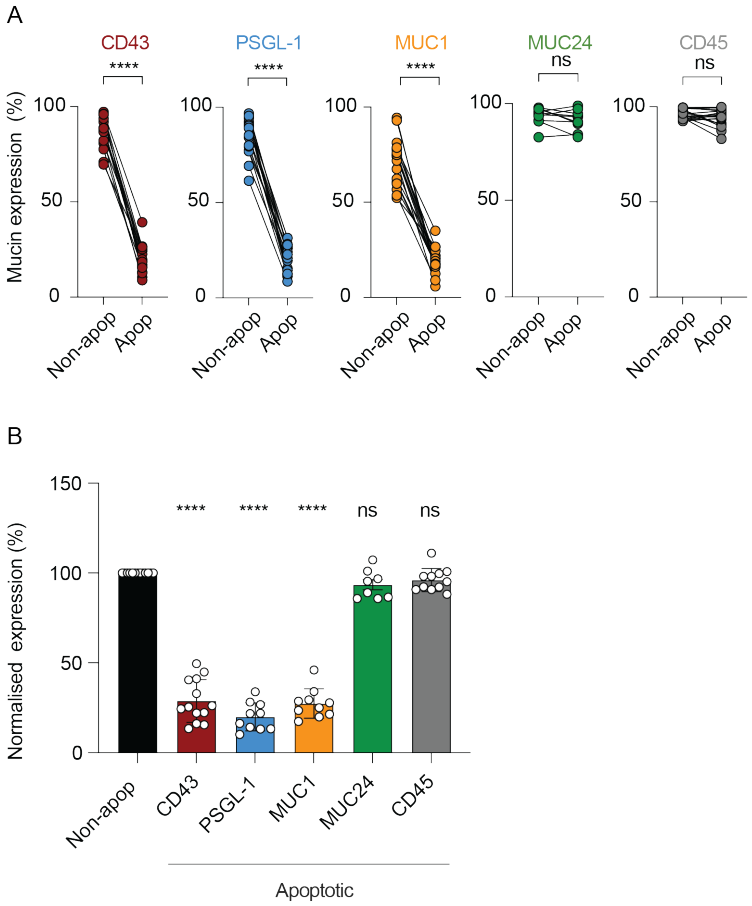


*Figure 16: CD43, PSGL-1 and MUC1 but not MUC24 and CD45 are significantly downregulated on apoptotic CEM T cells. CD43 (red), PSGL-1 (blue), MUC1 (yellow), MUC24 (green), CD45 (dark grey) and non-apoptotic (black). A) Absolute mucin expression on non-apoptotic and apoptotic cells. n = 10-18, student's paired t-tests were performed for each marker. B) Mucin expression normalised to signal on non-apoptotic cells. n = 8-13. Data were log_{10} transformed, followed by a one-way ANOVA corrected for multiple comparisons using Dunnett's multiple comparisons test. **** $p<0.0001$, ns = not significant.*

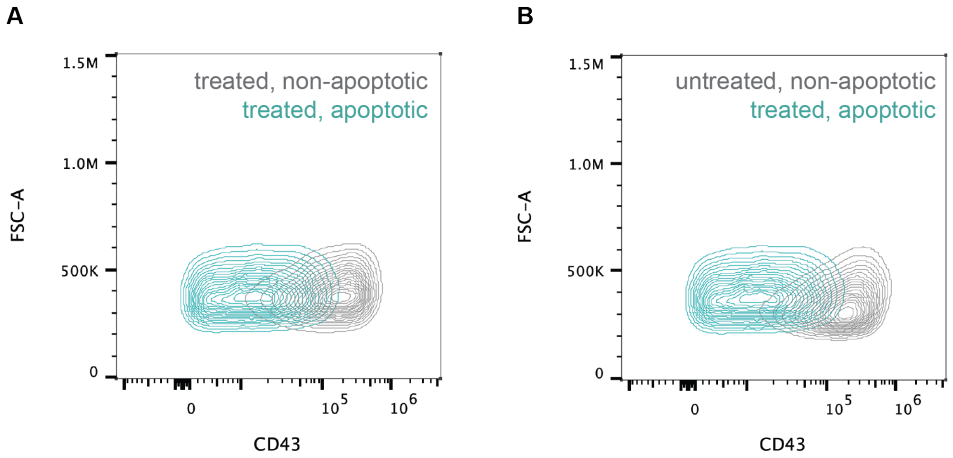


Figure 17: Mucin labelling is comparable in treated, non-apoptotic cells and untreated, non-apoptotic cells. A) Overlay of staurosporine-treated, non-apoptotic cells (grey) and staurosporine, apoptotic cells (teal). B) Plot of DMSO-treated (untreated), non-apoptotic cells (grey) and staurosporine-treated, apoptotic cells (teal).

original signal. MUC24 and CD45 were highly expressed at around 95% and remained unchanged. CD43, PSGL-1 and MUC1 were significantly downregulated on apoptotic cells ($p < 0.0001$), while MUC24 and CD45 expression did not significantly change. Figure 15B shows an overview of all mucins displayed as normalised values to their baseline expression.

As previously mentioned, the above mucin data were gated on the apoptotic or non-apoptotic fraction of the same treated samples. However, when analysis was performed based on the apoptotic fraction within a staurosporine-treated sample and the non-apoptotic fraction within a DMSO-only sample, the same pattern of results was obtained (Figure 17). We considered that data would be biologically more comparable when derived from cells within the same sample, and therefore all further data are displayed fully gated on staurosporine-treated Casp3/annexin-V positive and negative samples as in Figure 12.

3.2.3 Mucin labelling of CEM with UV light-induced apoptosis

Although staurosporine is used as a widespread and well accepted apoptosis inducer, it needed to be confirmed that the effects observed in downregulation of mucin labelling were not due to off-target effects of chemically-induced apoptosis. To confirm this a UV apoptosis induction protocol was established in which CEM were exposed to UV-C light at 50 J/m^2/s for 2 min to cells followed by 24 h of incubation (see Material and Methods on page 53). Normalised mucin labelling of CD43, PSGL-1 and MUC1 was significantly reduced to background

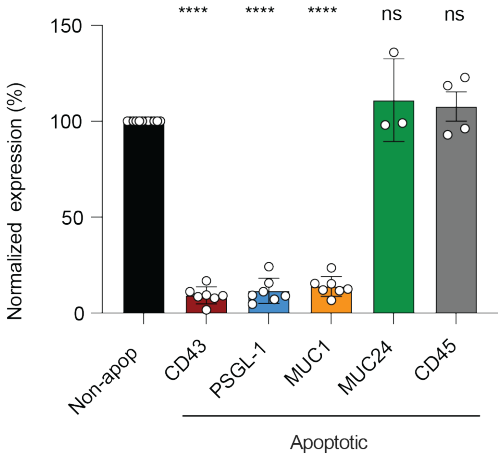


*Figure 18: CD43, PSGL-1 and MUC1 but not MUC24 and CD45 labelling is significantly down-regulated on UV-induced apoptotic CEM T cells. CD43 (red), PSGL-1 (blue), MUC1 (yellow), MUC24 (green), CD45 (dark grey) and non-apoptotic (black). Mucin labelling normalised to signal on non-apoptotic cells. n = 3-7. Data were log_{10} transformed followed by a one-way ANOVA corrected for multiple comparisons using Dunnett's multiple comparisons test. **** $p<0.0001$, ns = not significant*

levels at approximately 10% with unchanged MUC24 and CD45 labelling (Figure 18).

3.2.4 Mucin labelling of apoptotic Jurkat cells

To exclude that this was a cell line-specific observation another $CD4^+$ T cell line, Jurkat, was tested for mucin labelling. CD43, PSGL-1, MUC1, MUC24 and CD45 were well expressed on Jurkat and once treated with staurosporine showed similar patterns of downregulation (Figure 19). CD43, PSGL-1 and MUC1 labelling was significantly downregulated to approximately 40, 20 and 40% of their respective baseline labelling, whereas MUC24 and CD45 labelling was not significantly changed.

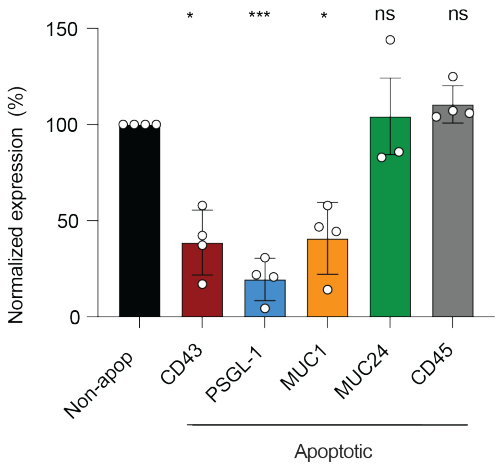


*Figure 19: Labelling of CD43, PSGL-1 and MUC1 but not MUC24 and CD45 is significantly downregulated on apoptotic Jurkat T cells. CD43 (red), PSGL-1 (blue), MUC1 (yellow), MUC24 (green), CD45 (dark grey) and non-apoptotic (black). Mucin labelling normalised to signal on non-apoptotic cells. n = 3-4. Data were log_{10}-transformed followed by a one-way ANOVA corrected for multiple comparisons using Dunnett's multiple comparisons test. *** $p<0.001$, * $p<0.05$, ns = not significant*

3.2.5 Mucin labelling of apoptotic primary CD4$^+$ cells

As CD43, PSGL-1 and MUC1 labelling was significantly downregulated on apoptotic CEM and Jurkat T cell lines, next these observations were confirmed in primary CD4$^+$ T cells to ensure that this phenomenon was reproducible in a more physiologically-relevant system. PBMCs were isolated from blood of healthy donors and T cells activated and expanded with IL-2 and PHA for 48 h (Figure 20A). This was an essential step as MUC1 and MUC24 are not expressed on resting T cells but are upregulated under activating conditions [83, 97]. Apoptosis was chemically induced as previously described using staurosporine and cells stained and analysed by flow cytometry.

CD43, PSGL-1, MUC1 and CD45 were well expressed on activated CD4$^+$ T cells, while unlike on CEM and Jurkat, MUC24 labelling was low (Figure 20B). Contour overlay plots show a reduction of signal intensity when cells became positive for cleaved Casp3/annexin-V in the case of CD43, PSGL-1 and MUC1, but not for CD45 or MUC24. Repeats with different donors confirmed the significant reduction of CD43, PSGL-1 and MUC1 in the apoptotic population, whereas MUC24 and CD45 labelling remained unchanged (Figure 20C).

I also measured mucins on CD8$^+$ T cells which had undergone the same processing as outlined in Figure 20. Healthy and apoptotic primary CD8$^+$ T cells revealed significant loss of

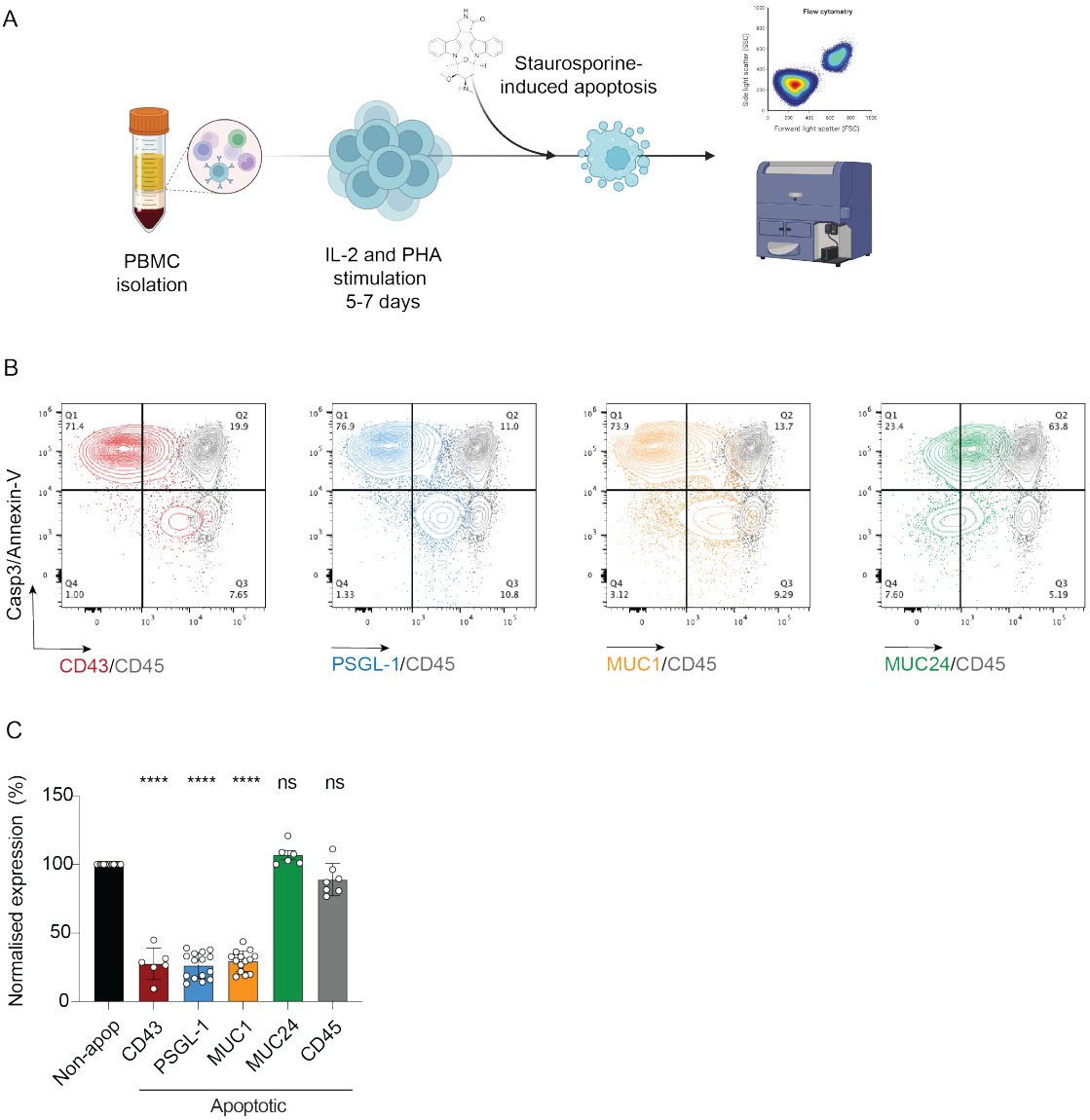


*Figure 20: CD43, PSGL-1 and MUC1 but not MUC24 and CD45 are significantly downregulated on apoptotic primary CD4⁺ T cells. A) Overview of primary T cell apoptosis assay. B) Contour plots of staurosporine-treated primary CD4⁺ T cells overlaying one mucin of interest and CD45 as a control mucin, respectively. Mucin labelling normalised to signal on non-apoptotic cells. CD43 (red), PSGL-1 (blue), MUC1 (yellow), MUC24 (green), CD45 (dark grey) and non-apoptotic (black). n = 6-15. Data were log_{10} transformed, followed by a one-way ANOVA corrected for multiple comparisons using Dunnett's multiple comparisons test. **** $p<0.0001$, ns = not significant.*

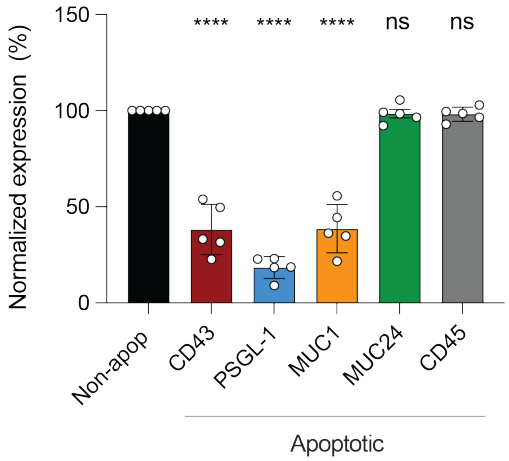


*Figure 21: CD43, PSGL-1 and MUC1 but not MUC24 and CD45 signal is significantly reduced on apoptotic primary CD8⁺ T cells. Mucin labelling normalised to signal on non-apoptotic cells. CD43 (red), PSGL-1 (blue), MUC1 (yellow), MUC24 (green), CD45 (grey) and non-apoptotic (black). n = 4-10. Data were log_{10} transformed, followed by a one-way ANOVA corrected for multiple comparisons using Dunnett's multiple comparisons test. * $p<0.05$, **** $p<0.0001$, ns = not significant.*

signal for CD43, PSGL-1 and MUC1, but not MUC24 and CD45 (Figure 21).

3.2.6 Mucin labelling of other apoptotic immune cell types

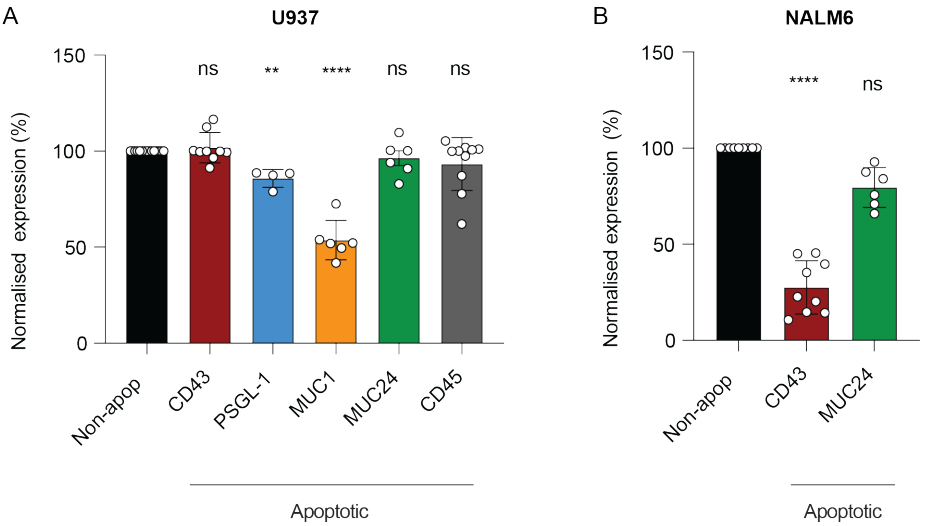


*Figure 22: Mucin labelling normalised to signal on non-apoptotic cells. CD43 (red), PSGL1 (blue), MUC1 (yellow), MUC24 (green), CD45 (dark grey) and non-apoptotic (black). n = 6-15, data were transformed, followed by a one-way ANOVA corrected for multiple comparisons using Dunnett's multiple comparisons test. ** $p<0.01$, **** $p<0.0001$, ns = not significant.*

To see whether this phenomenon applied to other immune cell types, the human cell lines U937 and NALM6 were tested: U937 is a pro-monocytic lymphoma cell line and NALM6 is a B cell precursor leukemic cell line. U937 cells expressed CD43, PSGL-1, MUC1, MUC24 and CD45 (Figure 22A). Interestingly, CD43 labelling was not significantly reduced on apoptotic NALM6 cells. PSGL-1 and MUC1 labelling was reduced by approximately 20% and 50% on

apoptotic cells, respectively. MUC24 and CD45 labelling remained stable.

NALM6 cells expressed CD43 and MUC24 but not PSGL-1, MUC1 or CD45. CD43 labelling was significantly reduced by approximately 70% on apoptotic NALM6 cells, while MUC24 levels were not significantly changed (Figure 22B).

3.2.7 Mucin labelling of CEM, Jurkat and primary CD4$^+$ cells with dexamethasone-induced apoptosis

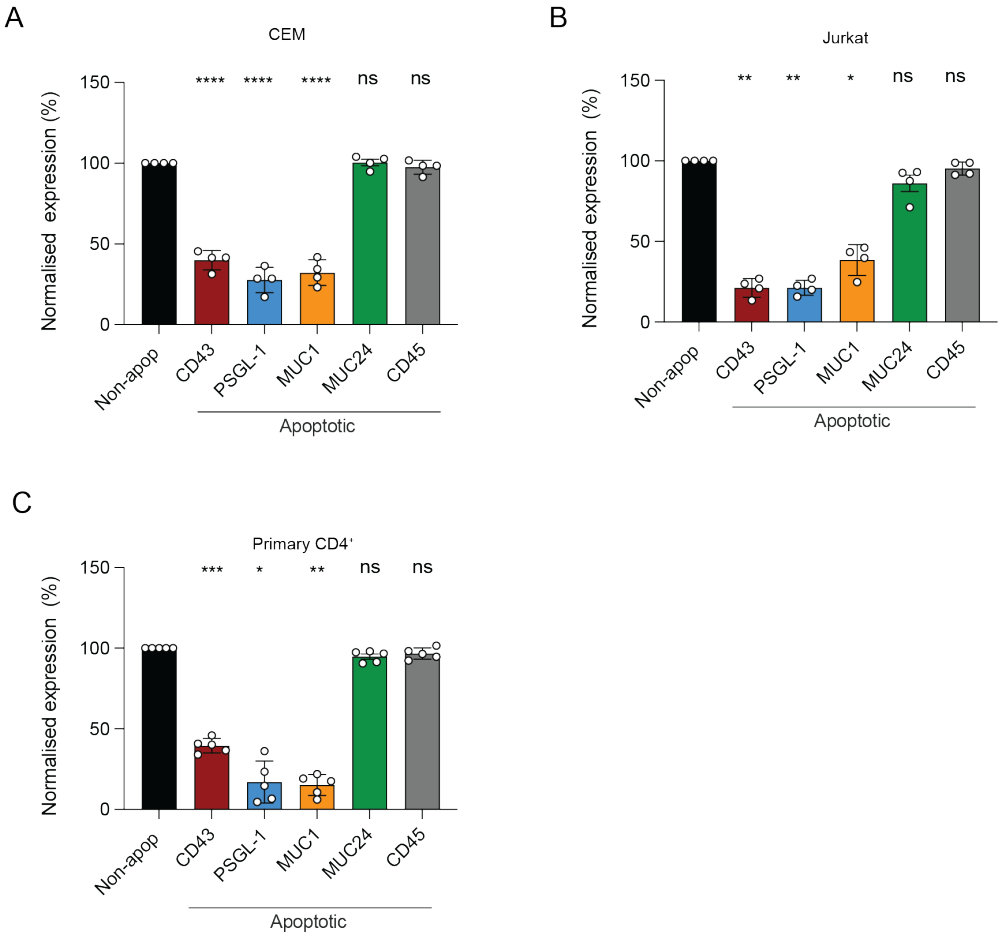


*Figure 23: Mucin labelling of dexamethasone-treated cells. CD43 (red), PSGL1 (blue), MUC1 (yellow), MUC24 (green), CD45 (dark grey) and non-apoptotic (black). Values have been normalised to mucin levels on non-apoptotic cells. A) Mucin labelling of apoptotic CEM B) Jurkat and C) primary CD4$^+$ cells that have been treated with dexamethasone. n = 4-5, data were transformed, followed by a one-way ANOVA corrected for multiple comparisons using Dunnett's multiple comparisons test. * $p<0.05$, ** $p<0.01$, *** $p<0.001$, **** $p<0.0001$, ns = not significant*

In vivo, one of the most striking examples of regulated T cell death is during positive and negative selection in the thymus. Glucocorticoid hormones are a class of steroid hormones produced and secreted by the thymus, and induce apoptosis in T cells via binding of the glucocorticoid hormone receptor (GR) and downstream activation of caspase 3, 8 and 9 [455,

456]. The synthetic glucocorticoid hormone dexamethasone has been shown to readily trigger apoptosis in murine thymocytes and T lymphocytes [205, 457]. Using this physiologically relevant model of T cell apoptosis induction CD43, PSGL-1 and MUC1 but not MUC24 and CD45 labelling was significantly reduced on apoptotic CEM, Jurkat and primary $CD4^+$ T cells (Figure 23A-C).

3.3 Discussion

Previous results from the Sattentau led me to hypothesise that not only CD43 labelling was reduced on apoptotic T cells, but that labelling of other mucins might also be selectively down-regulated. This chapter aimed to test this hypothesis by screening the mucin-like molecules CD43, PSGL-1, MUC1, MUC24 and CD45 on healthy and apoptotic T cell lines, primary $CD4^+$ and $CD8^+$ T cells, monocytic and B cell lines.

Surface staining of healthy CEM T cells revealed the labelling of MUC1, CD45, MUC24, PSGL-1, CD43 and CD44, but not MUC15, MUC18 and TIM1. This confirmed my hypothesis that many mucins are expressed on T cells, even though traditionally those markers are best characterised on mucosal tissues and epithelial cells. CD47 was used as a positive control molecule for expression on T cells, on the basis that whilst it is not classed as a mucin-like molecule, it has previously been reported as a don't eat-me signal [458] and a co-activating receptor during TCR activation. As my data were reported as relative labelling using conventional flow cytometry in which the signal is not proportional to the number of molecules analysed, the MESF approach helped me to quantify absolute labelling of CD43, PSGL-1, MUC1, MUC24 and CD45. MUC1 labelling was by far the lowest, while CD43, PSGL-1, MUC24 and CD45 were strongly expressed. These results confirm previously observed labelling of CD43 [31], PSGL-1 [459], MUC24 [91] and CD45 [448] on CEM specifically, and laid valuable groundwork to characterise mucin expression on T cells, independent of operator and machine settings. My results confirm that staurosporine is a potent inducer of apoptosis, as defined here by cleaved Casp3 expression and annexin-V binding. Three h at 10 μM induces approximately 70% apoptosis, while maintaining good cell viability. Being able to differentiate between live and dead cells was important in order to ensure the effects observed were truly

of the subset of cells that were in the apoptotic stage, as dead cells included in the analysis might have died by other means such as necrotic cell death induced by pipetting-induced shear forces. Shear force might also impact the surface expression of some mucins via other mechanisms, for example MUC1, which has a SEA domain that is known to be released when exposed to strong shear forces [460]. Screening mucins on apoptotic CEM T cells revealed significantly reduced labelling of CD43, PSGL-1 and MUC1, but not MUC24 or CD45. This highlighted that simply the large size and heavy glycosylation do not seem to be the sole criteria for the observed loss of signal, but that this most likely reflects other more selective mechanisms. Interestingly, CD43, PSGL-1 and MUC1 expression reduce to a plateau of approximately 15% expression at around 4 h, which was retained through to 6 h and did not drop any further. This suggests that there is either a threshold of maximum downregulation when using staurosporine, or that an equilibrium of downregulation and re-circulation of intracellular full-length mucins is reached. Apoptosis induction by UV-C radiation in CEM, CD43, PSGL-1 and MUC1 showed a greater reduction in mucin labelling to around 8-10% of maximum signal, indicating that whilst the outcome is independent of the method of apoptosis induction, the degree of loss of mucin labelling is influenced by the mechanism of apoptosis induction. To ensure this was not a cell-line specific phenomenon, the staurosporine assay was repeated with another $CD4^+$ T cell line, Jurkat. The pattern of results was the same as with CEM, excluding that this is a CEM-specific phenomenon. While CEM and Jurkat T cells are well established cell lines, and particularly Jurkat cells are a frequent choice in immunological research, both are leukaemic lines and as such might have cancer-specific glycocalyx regulation and expression dynamics. Therefore, the hypothesis was tested that CD43, PSGL-1 and MUC1 are downregulated on apoptotic T cells in primary T cells. MUC1 and MUC24 are not expressed on resting T cells, hence donor cells required activation prior to conducting the apoptosis assay. Staurosporine treatment yielded similar apoptosis levels as with T cell lines. As previously, CD43, PSGL-1 and MUC1 labelling was downregulated while MUC24 and CD45 did not significantly change. This shows that the reduction in labelling observed in cell lines also applies to primary T cells. Testing primary $CD8^+$ T cells yielded very similar results. To test if mucins are expressed and perhaps even downregulated on other apoptotic immune cell types, a monocytic (U937) and B cell (NALM6) line were screened. All mucins were expressed on U937 cells, while only CD43 and MUC24 had detectable staining signal

on NALM6 cells. Lack of PSGL-1 expression on NALM6 was previously reported [459]. CD43 labelling was downregulated on apoptotic NALM6 cells, while MUC24 retained its baseline signal. Interestingly, on apoptotic U937 cells, PSGL-1 and MUC1 staining was significantly reduced but was not downregulated as much as on T cells. CD43, MUC24 and CD45 were not significantly changed. Previous studies by Seo et al. in mice reported that CD43 is shed from activated granulocytes, mast cells and T cells, but not from macrophages [33], consistent with my results although not based on apoptotic cells. Treatment with the synthetic glucocorticoid hormone dexamethasone showed reduced labelling of CD43, PSGL-1 and MUC1 but not MUC24, CD45 on apoptotic CEM, Jurkat and primary $CD4^+$ T cells. These data confirm consistent modulation of mucin labelling on apoptotic T cells across different apoptosis induction approaches.

These results show that changes in mucin labelling of immune cells is a wider phenomenon, however selectively regulated across different cell types. Although reduced membrane labelling of selected mucins was demonstrated during apoptosis, the mechanism remained obscure at this point. In the published literature, CD43 downregulation in human cells has previously been described in the context of neutrophil activation and apoptosis [35, 37, 461]. Nusbaum et al. were able to exclude internalisation and membrane blebbing as reasons for the reduced signal, and interestingly they found a 26-kDa membrane-bound fragment, indicating that proteolytic cleavage could be the underlying mechanism. This was subsequently confirmed for CD43 shedding on activated neutrophils by cathepsin G [32]. Stampfuss et al. showed PSGL-1 was proteolytically shed from apoptotic U937s and primary monocytes and that cleavage was exerted by an N-ethylmaleimide (NEM)–inhibitable metalloproteinase of the ADAM family [462]. MUC1 shedding has been reported on various cell types, however mainly on epithelial and not in the context of apoptosis. Thathiah et al. described enzymatic shedding of the MUC1 extracellular N-terminus by ADAM17 [79, 463]. Based on these previous studies it was therefore considered that a potential mechanism for the loss of mucins was proteolytic cleavage. However, other potential mechanisms such as mucin internalisation or antigenic changes such as conformational change in mucin protein backbone or modification of glycosylation reducing antibody binding, could not at this stage be excluded. Therefore in the next chapter, a focus was put on on elucidating the mechanism(s) underlying CD43, PSGL-1

and MUC1 downregulation of labelling of apoptotic T cells with an emphasis on proteolytic cleavage.

4 The mechanism of mucin downregulation in apoptosis

4.1 Introduction

In this chapter the mechanism(s) underlying the loss of mucin labelling during T cell apoptosis are investigated, that were observed in the previous chapter. There is a plethora of mechanisms underlying regulation of membrane proteins, among which endocytosis is central. Endocytosis describes the transport of substances or molecules via cell-membrane engulfment and is considered the main mechanism for removal of cell surface proteins [464–466]. Whilst there are diverse processes clustered under the umbrella term endocytosis, clathrin-dependent endocytosis is responsible for re-distribution of transmembrane molecules, thereby exerting a regulatory function on plasma membrane-embedded proteins [466]. Adaptor protein complex 2 (AP2) attaches to the intracellular portion of a transmembrane molecule, after which clathrin binds and assembles further proteins around the growing vesicle. F-actin and Dynamin cause scission at the neck of the vesicle containing the transmembrane molecules and led to subsequent inwards movement of the vesicle into the cell. Endocytosed membrane proteins are redistributed intracellulary via the proteosomal or endosomal pathway or degraded by the proteasome. The CD43 C-terminus has been shown to localise to the nucleus in murine bone marrow cells after its release from the membrane by γ-secretase [33], suggesting the involvement of an endocytic process for at least a portion of the protein. MUC1 has been shown to undergo continuous internalisation and recycling between the apical membrane and the Golgi apparatus in ductal epithelial cells and has specifically been shown to be internalised by clathrin-dependent endocytosis in Chinese hamster ovary (CHO) cells [467, 468]. These findings set a precedent for intracellular re-localisation in the case of CD43 and MUC1. When endocytosed proteins are not redistributed, they can be selected for degradation in lysosomal compartments leading to quick protein-turnover, as in the case of MUC1, which despite its large size, has a metabolic half-life estimated to be 12-16 h [469]. Internalisation and subsequent re-distribution or degradation could both account for loss of cell surface labelling [470, 471], for example as in the potential case of CD43, PSGL-1 and MUC1 on apoptotic T cells.

A second possibility for the loss of mucin signal during T cell apoptosis might result from

changes in glycosylation influencing glycan-dependent mAb epitopes. As integral members of the glycocalyx, the glycosylation patterns of cell-anchored mucins depend on a myriad of factors. Notably, the glyco-composition of MUC1 shows significant variability depending on the tissue of origin [472]. In the case of CD43, different glycoforms have been described on T cells: resting T cells express a 115 kDa glycoform of CD43 which is exchanged for a 130 kDa glycoform when entering activation [473]. On primary $CD8^+$ T cells there is a functional link between terminal glycosylation of PSGL-1, which influences ligand interaction and alters the pool of T cell interaction molecules [62]. In the context of apoptosis, sialic acid residues can be enzymatically cleaved on glycoproteins of dying cells [474]. This highlights that glycosylation patterns of MUC1, PSGL-1, and CD43 may undergo modifications according to the cell's tissue localisation and cell fate such as activation or cell death. Thus modification of mucin antigenicity by glycosylation changes could potentially lead to reduced labelling of CD43, PSGL-1 and MUC1 on apoptotic cells.

While the specificity of deglycosylation is limited to sugars, proteins can undergo conformational changes, induced by various mechanisms such as via post-translational modification or interaction with other molecules, which may reduce or eliminate the epitopes of monoclonal antibodies [475–478]. Proteolytic cleavage can result in more dramatic alterations in the cell surface glycoprotein expression profile. Soluble CD43, PSGL-1 and MUC1 have been detected in human plasma [36, 479, 480], raising the idea that mucins can be released from the cell surface in certain contexts. CD43 is shed on activated human lymphocytes and granulocytes [481], PMA-activated neutrophils [37, 482, 483] and PMA-activated mast cells [484]. Proteolytic cleavage of PSGL-1 has been reported for apoptotic U937s and primary monocytes, and activated HL-60 and neutrophils [462, 485, 486]. MUC1 cleavage has been reported on various cell types, however mainly of epithelial origin [79, 463]. Different proteases have been described to be responsible for mucin cleavage on these cells. In the case of CD43, neutrophil elastase and cathepsin G were proposed to be the cleaving proteases [32, 483], with metalloproteases suspected to cleave CD43 on other immune cells [481]. PSGL-1 cleavage is carried out by the aspartyl protease BACE1 and the metalloproteases ADAM8 and ADAM10 on U937 [462, 486, 487] and neutrophils [488], and by ADAM8 on HL-60 [486]. ADAM17, which is a close relative of ADAM10, ADAM9 and MT1 are ca-

pable of shedding MUC1 on epithelial cells [78, 79, 463, 469]. This indicates that while the same mucin is cleaved, different sheddases might be responsible depending on cell type and context of cleavage, such as activation or apoptosis.

Under steady-state conditions, healthy cells continuously release vesicles as a means of intercellular communication. Under these conditions, CD43, PSGL-1 and MUC1 have been detected in vesicles shed from human primary cells and cell lines [489–491]. However during apoptosis, different types of vesicles can be discharged from the dying cell as part of the immunologically silent disintegration of the cell. Apoptotic bodies are a subclass of these vesicles, ranging in size from 1 to 4 μm. Originating from the plasma membrane, they carry cell surface proteins [492]. Secretion of mucins via apoptotic bodies might result in reduced surface labelling of apoptotic cells. Finally, the ectodomains of some mucins contains a SEA (sea-urchin sperm protein, enterokinase, and agrin) domain. This domain is non-covalently connected to the transmembrane domain and can undergo auto-proteolysis in response to diverse stimuli [493]. Notably, among MUC1, CD43, PSGL-1, MUC24, and CD45, only MUC1 features a SEA module, which has been reported to lead to its ectodomain release [77]. Thus, the decline in MUC1 labeling during T cell apoptosis could potentially be attributed to the SEA domain-mediated release of its ectodomain.

In this chapter, the mechanism underlying CD43, PSGL-1 and MUC1 loss of labelling during T cell apoptosis are addressed. While there is existing literature on mucins in the context of internalisation, changes in antigenicity and non-proteolytic removal of mucins from the surface, no extensive reports have been published in the context of T cell apoptosis. When reviewing the existing literature it becomes evident that proteases and enzymatic cleavage are a recurring observation in the context of mucin shedding across various cell types, both on activated and apoptotic cells. This led me to hypothesise that proteolytic cleavage might be the underlying mechanism of CD43, PSGL-1 and MUC1 signal loss during apoptosis.

4.1.1 Hypothesis

That a protease or proteases may selectively cleave CD43, PSGL-1 and MUC1, but not MUC24 and CD45 on apoptotic T cells.

4.1.2 Specific aims

I explore the mechanism(s) for mucin downmodulation in apoptotic T cells by:

1. Assaying for mucin internalisation
2. Probing for antigenic changes in mucin expression
3. Interrogating mucin cleavage by a cellular protease or proteases
4. Investigating the regulation of the cleaving protease

4.2 Results

4.2.1 Intracellular mucin labelling of healthy and apoptotic CEM

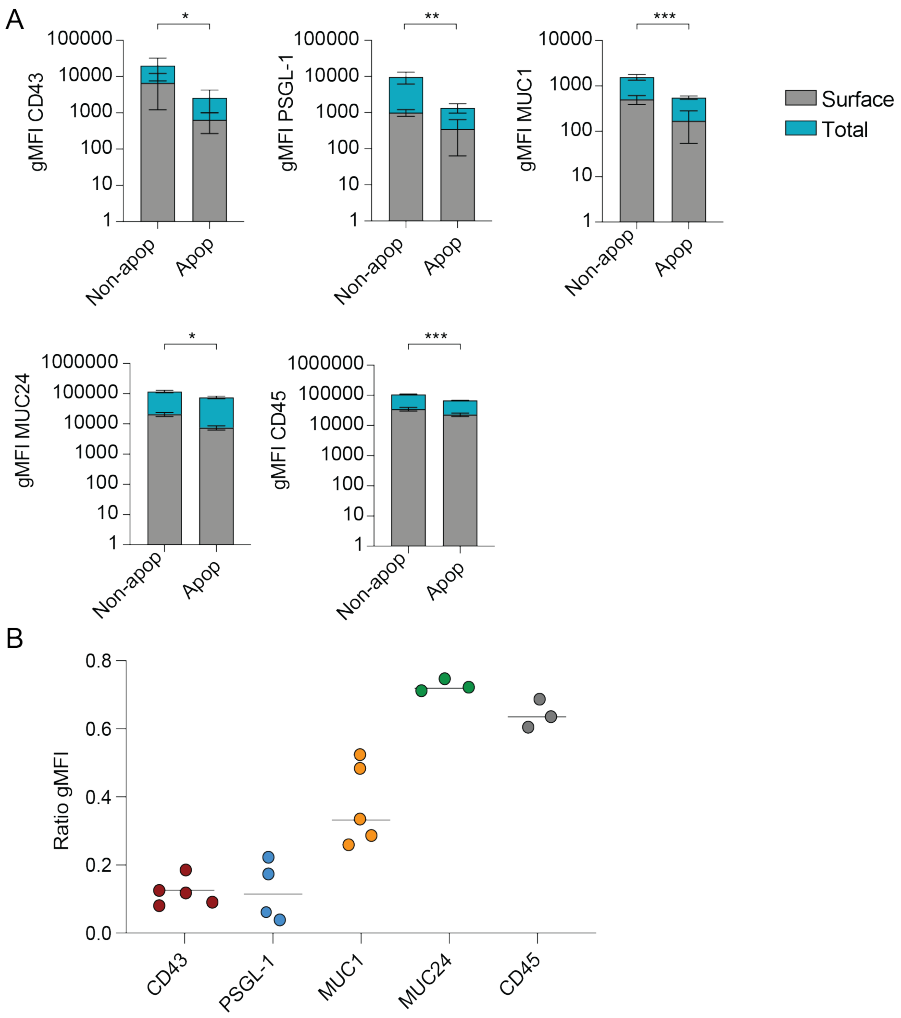


*Figure 24: Total cell gMFI expression of CD43, PSGL-1, MUC1, MUC24 and CD45 is not increased in apoptotic samples. Overlay bar charts of apoptotic and non-apoptotic samples. A) gMFI of surface labelling is plotted in grey, total cell signal in teal. B) Ratio of apoptotic to non-apoptotic labelling of total cell labelling. CD43 (red), PSGL-1 (blue), MUC1 (yellow), MUC24 (green) and CD45 (grey). n = 3-5, unpaired t-tests were performed on non-apoptotic and apoptotic data of total cell samples. *** $p<0.001$, ** $p<0.01$, * $p<0.05$*

To exclude other mechanisms, the reduction in CD43, PSGL-1 and MUC1 fluorescence signal was due to internalisation was assessed. To achieve this, mucin surface signal was compared to intracellular signal with the idea that if mucins were being internalised, the ratio of surface to internal mucin signal would decrease but the total signal would remain the same. If however the internalised mucins were being trafficked to a degradative compartment then the intracellular and therefore total labelling would decrease. The control mucins MUC24 and CD45 would be expected to maintain both an unchanged surface and total cell signal. Apoptotic and non-apoptotic samples were surface stained for annexin-V and the mucins, split the samples

in half and proceeded with either a Casp3 intracellular staining only, or a combined intracellular staining of both mucins and Casp3, resulting in samples that will henceforth be referred to as ”surface” staining and ”total cell” staining. When comparing apoptotic surface and apoptotic total cell samples, the gMFI was significantly reduced for all markers (Figure 24A). To facilitate comparison, a ratio was calculated of the total cell gMFI between apoptotic and non-apoptotic cells. If internalisation occurred, a ratio of 1 would be expected, as the sum of all mucins in or on each cell would remain constant. CD43, PSGL-1 and MUC1 had an average ratio of 0.23 0.14 and 0.37, respectively, MUC24 and CD45 had an average ratio of 0.70 and 0.62 (Figure 24B). The observation of a total cell ratio substantially below 1 for CD43, PSGL-1, MUC1 hints at the possibility that these mucins either might not be internalised, or might be internalised into a degradative compartment.

4.2.2 Creation of a C and N-terminally tagged CD43 CEM cell line

While flow cytometric analysis did not show obvious evidence of internalisation, other factors besides proteolytic cleavage need to be considered as potential explanations for the reduction in staining signal. Loss of antibody binding to glycoproteins may occur as a result of altered antigenicity in the form of conformational change in the protein backbone which alters the epitope, or glycosylation modification (some mucin-specific antibodies are sensitive to sialylation), or both, as described in the introduction. To exclude that the previous results were observed due to changes in antigenicity, a fluorescent reporter CD43 construct was created, which was then stably expressed in CEM knocked out for endogenous CD43 ($CD43^{-/-}$ CEM). N-terminally tagged CD43 (Halo) and C-terminally tagged CD43 (SNAP) plasmids were kindly provided by the Davis lab [494]. After incubation with the unique cutters BstXI and NotI of Halo-CD43 and CD43-SNAP, sticky end fragments were created of Halo-CD43 and CD43-SNAP (Figure 25A). Fragments were validated by size using agarose gel electrophoresis and purified by subsequent gel extraction (Halo fragment 10,252 bp, SNAP fragment 1046 bp). Fragments were ligated using T4 ligase and StablE cells were transduced with the ligated construct. The plasmid backbone carried an ampicillin (Amp) resistance gene, which allowed for selection of Amp-resistant colonies. Successful colonies were expanded, extracted, and the sequence confirmed by Sanger sequencing. The purified plasmids were transfected into

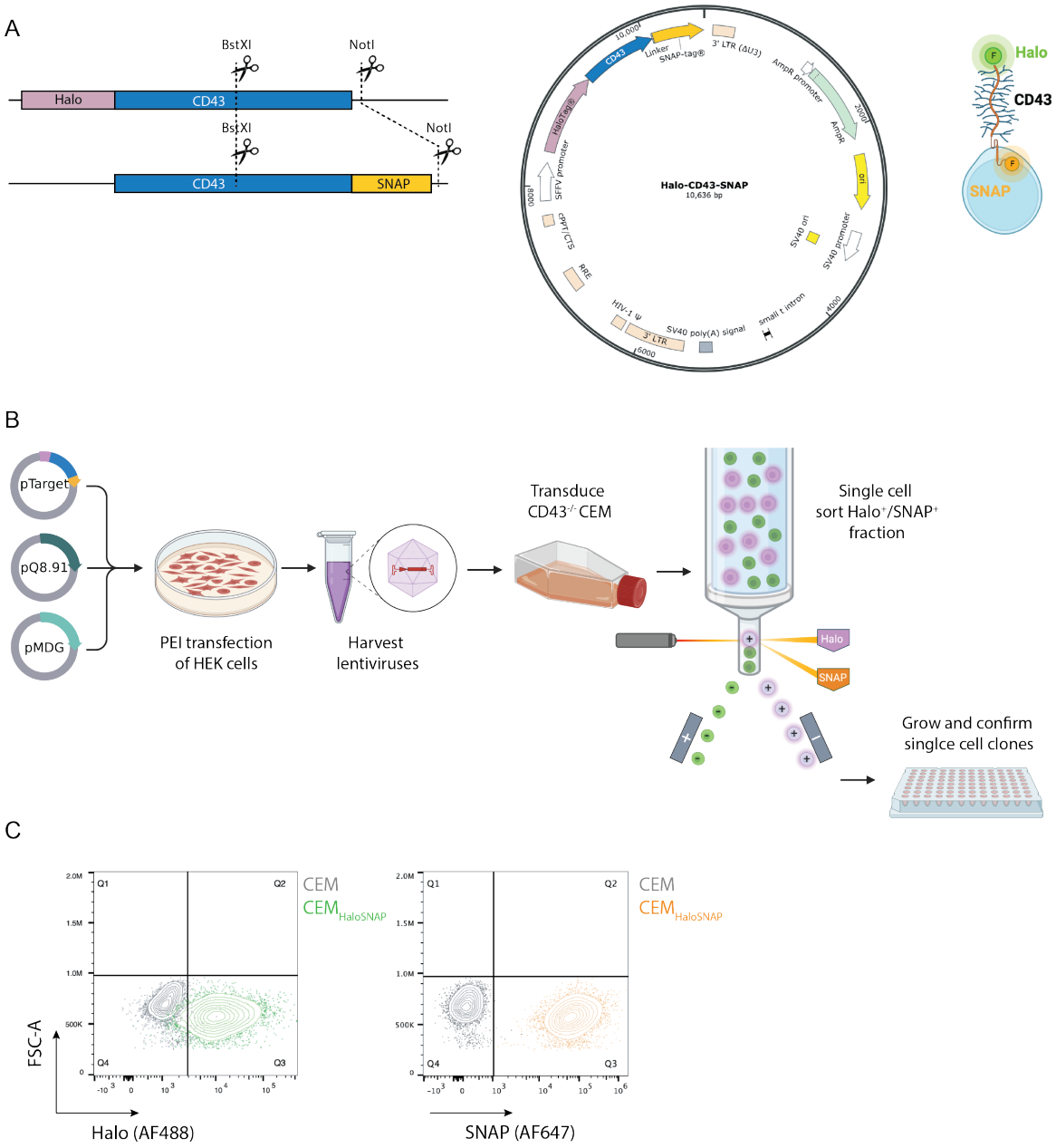


Figure 25: Generation of CD43$_{Halo/SNAP}$ CEM cell line. A) Cloning strategy using unique cutters BstXI and NotI and plasmid map with N-terminal Halo and C-terminal SNAP tag and a schematic representation of double-tagged CD43 on a CEM cell. B) Schematic overview of lentiviral production, transduction and Halo/SNAP cell line generation. C) Contour plots of substrate staining of WT CEM (grey) and stably transduced CEM$_{Halo/SNAP}$ (green and orange for Halo and SNAP substrate, respectively).

HEK293T cells together with pQ8.91 and pMDG using polyethylenimine (PEI) (Figure 25B). After 48 and 72 h of incubation the cell culture supernatant containing the lentiviruses was carefully harvested, filtered (0.45 μM cutoff) and concentrated using Lenti-X. Healthy CD43$^{-/-}$ CEM were transduced in three dilutions of concentrated virus to titrate the virus and in the presence of polybrene, to achieve an increased transduction efficiency. After appropriate expansion, cells were stained with live/dead dye, Halo and SNAP substrate and sorted using an Aria III cell sorter. After recovery and expansion, the cells were re-tested to confirm stable expression of the CD43$_{Halo/SNAP}$ construct. The newly generated cell line could be successfully tagged with either Halo or SNAP substrates or both substrates at the same time using different fluorophores (Figure 25B). Since the substrates form a covalent bond with the tag, this tool enabled me to investigate dynamics of the CD43 C- and N-termini, independent of CD43 antigenicity.

4.2.3 CD43$_{Halo/SNAP}$CEM labelling during apoptosis

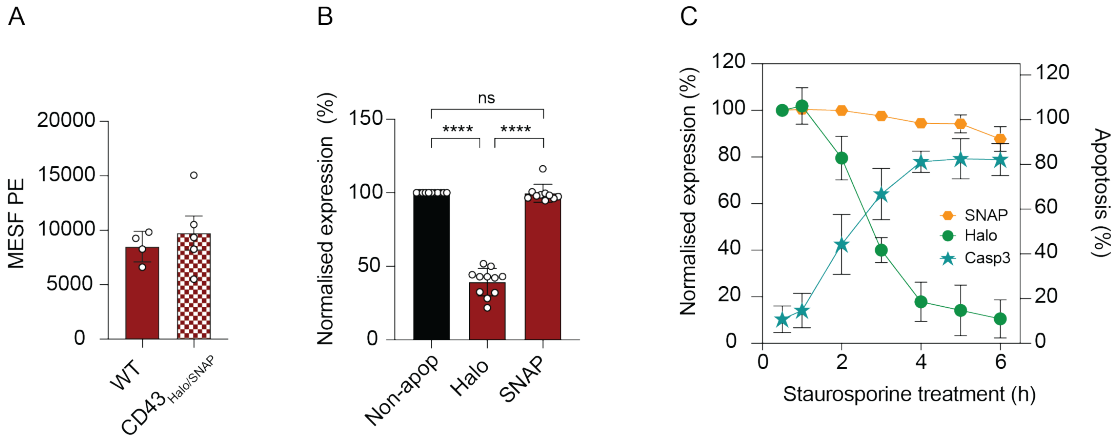


*Figure 26: Halo, but not SNAP is downregulated on apoptotic CEM. A) MESF quantification of CD43 on WT CEM (filled) and CD43$_{Halo/SNAP}$ CEM (chequered). B) Expression of Halo and SNAP substrate signal on apoptotic cells (red) normalised to their respective non-apoptotic levels (black). C) timecourse of Halo (green) and SNAP (orange) substrate signal and Casp3/annexin-V expression (teal, "Casp3"). n = 4-11, data were transformed, followed by a one-way ANOVA corrected for multiple comparisons using Dunnett's multiple comparisons test. **** $p<0.0001$, ns = not significant*

MESF quantification showed that CD43 surface expression on transduced CD43$_{Halo/SNAP}$ CEM was equivalent to WT CEM (Figure 26A). These experiments ensured that expression was comparable to physiological levels, excluding the possibility that subsequent observations could be influenced by over- or under-expression. Individual substrate staining of the Halo and SNAP tag on staurosporine-induced apoptotic cells compared to non-apoptotic cells re-

vealed a significant reduction in Halo, but not SNAP signal (Figure 26B). In a staurosporine timecourse experiment, gradual reduction of Halo signal was observed in apoptotic cells, plateauing at 10-20% after 4 h of treatment. SNAP signal remained high throughout the 6 h of treatment. These results indicate that CD43 is neither internalised on apoptotic cells nor that the reduction in CD43 labelling is caused by antigenic changes, but instead that the N-terminal portion of CD43 carrying the Halo tag is lost from the cells while the C-terminus remains.

4.2.4 ADAM10 inhibition in apoptotic CEM and primary T cells

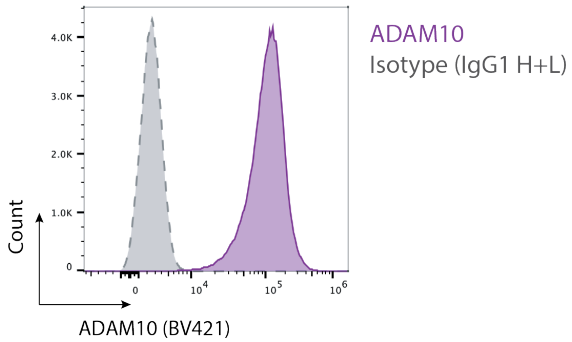


Figure 27: ADAM10 is expressed on healthy CEM T cells. Anti-ADAM10 clone 11G2 (purple) and a matching isotype control (grey, dashed) were stained for in BV421 and plotted against each other.

Based on the fact that CD43, PSGL-1 and MUC1 did not seem to be internalised along with the loss of CD43 N-terminus from apoptotic cells, I hypothesised that a protease might be responsible for cleaving the ectodomain of these proteins. As described in the introduction to this chapter, metalloproteases have been implicated in the shedding of mucins, and particularly of PSGL-1 and MUC1, from the surface of activated immune cells. Specifically, the metalloprotease ADAM10 was described to cleave PSGL-1 expression on U937 cells [487], and the Sattentau lab had previously described the implication of ADAM10 activity in CD43 cleavage. In order to explore the possibility of ADAM10 being the sheddase accountable for the decline in mucin signal on apoptotic T cells, my initial objective was twofold. The first aim was to verify previous reports indicating the expression of ADAM10 on CEM cells [495]. Secondly, the validation and the suitability of the anti-ADAM10 antibody clone 11G2 for flow cytometry experiments was assessed. Healthy CEM showed a robust surface ADAM10 staining signal, confirming its expression (Figure 27).

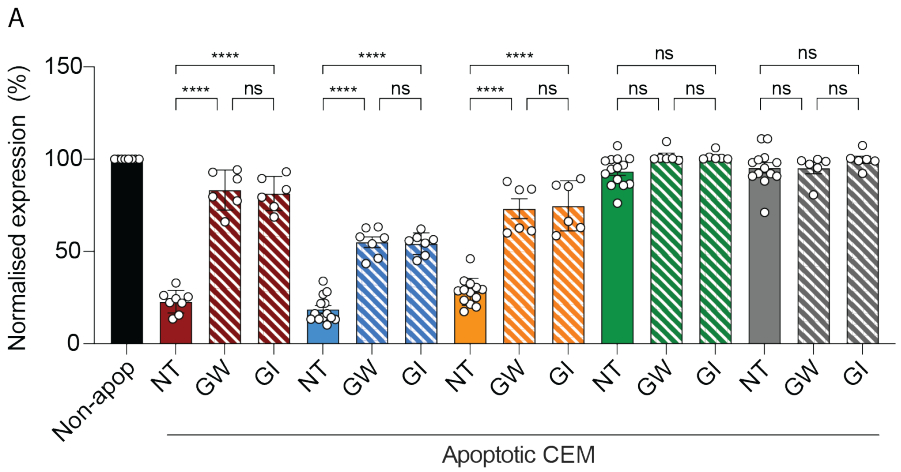


*Figure 28: GI and GW inhibitors reduce loss of CD43, PSGL-1 and MUC1, but not MUC24 and CD45, on apoptotic CEM. Non-apoptotic cells (black), CD43 (red), PSGL-1 (blue), MUC1 (yellow), MUC24 (green), CD45 (grey). Dashes indicate treatment with inhibitor. Non-treated (NT), GW-treated (GW) and GI-treated (GI) samples are clustered per mucin. n = 6-14. Data were log_{10} transformed followed by a one-way ANOVA corrected for multiple comparisons using Dunnett's multiple comparisons test. **** $p<0.0001$, ns = not significant*

Next, the small molecule inhibitor GW280264X was used, which inhibits the closely related metalloproteases ADAM17 and ADAM10 (IC_{50} values of 8 nM and 11.5 nM, respectively), which will be referred to as GW. GI254023X is a potent inhibitor of ADAM10 and a weak inhibitor of ADAM17 (IC_{50} values of 5.3 nM and 541 nM, respectively), which will be referred to as GI. Both inhibitors are reversible and function by forming a bidentate complex with the enzyme active site zinc molecule, thereby blocking substrate binding and shedding [496]. When CEM were treated with GW or GI inhibitors prior to inducing apoptosis through staurosporine treatment, CD43, PSGL-1 and MUC1 expression was significantly higher compared to the inhibitor-free samples on apoptotic CEM (Figure 28). Apoptotic, non-treated (NT) CD43, PSGL-1 and MUC1 expression was around 20-30%, while apoptotic GW and GI-treated samples retained around 60-80% of the respective marker expression. MUC24 and CD45 expression remained at baseline levels, regardless of apoptosis induction and inhibitor treatment.

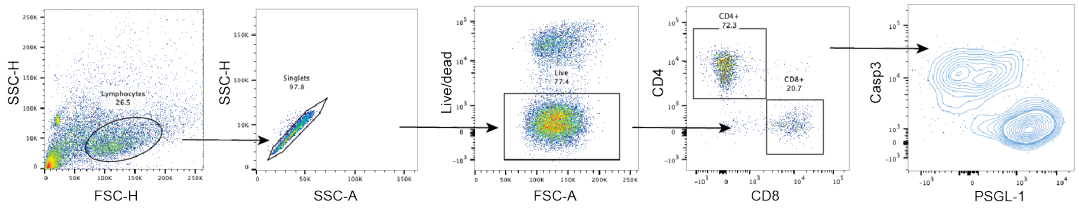


Figure 29: Gating strategy for CD4⁺ and CD8⁺ T cells within PBMC⁺. Gating on lymphocytes, doublet and dead cell exclusion, CD4/CD8, and subsequent mucin or apoptosis markers, here PSGL-1.

To confirm these results in primary T cells, PBMCs were isolated as before, monocytes were depleted by adherence and the remaining PBMC$^+$ population used for experiments. Additional gating permitted the distinction of T cell subsets (Figure 29, method section 2.7). When using GI and GW inhibitors on apoptotic CD4$^+$ and CD8$^+$ T cells, similar results were obtained (Figure 30). These data demonstrate that GW and GI are potent inhibitors of CD43, PSGL-1 and MUC1 cleavage in apoptotic CEM and primary T cells.

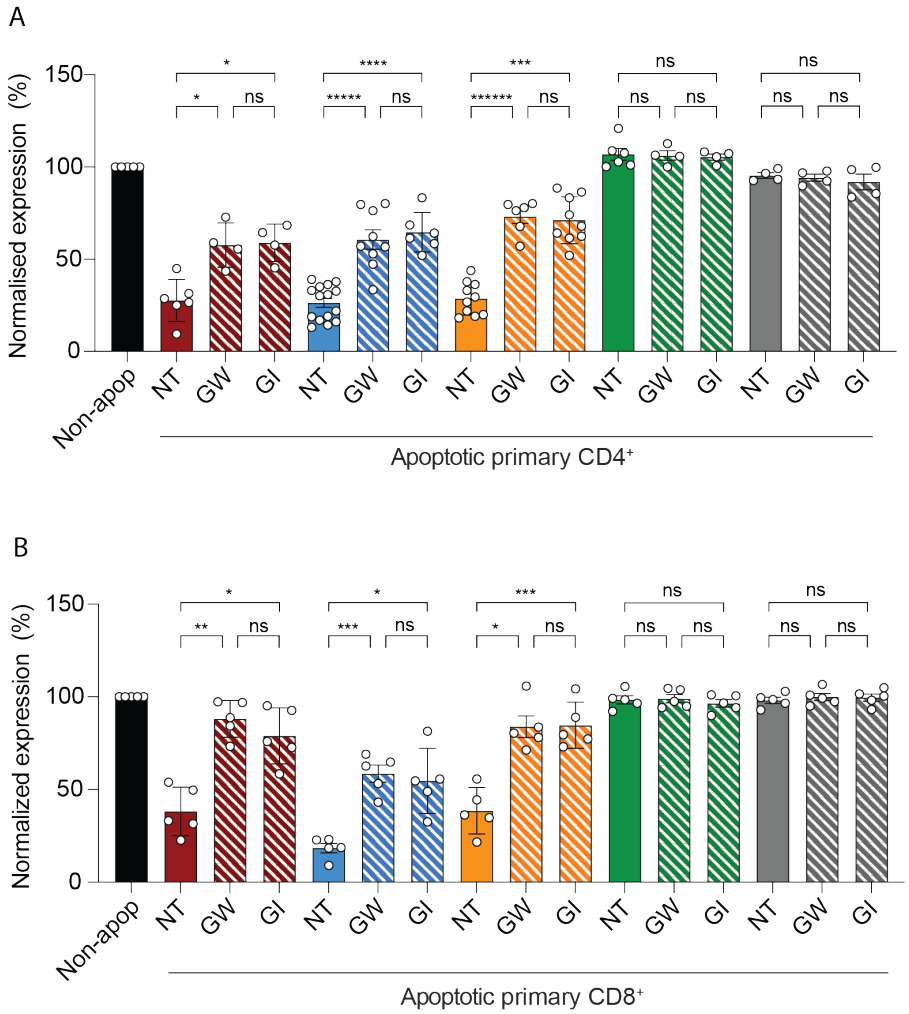


*Figure 30: GI and GW inhibitors reduce loss of CD43, PSGL-1 and MUC1, but not MUC24 and CD45, on apoptotic primary CD4$^+$ and CD8$^+$ T cells. Non-apoptotic cells (black), CD43 (red), PSGL-1 (blue), MUC1 (yellow), MUC24 (green), CD45 (grey). Dashes indicate treatment with inhibitor. Non-treated (NT), GW-treated (GW) and GI-treated (GI) samples are clustered per mucin. n = 4-9. Data were log_{10} transformed followed by a one-way ANOVA corrected for multiple comparisons using Dunnett's multiple comparisons test. **** $p<0.0001$, ns = not significant.*

Next, the replication of the above findings was attempted in UV-C-irradiated CEM. As before, cells were pre-incubated with GW and GI inhibitor for 1 h and then exposed to UV-C light for 2 min (Figure 31). Unexpectedly, GW was UV sensitive and therefore required re-addition post UV treatment, while GI remained stable. CD43, PSGL-1 and MUC1 expression was heavily

reduced to approximately 10% on UV-induced apoptotic cells, while GI and GW allowed the cells to retain 70-80% expression. There was no significant difference between GW and GI treatment. Due to time constraints with my DPhil deadline, these data unfortunately could not be acquired for the control mucins MUC24 and CD45.

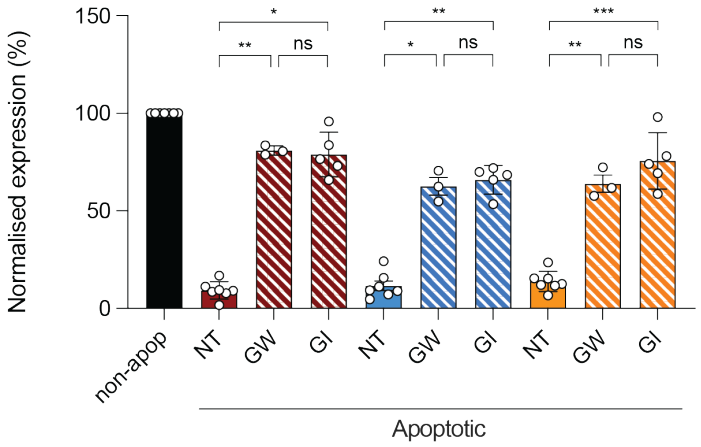


*Figure 31: GI and GW inhibitors reduce loss of CD43, PSGL-1 and MUC1 on CEM during UV-C-induced apoptosis. Non-apoptotic cells (black), CD43 (red), PSGL-1 (blue), MUC1 (yellow). Dashes indicate treatment with inhibitor. Non-treated (NT), GW-treated (GW) and GI-treated (GI) samples are clustered per mucin. n = 5-7. Data were log_{10} transformed followed by a one-way ANOVA corrected for multiple comparisons using Dunnett's multiple comparisons test. * $p<0.05$, ** $p<0.01$, *** $p<0.001$, ns = not significant.*

4.2.5 ADAM10 inhibition in dexamethasone-treated T cells

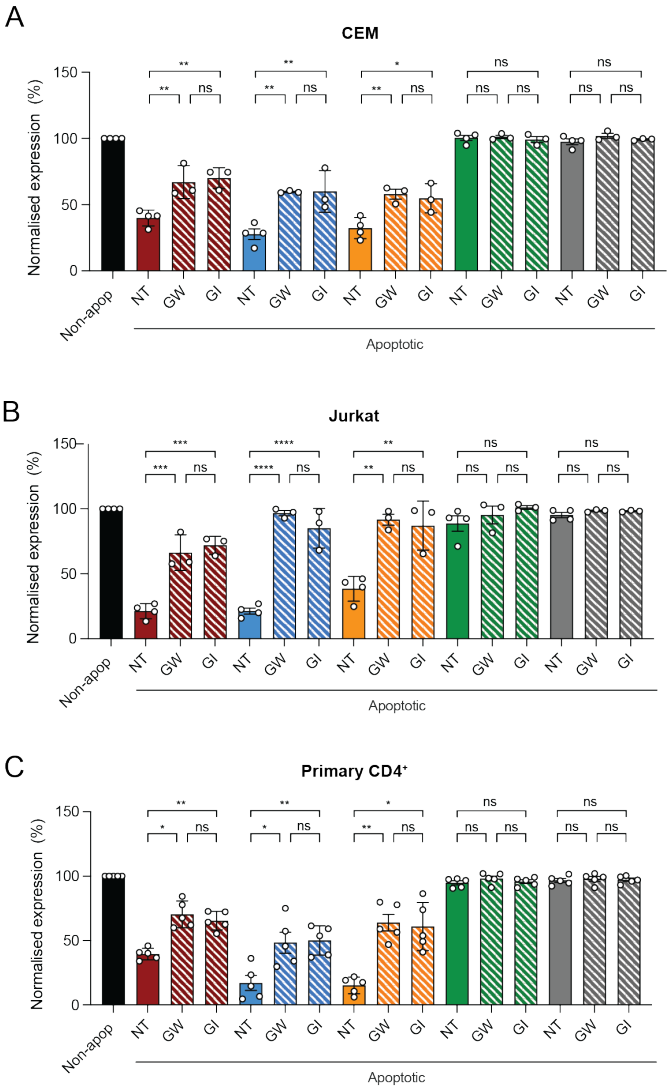


*Figure 32: GI and GW inhibitors reduce loss of CD43, PSGL-1 and MUC1 on CEM during dexamethasone-induced apoptosis. Non-apoptotic cells (black), CD43 (red), PSGL-1 (blue), MUC1 (yellow). Dashes indicate treatment with inhibitor. Non-treated (NT), GW-treated (GW) and GI-treated (GI) samples are clustered per mucin. n = 3-5. Data were log_{10} transformed followed by a one-way ANOVA corrected for multiple comparisons using Dunnett's multiple comparisons test. * $p<0.05$, ** $p<0.01$, *** $p<0.001$, ns = not significant.*

To validate the above findings in a more physiological model of T cell apoptosis, CEM, Jurkat and primary $CD4^+$ T cells were incubated with dexamethasone [497] either in the presence or absence of GW or GI inhibitor. As before, reduction of labelling of CD43, PSGL-1 and MUC1 was significantly reduced in GW and GI-treated cells, whilst MUC24 and CD45 expression remained stable. There were no significant differences between labelling of GW and GI-treated cells in any of the samples. The observation that there is no significant difference between GW and GI-treated samples for CD43, PSGL-1 and MUC1 on apoptotic CEM, primary $CD4^+$ and $CD8^+$ T cells indicates that ADAM10 could be the main sheddase at play. Both GW and

GI inhibitors are reversible and cannot achieve 100% inhibition. Hence, a more refined approach was attempted using the ADAM10$^{-/-}$ CEM cell line available in the Sattentau lab. The cell line was kindly generated by Dr Rebecca Russell using a CRISPR/Cas9 electroporation system, after which she confirmed successful knockout by western blot prior to my affiliation with the lab.

4.2.6 ADAM10 knockout in CEM

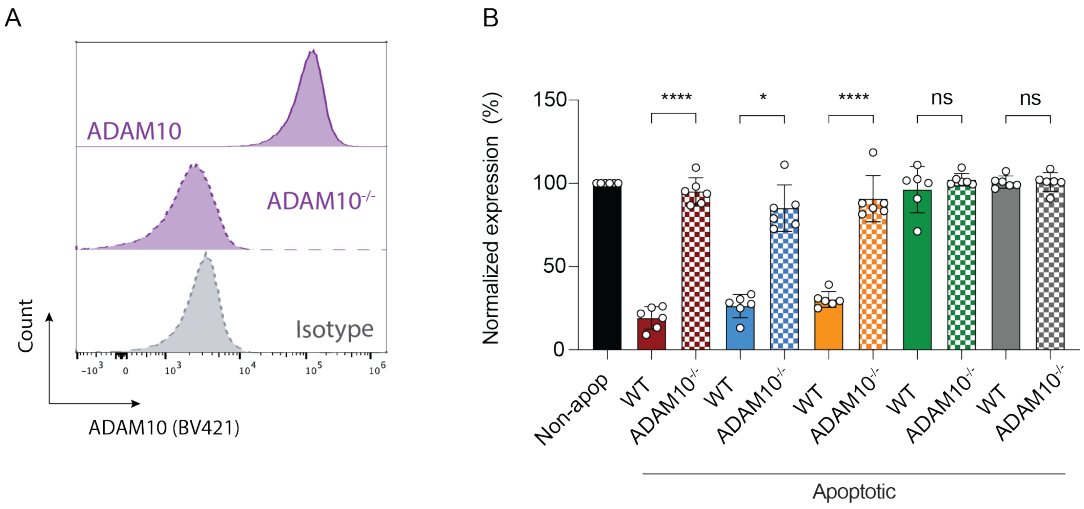


*Figure 33: A) ADAM10 expression profile on WT CEM (purple) and ADAM10$^{-/-}$ CEM (purple, dashed) compared to an isotype control (grey, dashed). B) Mucin expression on apoptotic WT (filled) and ADAM10$^{-/-}$ CEM (chequered). Bars represent non-apoptotic cells (black), CD43 (red), PSGL-1 (blue), MUC1 (yellow), MUC24 (green), CD45 (grey). n = 6. Data were log$_{10}$ transformed followed by a one-way ANOVA corrected for multiple comparisons using Dunnett's multiple comparisons test. * $p<0.05$, **** $p<0.0001$, ns = not significant*

First, ADAM10 expression was analysed on WT and ADAM10$^{-/-}$ CEM by flow cytometry. As before, ADAM10 yielded a strong signal on WT cells. On ADAM10$^{-/-}$ cells, the fluorescent signal was comparable to that of the isotype control (Figure 33A), confirming specific binding of the antibody. When inducing apoptosis with staurosporine, CD43, PSGL-1 and MUC1 were significantly downregulated on WT cells as in previous experiments (20-30%, Figure 33B). Strikingly, on apoptotic ADAM10$^{-/-}$ cells, CD43, PSGL-1 and MUC1 expression remained high (90-100%). MUC24 and CD45 expression levels remained unchanged in the apoptotic populations of both WT and ADAM10$^{-/-}$ CEM.

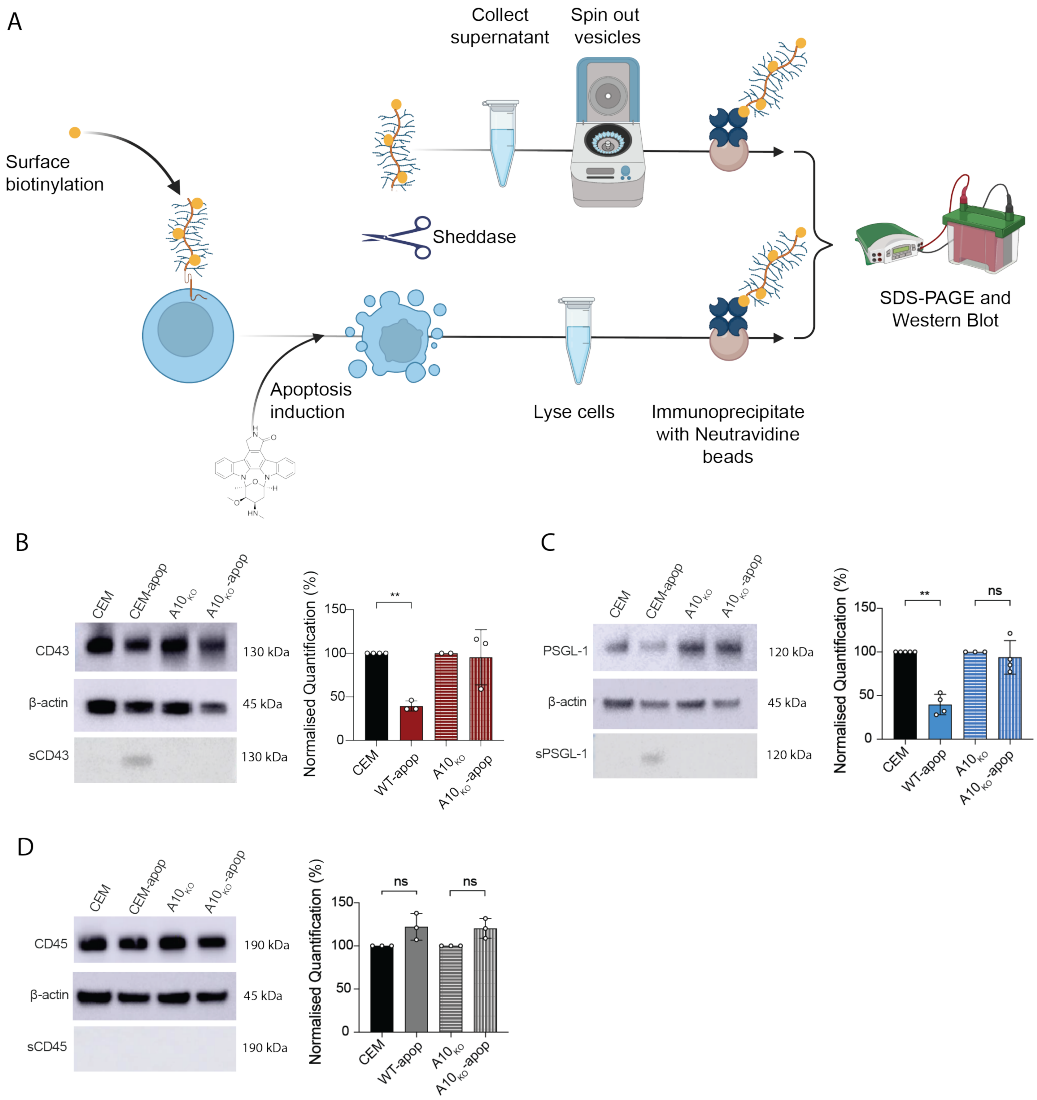


*Figure 34: A) Schematic of surface biotinylation assay and Western blot sample preparation. B) Western blot of CD43 on surface fraction, and supernatant, β-actin loading control on flow-through. Normalised signal quantification histograms. C) Western blot of PSGL-1 on surface fraction, and supernatant, β-actin loading control on flow-through. Normalised signal quantification histograms. C-D) Western blot on surface fraction, β-actin loading control on flow-through and supernatant. Untreated WT CEM ("CEM"), staurosporine-treated CEM ("CEM-apop"), untreated ADAM10$^{-/-}$ ("A10") and staurosporine-treated ADAM10$^{-/-}$ ("A10-apop"). Normalised signal quantification histograms. B) CD43, β-actin, soluble CD43 (sCD43) ; C) PSGL-1, β-actin, soluble PSGL-1 (sPSGL-1) and D) CD45, β-actin, soluble CD45 (sCD45). n = 2-4. Data were $\log_{10}$ transformed followed by a one-way ANOVA corrected for multiple comparisons using Dunnett's multiple comparisons test. ** $p<0.01$, ns = not significant.*

4.2.7 Surface biotinylation and pull-down of WT and ADAM10$^{-/-}$ CEM lysates and supernatants during apoptosis

Considering that the expression of all mucins on apoptotic ADAM10$^{-/-}$ CEM was comparable to expression on non-apoptotic cells, these data suggest that ADAM10 serves as the major sheddase of CD43, PSGL-1 and MUC1 on CEM T cells. Based on these results, I hypothesised that the soluble ectodomain of CD43, PSGL-1 and MUC1, but not of MUC24 and CD45 might be detectable in the cell culture supernatant of apoptotic CEM. Running glycoproteins such as mucins on polyacrylamide gels and conducting Western blots has posed significant difficulties in the past due to the mucins' high molecular weight and strong negative charge of the mucins. Additionally, a significant amount of sample can be lost due to adhesion to plastic tubing owed to the sticky nature of mucins [498]. Following a comprehensive series of optimisation experiments, the development of an assay was achieved that allowed the detection of mucins by Western blot analysis. Using the Pierce™ Cell Surface Biotinylation and Isolation Kit, all surface molecules of WT and ADAM10$^{-/-}$ CEM were biotinylated(Figure 34A). After extensive washing, samples were split in half and apoptosis induced by staurosporine, allowing the mucins to be shed from the cell surface and released into the supernatant. After 3 h, the supernatant was collected, potentially containing the biotinylated mucin ectodomains. The cell pellet, containing non-shed, biotinylated cell surface molecules was collected in a separate tube. To exclude the possibility that mucins might be released from the cell surface as part of apoptotic bodies, the supernatant was spun for 30 mins at 14,000 g [499], while simultaneously lysing the cell fraction. Biotinylated protein was pulled down using Neutravidin beads. The non-bead-binding fraction of the lysate samples (flow-through) was saved to be able to perform a loading control using β-actin. Samples were boiled at 95ºC in sample buffer, run on a 4-12% gradient SDS-PAGE and transferred onto a nitrocellulose membrane. Antibodies for Western blots were validated for CD43, PSGL-1 and CD45 on CEM cells. This was a crucial step as some antibodies previously validated for specific cell lines or primary cells did not exhibit the same specificity for proteins on CEM cells. ECL substrate (low picogram detection limit) was used for lysates and SuperSignal West Femto Maximum Sensitivity Substrate (low femtogram detection limit) was used for supernatant samples. As shown by MESF quantification in Chapter 1, MUC1 expression is low on CEM cells and therefore too low for reliable

probing and meaningful comparison by Western blot. When probing the surface-biotinylated fraction from the lysate, a fainter band can be seen in staurosporine-treated CEM compared to untreated CEM for CD43 and PSGL-1, but not CD45 (Figure 34B-D). No difference was observed in the case of PSGL-1 and CD45 on ADAM10$^{-/-}$ CEM. Due to difficulties with the assay, the sample size was too small in the case of CD43 to conduct statistical analyses. When probing the supernatant samples with femto-substrate, faint bands can be seen for sCD43 and sPSGL-1, while no signal was detected for CD45. sCD43 and sPSGL-1 appeared around the same molecular weight as surface CD43 and PSGL-1. These results support the idea that CD43 and PSGL-1, in contrast to CD45, undergo ADAM10-mediated shedding from the cell surface of apoptotic cells with the soluble ectodomain released into the supernatant.

4.2.8 Mass spectrometric analysis of WT and ADAM10$^{-/-}$ CEM during apoptosis

Considering the low detection limit, the difficulty of the assay and the number of processing steps from biological sample to read-out, mass spectrometric analysis was considered as potentially a more suitable approach to detect shed mucin ectodomains. Through mass spectrometry, not only CD43, PSGL-1, and MUC1 but all molecules potentially shed under apoptotic conditions that are detectable by MS methods could be characterised, offering a comprehensive, unbiased ”big picture” perspective. Further to that, utilising ADAM10$^{-/-}$ CEM would permit the definition of the ADAM10 sheddome on apoptotic CEM. Professor Mertins is the head of proteomics facility at the Max-Delbrück-Centre for Molecular Medicine (MDC) and Kerstin Fentker, one of the PhD students in the laboratory, specialises in mucin proteomics. Due to their charge and tandem repeats, MS on mucin-like molecules presents a challenging task. As a result there are few laboratories in the world that specialise in this field. For this collaboration, samples were created as per the workflow in Figure 34A with the following exceptions: Instead of sample buffer addition and SDS-PAGE, samples were resuspended in PBS and frozen on beads at -80ºC. The Neutravidin-purified lysate and supernatant samples of three independent biological repeats were shipped to Kerstin Fentker and run and analysed in Berlin.

The experimental setup as described above resulted in eight conditions: WT untreated, WT staurosporine-treated, ADAM10$^{-/-}$ untreated, ADAM10$^{-/-}$ staurosporine-treated; for both lysate

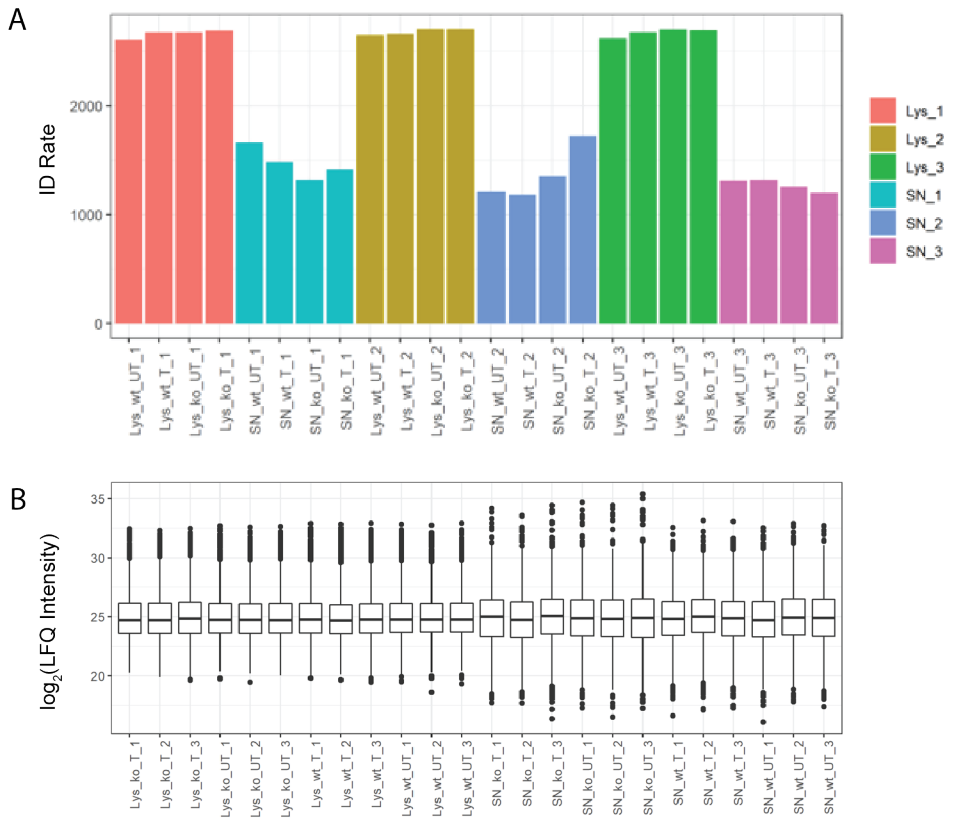


Figure 35: MS quality control. A) ID rates across sample types and repeats clustered by colour. B) Boxplot analysis of log_2 of each sample's LFQ intensity. Boxplots show means with upper and lower quartiles, standard deviation and outliers.

and supernatant. Three biological replicates of these conditions were run and analysed. Data were filtered for 50% valid values in all samples, after which 2786 proteins were quantified. To assure sample quality, the ID rate across the different sample conditions was plotted in Figure 35A. The sample ID rate assesses the number of proteins identified per sample. A higher ID rate was observed in lysate samples compared to supernatant samples meaning more proteins could be identified in the lysate than in the supernatant. ID rates were consistent across sample conditions, which confirmed that the biological repeats were comparable. Label-free quantification (LFQ) assesses the peak intensity or area under the curve of a detected peptide ion, allowing relative quantification of peptides across samples. Boxplots of the log_2(LFQ intensity) confirmed similarity between all samples and repeats (Figure 35B).

To assess differences caused by the knockout of ADAM10, lysate samples from WT and ADAM10$^{-/-}$ were compared first. 1098 proteins including PSGL-1 (SELPLG) and CD45 (PTPRC) were significantly different (Figure 36A). CD43 (SPN) was not significantly changed. In the supernatant, a total of 139 proteins were significantly different, including CD43 and CD45

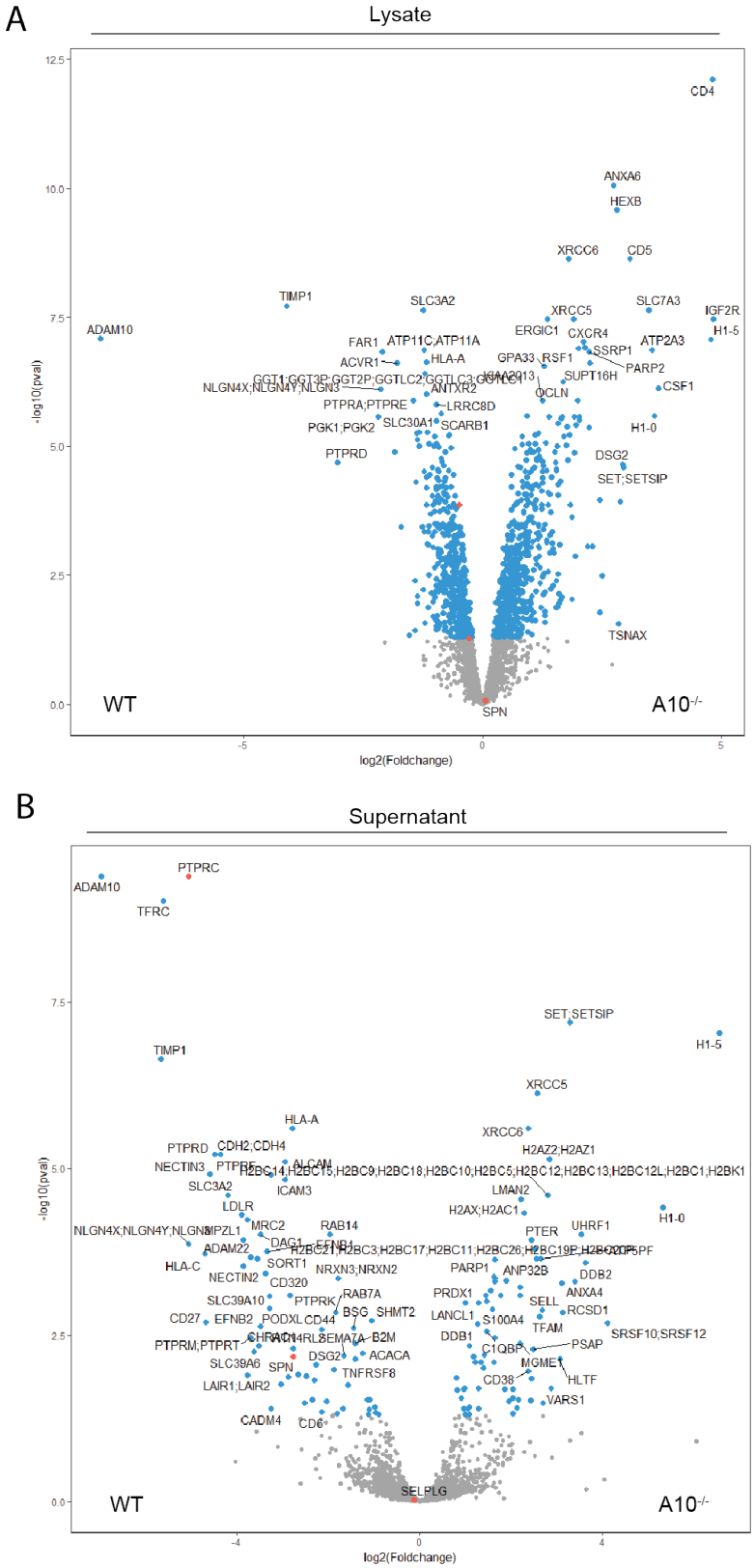


Figure 36: Volcano plots comparing WT and ADAM10$^{-/-}$ (A10). Lysates (A) and supernatant samples (B) Each dot represents one protein. Grey proteins are not significantly changed, blue are significantly changed and red are mucins of interest CD43 (SPN), PSGL-1 (SELPLG) and CD45 (PTPRC). Y-axes show log_{10} of the p-value and x-axes show log_2 fold-change between the samples. n = 3, moderated t-tests were performed. Adjusted p-value < 0.05.

(Figure 36B). When comparing non-treated (NT) and staurosporine-treated (ST) lysate samples, 127 proteins were changed, none of which included CD43, PSGL-1 or CD45 (Figure 37). In supernatant samples, 24 proteins were changed, none of which included my mucins of interest. Notably, the cellular knockout of ADAM10 seemed to result in higher numbers of different proteins in both lysate and supernatant, compared to cells subjected to staurosporine treatment. As expected, ADAM10 notably differed in fold-change and p-value in both lysates and supernatants of WT and ADAM10$^{-/-}$ samples.

When comparing all lysates, there were no changes in CD43 intensity (Figure 38). However, a discernible increase in CD43 intensity was detected in WT supernatant when compared to ADAM10$^{-/-}$ samples. The $\log_2$ fold-change interval for PSGL-1 was consistently narrow, ranging from 26 to 27, and attempts to measure PSGL-1 in supernatant samples were unsuccessful. There was a significant difference between all CD45 samples with the exception of untreated WT and treated WT in the lysates, untreated WT and treated WT, and untreated ADAM10$^{-/-}$ and treated ADAM10$^{-/-}$. Generally, the intensities of lysate samples exhibited higher levels compared to supernatant samples for both CD43 and CD45.

ACTG1 encodes for γ-actin, H2BC12 encodes for a protein bearing the same name, which is a member of the histone H2B family. GAPDH encodes for a protein of the same name which is a key regulatory protein in glycolysis and frequently used as a loading control in Western blotting. All three are considered intracellular housekeeping proteins. Notably, ACTG1, H2BC12 and GAPDH are detected in all sample conditions of both lysate and supernatant (Figure 39A-C). Considering that all samples underwent surface-biotinylation and subsequent pull-down, no intracellular proteins were expected in the supernatant. This means that despite the careful sample preparation, intracellular proteins contaminated the supernatant samples and hence all data should be interpreted with great care. Due to time constraints with my DPhil deadline, these experiments unfortunately could not be repeated.

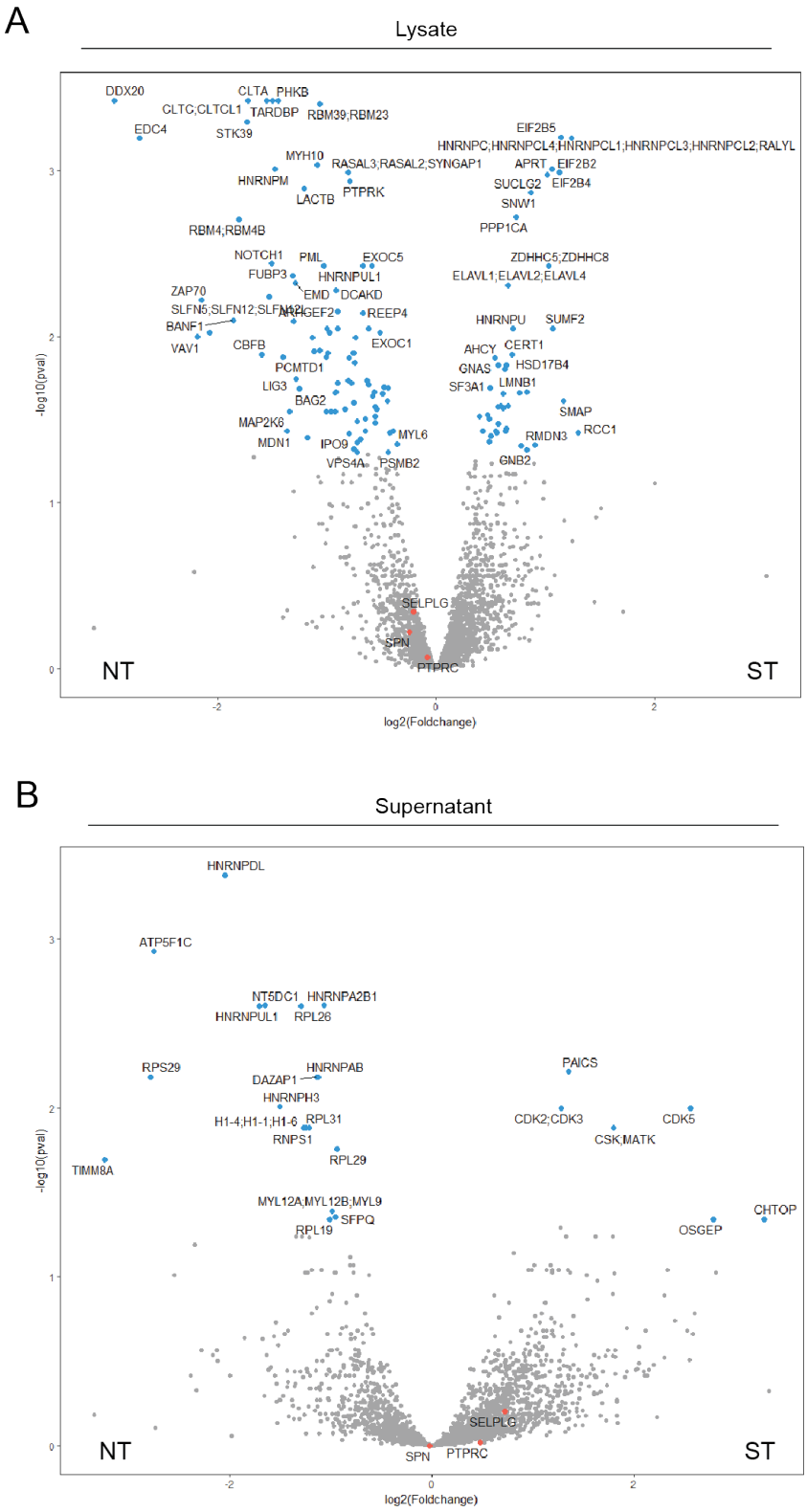


Figure 37: Volcano plots comparing non-treated (NT) and staurosporine-treated (ST) samples. Lysates (A) and supernatant samples (B). Each dot represents one protein. Grey proteins are not significantly changed, blue are significantly changed and red are mucins of interest CD43 (SPN), PSGL-1 (SELPLG) and CD45 (PTPRC). Y-axes show log_{10} of the p-value and x-axes show log_2 fold-change between the samples. n = 3, moderated t-tests were performed. Adjusted p-value < 0.05.

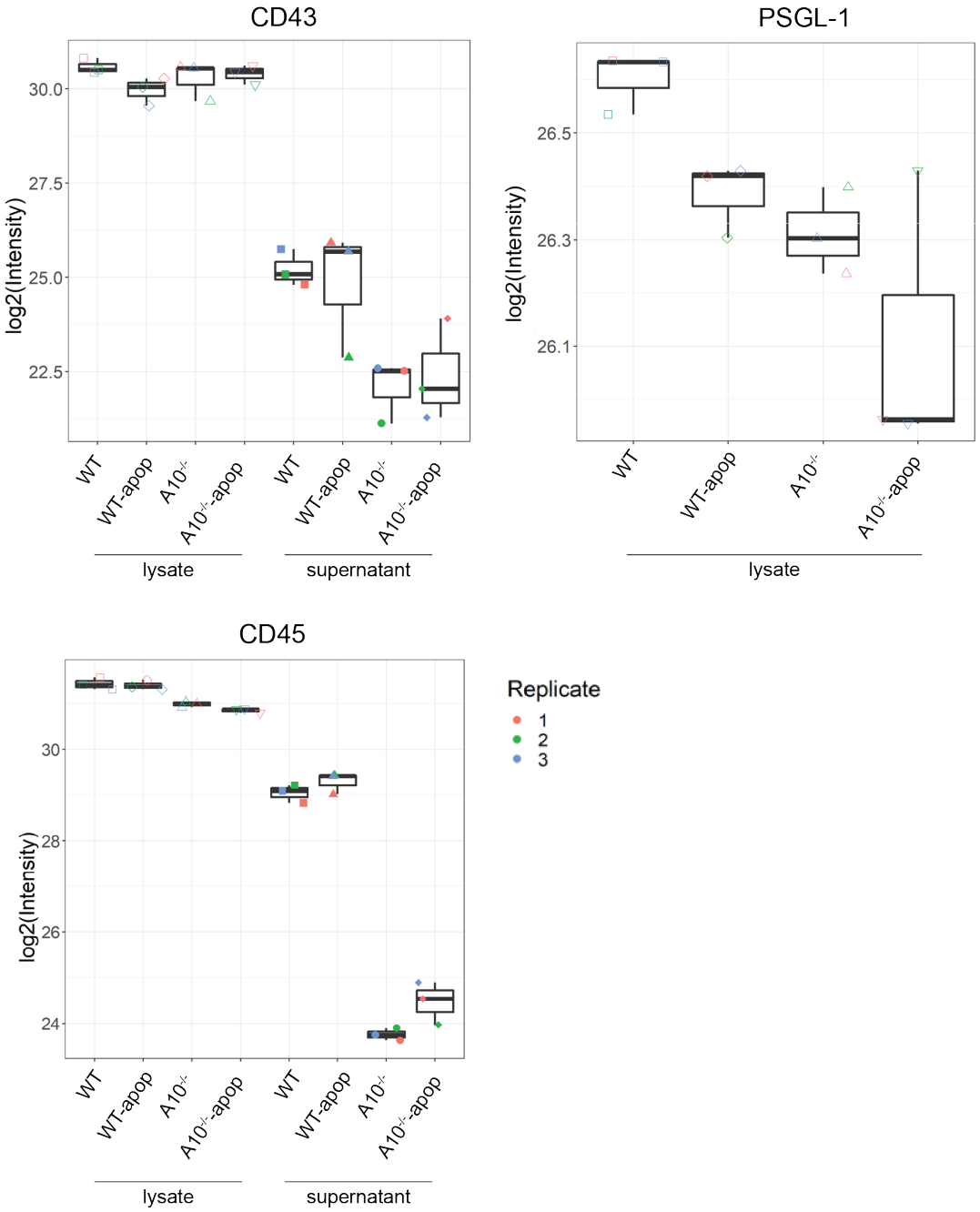


Figure 38: MS protein intensities of CD43, PSGL-1 and CD45. Values are plotted as log_2(intensities). Replicate 1 (red), 2 (green) and 3 (blue), lysate (solid symbols) and supernatant (empty symbols). Boxplots show means with upper and lower quartiles, standard deviation and outliers.

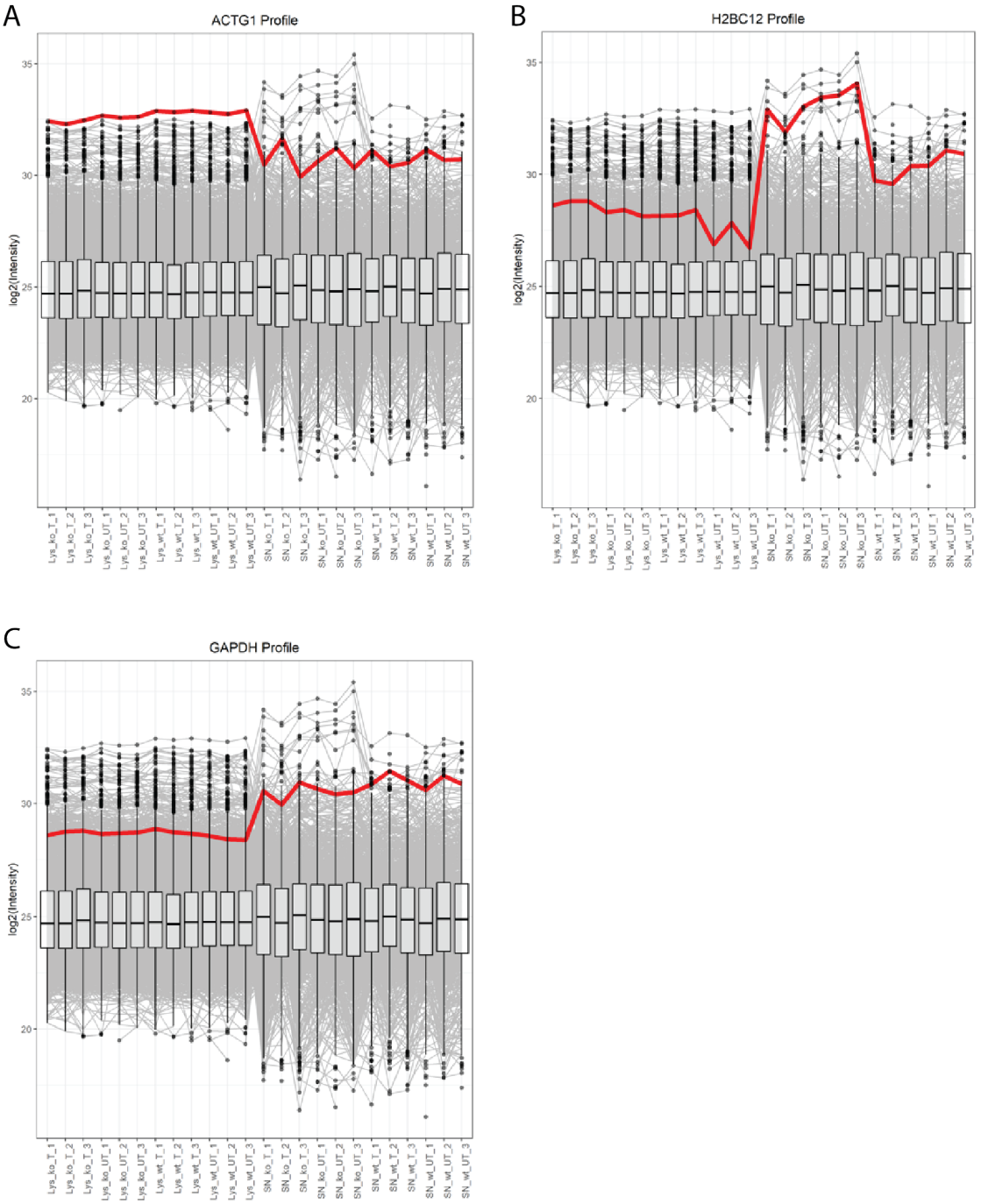


Figure 39: Detection of intracellular proteins across lysate and supernatant samples. Boxplots show means with upper and lower quartiles, standard deviation and outliers. log_2 of sample intensity was plotted for all hits and A) ACTG1; B) H2BC12 and C) GAPDH were highlighted in red.

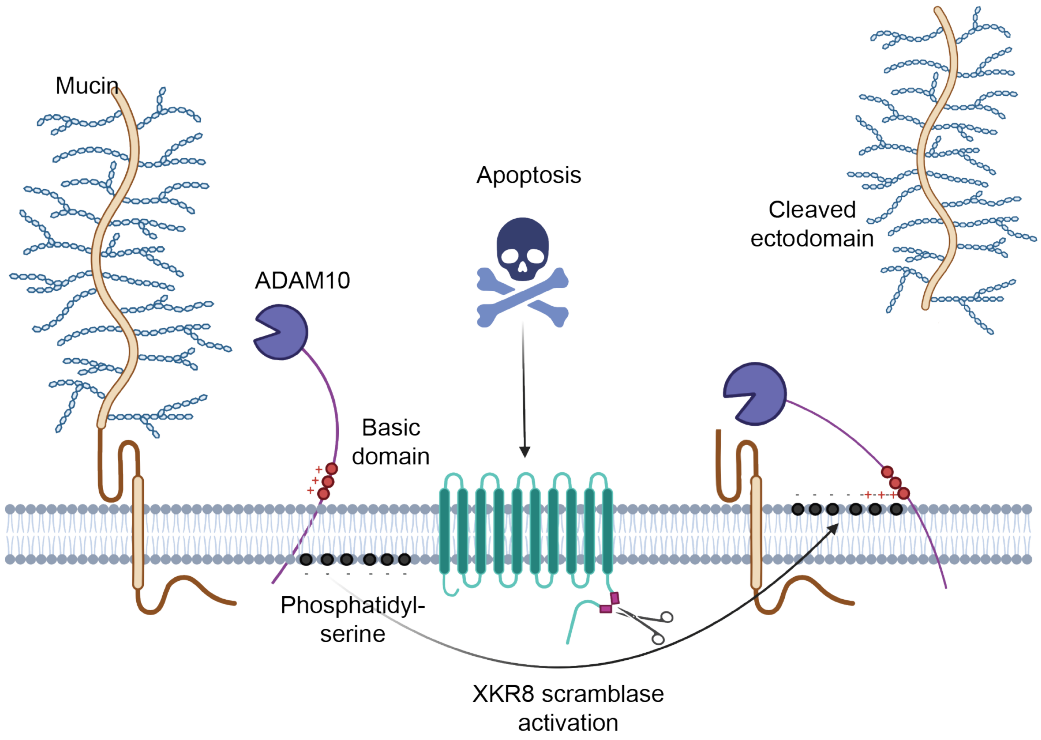


Figure 40: Schematic overview of mucin shedding through ADAM10 during apoptosis

4.2.9 XKR8 function in apoptotic CEM

The activation of ADAM10 is attributed to PS flipping to the outer leaflet where the negatively charged phospholipid electrostatically interacts with the basic patch of the ADAM10 stalk region, thereby inducing movement of the enzyme's active site closer to plasma membrane-proximal substrates [377]. However, this mechanism has previously only been published in the context of Ca^{2+} flux-induced PS flipping mediated by TMEM16F (ANO6) [375]. I therefore hypothesised that XKR8, a PS scramblase with a Casp3 motif [402], might be responsible for PS flipping in apoptosis and ADAM10 activation.

To explore this hypothesis, CRISPR/Cas9 editing was used as before (see Material and Methods on page 49) to achieve a knockout of XKR8 in CEM cells and investigate the impact on mucin shedding during apoptosis (Figure 41A). Ribonucleoproteins (RNP) consisting of Cas9 protein, tracrRNA and crRNA were transfected into WT CEM using the Neon NxT electroporation system (ThermoFisher). Three guide RNAs (gRNAs) targeting XKR8 exon 2 were used at the same time to increase efficiency. Human XKR8 has 5 exons. Targeting downstream exons, truncated proteins and shorter isoforms could potentially retain functionality. However, directing gRNAs towards the first exon might result in gene silencing rather than achieving a complete knockout. Therefore the gRNAs were designed to target exon 2. Due to failed

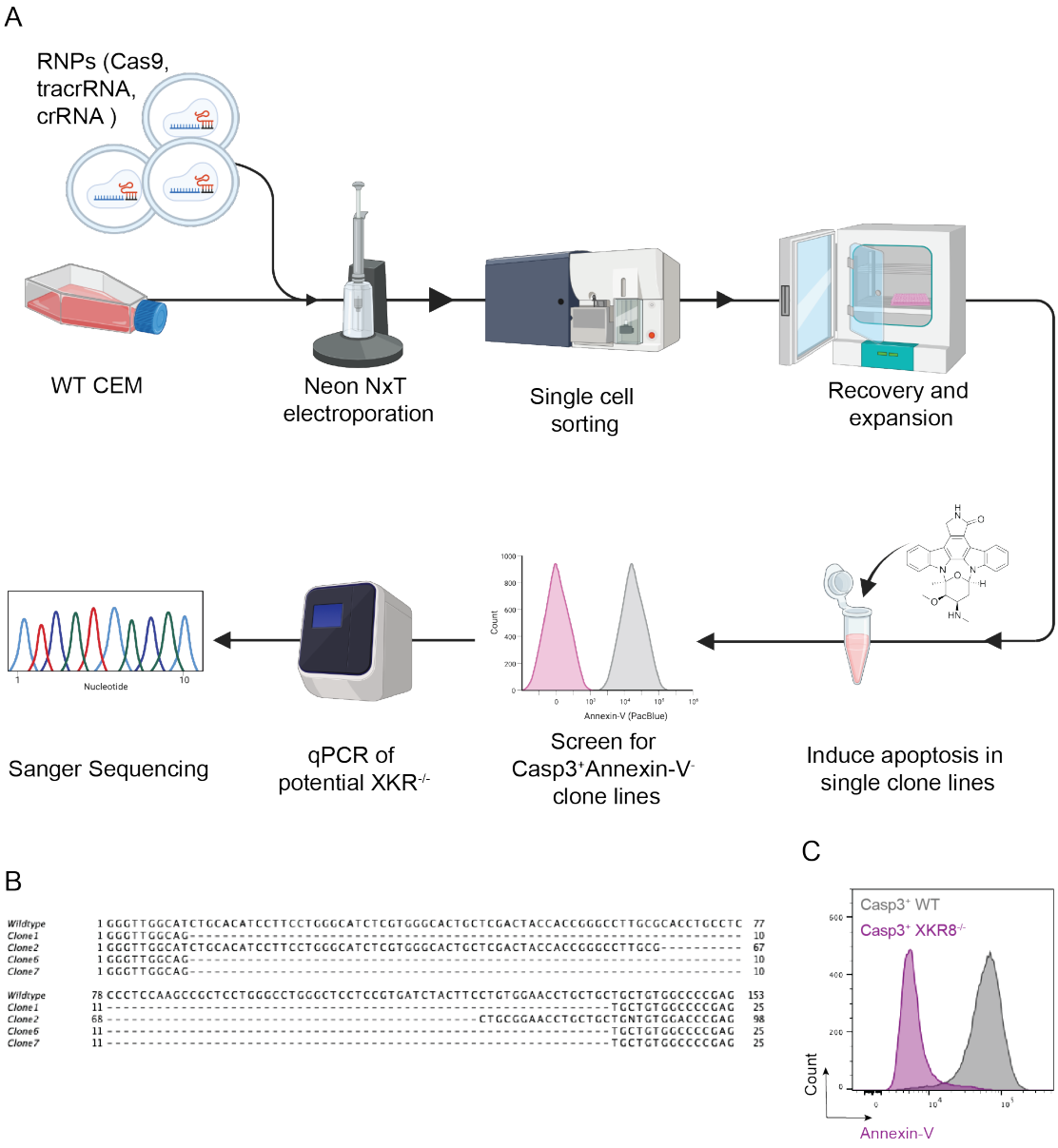


Figure 41: XKR8$^{-/-}$ CEM generation and validation. A) Cartoon of CRISPR workflow and validation B) Comparative sequence sections of exon 2 from single cell clones C) Functional knockout confirmation by apoptosis induction. WT CEM in grey, XKR8$^{-/-}$ CEM in purple. Histograms show count against annexin-V.

validation of commercially available antibodies, a single cell sort of single, live and annexin-V-negative apoptotic (Casp3-positive) cells was performed. WT CEM that became apoptotic due to the effects of electroporation or otherwise would be positive for annexin-V staining, thus a sort of the annexin-V-negative population was performed to refine the pool of potential successful KOs. Once the single cell clones had been recovered and expanded, genomic DNA (gDNA) was extracted and quantitative Polymerase Chain Reaction (qPCR) performed using primers targeting exon 2 of XKR8. Subsequent Sanger sequencing confirmed large deletions in exon 2 for clones 2, 3, 6 and 7 (Figure 41B). When apoptosis was induced in the sequenced XKR8$^{-/-}$ CEM clones, the Casp3-positive cells were negative for annexin-V, contrary to their WT counterparts (Figure 41C). These results functionally confirmed the successful knockout and demonstrated that CEM lacking XKR8 are unable to flip PS during apoptosis.

According to my hypothesis, on cells that are prevented from flipping PS during apoptosis, ADAM10 conformation should remain unchanged, thereby preventing CD43, PSGL-1 and MUC1 cleavage from the cell surface (Figure 40). To test this, apoptosis was induced in XKR8$^{-/-}$ CEM using staurosporine and mucin expression analysed by flow cytometry. When comparing annexin-V binding on untreated WT and XKR8$^{-/-}$ cells, both showed comparable binding at approximately 10%. However staurosporine-treated WT CEM were approximately 80% positive for annexin-V binding, significantly more than staurosporine-treated XKR8$^{-/-}$ cells, which showed annexin-V binding comparable to untreated samples (Figure 42A). Casp3^{+} (apoptotic) XKR8$^{-/-}$ cells had significantly higher CD43, PSGL-1 and MUC1 expression compared to apoptotic WT CEM. MUC24 and CD45 expression was not changed (Figure 42B). A histogram comparing all mucins on apoptotic WT and XKR8$^{-/-}$ CEM showed a peak shift in WT but not XKR8$^{-/-}$ cells (Figure 42C). These results suggested that XKR8 is crucial for ADAM10 activity and subsequent shedding of CD43, PSGL-1 and MUC1.

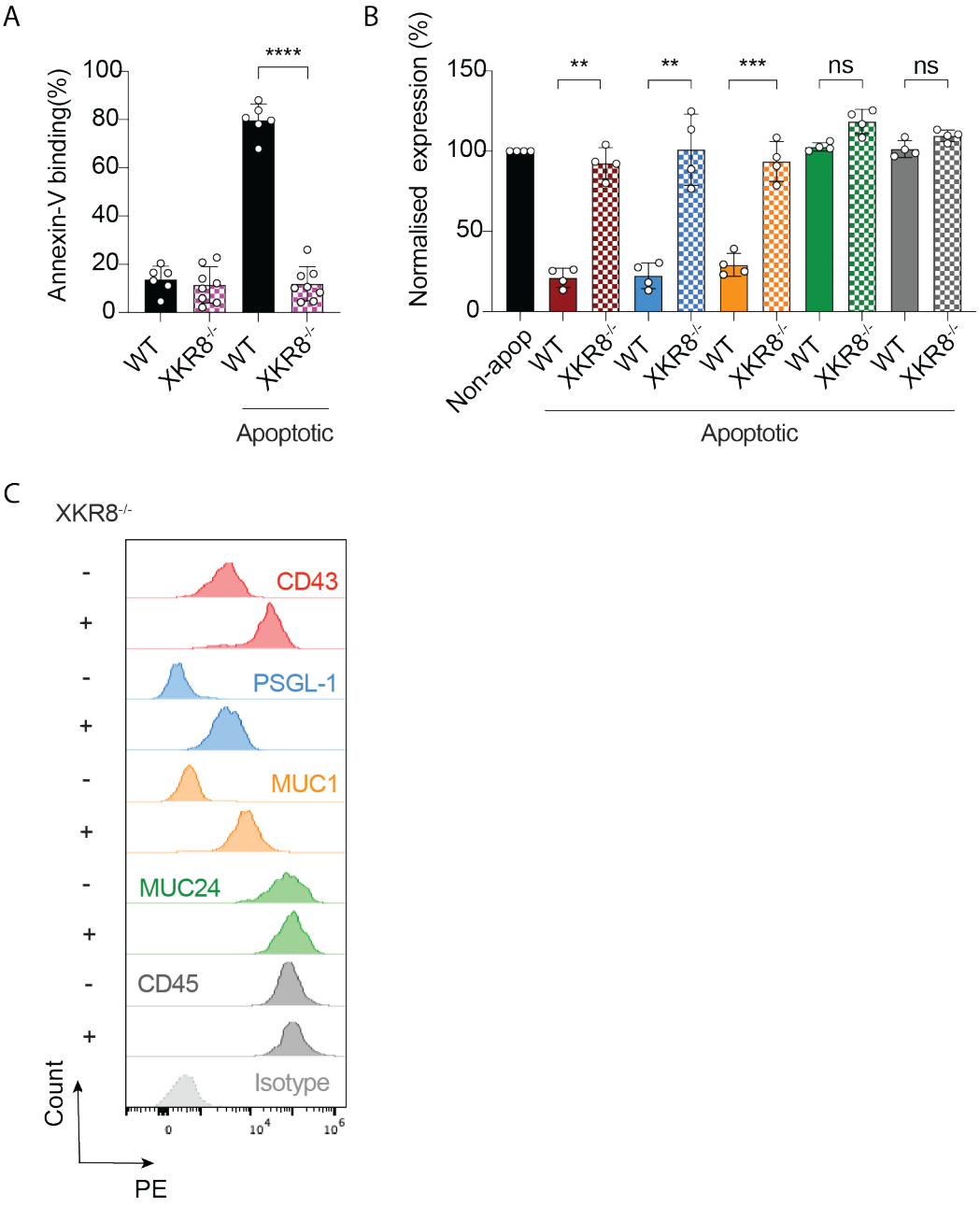


*Figure 42: XKR8$^{-/-}$ CEM in apoptosis. A) Annexin-V expression on healthy WT and XKR8$^{-/-}$ CEM and apoptotic WT and XKR8$^{-/-}$ CEM. B) Mucin expression on apoptotic WT and XKR8$^{-/-}$ CEM, normalised to non-apoptotic expression. C) Histograms of WT (-) and XKR8$^{-/-}$ (+) CEM of mucins on apoptotic cells. CD43 (red), PSGL-1 (blue), MUC1 (yellow), MUC24 (green), CD45 (dark grey) and non-apoptotic (black). n = 4-6. Data were log$_{10}$-transformed followed by a one-way ANOVA corrected for multiple comparisons using Dunnett's multiple comparisons test. **** $p<0.0001$, *** $p<0.001$, ** $p<0.01$, ns = not significant.*

4.3 Discussion

Previous results from my first chapter led me to hypothesise that CD43, PGSL-1 and MUC1, but not MUC24 and CD45 labelling was selectively downregulated on apoptotic T cells. In the current chapter the aim was to test this hypothesis by investigating internalisation, changes of antigenicity and enzymatic cleavage of CD43, PSGL-1 and MUC1. Surface and total cell staining of CD43, PSGL-1, MUC1, MUC24 and CD45 on healthy and apoptotic cells aimed to investigate if the mucins are internalised upon apoptosis induction. While a significant decrease in labelling and a reduced ratio were observed for CD43, PSGL-1 and MUC1, MUC24 and CD45 were also significantly reduced and had a ratio below 1. While this was unexpected, the ratios of MUC24 and CD45 were only slightly below, while the CD43, PSGL-1 and MUC1 had much smaller ratios of 0.1 - 0.4. This indicates that the reduction of CD43, PSGL-1 and MUC1 labelling is much more pronounced. Overall it should be noted that a purely intracellular staining would have given cleaner results when comparing surface and intracellular protein labelling. Furthermore one should consider that the readout of this experiment relies on antibody labelling and any loss of antigenicity such as conformational changes or shifts in glycosylation pattern could potentially contribute to a reduced signal. These findings serve as a promising indicator that antibody binding to CD43, PSGL-1, and MUC1 also decreases intracellularly during apoptosis, however without further experiments, these results should be interpreted with caution. Nusabum et al previously published that CD43 downregulation is not due to internalisation or membrane blebbing during neutrophil activation and apoptosis [37, 461], which is in line with my results.

Apoptosis induction of double-tagged CD43 shows a reduction in N-terminal Halo over time. As a covalently linked substrate was used to stain both tags and not antibodies as before, a conformational change and the state of glycosylation can be excluded as possible reasons for reduction in signal. The CD43 C-terminal SNAP fluorochrome remained stable even at high cellular apoptosis percentages. This indicates that while the N-terminus is lost from the apoptotic cells, the C terminus remains intact. Notably, this effect is not influenced by overexpression of CD43 on the cell line, as confirmed by MESF quantification. This outcome supports my hypothesis that CD43 might be enzymatically cleaved. Our collaborators in the Sezgin lab at the Karolinska Institutet used my $CD43_{Halo/SNAP}$ construct for fluorescent correlation spec-

troscopy (FCS) to analyse the release of soluble $CD43_{Halo}$ ectodomain in supernatants. They found diffusion over time of labelled Halo, but not SNAP in cell culture supernatants, excluding shedding of full-length CD43 by apoptotic bodies [500].

After confirming antibody labelling of ADAM10 on CEM cells, the ADAM17 and ADAM10 inhibitor GW and the ADAM10 inhibitor GI were tested during apoptosis induced by staurosporine. Both inhibitors effectively prevented loss of CD43, PSGL-1 and MUC1 on apoptotic cells. The same results were confirmed on primary $CD4^+$ and $CD8^+$ T cells. No significant difference between GW and GI inhibition was found in any of the samples, indicating that not ADAM17 but ADAM10 might be the major sheddase of CD43, PSGL-1 and MUC1 on CEM and primary T cells. Using UV-C radiation to induce apoptosis in CEM rendered the same results for all mucins, expect for MUC24 and CD45, which were not tested. For completeness, these data should be repeated including MUC24 and CD45 as negative controls to ensure that there were no off-target drug effects on mucins in general. The inhibitor-based outcomes remained consistent across CEM, Jurkat, and primary $CD4^+$ cells under conditions of both staurosporine and dexamethasone-induced apoptosis. This confirms that the inhibitors' effectiveness in preventing CD43, PSGL-1, and MUC1 shedding is not contingent upon the specific T cell line used or the method of apoptosis induction. To exclude any effects small molecule inhibitors could have had on these results, mucin expression was investigated during apoptosis induction in the $ADAM10^{-/-}$ CEM line available in the lab. Interestingly, CD43, PSGL-1 and MUC1 shedding was strongly inhibited. My previous inhibitor data showed that GW/GI treatment of apoptotic WT CEM resulted in approximately 70% retention of mucin expression. However, on apoptotic $ADAM10^{-/-}$ CEM mucin labelling was comparable to non-apoptotic levels, indicating that, as expected, the GW and GI inhibitors did not fully suppress ADAM10 activity. These observations could potentially be attributed to the reversible nature of the inhibitors, the continuous intracellular recycling of functional ADAM10 to the cell surface, or possibly the use of a concentration that was too low to fully out-compete dissociation of the inhibitor or ADAM10 re-cycling. Together, these data confirmed that ADAM10 is the major sheddase of CD43, PSGL-1 and MUC1 on apoptotic T cells. The only preceding evidence of ADAM10 cleaving CD43, PSGL-1 or MUC1 has been in an ADAM10 overexpression model in the epithelial cell line HEK 293, which led to cleavage of PSGL-1 [487]. To our knowledge,

this is the first report that these mucins are cleaved on apoptotic T cells and by ADAM10. The tetraspanins Tspan5, Tspan10, Tspan14, Tspan15, Tspan17, and Tspan33 can interact with ADAM10 and regulate its maturation, trafficking, stability and enzymatic function [378–381]. The specific tetraspanin associated with ADAM10 determines the substrate specificity and half-life of ADAM10 [501–505]. The Tspan15:ADAM10 interaction is particularly well researched and defining which Tspan is involved in ADAM10-mediated shedding of mucins under apoptotic conditions might yield interesting results.

When probing for mucin loss via Western blot detection, only CD43, PSGL-1 and CD45 could be successfully detected. Possible explanations for the challenges in detecting MUC1 could be attributed to its low expression levels on CEM and the lack of an appropriate antibody. A significant decrease in CD43 and PSGL-1 but not CD45 was found for apoptotic WT CEM, whereas PSGL-1 and CD45 levels in ADAM10$^{-/-}$ remained unchanged. Interestingly, CD43 and PSGL-1 were also detected in cell culture supernatant with molecular weights that were similar to lysate samples. The high molecular weight of mucins is mainly due to substantial glycosylation, as their predicted weight based on their polypeptide backbones is much lower. In the case of CD43, PSGL-1 and CD45 the predicted weights are 44 kDa [473], 43 kDa [506] and 120 kDa [507], respectively. The C-terminus and transmembrane regions, which do not carry carbohydrates, are therefore of such small molecular weight that any potential contamination with the full-length mucin in supernatant samples might be indiscernible on a gradient gel. CD43 is shed on PMA-activated neutrophils, resulting in three bands 130, 49 and 34 kDa [482], while Bazil et al. reported fragments of 120, 60 and 47 kDa [35]. Weber et al. observed a 123 kDa fragment in the supernatant upon stimulating HMC-1 cells with PMA [484]. These findings suggest that the varied cleavage products observed could stem from distinct proteases engaging in the cleavage of CD43, depending on cell type and context, such as activation or apoptosis. PSGL-1 was blotted as a single band of 100–120 kDa in the supernatant of activated neutrophils [508], similar to my results in apoptotic T cells. Lichtenthaler and colleagues showed a 120 kDa fragment in the supernatant and a C-terminal fragment of 20 kDa in the lysate, which was only visible with long exposure [487]. While in my hands apoptotic CEM did not reveal bands indicating cell-bound, truncated CD43 and PSGL-1, this outcome could potentially stem from insufficient exposure as in the case of Lichtenthaler

et al. extensive exposure was required to make the band visible. Alternatively, the truncated mucins could be subject to γ-secretase-mediated intramembrane proteolysis and degraded intracellularly, as was shown for CD43 [509]. While the system was substantially optimised to obtain these results, the assay was still prone to variability. Moreover, any future repeats performed should include pre-clearing agarose beads to remove nonspecific binding.

When analysing untreated and staurosporine-treated WT and ADAM10$^{-/-}$ CEM by mass spectrometry, a higher ID rate was observed in lysate samples compared to the supernatant samples meaning more proteins could be identified in the lysate than in the supernatant, which was coherent with expectations. ID rates were consistent across sample conditions, confirming comparability between repeats. MUC1 could not be detected in any of the samples. This could potentially be attributed to its modest expression levels on CEM and its tandem repeats, which make it difficult to detect by MS. When comparing protein changes in lysate and supernatant, the knockout of ADAM10 resulted in more change compared to apoptosis induction. Given how extensive the substrate pool is for ADAM10, substantial change in protein expression would be expected. Nevertheless stronger changes caused by apoptosis induction were anticipated. Among the staurosporine-treated samples, apoptosis was induced in only approximately 50% of samples due to high cell numbers and density. Increasing this percentage might result in stronger differences. While there seemed to have been no difference of CD43 in any lysate sample, more CD43 was found in supernatants from WT cells compared to ADAM10$^{-/-}$, potentially indicating more CD43 molecules are shed on CEM with active ADAM10. PSGL-1 was undetectable in any supernatant sample, and PSGL-1 intensity was unchanged in all lysate samples. While the expectation was that CD45 intensity would be stable across all samples, CD45 was significantly changed across a range of conditions, yielding inconclusive results. All supernatant samples showed high levels of the intracellular control proteins ACTG1, H2BC12 and GAPDH, highlighting that all supernatant samples had significant intracellular contamination. While intracellular contamination is a common issue in this type of experiment, this was prevented by utilising the surface biotinylation paired with extensive washing steps. This unfortunately remained unsuccessful and agarose pre-clearing beads and an elution step are advised for any repeats. Prior to my study, ADAM10 shedding activity had been analysed by MS using ADAM10 knockout cells for murine neurons [510],

and the human B cell lines SEM and NALM6 [511]. Scharfenberg and colleagues have also published an MS-based characterisation of soluble ADAM10 and the secretome of murine cardiomyocytes [512]. However, to my knowledge, no such analysis has been published in the case of T cells. Regrettably, my samples sent to Berlin for MS analysis thawed during delivery to the Berlin institute. As a result, all MS data should be interpreted with caution and repeated with new samples to ensure the accuracy of any observed effects.

Staurosporine-treated XKR8$^{-/-}$ CEM strongly expressed Casp3, while annexin-V binding was comparable to background levels. Among the 10 human XKR family members XKR4, XKR8, and XKR9 undergo caspase-mediated cleavage during apoptosis. While XKR8 is presumed to be ubiquitously expressed, XKR4 and XKR9 expression is tissue-specific [353, 402] and has not yet been characterised in T cells. The observation that apoptotic XKR8$^{-/-}$ cells exhibited a near absence of PS flipping implies that XKR4 and XKR9 might not be expressed or are functionally inactive in CEM T cells. TMEM16F (ANO6) is the dominant lipid scramblase in T cells and can flip PS to the outer leaflet of the membrane when activated by Ca^{2+} [513]. During apoptosis, intracellular Ca^{2+} concentrations increase [514, 515], which could lead to TMEM16F activity and subsequent PS flipping during apoptosis. My observation that Casp3-positive XKR8$^{-/-}$ cells displayed baseline levels of annexin-V binding, suggests that TMEM16F does not play a role in apoptosis-induced PS flipping within the CEM cell line. Suzuki and colleagues over-expressed XKR8 in the mouse T cell line WR19L, which led to an increase of PS exposure on the cell surface when apoptosis was triggered by FasL [353]. FuOXP is a chemotherapy drug that leads to XKR8 overexpression and concomitant PS flipping in the murine colorectal carcinoma cell line CT26 [516]. Knockdown of XKR8 with short interfering RNA (siRNA) in these cells led to almost abolished PS cell surface exposure and slowed tumour growth in an *in vivo* mouse tumour model [517]. The knockout of XKR8 in human haploid HAP1 cells resulted in a reduction in the release of both stomatitis virus particles and Ebola virus-like particles, an outcome attributed to the potentially adverse effect of the knockout on PS-induced membrane curvature [518]. These studies confirm the universal impact of XKR8 function in murine and human models. Previous studies infer that ADAM10 activity is activated by PS flipping to the outer leaflet, which draws the enzyme's active site toward the substrate in close proximity to the plasma membrane, mediated by electrostatic

interactions between the PS head groups and a basic patch on ADAM10 [377]. I therefore hypothesised that XKR8, a PS scramblase with a Casp3 motif [402], might be responsible for PS flipping in apoptosis, leading to ADAM10 activation and subsequent mucin cleavage. Strikingly, XKR8 knockout in CEM led to the retention of CD43, MUC1 and PSGL-1 on the cell surface of Casp3-positive cells. These results close the mechanistic loop (Figure 40) by demonstrating that XKR8 activity is necessary for PS flipping leading to ADAM10 activation on apoptotic CEM T cells.

Based on the stringent regulation of mucin shedding during apoptosis, the question of how mucin cleavage might impact cell-cell interactions during apoptotic cell clearance was considered. Therefore the next chapter focusses on elucidating the impact of mucin expression on apoptotic T cell uptake by macrophages.

5 Efferocytic uptake of apoptotic T cells by MDMs

5.1 Introduction

The aim of this chapter was to shed light on the potential biological significance of mucin shedding during T cell apoptosis. Swift efferocytic uptake of apoptotic cells is crucial for maintenance of tissue homeostasis [286, 519–521]. In the case of insufficient or delayed clearance, apoptotic cells are at risk of progressing to secondary necrosis, a lytic form of cell death which involves the unregulated release of intracellular auto-antigens and danger-associated molecular patterns (DAMPs) such as IL-1β, IL-18, high-mobility group box 1 (HGMB1), and ATP [522]. The release of DAMPs attracts pro-inflammatory innate immune cells and can ultimately result in chronic inflammation and autoimmune responses. For example, patients suffering from SLE show increased occurrence of secondary necrotic cells. In about 50% of patients with SLE, efferocytic function of macrophages is compromised, leading to increased secondary necrotic burden [523]. Accumulation of secondary necrotic cells in germinal centers leads to auto-antigen presentation by follicular DCs to auto-reactive B cells, resulting in the production of auto-antibodies [524]. Thus to maintain tissue homeostasis, a progression from immunologically silent apoptosis to immunogenic secondary necrotic outcome is undesirable, highlighting the importance of efficient efferocytosis by professional phagocytes. The notion that mucins compose an electrostatic barrier that negatively modulates cell-cell interactions has been in existence for three decades [525, 526]. Over-expression of CD43 on HeLa cells interfered with T cell adhesion in a co-culture assay [527] and in a transgenic mouse model of CD43 over-expression, B cell-T cell interactions were negatively impacted [528]. Conversely, knockout of CD43 enhanced T cell interaction [124] and during T cell migration and activation with anti-CD3 and anti-CD28, CD43 is clustered to the uropod, freeing up the leading-edge facilitating interaction and adhesion [124, 529, 530]. This highlights the wide-ranging negative impacts of CD43 expression on cell-cell interactions. PSGL-1 has the potential to be a ligand for all three members of the adhesion molecule family of selectins, however the binding capacity critically depends on its glycosylation and sulfation [55, 139, 531, 532]. Based on this, PSGL-1 has the potential to act as a pro-adhesive molecule, or can have anti-adhesive properties depending on its modifications. PSGL-1 knockout in mice caused enhanced T cell adhesion and proliferation [532] showing clear impacts pf PSGL-1 on cell-cell interactions.

Predominantly characterised on epithelial cells, MUC1 has been reported in many contexts associated with adhesion. MUC1 expression was lost from the epithelial cells at the site of embryo attachment, while MUC1 expression was normal on surrounding cells [533], showing exclusion of MUC1 during cell-cell interactions. On the surface of activated T cells MUC1 is expressed evenly but becomes polarised to the leading edge when stimulated with the migratory chemokine RANTES, suggesting early involvement in interactions between T cells and endothelial cells [83]. This shows that while CD43, PSGL-1 and MUC1 vary in expression and localisation during cell activation and migration, all three undergo active relocation to some extent, highlighting their importance in cell-cell interactions. In recent decades, the exploration of the contribution of mucins to cancer progression and metastasis has gained significant attention. CD43 and MUC1 are over-expressed and aberrantly glycosylated on cancer cells and expression correlates with worse disease progression and survival [534, 535]. PSGL-1 specifically has been identified as a novel checkpoint inhibitor that suppresses T cell responses and serves as a prognostic biomarker [146, 536]. These examples serve to highlight the extensive implications of mucins in cell-cell interactions. Considering our novel finding of mucin down-regulation during T cell apoptosis, I hypothesised that through their size and negative charge, mucins create a biophysical barrier or shield, which must be reduced during apoptosis for efficient efferocytosis to occur. This, in turn, may position CD43, PSGL-1, and MUC1 as potential novel ”don’t-eat-me” signals.

5.1.1 Hypothesis

That CD43, MUC1 and PSGL-1 act as a “don’t-eat-me” barrier on T cells that is removed during apoptosis to facilitate efferocytic uptake.

5.1.2 Specific aims

I explore the impact of mucins on efferocytosis by:

1. Setting up a co-culture assay that allows apoptotic T cell uptake quantification
2. Assessing the impact of mucin and ADAM10 expression on uptake
3. Assessing the influence of the mucinase StcE on uptake

5.2 Results

5.2.1 Establishment of an MDM-apoptotic T cell co-culture assay

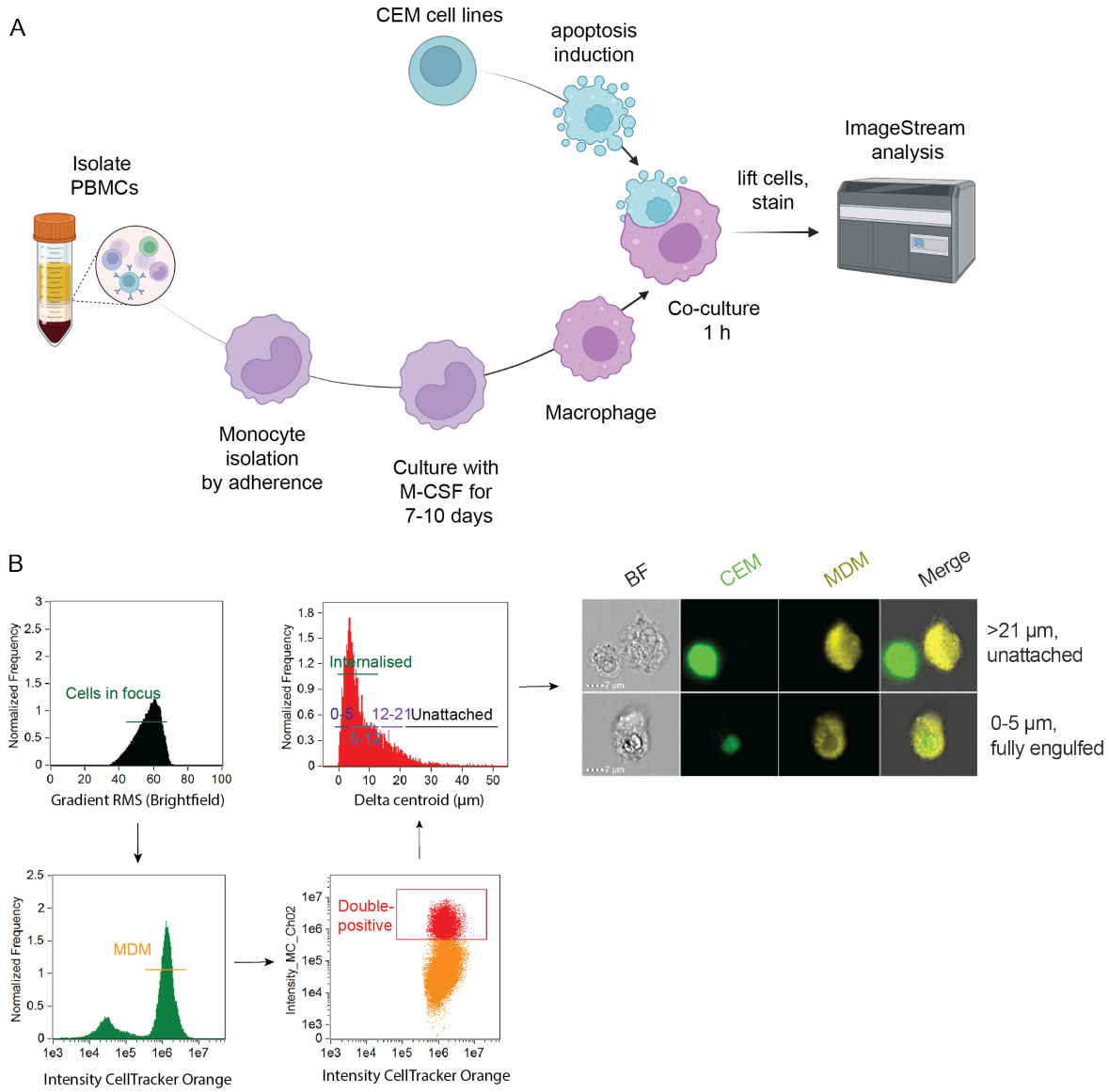


Figure 43: Effero Assay A) Schematic overview of the co-culture assay. B) Gating strategy on ImageStream software IDEAS. Cells were gated on cells in focus, monocyte-derived macrophages (MDMs), CellTracker Orange and CellTracker Green double-positive events, and the Delta Centroid function applied to cluster events into a 0-5 μm (engulfed), 5-12 μm (partially engulfed), 12-21 μm (attached) and $<$ 21 μm (unattached).

To establish the effects of mucins on efferocytic uptake, a co-culture assay was developed by a postdoctoral researcher Dr Maeva Dupont, along with Shengpan Zhang, a PhD student in the laboratory. Subsequent efferocytic quantification was performed using ImageStream, building on the methodology established previously in the lab by Baxter and colleagues [537] and subsequently modified according to Zhou and colleagues [538]. PBMCs were isolated from enriched donor blood and left to adhere on tissue culture plates in the absence of FCS (Figure

43A). The monocytes were then differentiated into monocyte-derived macrophages (MDM) in the presence of M-CSF for 7-10 days. M-CSF was used to polarise the MDM toward a more phagocytic and less inflammatory phenotype (M2-type), allowing us to study the efferocytic capacity of the donor macrophages. After complete differentiation, MDM were stained with CellTracker Orange and CEM were stained with CellTracker Green. In half the samples, apoptosis was induced using staurosporine as before and the other half were incubated with carrier (DMSO) as a control condition. After washing, CEM were stained with live/dead dye, washed again and added to the MDM for 1 h at a ratio of 1:1. Wells were carefully rinsed, and MDMs lifted using EDTA and gentle scraping. Cells were fixed, stained for Casp3 and run on an ImageStream, a flow cytometer with added fluorescence imaging capacity. Gating was performed on cells in focus, MDMs and CellTracker positive cells to isolate the green and orange events containing both MDMs and T cells (Figure 43B). The delta centroid function defines distances between the centre of two cells and allows gating based on distance: fully engulfed (0-5 μm), partially engulfed (5-12 μm), attached (12-21 μm) and unattached ($>$ 21 μm). Together, this allowed me to quantify how many apoptotic (Casp3-positive) and non-apoptotic (Casp3-negative) T cells were fully engulfed during the co-culture.

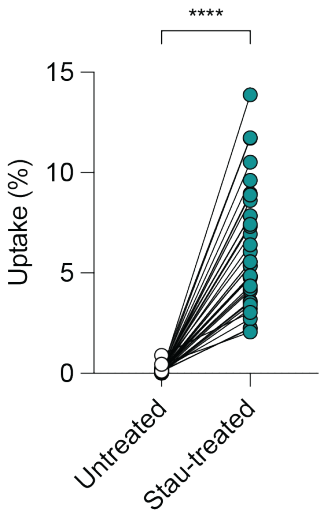


*Figure 44: Efferocytic uptake of healthy and apoptotic CEM by MDMs. Percent uptake of untreated or staurosporine-treated CEMs based on ImageStream assay. Each symbol represents one donor. Symbol fill colour indicates treatment: untreated (white), staurosporine-treated (teal) n = 36. Student t-test was performed **** $p<0.0001$.*

Using the ImageStream assay as outlined above, the percentage of MDM containing one or more apoptotic T cells was recorded. As samples would vary slightly in % apoptosis, an aliquot of T cells post-staurosporine treatment and before co-culture was saved to assess

apoptosis (% Casp3$^+$) by flow cytometry. This allowed me to normalise between experiments by dividing the % internalised, apoptotic T cells by the % of apoptotic T cells prior to co-culture. ”Uptake (%)” is henceforth defined as [% MDM-engulfed apoptotic T cells / % apoptotic T cells prior to co-culture] x 100. When testing untreated and staurosporine-treated WT CEM, uptake was significantly increased in CEM that had been treated with staurosporine (Figure 44). This confirmed efferocytic capacity of the MDM *in vitro* and indicates that MDM preferably take up apoptotic cells, validating this assay.

5.2.2 Efferocytic clearance of apoptotic MUC1$^{-/-}$ and PSGL-1$^{-/-}$ CEM

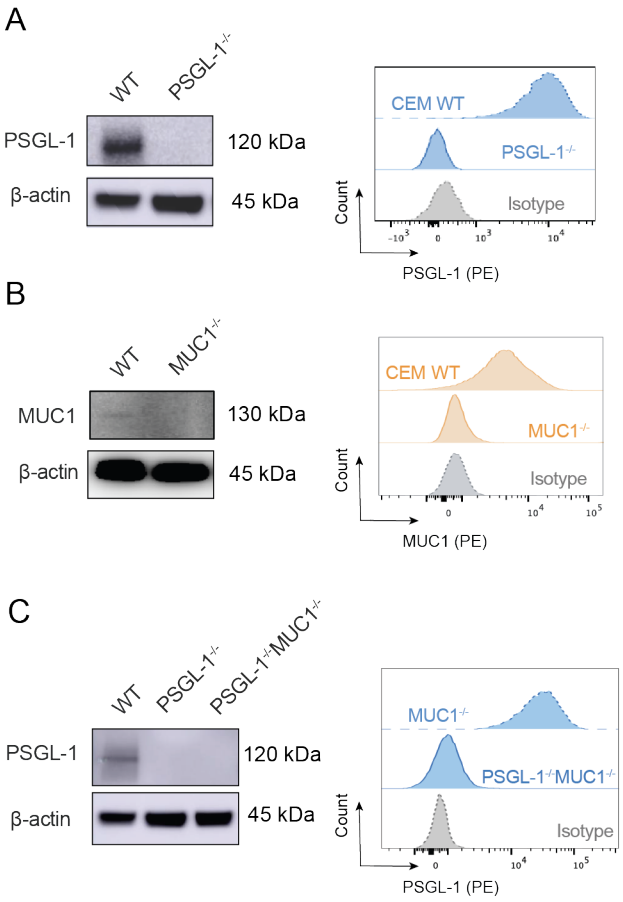


Figure 45: Validation of mucin knockouts by Western blot and flow cytometry. A Western blot was performed for WT and knockout cells probing for PSGL-1 (A, C) or MUC1 (B) and β-actin. Healthy cells were stained and analysed by flow cytometry. A) PSGL-1 WT (blue, dashed), PSGL-1$^{-/-}$ (blue), IgG$_1$-PE isotype control (grey, dashed) B) MUC1 WT (yellow, dashed), MUC1$^{-/-}$ (yellow), IgG$_1$-PE isotype control (grey, dashed) C) MUC1 WT (blue, dashed), PSGL-1$^{-/-}$MUC1$^{-/-}$ (blue), IgG$_1$-PE isotype control (grey, dashed)

To test the potential impact of different mucins on efferocytosis PSGL-1 was knocked out in CEM cells using a CRISPR/Cas9 system as described in Material and Methods on page 49. Cells were single-cell sorted and pre-screened for PSGL-1 and MUC1 expression by flow cytometry. Promising clones were pooled and tested by Western blot to confirm expression in the whole cell lysate (Figure 45A, B). As discussed in Chapter 1, MUC1 expression on CEM cells is weak and probing MUC1 yielded a faint, but visible signal (Figure 45B). In order to generate a double knockout cell line (PSGL-1$^{-/-}$MUC1$^{-/-}$ CEM), PSGL-1 was knocked out in the MUC1$^{-/-}$ CEM. This decision was motivated by a lower CRISPR efficiency observed during the creation of the MUC1$^{-/-}$ CEM combined with difficult detection by Western blot. The challenges encountered when blotting and staining for MUC1 meant that knocking out PSGL-1 in an already confirmed MUC1$^{-/-}$ cell line allowed me to probe for PSGL-1 instead

(Figure 45C). PSGL-1$^{-/-}$MUC1$^{-/-}$ CEM cells were more susceptible to staurosporine treatment, whereby using the same concentration and duration as previously resulted in a more pronounced apoptotic population compared to WT or single knockout cells.

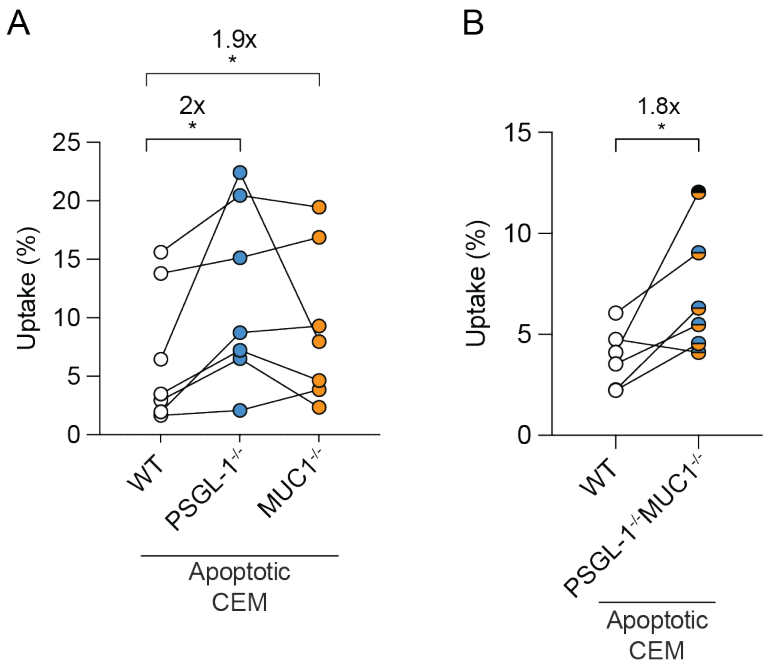


*Figure 46: Efferocytic uptake of apoptotic CEM by MDMs. Percent uptake of apoptotic CEM cell lines based on ImageStream assay. Each symbol represents one donor. Symbol fill colour indicates cell line: WT (white), PSGL-1$^{-/-}$ (blue), MUC1$^{-/-}$ (yellow), and PSGL-1$^{-/-}$MUC1$^{-/-}$ (half blue, half yellow). n = 5-7. A) One-way ANOVA and B) student t-test was performed * $p<0.05$*

Next the above cell lines were tested in the ImageStream assay (Figure 46). When calculating the uptake of apoptotic WT CEM compared to apoptotic PSGL$^{-/-}$ CEM, the latter cell line was efferocytosed more (a factor of 2-fold). Uptake was similarly increased when MUC1 was knocked out (1.9-fold). When both PSGL-1 and MUC1 were knocked out, an increased uptake was recorded (1.8-fold), however the uptake of the double knockout cell line was comparable to the single knockout lines. These data indicate that loss of mucins facilitates uptake by MDM *in vitro*. Shengpan Zhang conducted analogous experiments using the CD43$^{-/-}$ CEM cells available in the Sattentau laboratory. Hence, CD43$^{-/-}$ CEM cells are not investigated in this thesis.

5.2.3 Influence of modified ADAM10 activity and mucinase treatment on efferocytosis

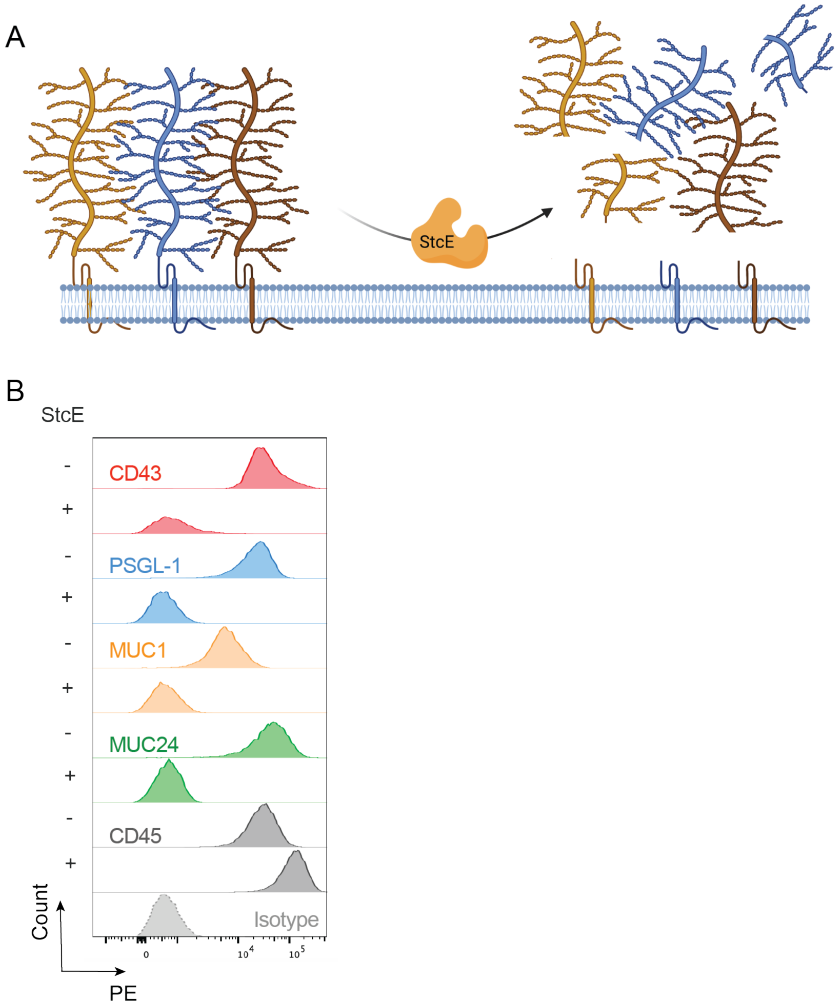


Figure 47: Mucinase StcE cleaves CD43, PSGL-1, MUC1 and MUC24, but not CD45 on healthy CEM. A) Schematic overview of StcE cleaving mucins. B) Histograms showing health CEM that remained untreated (-) or have received (+) StcE treatment. CD43 (red), PSGL-1 (blue), MUC1 (yellow), MUC24 (green), CD45 (dark grey), IgG_1-PE isotype control (light grey, dashed)

StcE (secreted protease of C1-esterase inhibitor) is a zinc metalloprotease secreted by Enterohemorrhagic *Escherichia coli* (EHEC) [539], that specifically cleaves the glycosylated extracellular domain of mucin-like molecules such as CD43, PSGL-1, MUC1 and CD45 [540]. While this has been established on neutrophils, soluble mucins, and the epithelial cell lines CF10A and MCF10A [23, 539, 540], StcE function was characterised on CEM cells (Figure 47A). The Bertozzi lab kindly provided purified, entodoxin-free StcE enzyme. Healthy CEM were treated with 2 μg/mL StcE for 1 h prior to surface staining and subsequent analysis by flow cytometry. Interestingly, a rapid decrease in antibody binding was observed for CD43, PSGL-1, MUC1 and MUC24 and fluorescence in StcE-treated samples for those molecules

were comparable to background levels and the isotype control (Figure 47B). Only a small shift in CD45 labelling was recorded. Overall, StcE treatment provided a rapid method for rapidly and simultaneously eliminating mucins from the cell surface of CEM.

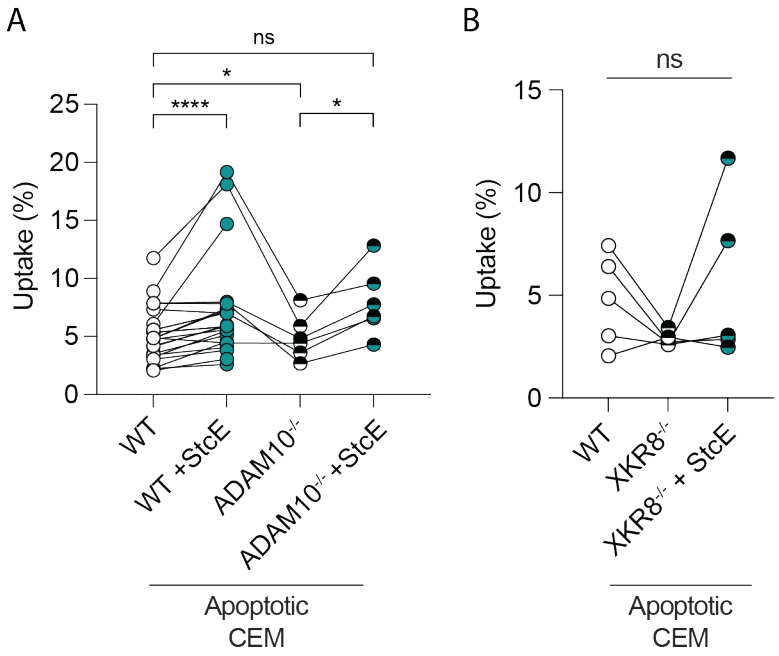


*Figure 48: Efferocytic uptake of apoptotic ADAM10$^{-/-}$ and XKR8$^{-/-}$ CEM by MDMs. Percent uptake of apoptotic CEM cell lines based on the ImageStream assay. All data represent the uptake (%) of staurosporine-treated CEM cells. Each symbol represents one donor. Teal colour indicates StcE treatment. Half-filled symbols represent knockout cell lines: A) ADAM10$^{-/-}$ and B) XKR8$^{-/-}$. n = 5-21. One-way ANOVAs were performed *** $p<0.001$, * $p<0.05$, ns = not significant*

Considering that the PSGL-1$^{-/-}$ and MUC1$^{-/-}$ CEM showed preferential uptake by MDMs in the co-culture assay, I hypothesised that simultaneous removal of multiple mucins by StcE on CEM might lead to an increase in uptake by MDM. As shown in Chapter 2, CD43, PSGL-1 and MUC1 cleavage is inhibited on apoptotic ADAM10$^{-/-}$ CEM. I further hypothesised that mucin retention on the cell surface through ADAM10 inactivity might result in the decreased efferocytic uptake of apoptotic ADAM10$^{-/-}$ CEM by MDMs. To investigate this, the co-culture assay was repeated with WT and ADAM10$^{-/-}$ CEM. Seeing as StcE reduces the glycan shield to a minimum [23], half the conditions were treated with StcE prior to apoptosis induction and co-culture. Compared with apoptotic WT cells, uptake of apoptotic, StcE-treated WT cells was significantly increased (Figure 48A). Apoptotic ADAM10$^{-/-}$ CEM uptake was reduced compared to WT cells with functional expression of ADAM10. As anticipated, more StcE-treated ADAM10$^{-/-}$ CEM were efferocytosed than untreated ADAM10$^{-/-}$ whereas there was no difference between WT cells and StcE-treated ADAM10$^{-/-}$ CEM. This implied that StcE

treatment potentially mitigated ADAM10 deficiency. To investigate if lack of PS scrambling through XKR8 knockout had similar effects on efferocytosis as ADAM10 knockout, the assay was repeated with $XKR^{-/-}$ CEM. The data depicted in Figure 48B exhibited a potential trend in decreased uptake of $XKR8^{-/-}$ compared to WT cells, which seemed to increase again with StcE treatment, however none of the conditions achieved statistical significance.

5.2.4 Efferocytic clearance of apoptotic primary CD4⁺ CD43$^{-/-}$ CEM

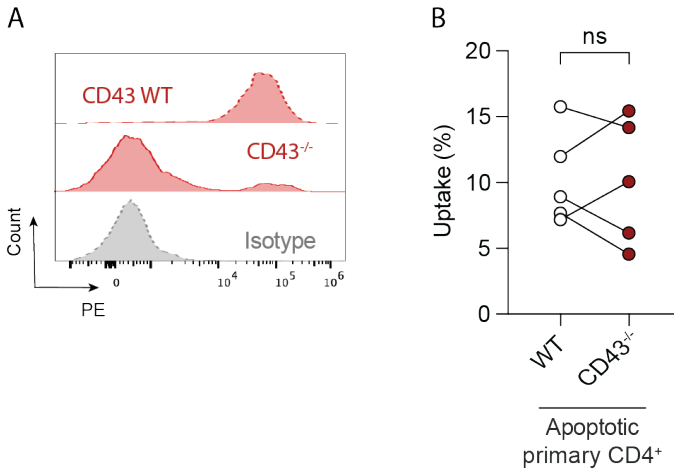


Figure 49: CD43 knockout in primary CD4⁺ T cells. A) WT and knockout cells were probed and analysed by flow cytometry: CD43 WT (red, dashed), CD43$^{-/-}$ (red), IgG$_1$-PE isotype control (grey, dashed) B) CD43 WT (white), CD43$^{-/-}$ (red). n = 5. A student's t-test was performed. ns = not significant

Next, CD43 was knocked out in primary T cells. For this a platform for primary cell CRISPR-knockouts was used which was established by Jose Cabezas Caballero, a DPhil student in Prof Omer Dushek's lab. In short, CD4⁺ T cells were isolated from human cone blood and knocked out for CD43 using a CRISPR/Cas9 system as described in Materials and Methods on page 50. Due to the limited number of these cells, the knockout efficiency was evaluated, without performing a Western blot, by flow cytometry (Figure 49A), which was approximately 90%. For all previous knockouts, a cell sort was performed to attain a full knockout population. However it was considered that sorting cells might impact their health and subsequent behaviour in a functional assay, particularly given the limited size of the cell population that retained CD43 expression. Therefore a bead pull-down was conducted of all positive cells by labelling with anti-CD43-APC and using anti-APC beads. Subsequently the primary WT and CD43$^{-/-}$ CD4⁺ T cells were treated with staurosporine and conducted an efferocytosis assay, however no significant difference was observed (Figure 49B).

5.3 Discussion

The findings obtained in Chapter 2 prompted me to hypothesise that T cells downregulate CD43, PSGL-1, and MUC1 during apoptosis to diminish the steric hindrance imposed by these mucins on the cell surface and that downregulation might facilitate clearance by phagocytes. This chapter aimed to test this hypothesis by modifying mucin expression on CEM cells and by quantifying efferocytic uptake in a co-culture assay. When testing apoptotic PSGL-$1^{-/-}$ CEM and $MUC1^{-/-}$ CEM, both were preferentially engulfed by MDMs compared to WT CEM expressing PSGL-1 or MUC1. While expression of CD43, PSGL-1 and MUC1 is downregulated on apoptotic T cells, residual mucins of approximately 10-20% still remained on the cell surface. The increased efferocytic uptake observed with the knockouts confirmed these expectations. Apoptotic PSGL-$1^{-/-}$$MUC1^{-/-}$ double-knockout CEM were also preferentially taken up compared to their WT counterparts, however a similar increase of uptake was observed compared to the single knockout cells. Since the knockout of PSGL-1 or MUC1 alone led to a two-fold uptake, a greater impact of both mucins lacking on the cell surface was expected. While the double-knockout cell line survived genetic editing and did grow, cell doubling time was longer compared to all other CEM cell lines and an increased susceptibility to staurosporine treatment was observed. While the quantified efferocytic uptake (%) accounts for fluctuations of apoptosis percentages between samples, this might only compensate for differences to a certain extent. Titrating staurosporine to induce similar levels of apoptosis in PSGL-$1^{-/-}$$MUC1^{-/-}$ CEM and WT CEM would confirm if the same or an increased uptake can be observed. To my knowledge, there have been no prior reports of PSGL-$1^{-/-}$$MUC1^{-/-}$ double knockout cell lines or organisms. Consequently it is difficult to know if the observed phenotype of slowed growth and increased susceptibility to apoptosis inducers results from potential off-target effects of the gRNAs used or if it reflects a inherent cellular response to the absence of both mucins. If this reflects the inherent phenotype of PSGL-$1^{-/-}$$MUC1^{-/-}$ knockout, the possibility of a compensatory over-expression of alternative mucins or other don't-eat-me signals must be considered, which might explain the limited increase in uptake. A limitation of the assay is that the uptake index reflects the proportion of MDMs that have internalised one or more apoptotic CEM, but does not discriminate between the actual number of apoptotic cells that were ingested, given that macrophages can phagocytose multiple cells simultane-

ously [541]. Therefore in the case of my knockout CEM, an upper limit for MDM ingestion might have been reached through which no further increase might have been possible in the case of the PSGL-1$^{-/-}$MUC1$^{-/-}$ CEM. Interestingly, in an *in vivo* embryonic development model, macrophages have been shown to efferocytose apoptotic corpses in numbers as high as 20 per macrophage [541]. In my system co-culture was conducted at a ratio of 1:1, whereby approximately 40-60% of CEM were apoptotic. Therefore based on cell numbers, MDMs were unlikely to become overburdened in my specific experimental settings. However, the apoptotic corpses described by Raymond and colleagues are roughly 3 μm in size, whereas CEMs are notably larger, measuring around 10 μm in diameter [542]. Assuming the overall efferocytic capacity of *in vivo* macrophages and the MDMs in the *ex vivo* assay performed in this thesis are equivalent, macrophages are likely to engulf fewer apoptotic cells in the case of CEM. Despite these considerations, the factors contributing to the observed plateau in uptake when knocking out both PSGL-1 and MUC1 might be more likely due to phenotypic reasons, as PSGL-1$^{-/-}$MUC1$^{-/-}$ cells were highly susceptible to Staurosporine treatment. Further reasons could be the variability of the assay or a combination of all above reasons.

StcE treatment led to rapid cleavage of CD43, PSGL-1, MUC1 and MUC24, which aligns with previous reports [540, 543, 544] apart from MUC24, which to my knowledge has not previously been investigated for StcE mucinase cleavage. CD45 cleavage was not observed post-StcE treatment, contrary to previous findings by Malaker and colleagues [540], who reported that recombinant CD45 is cleaved by StcE. In their study CD45 was expressed by NS0 murine hybridoma cells [540] and little is known about the O-glycosylation profile of those cells [545]. Given that StcE cleavage is dependent on the glycosylation profile of a glycoprotein, this could explain why on CEM cells, no reduction of CD45 antibody binding could be observed post StcE treatment. CD45 has six described isoforms that vary in length and glycosylation [101]. The CD45 mucin domain is located at the N-terminus, which might influence cleavage and antibody binding depending upon the epitope location. Furthermore, specific isoforms can be targeted depending on the antibody used, or all isoforms can be detected by binding a conserved portion of the protein. Goh and colleagues tested CD45 cleavage by StcE on neutrophils using the antibody clone UCHL1, which binds to the R0 isoform of CD45 [545]. The clone that was used in this thesis is MEM-28. According to the manufacturer, MEM-

28 was prepared from human thymocytes and T lymphocytes and reacts with all alternative forms of human CD45 antigen. This suggests that this antibody binds to a conserved part of the molecule distal from the N-terminal mucin domains. Thus the absence of reduced anti-CD45 labeling on CEM cells could potentially be attributed to cleavage occurring N-terminally to the antibody binding site. Based on the existing literature, it can be inferred that CD45 undergoes cleavage; however cleavage remains undetected by MEM-28.

Apoptotic WT CEM were preferentially taken up if treated with StcE mucinase prior to co-culture and ADAM10 knockout led to decreased uptake. ADAM10$^{-/-}$ can be expected to retain expression of CD43, PSGL-1, MUC1 and perhaps other unidentified mucins during apoptosis and reduced uptake indicates that the lack of removal of these mucins results in decreased efferocytosis. A stronger effect might have perhaps been expected, however several parallel mechanisms might have contributed to a reduced reduction in uptake. During apoptosis, sialic acid residues are removed on glycoproteins of lymphocytes [474, 546], which reduces the charge of the biophysical barrier and probably makes the cell more accessible for phagocytosis. For example, additional treatment of apoptotic lymphocytes with neuraminidase led to increased engulfment [474]. This highlights a natural removal of charge from the mucin-shield, which together with other eat-me signals such as PS [547] might lead to moderate uptake even if ADAM10-mediated shedding was impaired, explaining only slightly reduced uptake in ADAM10$^{-/-}$ versus WT cells. When apoptotic ADAM10$^{-/-}$ CEM were treated with StcE more cells were taken up than before treatment and uptake was comparable with WT cells indicating a rescue effect imposed by StcE. Interestingly, in other studies NK-mediated cytotoxicity increased when target cells were de-mucinated by StcE [543, 548], indicating increased interaction when the steric barrier imposed by mucins is reduced. While PS exposure by itself was not enough to trigger engulfment of healthy cells [474], PS exposure paired with desialylation led to uptake of even non-apoptotic cells [549]. However some studies suggest that removing the charge of the mucin shield might not be as important as the physical size of the mucins. Park and colleagues described that the specific glycocalyx composition is less important than the glycocalyx thickness [548] and the John lab have found that the length of MUC1 is the determining factor during inhibition of ligand-mediated cell-cell interactions rather than its charge [525]. Future studies including parallel experiments with StcE or siali-

dase treatment of apoptotic cells might offer valuable insights into the relative importance of size and charge of the mucin shield during efferocytosis.

StcE not only cleaves CD43, PSGL-1 and MUC1 but also the strongly expressed MUC24 and, as reported, a component of CD45. Therefore, StcE treatment of ADAM10$^{-/-}$ CEM was expected to exceed WT levels. However this could be due to the limited sample size used for ADAM10$^{-/-}$ experiments and repeating the experiment with more donors might confirm trends more clearly. Uptake of apoptotic XKR8$^{-/-}$ CEM was indifferent from that of apoptotic WT cells, and did not change further when treated with StcE, however certain trends are visible that suggest cells lacking XKR8 expression might be engulfed less and that there might be a potential rescue effect of StcE. This was somewhat surprising as apoptotic XKR8$^{-/-}$ cells not only still express CD43, PSGL-1 and MUC1 but also lack the strong eat-me signal of PS expression on the cell surface. Therefore the XKR8 knockout was expected to cause an even stronger phenotype than ADAM10 knockout, however more repeats might be able to confirm the trends observed in my data. Kawano and Nagata have shown that whereas apoptotic murine lymphocytes and neutrophils are well efferocytosed but if XKR8, the only XKR protein containing a Casp3 cleavage site expressed in murine haematopoietic cells, is knocked out, apoptotic cells were hardly engulfed [422], supporting the trend seen in my data. Further they saw increased accumulation of apoptotic thymocytes in the thymus and an increase in senescent neutrophils in the spleen. XKR8-null mice presented with SLE-like symptoms, auto-antibodies and splenomegaly, which aligns with symptoms of impaired efferocytosis and secondary necrosis in other studies [235, 286, 288, 522]. The observation of increased senescence in XKR8-deficient neutrophils underscores the broader implications of XKR8 beyond apoptosis and that its role in ADAM10-mediated mucin cleavage and efferocytic uptake should be explored further.

Due to limited cell numbers, primary CD43$^{-/-}$ T cells were confirmed for knock out by flow cytometry with subsequent bead-pull down of CD43-expressing cells and not Western blot or PCR. If repeated, the experimental settings should be adjusted to allow for testing by Western blot, for example reducing the co-culture step from a 6-well plate layout to a smaller 24-well plate. The absence of any differences in uptake between WT primary cells was unexpected,

but could potentially be attributed to the limited number of donors used. This was the first time the assay was used for primary T cells and including an StcE condition as a positive control would have been beneficial for comparison and validation. However, similar to my results, Yi-Yi and colleagues found that in a non-apoptosis phagocytosis assay, uptake of $CD43^{-/-}$ tumour cells and WT tumour cells by murine macrophages was at similar levels [550]. CD47, a member of the immunoglobolin superfamily and a well characterised don't-eat-me signal, is clustered in lipid rafts eliciting an inhibitory signal upon ligation with SIRPα on phagocytes. During apoptosis however, CD47 becomes dispersed, reducing its inhibitory potential [551]. While CD47 does not belong to the mucin family and its mechanism as a don't-eat-me signal is distinct from the mechanism described in this thesis, a similar study based on CD43 localisation has shown that CD43 moves to the uropod via lipid rafts during T cell activation [530]. Freeman and colleagues showed specific exclusion of chimeric molecules expressing the CD43 ectodomain during frustrated phagocytosis [552]. Hence, the combined effects of ADAM10-mediated CD43 shedding and potential re-distribution of any remaining CD43 molecules could result in a highly efficient reduction or removal of the contribution of CD43 to the biophysical barrier on apoptotic T cells. This might explain why a knockout of CD43 does not exhibit any additional impact on efferocytosis in my experiments. Regardless of this however, expanding the sample size should be considered.

My findings in this chapter confirm the importance of ADAM10-mediated mucin shedding during apoptosis for efficient efferocytic clearance. Other scramblases such as the Ca^{2+}-inducible TMEM16 proteins are capable of altering PS symmetry [376]. PS has previously been detected on the outer membrane of $CD4^{+}$ $CD25^{hi}$ T_{reg} cells [553] and is externalised rapidly in T cells upon TCR signalling by pMHC engagement [554]. Considering the broader influence of mucins on cell-cell interactions beyond efferocytosis, the hypothesis was formulated that PS-activated ADAM10 might cleave mucins on activated T cells, which was explored in the following chapter.

6 Downregulation of Mucin-like Molecules in Activated T cells

6.1 Introduction

In this chapter I investigate mucin expression during T cell activation. Shortly after the discovery of mucin expression on T cells, the role of mucins in T cell activation was explored. CD43, PSGL-1, MUC1 and CD45 have all been attributed regulatory roles during T cell activation. CD43 is capable of prolonging the duration of TCR signalling by lowering the T cell activation threshold [555, 556]. MUC1 has been attributed a co-inhibitory role during T cell activation [557, 558], similar to PSGL-1, which has been described as a checkpoint molecule by regulating TCR signalling, increasing inhibitory receptor expression and exacerbating T cell exhaustion through low-pH dependent binding of VISTA [61, 146, 532, 557, 559]. CD45 has been shown to activate Lck, which in turn phosphorylates the TCR [560, 561]. At the same time CD45 can suppress CD3ζ-chain phosphorylation in response to both antigen-independent and low-affinity antigen signals [562]. Due to its dual role in modulating TCR signaling, CD45 has been termed a ”gatekeeper” of TCR signalling [562]. To my knowledge, MUC24 has not yet been studied in T cell activation. While CD43, PSGL-1, MUC1, and CD45 are traditionally associated with adhesion and proliferation [55, 83, 124, 139, 527, 529–533, 563–565], it is evident that they also play important regulatory roles in T cell activation. Further to its regulatory function, Tinoco and colleagues found that PSGL-1 is excluded from the immunological synapse by interactions with the cytoskeletal adaptor ERM proteins ezrin, radixin and moesin [62, 566]. Even though one group described that CD43-mediated regulation of T cell activation is not due to steric hindrance [567], others have found that is still excluded from the T cell synapse in a similar way by ERM proteins, and that blocking removal of CD43 from the immunological synapse led to decreased IL-2 and IFN-γ production, crucial for successful T_h1-type cell activation [424, 568, 569]. Interestingly, CD45 is not only removed from the T cell synapse [425], but is pre-excluded from microvilli even prior to antigen encounter [570]. The relationship between the regulatory roles of mucins and their molecular attributes, such as their large size and negative charge, has not yet been fully characterised, particularly in the context of lymphocyte activation.

A common activation model for use *in vitro* is treatment with PMA/ionomycin [571]. PMA is a phorbol ester which activates protein kinase C (PKC) and leads to a slight elevation in intracellular Ca^{2+} [572–574]. Ionomycin, while also capable of activating PKC (Protein Kinase C) [571], chemically functions as an ionophore by inducing an intracellular Ca^{2+} flux in T cells through Ca^{2+} release from intracellular stores into the cytosol [571, 575, 576]. TMEM16F is an intra-membrane protein that has functional properties of both an ion channel and a phospholipid scramblase and its activity is regulated through a Ca^{2+}-binding site at its N-terminal domain [376, 577, 578]. It is recognised as the dominant lipid scramblase in murine T cells and is capable of flipping PS to the outer leaflet of the membrane of $CD4^+$ and $CD8^+$ T cells when stimulated with the calcium ionophore A23187 [513]. Similarly, Bricogne and colleagues have showed that in Jurkat T cells, ionomycin treatment leads to the rapid elevation of cytoplasmic Ca^{2+}, which results in membrane expansion, TMEM16F activation and subsequent PS flipping [401]. During TCR-mediated activation, TMEM16F is recruited to the immunological synapse, where it plays an essential role in cSMAC formation. Additionally, it can be included in late endosomes, sequestering intracellular TCR signaling complexes for subsequent lysosomal degradation, contributing to the termination of T cell activation [513]. During TCR-mediated activation of T cells, PS is also flipped to the outer leaflet of the membrane [554]. This highlights the importance of TEMEM16F-mediated PS flipping during T cell activation though both ionophore stimulation and TCR-mediated activation.

Based on my findings from Chapter 3, 4 and 5 and the above literature, it was considered that CD43, PSGL-1 and MUC1 might negatively affect T cell : APC interaction either through steric hindrance or negative signalling and thus shedding of mucins from activated T cells might enhance T cell activation. Furthermore it was considered that that their exclusion from the immunological synapse might be the initial step preceding cleavage by a PS-activated ADAM10. Therefore, characterising the dynamics of mucins on PMA/ionomycin and TCR-activated T cells could help us gain a deeper understanding of their role in T cell activation.

6.1.1 Hypothesis

That mucins are shed during T cell activation as a potential mechanism to positively regulate T cell activation.

6.1.2 Specific aims

I explore the expression of cell surface mucins during T cell activation through:

1. Monitoring mucin expression on T cells in an ionophore activation assay

2. Assessing mucin expression during TCR-mediated activation in a T cell-antigen presenting cell (APC) co-culture assay

6.2 Results

6.2.1 Mucin expression on ionophore-activated Jurkat cells

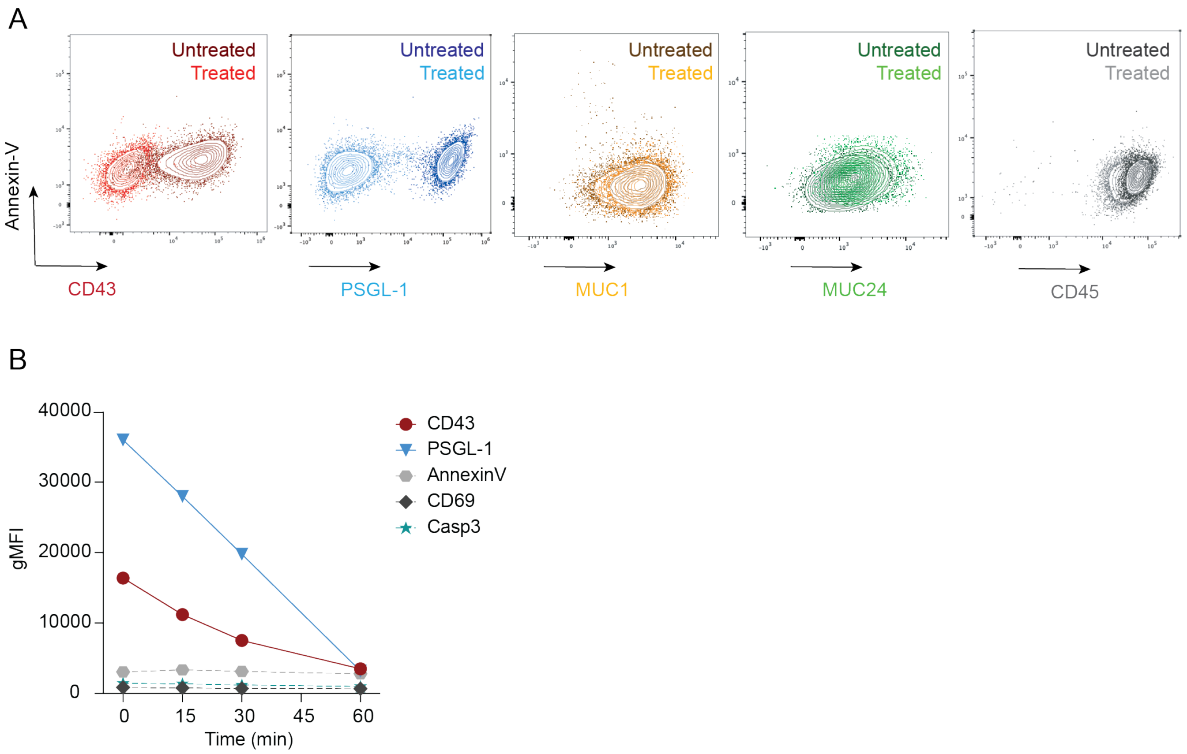


Figure 50: Jurkat lose CD43 and PSGL-1 labelling when treated with ionophores. A) Contour plots of CD43 (red), PSGL-1 (blue) and CD45 (dark grey) against annexin-V of PMA/ionomycin-untreated and treated cells B) Timecourse experiment of treatment at 0, 15, 30 or 60 min with PMA/ionomycin. gMFI is plotted over time for all markers: CD43 (red circle), PSGL-1 (blue triangle), annexin-V (light grey hexagon), CD69 (dark grey rhombus) and Casp3 (teal star). n = 1

To develop an activation assay, Jurkats cells were used as they are a well-established $CD4^+$ T cell line used for immunological research in general, and signalling and activation studies in particular [579]. Based on the literature [401], an initial experiment was performed in which healthy Jurkats were treated using ionomycin and PMA at 25 μg/mL or carrier only (DMSO) at 37ºC for 60 min. The samples were immediately put at 4ºC following the completion of the experiment, and the subsequent antibody staining was also carried out at 4ºC to stop any potential endocytic processes [580]. Samples were subsequently stained for CD43, PSGL-1, MUC1, MUC24 and CD45 (Figure 50A). After treatment, a significant reduction in CD43 and PSGL-1 labelling was observed, whereas MUC1, MUC24, and CD45 levels remained unchanged. As a result, CD43, PSGL-1, and CD45 were chosen as a focus for further analysis, with CD45 serving as a negative control. When repeating the experiment as a timecourse with 0, 15, 30 and 60 min of treatment, PSGL-1 and CD43 labelling was gradually lost from the

cells and staining is comparable to background after 60 min (Figure 50B). To ensure any observed effects seen in mucin labelling were not due to apoptosis-induced shedding, a Casp3 staining was included, which remained negative throughout the timecourse. CD69 is an early activation marker on T cells [581], however staining remained negative. Annexin-V labelling was negative also (Figure 50B).

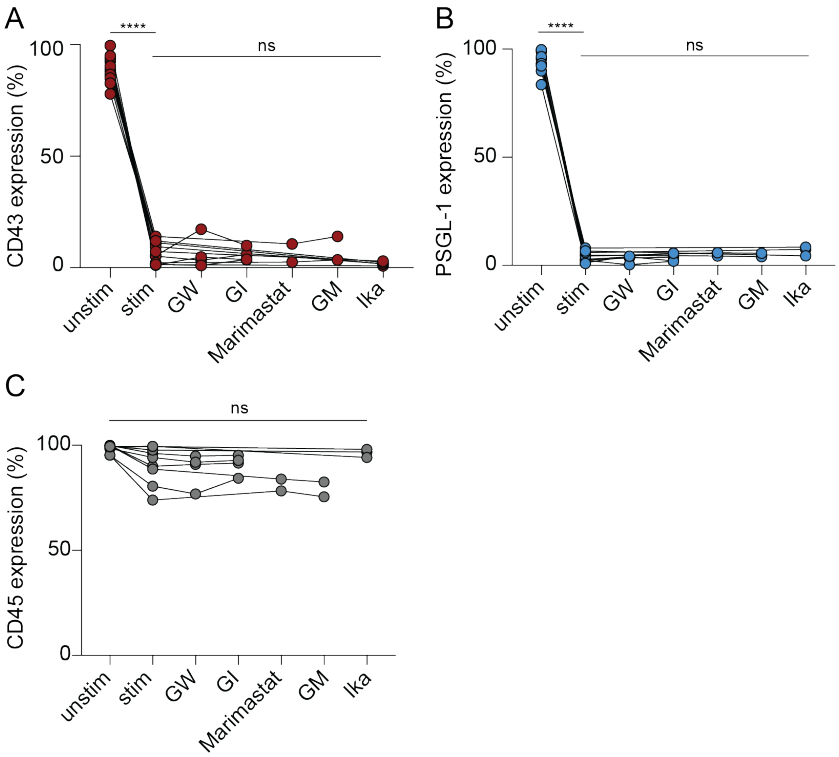


*Figure 51: Metalloprotease and endocytosis inhibitor-treated, stimulated Jurkat cells lose labelling of CD43 and PSGL-1 but not CD45. Jurkat cells were either treated with carrier only (unstim), with PMA/ionomycin (stim) or were pre-incubated with GW, GI, Marimastat, GM or Ikaraguamycin (Ika) in addition to PMA/ionomycin treatment. A) CD43 (red) B) PSGL-1 (blue) C) CD45 (grey). n = 3-13 one-way ANOVA was performed. **** $p<0.0001$, ns $p>0.05$*

To investigate if the observed loss of antibody labelling was due to ADAM10, healthy Jurkats were pre-incubated with GW and GI inhibitor prior to stimulation with PMA/ionomycin as before, and maintained their presence during the stimulation. GW and GI had no effect on loss of CD43 and PSGL-1 antibody labelling (Figure 51A,B) and no changes were observed in CD45 labelling (Figure 51C). To investigate a possible loss of binding due to shedding by other metalloproteases, the broad-spectrum matrix metalloprotease inhibitors Marimastat and GM6001 (GM, also known as Ilomastat) were used. Both are strong pan-metalloprotease inhibitors with small differences in the efficiency of their inhibition of various matrix metalloproteinase classes [582]. Marimastat and GM treatment resulted in no change of mucin loss. Considering the ineffectiveness of the several metalloprotease inhibitors combined with

the lack of annexin-V binding, I hypothesised that a different mechanism than ADAM10 (or another metalloprotease)-mediated shedding might be the underlying cause for CD43 and PSGL-1 loss of labelling during stimulation. To exclude internalisation, Ikaraguamycin (Ika) was used, which was first discovered as a macrolactam antibiotic however also functions as an efficient inhibitor of clathrin-mediated endocytosis [583]. Ika did not inhibit loss of CD43 or PSGL-1 labelling and had no effect on CD45 staining. More studies are needed to elucidate whether CD43 and PSGL-1 are degraded, shed by non-metalloproteases or undergo antigenic changes.

6.2.2 Mucin expression on primary T cells activated by TCR engagement

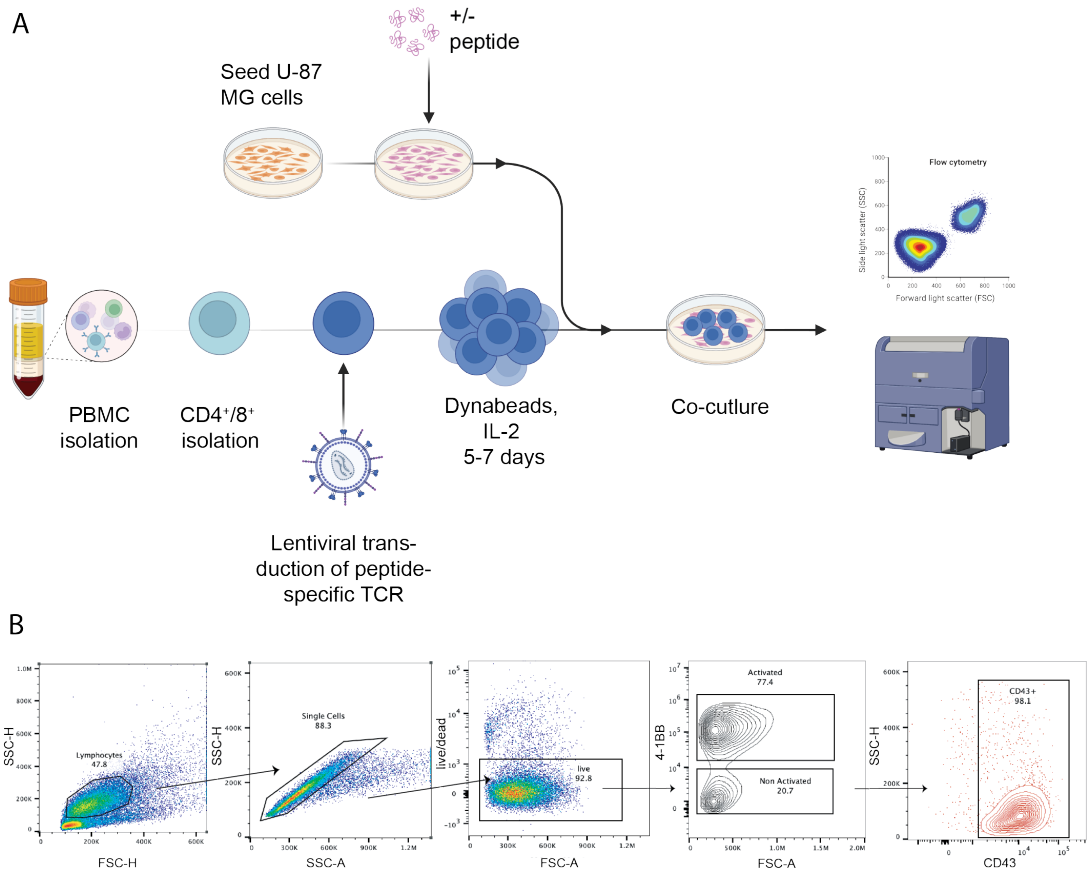


Figure 52: T cell activation by TCR engagement. A) Cartoon outlining the workflow of primary T cell isolation, transduction and co-culture with peptide loaded U-87 MG cells. B) Representative FACS plots of T cells after a 20 h co-culture. Gating strategy: lymphocytes, single cells, live cells, 4-1BB-positive and negative, followed by gating on the relevant marker, here 4-1BB-negative CD43-positive.

While *in vitro* T cell activation with PMA and ionomycin is well established, no T cell activation marker could reliably be used to verify activation in the prior experiment as the time-course was too short. To probe whether activation was the true trigger of the observations made

and to use a more physiological model, a method established in Prof Omer Dushek's lab was used with the help of Jose Cabezas Caballero, a DPhil student in the Dushek lab (Figure 52A). $CD4^+$ or $CD8^+$ T cells were isolated from human leukocyte cones and immediately transduced with lentiviruses containing a TCR specific for the NY-ESO-1 tumor-specific peptide. T cells subsequently received IL-2 and CD3/CD28 Dynabeads® for 5-7 days. After sufficient expansion, U-87 MG cells, an immortalised cell line from a glioblastoma patient with epithelial morphology [584], were seeded and either pulsed with 100 nM peptide or left untreated. U-87 cells endogenously express HLA-A*02:01, which is capable of binding the NY-ESO-1 peptide. T cells were co-cultured with U-87 MG cells at a ratio for 2:1 and analysed by flow cytometry. 4-1BB (CD137) is a glycoprotein receptor and a member of the TNF superfamily [585]. While CD69 is an early T cell activation marker which is detectable as early as 2-3 h post activation [581], 4-1BB is a widely used marker for mid-late T cell activation. 4-1BB expression is induced by TCR engagement and peaks at around 24 h [586], however its expression has been reported as detectable as early as 6 h post-activation [587, 588]. Signalling through interleukins and interferons such as IL-2, IL-4, IL-12, IFN-α and IFN-γ can increase surface expression of CD69, suggesting CD69 is most reliable when used in tandem with at least one other activation marker [589–591]. Therefore, CD69 was used in conjunction with 4-1BB for detection of activation in this assay. Gating was performed as follows: lymphocytes were gated based on forward scatter (FSC) and side scatter (SSC) before doublets and live/dead cell dye, to allow exclusion of dead cells with dye-permeable membranes. Subsequent gating was carried out on 4-1BB to differentiate between activated and non-activated T cells, followed by single mucin staining (Figure 52B).

To monitor the progression of activation over time, and several control markers were examined on T cells of one donor in a timecourse experiment. A single donor was used because the number of cells available per donor was limited, and this experiment was primarily designed to provide initial insights into the dynamics of this activation model. Figure 53A showed a gradual increase of 4-1BB in the first 4 h followed by a rapid increase, while CD69 expression increased immediately and then levelled off after 4 h. Annexin-V gradually increased and seemingly reached a plateau after 10 h. To ensure that my results were not affected by activation-induced cell death (AICD), a Casp3 staining was incorporated in samples from

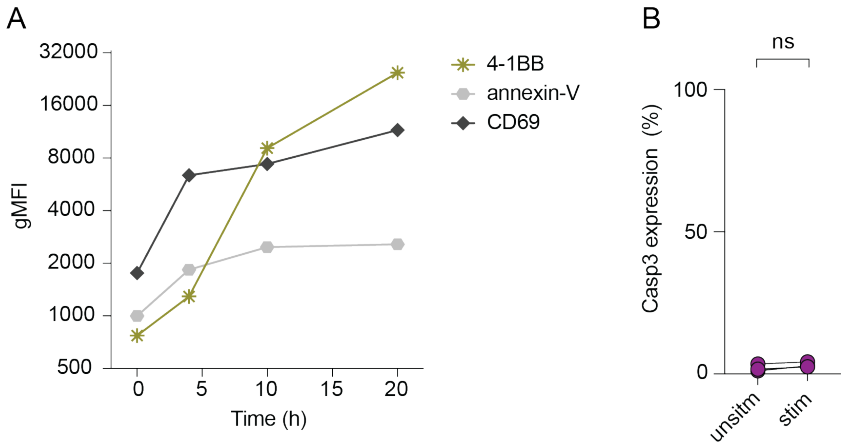


Figure 53: Validation of T cell activation by TCR engagement. A) timecourse of 4-1BB (asparagus star), annexin-V (light grey hexagon) and CD69 (dark grey rhombus) between 0 - 20 h of co-culture. Y-axis is displayed as log_2 gMFI. B) Intracellular Casp3 expression of T cells from 20 h co-cultures without (unstim) or with peptide-loaded U-87 MGs (stim). n = 1-3 donors, each circle in B) represents the average of 6 technical replicates per donor. Student's t-test was performed; ns = not significant

three donors (Figure 53B). These results confirmed that after 20 h of co-culture, T cells were activated and did not exhibit increased apoptosis.

When $CD4^+$ T cells were co-cultured for 20 h with U-87 MGs with or without peptide, CD43 and CD45 expression remained unchanged and PSGL-1 expression was reduced (Figure 54A). As discussed in Chapter 3, MUC1 and MUC24 are expressed on activated, rather than resting T cells, which was confirmed in my co-culture assay. Figure 54B shows example plots for annexin-V and mucin expression on $CD4^+$ T cells over time. While a gradual increase in annexin-V staining was observed in all samples, a simultaneous decrease in PSGL-1 expression was visible. Conversely, MUC1 and MUC24 exhibited the opposite trend. CD45 and CD43 expression remained comparable to baseline.

When the assay was repeated with $CD8^+$ T cells, similar results were obtained. After 20 h of co-culture, CD43 and CD45 expression was unchanged and MUC1 and MUC24 increased (Figure 55A). PSGL-1 was reduced to approximately 25% of its baseline expression compared to around 60% on $CD4^+$, thus the reduction in PSGL-1 labelling was seemingly greater on $CD8^+$ T cells compared to $CD4^+$ T cells. Annexin-V binding gradually increased over time when comparing 0, 4, 10 and 20 h of co-culture (Figure 55B). Increasing annexin-V expression and PSGL-1 loss of antibody binding led me to hypothesise that even though differences in mucin dynamics on apoptotic cells exist, PSGL-1 might be cleaved by PS-activated ADAM10 on activated $CD4^+$ and $CD8^+$ T cells. To test this, primary $CD4^+$ or $CD8^+$ T cells were pre-

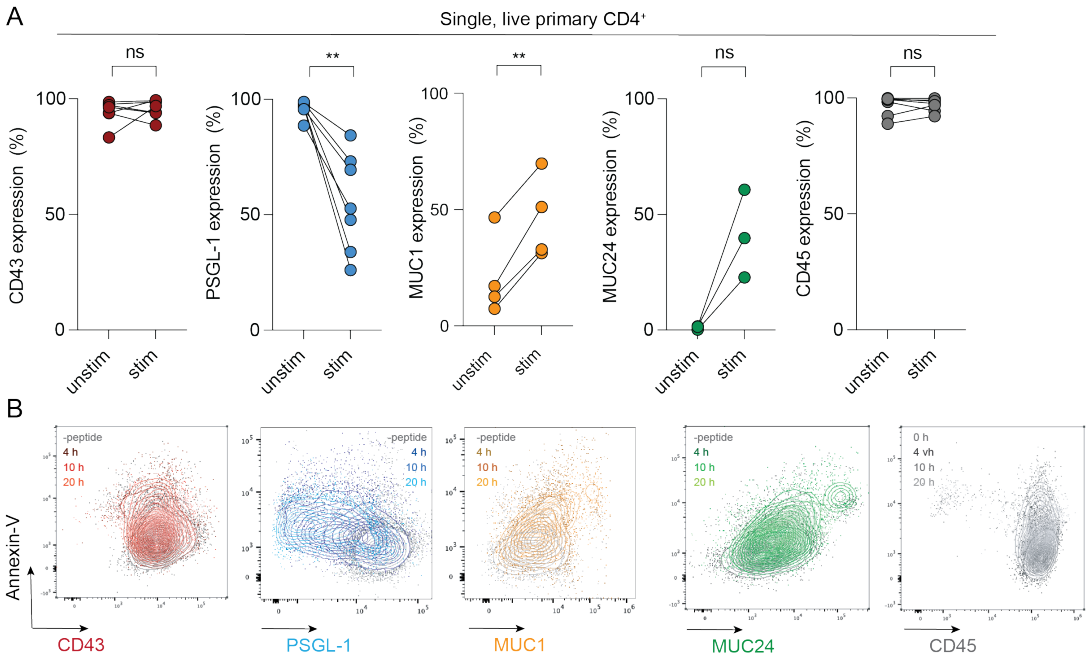


*Figure 54: Activation of CD4+ T cells by TCR engagement. Mucin colours are CD43 (red), PSGL-1 (blue), MUC1 (yellow), MUC24 (green), CD45 (grey). A) absolute mucin expression on T cells from co-cultures without (unstim) or with peptide-pulsed U-87 MGs (stim). B) Contour plots of mucins against annexin-V expression without TCR stimulation (-peptide), and with stimulation for 4 h, 10 h or 20 h. n = 3-7, student's t-tests were performed. ** $p<0.01$, ns = not significant*

incubated with GI and GW inhibitor at 10 μM for 45 min and without removing the inhibitor proceeded with the co-culture as before.

No difference was detected in the control mucins CD43 and CD45 on either CD4+ or CD8+ T cells when T cells were treated with ADAM10 or ADAM17 inhibitor (Figure 56). By contrast, GW and GI treatment resulted in a significantly reduced loss of PSGL-1 on CD8+ T cells compared to stimulated cells without inhibitor. On CD4+ T cells, PSGL-1 expression was higher on GI-treated, stimulated cells compared to stimulated cells without inhibitor. This indicates that ADAM10 and ADAM17 might be involved in the downregulation of PSGL-1 during TCR-mediated activation of primary CD4+ and CD8+ T cells.

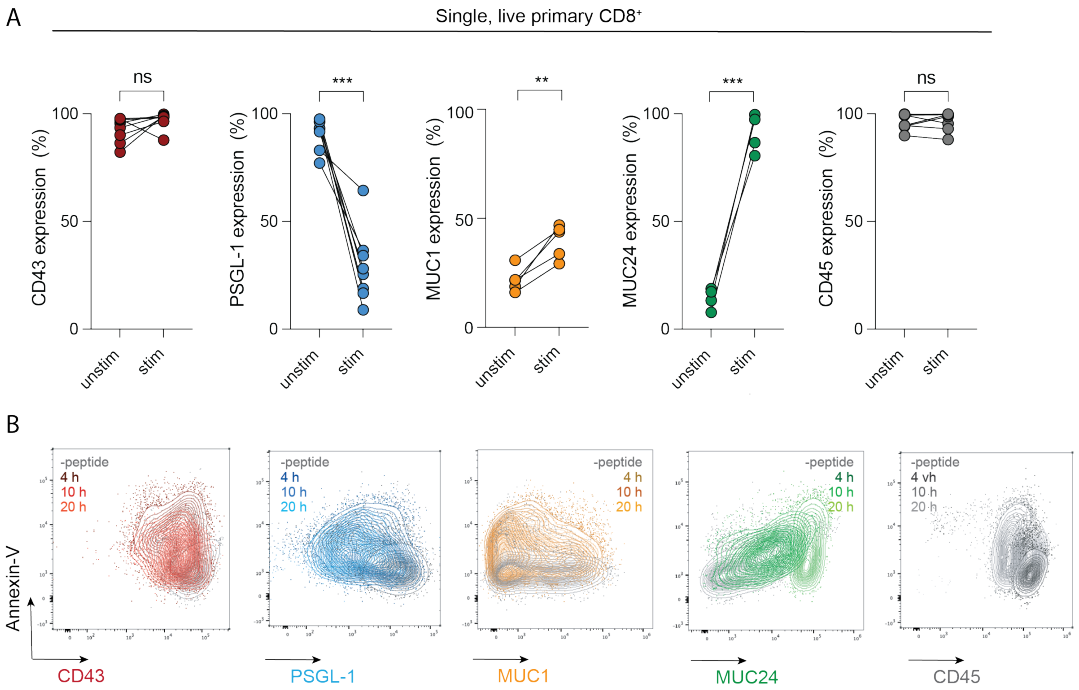


*Figure 55: Activation of CD8+ T cells by TCR engagement. CD43 (red), PSGL-1 (blue), MUC1 (yellow), MUC24 (green), CD45 (grey). A) absolute mucin expression on T cells from co-cultures without (unstim) or with peptide-pulsed U-87 MGs (stim). B) Contour plots of mucins against annexin-V expression without TCR stimulation (-peptide), and with stimulation for 4 h, 10 h or 20 h. n = 4-8, student's t-tests were performed. *** p<0.001, ** p<0.01, ns = not significant*

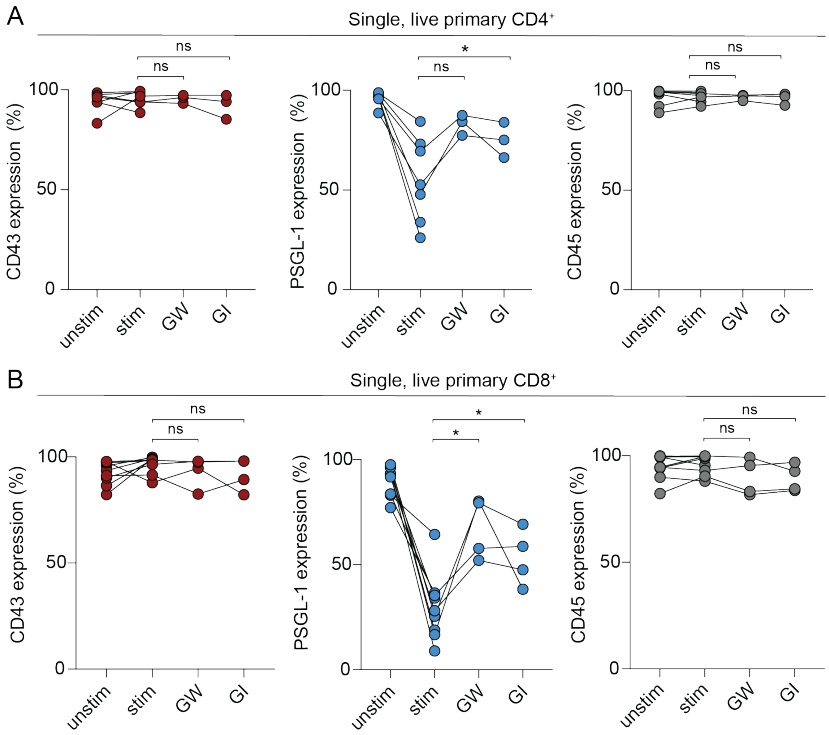


*Figure 56: Activation of inhibitor-treated CD4+ and CD8+ T cells by TCR engagement. CD43 (red), PSGL-1 (blue), CD45 (grey). Absolute mucin expression on T cells from co-cultures without (unstim) or with peptide-pulsed U-87 MGs (stim), with GW-treatment and peptide stimulation (GW) and with GI-treatment and peptide stimulation (GI) A) CD4+ T cells B) CD8+ T cells. n = 3-8, one-way ANOVA was performed. * p<0.05, ns = not significant*

6.2.3 Discussion

The results obtained in Chapters 3-5 led me to propose the hypothesis that optimal T cell activation might require the regulation of mucin expression to reduce their biophysical barrier function. Similar to mucin loss facilitating the uptake of apoptotic T cells by macrophages, mucin expression might also have negative biophysical effects on the interaction between T cells and APCs. This chapter aimed to test this hypothesis by stimulating T cells through stimulation with PMA/ionomycin and by utilising a TCR-mediated activation assay.

PMA and ionomycin treatment of Jurkats led to reduced labelling of CD43 and PSGL-1, but not MUC1, MUC24 or CD45. A negative Casp3 and annexin-V staining excluded PMA/ionomycin treatment-induced cell death [592, 593]. Therefore, the possibility that the reduced staining of CD43 and PSGL-1 was due to apoptosis-mediated shedding was excluded. Nonetheless, other types of cell death have been reported during T cell activation, such as necrosis [594, 595], during which PS exposure has been observed [393]. Therefore, including necrosis markers in future experiments would help to exclude other types of cell death. CD69 labelling remained negative, which was to be expected given that while it is an early activation marker, the earliest detectable increase is around 2-3 h post stimulation [581]. Annexin-V staining was negative, which is contrary to some reports in which ionomycin treatment led to PS exposure [401, 596, 597], however other studies such as those by Ho and colleagues have shown that after PMA/ionomycin treatment of Jurkats, CD69 can be detected but not PS [598]. It is worth noting that the studies which reported PS flipping treated target cells for a very short time (10 [596] and 15 min [401]), therefore PS flipping could be a very time-sensitive and short-lived process, which may explain the absence of annexin-V staining post-stimulation in my experiments. Additionally, before PS exposure had been linked with T cell activation, annexin-V binding was routinely used to measure activation-induced cell death and therefore might have been misinterpreted in older studies [599–602]. To explore both enzymatic shedding by metalloproteases and internalisation as potential mechanisms underlying loss of CD43 and PSGL-1 labelling, GW and GI inhibitors were utilised to investigate whether ADAM10 or ADAM17 shed CD43 and PSGL-1, which was apparently not the case. The broad-spectrum matrix metalloprotease inhibitors Marimastat and GM also failed to prevent loss of CD43 and PSGL-1 binding, excluding the possibility that other metalloprotease-mediated shedding led

to these observations. Inhibition of clathrin-mediated endocytosis by Ika treatment did not prevent CD43 and PSGL-1 reduction, however previous studies have found that Ika is a reversible inhibitor and only inhibits internalisation to approximately 60-80% [583]. Considering the rapid loss of antibody labelling, perhaps 20-40% active internalisation might have sufficed to yield the observed results. Despite these experiments, other possibilities remain to be explored. Ika only inhibits clathrin-mediated endocytosis [583] and other endocytic pathways might be responsible for the observed effects. Additionally, alterations in antigenicity might result in reduced antibody binding for CD43 and PSGL-1. Despite the lack of an explanation arising from my experiments probing metalloprotease shedding and clathrin-mediated internalisation, it appears that this phenomenon is specific rather than a general mechanism due to a lack of change in labelling of MUC1, MUC24, and CD45. Previous studies have found that CD43 is shed on PMA-activated neutrophils, granulocytes and HMC-1 cells, a human mast cell line [32, 481, 482, 484]. Walker and Green claimed that PMA treatment of CEM T cells did not lead to altered CD43 expression by flow cytometry, but did not show data supporting this statement [125]. The discrepancies in these reports suggest that small differences in experimental conditions, such as concentrations and incubation time, may substantially influence the outcomes. If my experiments were to be repeated, it might be advisable to lower the concentration of PMA and ionomycin and extend the duration of stimulation. This would allow the use of appropriate markers to confirm the activation status of the cells. If CD43 and PSGL-1 were not enzymatically cleaved off the cell surface, the potential for changes in antigenicity, and alterations in internalisation and degradation processes remain a possibility. Using the $CD43_{Halo/SNAP}$ construct in a Jurkat cell line might provide insights into the stimulation-induced changes of CD43, especially if investigated using live cell fluorescence imaging.

Testing mucin expression in a human TCR-mediated activation model using primary $CD4^+$ and $CD8^+$ T cells showed an increase of the activation markers CD69, 4-1BB and of PS exposure. In a murine co-culture model of peptide-pulsed with cognate T cells from OT-I mice, PS flipping was detectable by annexin-V binding [554]. Exposure reached its peak at approximately 12 h, stayed high at 20 h and was fully reverted at approximately 72 h [554]. A similar study using $CD8^+$ T cells also from OT-I mice co-cultured with TC-1 tumor cells pulsed with OVA peptide found that PS exposure reached a plateau at 24 h [603]. In their experiments, CD69 labelling

reached its maximum at 6 h. These results are very similar to my findings, in which annexin-V binding peaked at around 10 h and stayed high at 20 h, and CD69 increased rapidly, reaching a plateau at 4 h. Naither Mao et al nor McDonald et al measured PS flipping between 0 and 12 h or 6 and 24 h, respectively [554, 603]. It is therefore possible that if they had done so, they might have observed the maximum exposure at approximately 10 h as well. However due to the limited sample size, the timecourse should be used merely to give an impression of marker expression. Additional repeats including later time points might yield interesting and more robust results. As discussed in Chapter 3, MUC1 and MUC24 are not expressed on resting T cells but are upregulated under activating conditions [83, 97]. Therefore the increase in MUC1 and MUC24 labelling of activated $CD4^+$ and $CD8^+$ results confirmed the said previous reports from the literature. CD43 and CD45 remained unchanged and PSGL-1 antibody labelling was reduced, and this reduction was more pronounced in $CD8^+$ cells. Jelly-Gibbs and colleagues generated a model in which murine $CD4^+$ Th_1 and Th_2-differentiated cells were co-cultured with peptide-pulsed splenic APCs [604]. They found PSGL-1 downregulation on activated Th_1 cells and a moderate reduction of CD43 in Th_1 and Th_2 cells. In the experimental setup used in this thesis, no differentiation was made between $CD4^+$ T cell subsets. Therefore, the possibility remains that CD43 regulation may differ among various subsets of $CD4^+$ T cells which were not visible in the bulk $CD4^+$ population. Additionally, species-specific differences could also play a role in these observations. On the other hand, the loss of PSGL-1 labelling might constitute a more general mechanism that is not subset or species-specific. Considering that CD43 and CD45 are reportedly excluded from the T cell synapse and moved to the dSMAC or uropod of the cell [424, 568], the stable labelling of CD45 and CD43 in my experiment could mean that re-distribution is sufficient to reduce steric hindrance and negative signalling in the case of CD45. Interestingly, while playing a specific role as a checkpoint molecule by regulating TCR signaling, increasing inhibitory receptor expression and exacerbating T cell exhaustion [61, 557, 559], PSGL-1 has also been reported to be removed from the T cell synapse [62, 566]. Hope et al. further published a conference abstract in which they summarise that repeated signalling though PSGL-1 prolongs TCR signalling and thus drives T cell exhaustion [605]. Hence, in cases of strong TCR-pMHC binding, removal of PSGL-1 from the cell surface could serve a biological purpose: PSGL-1 cleavage might aid in excluding this mucin from the immunological synapse while simultaneously eliminating ligation-induced

signalling [557], thus balancing TCR activation and limiting T cell exhaustion. In my experiments, no complete loss of PSGL-1 labelling was observed and some expression remained of approximately 60% and 30% on activated $CD4^+$ and $CD8^+$ T cells, respectively. Based on findings by Hope and colleagues, removal of certain PSGL-1 molecules might facilitate the termination of signalling, while simultaneously, retaining a fraction of PSGL-1 signalling might be advantageous in order to generate a significant TCR signal.

Loss of PSGL-1 antibody labelling during activation was reduced by incubation with GI inhibitor for $CD4^+$ and $CD8^+$ cells, and by GW inhibitor in $CD8^+$ cells. Sample size was limited in GW-treated, activated $CD4^+$ T cells precluding statistical analysis, however a trend can be observed. This suggests that ADAM10 might be the sheddase responsible for loss of antibody labelling of activated T cells. Tetraspanin-mediated ADAM10 substrate specificity could account for differences in downregulation between $CD4^+$ and $CD8^+$ cells [379, 380]. CD45 is excluded to facilitate the formation of a stable immunological synapse [570] and acts as a negative regulator for TCR signalling on T cells until the TCR encounters a cognate, high-affinity peptide-MHC complex [562, 606]. Compared to CD45, PSGL-1 is larger in size, forms dimers and exhibits different glycosylation patterns, and therefore effective reduction of negative signalling might necessitate enzymatic cleavage of PSGL-1 in addition to exclusion. To confirm potential ADAM10-mediated shedding of PSGL-1 during TCR activation, a CRISPR knockout of ADAM10 could be performed on the primary T cells prior to lentiviral transduction. Alternatively, a co-culture model could be developed using Jurkats transduced with the 1G4 TCR and in which ADAM10 has been knocked out. Additionally introducing a tagged PSGL-1 molecule would provide insights into molecular dynamics during activation. For example, a double-tagged (N- and C-termini) molecule might confirm shedding via flow cytometric analysis, and live cell imaging. Super-resolution imaging might elucidate whether, for example, PSGL-1 is initially excluded from the immunological synapse then subsequently cleaved. Additionally, exploring MUC24 and its potential exclusion from the T cell synapse might be interesting, as to my knowledge MUC24 has not yet been studied during T cell activation. Due to time constraints related to my DPhil deadline I was unable to further investigate these topics and I look forward to monitoring the developments in this field in the future.

7 Conclusion and future directions

Mucin-like molecules have primarily been well-characterised on epithelial cells as the luminal lining of mucosal tissues. However scant knowledge is available about the expression and regulation of transmembrane mucins on immune cells. Previous lab members have shown that CD43 labelling is reduced on apoptotic T cells, indicating that mucins might require removal from the cell surface to allow efferocytic clearance. The results presented in Chapter 3 reveal strong expression of CD43, PSGL-1, MUC24 and CD45 on T cells and weak expression of MUC1 on $CD4^+$ T cell lines and on primary $CD4^+$ and $CD8^+$ cells. CD43, PSGL-1 and MUC1, but not MUC24 and CD45 labelling was strongly reduced on apoptotic cells. A C- and N-terminally tagged CD43 cell line showed that during T cell apoptosis, the N-terminus but not the C-terminus is lost, indicating enzymatic shedding, further confirmed by Western blotting. The metalloprotease ADAM10 also sheds PSGL-1 on U937 cells [462, 487] and neutrophils [488], and its close relative ADAM17 reportedly cleaves MUC1 on epithelial cells [79, 463]. Based on these findings and those of previous lab members the ADAM10 inhibitors GI and GW and an $ADAM10^{-/-}$ cell line were used to confirm ADAM10 as the major sheddase of CD43, PSGL-1 and MUC1. Bleibaum and colleagues found that PS is needed for ADAM10 activity [377]. I therefore hypothesised that XKR8, a PS scramblase with a Casp3 motif [402], might be responsible for PS flipping in apoptosis and ADAM10 activation. Despite high levels of Casp3, $XKR8^{-/-}$ T cells showed lack of mucin shedding, suggesting that XKR8 is crucial for ADAM10 activity and subsequent shedding of CD43, PSGL-1 and MUC1. In Chapter 5, a co-culture assay and ImageStream technology were utilised to show increased uptake of MUC1 and PSGL-1 knockout cells, while ADAM10 knockout yielded opposite results. Treatment with StcE mucinase reversed the negative impact of $ADAM10^{-/-}$, consistent with mucins posing a biophysical barrier the reduction of which is required for efficient dead cell clearance. PS is exposed on activated T cells [513, 554], and CD43, PSGL-1 and CD45 are excluded from the immunological synapse [62, 424, 425, 566, 568–570, 607]. I therefore hypothesised that mucins might require shedding during T cell activation to facilitate cell-cell interactions. Ionophore-induced activation led to the loss of labelling of CD43 and PSGL-1, but not CD45 on Jurkats, the mechanism of which requires further exploration. In an APC:T cell co-culture with primary cells, PSGL-1 was downregulated on activated $CD4^+$ and $CD8^+$, potentially mediated

by ADAM10.

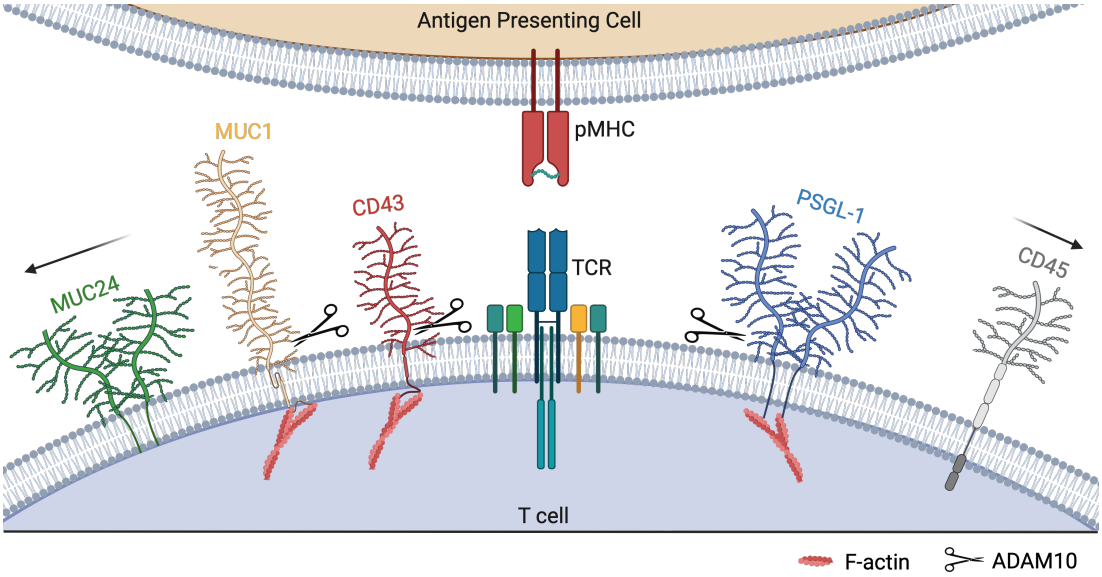


Figure 57: Interaction of an APC with a mucin-expressing T cell. Upon approximation of the peptide-loaded MHC molecule (pMHC) and the TCR, MUC24 and CD45 can be laterally excluded from the forming T cell synapse, while CD43, MUC1 and PSGL-1 require cytoskeletal rearrangement or enzymatic cleavage to facilitate a close interaction of the cells.

According to current literature, CD43, PSGL-1 and MUC1 can be connected to the cytoskeleton via F-actin and ERM adaptor proteins [34, 566, 607] while the same has not yet been described for MUC24 and CD45. Based on the findings of this thesis and current literature the following model may be suggested: MUC24 and CD45 are both laterally mobile and can be passively excluded from the forming site of interaction. CD43, PSGL-1 and MUC1 are anchored and hence either require active movement by the cytoskeleton or cleavage by a metalloprotease such as ADAM10 (Figure 57).

7.1 Suggestions for future studies

7.1.1 Mucin cleavage and ADAM10 specificity

Alongside repeating MS analysis of the ADAM10 sheddome, there is a set of experiments which might help further our understanding of the role of mucins in immune cell interactions. The ADAM metalloprotease substrate pool is large and its specificity is edited through association with tetraspanins. However not much is known about the substrate cleavage motif of ADAM10 and while other studies have used MS to investigate it further, attempts have had limited success [608]. A bottom-up approach using mutagenesis of CD43, PSGL-1 and

MUC1 in CEM cells with subsequent validation in an apoptosis assay would be possible. This could be realised in two ways: 1) by site-directed mutagenesis based on known literature and defining the target amino acids by educated guessing; 2) By harnessing tools used in random mutagenesis, such as error-prone PCR (epPCR) for directed evolution. In this method, a polymerase introduces random errors, thus mutations, into the sequence during extension. In this case, the target sequence could be the membrane-proximal domain of the mucins. Subsequent transformation into a mucin-knockout cell line and validation in an apoptosis assay would provide a high-throughput method for screening and might lead to the discovery of the ADAM10 cleavage motif for these molecules. Together with the newly unveiled structures of both the inactive and active ADAM10-Tspan15 complex [337, 339], these findings would serve to broaden our understanding of the ADAM10 cleavage mechanisms.

7.1.2 The efferocytosis assay

Performing additional repeats of primary CD43$^{-/-}$ efferocytosis experiments will increase their statistical power. The cell lines studied in this work were particularly used for the exploration of knockout models. Nonetheless an overexpression system would be interesting to study the effects of an reinforced glycocalyx shield. It would furthermore be interesting to quantify which mucins, if overexpressed, have the greater effect on uptake given that a previous study claimed that the size of MUC1 is of greater significance than its charge [525]. One limitation inherent to ImageStream analysis is the potential for misinterpretation due to the imaging perspective. It could create an illusion of cellular internalisation when in fact the cell of interest may be adhering at the front or rear surface of a macrophage or behind it. Confocal imaging of samples from the co-culture assay would enable the acquisition of z-stacks and facilitate the reconstruction of a three-dimensional representation of the cells. This approach would offer a more comprehensive visualisation of the engulfment process in a 3D space. The CharON construct designed by Raymon and colleagues [541] is comprised of a GFP reporter that is activated upon apoptosis induction in a Casp3-dependent manner. After engulfment by a macrophage and acidification in the phagolysosome, the pH sensitive expression of pHlorina is triggered. Utilising the CharON-Jurkat model in the efferocytosis assay with analysis via ImageStream or microscopy would provide further proof of internalisation. Further validation

of the assay could be performed by using actin inhibitors, since immobilising the cytoskeleton of MDM should prevent efferocytosis resulting in diminished uptake [500].

7.1.3 The role of ADAM10 in efferocytosis

ADAM10 cleaves Amyloid precursor protein (APP) and ADAM10-dysregulation is one hallmark of Alzheimer's disease. Scharfenberg et al. were the first to create a soluble version of ADAM10 that was capable of cleaving substrates in suspension [512]. Since then, Hershkovits and colleagues have created a novel form of sADAM10 that was based on the isolated catalytic metalloprotease domain. In their study, sADAM10 successfully caused APP cleavage when added to cell culture and was able to cleave overexpressed protein on the membrane of live cells [609]. Several mucins such as CD43, CD44, PSGL-1, MUC1, MUC24 and CD45 are overexpressed on cancers and their enhanced expression negatively correlates with disease progression and outcome [436–438]. Exploring the potential effects of soluble ADAM10 in an animal tumour model would yield interesting results.

7.1.4 Immune cell activation and mucin expression

Conducting additional experiments to investigate mucin expression dynamics during T cell activation would yield insights into the sequence of events from first contact between a T cell and an APC, the exclusion and shedding of mucins, and the role of ADAM10 in this process. ADAM10 knockout in primary T cells prior to co-culture with and without peptide-pulsed APCs would provide ideal samples for the analysis of the ADAM10 sheddome by mass spectrometry for an unbiased approach, and Western blot or ELISA for specific protein targets. Further to those experiments, a TMEM16F knockout would address the hypothesis that during activation, Ca^{2+}-activated TMEM16F flips PS, which in turn activates ADAM10 shedding. Interestingly, Sakuragi et al. described that XKR8, while carrying a Casp3 motif, is capable of PS scrambling through its phosphorylation motif in a murine B cell line [421]. Therefore it might be of interest to also knock out XKR8 when addressing which scramblase might be responsible for PS exposure during T cell activation. Finally, the phenomenon of ADAM10-mediated mucin shedding and its significance in cell-cell interactions may have broader implications, potentially extending to various other immune cells like B cells and additional antigen-presenting

cells (APCs). Investigating mucin expression patterns under apoptotic conditions on other immune cell lines and *in vivo* could provide valuable insights into the generality of this mechanism.

Collectively, the experiments discussed here might enable a fuller understanding of the influence of mucin dynamics on immune cell interactions. This thesis has not only uncovered apoptosis-triggered mucin shedding but has also shown the positive impact of mucin shedding on efferocytic uptake. Furthermore, it is the first report on ADAM10 activation triggered by XKR8-mediated PS flipping. Together with the novel observation of PSGL-1 shedding by ADAM10 on during T cell activation, these observations highlight a new role of mucins on immune cells.

References

1. Bansil, R. & Turner, B. S. The biology of mucus: Composition, synthesis and organization. *Advanced drug delivery reviews* **124,** 3–15 (2018).
2. Johansson, M. E., Sjövall, H. & Hansson, G. C. The gastrointestinal mucus system in health and disease. *Nature reviews Gastroenterology & hepatology* **10,** 352–361 (2013).
3. Pinzón Martıén, S., Seeberger, P. H. & Varón Silva, D. Mucins and pathogenic mucin-like molecules are immunomodulators during infection and targets for diagnostics and vaccines. *Frontiers in chemistry* **7,** 710 (2019).
4. Corfield, A. P. Mucins: a biologically relevant glycan barrier in mucosal protection. *Biochimica et Biophysica Acta (BBA)-General Subjects* **1850,** 236–252 (2015).
5. Rachagani, S., Torres, M. P., Moniaux, N. & Batra, S. K. Current status of mucins in the diagnosis and therapy of cancer. *Biofactors* **35,** 509–527 (2009).
6. Cox, K. E. *et al.* The mucin family of proteins: candidates as potential biomarkers for colon cancer. *Cancers* **15,** 1491 (2023).
7. Kaur, S., Kumar, S., Momi, N., Sasson, A. R. & Batra, S. K. Mucins in pancreatic cancer and its microenvironment. *Nature reviews Gastroenterology & hepatology* **10,** 607–620 (2013).
8. Bhatia, R. *et al.* Cancer-associated mucins: role in immune modulation and metastasis. *Cancer and Metastasis Reviews* **38,** 223–236 (2019).
9. Wagner, C., Wheeler, K. & Ribbeck, K. Mucins and their role in shaping the functions of mucus barriers. *Annual review of cell and developmental biology* **34,** 189–215 (2018).
10. Jonckheere, N., Skrypek, N., Frénois, F. & Van Seuningen, I. Membrane-bound mucin modular domains: from structure to function. *Biochimie* **95,** 1077–1086 (2013).
11. Johansson, M. E. & Hansson, G. C. Immunological aspects of intestinal mucus and mucins. *Nature Reviews Immunology* **16,** 639–649 (2016).
12. Campo, V. A., Buscaglia, C. A., Di Noia, J. M. & Frasch, A. C. C. Immunocharacterization of the mucin-type proteins from the intracellular stage of Trypanosoma cruzi. *Microbes and infection* **8,** 401–409 (2006).

13. Senapati, S., Das, S. & Batra, S. K. Mucin-interacting proteins: from function to therapeutics. *Trends in biochemical sciences* **35,** 236–245 (2010).

14. Kufe, D. W. Mucins in cancer: function, prognosis and therapy. *Nature Reviews Cancer* **9,** 874–885 (2009).

15. Gendler, S. J. MUC1, the renaissance molecule. *Journal of mammary gland biology and neoplasia* **6,** 339–353 (2001).

16. Hollingsworth, M. A. & Swanson, B. J. Mucins in cancer: protection and control of the cell surface. *Nature Reviews Cancer* **4,** 45–60 (2004).

17. Hattrup, C. L. & Gendler, S. J. Structure and function of the cell surface (tethered) mucins. *Annu. Rev. Physiol.* **70,** 431–457 (2008).

18. Ueda, A., Shimomura, M., Ikeda, M., Yamaguchi, R. & Tanishita, K. Effect of glycocalyx on shear-dependent albumin uptake in endothelial cells. *American Journal of Physiology-Heart and Circulatory Physiology* **287,** H2287–H2294 (2004).

19. Janczyk, P., Hansen, S., Bahramsoltani, M. & Plendl, J. The glycocalyx of human, bovine and murine microvascular endothelial cells cultured in vitro. *Journal of electron microscopy* **59,** 291–298 (2010).

20. Zausig, Y. A. *et al.* The impact of crystalloidal and colloidal infusion preparations on coronary vascular integrity, interstitial oedema and cardiac performance in isolated hearts. *Critical Care* **17,** 1–10 (2013).

21. Oltean, S. *et al.* Vascular endothelial growth factor-A165b is protective and restores endothelial glycocalyx in diabetic nephropathy. *Journal of the American Society of Nephrology: JASN* **26,** 1889 (2015).

22. Kesimer, M. *et al.* Molecular organization of the mucins and glycocalyx underlying mucus transport over mucosal surfaces of the airways. *Mucosal immunology* **6,** 379–392 (2013).

23. Shurer, C. R. *et al.* Physical principles of membrane shape regulation by the glycocalyx. *Cell* **177,** 1757–1770 (2019).

24. Janeway Jr, C. A., Travers, P., Walport, M. & Shlomchik, M. J. in *Immunobiology: The Immune System in Health and Disease. 5th edition* (Garland Science, 2001).

25. Cyster, J. G., Shotton, D. M. & Williams, A. F. The dimensions of the T lymphocyte glycoprotein leukosialin and identification of linear protein epitopes that can be modified by glycosylation. *The EMBO journal* **10,** 893–902 (1991).

26. Marth, J. D. & Grewal, P. K. Mammalian glycosylation in immunity. *Nature Reviews Immunology* **8,** 874–887 (2008).

27. Remold-O'Donnell, E. & Rosen, F. S. Sialophorin (CD43) and the Wiskott-Aldrich syndrome. *Immunodeficiency Reviews* **2,** 151–174 (1990).

28. Van der Merwe, P. A. Formation and function of the immunological synapse. *Current opinion in immunology* **14,** 293–298 (2002).

29. Sabri, S. *et al.* Glycocalyx modulation is a physiological means of regulating cell adhesion. *Journal of Cell Science* **113,** 1589–1600 (2000).

30. Soler, M. *et al.* Leukosialin (CD43) behavior during adhesion of human monocytic THP-1 cells to red blood cells. *Journal of leukocyte biology* **61,** 609–618 (1997).

31. Mody, P. D. *et al.* Signaling through CD43 regulates CD4 T-cell trafficking. *Blood, The Journal of the American Society of Hematology* **110,** 2974–2982 (2007).

32. Mambole, A. *et al.* The cleavage of neutrophil leukosialin (CD43) by cathepsin G releases its extracellular domain and triggers its intramembrane proteolysis by presenilin/γ-secretase. *Journal of Biological Chemistry* **283,** 23627–23635 (2008).

33. Seo, W. & Ziltener, H. J. CD43 processing and nuclear translocation of CD43 cytoplasmic tail are required for cell homeostasis. *Blood, The Journal of the American Society of Hematology* **114,** 3567–3577 (2009).

34. Cannon, J. *et al.* CD43 interaction with ezrin-radixin-moesin (ERM) proteins regulates T-cell trafficking and CD43 phosphorylation. *Molecular biology of the cell* **22,** 954–963 (2011).

35. Bazil, V. & Strominger, J. L. CD43, the major sialoglycoprotein of human leukocytes, is proteolytically cleaved from the surface of stimulated lymphocytes and granulocytes. *Proceedings of the National Academy of Sciences* **90,** 3792–3796 (1993).

36. Schmid, K. *et al.* Amino acid sequence of human plasma galactoglycoprotein: identity with the extracellular region of CD43 (sialophorin). *Proceedings of the National Academy of Sciences* **89,** 663–667 (1992).

37. Nusbaum, P. *et al.* Distinct signaling pathways are involved in leukosialin (CD43) down-regulation, membrane blebbing, and phospholipid scrambling during neutrophil apoptosis. *Journal of Biological Chemistry* **280,** 5843–5853 (2005).

38. Oguri, E., Miki, Y., Hirano, K., Yamanaka, M. & Beppu, M. Clearance of CD43-capped cells by macrophages: capping alone leads to phagocytosis. *Biological and Pharmaceutical Bulletin* **35,** 551–558 (2012).

39. Kim, H. J., Park, H. J., Park, W. S. & Bae, Y. CD43 cross-linking increases the Fas-induced apoptosis through induction of Fas aggregation in Jurkat T-cells. *Experimental & molecular medicine* **38,** 357–363 (2006).

40. Andersson, C. X. *et al.* CD43 has a functional NLS, interacts with β-catenin, and affects gene expression. *Biochemical and biophysical research communications* **316,** 12–17 (2004).

41. Fay, K. T. *et al.* Increased mortality in CD43-deficient mice during sepsis. *Plos one* **13,** e0202656 (2018).

42. Baeckström, D. *et al.* Expression of the Leukocyte-associated Sialoglycoprotein CD43 by a Colon Carcinoma Cell Line. *Journal of Biological Chemistry* **270,** 13688–13692 (1995).

43. Fernandez-Rodriguez, J. *et al.* The leukocyte antigen CD43 is expressed in different cell lines of nonhematopoietic origin. *Tumor biology* **23,** 193–201 (2002).

44. Ziprin, P., Alkhamesi, N. A., Ridgway, P. F., Peck, D. H. & Darzi, A. W. Tumour-expressed CD43 (sialophorin) mediates tumour-mesothelial cell adhesion (2004).

45. Fiume, G. *et al.* Human immunodeficiency virus-1 Tat activates NF-κB via physical interaction with IκB-α and p65. *Nucleic acids research* **40,** 3548–3562 (2012).

46. Fiume, G. *et al.* Eukaryotic initiation factor 4H is under transcriptional control of p65/NF-κB. *PloS one* **8,** e66087 (2013).

47. Moore, K. Stults NL, Diaz S, Smith DF, Cummings RD, Varki A, and McEver RP. *Identification of a specific glycoprotein ligand for P-selectin (CD62) on myeloid cells. J Cell Biol* **118,** 445–456 (1992).

48. Li, F. *et al.* Visualization of P-selectin Glycoprotein Ligand-1 as a Highly Extended Molecule and Mapping of Protein Epitopes for Monoclonal Antibodies. *Journal of Biological Chemistry* **271,** 6342–6348 (1996).

49. Patel, K. D., Nollert, M. U. & McEver, R. P. P-selectin must extend a sufficient length from the plasma membrane to mediate rolling of neutrophils. *The Journal of cell biology* **131,** 1893–1902 (1995).

50. Yang, J., Furie, B. C. & Furie, B. The biology of P-selectin glycoprotein ligand-1: its role as a selectin counterreceptor in leukocyte-endothelial and leukocyte-platelet interaction. *Thrombosis and haemostasis* **81,** 1–7 (1999).

51. Kieffer, J. D. *et al.* Neutrophils, monocytes, and dendritic cells express the same specialized form of PSGL-1 as do skin-homing memory T cells: cutaneous lymphocyte antigen. *Biochemical and biophysical research communications* **285,** 577–587 (2001).

52. Nuñez-Andrade, N. *et al.* P-selectin glycoprotein ligand-1 modulates immune inflammatory responses in the enteric lamina propria. *The Journal of pathology* **224,** 212–221 (2011).

53. Tchernychev, B., Furie, B. & Furie, B. C. Peritoneal macrophages express both P-selectin and PSGL-1. *The Journal of cell biology* **163,** 1145–1155 (2003).

54. Spertini, O., Cordey, A.-S., Monai, N., Giuffrè, L. & Schapira, M. P-selectin glycoprotein ligand 1 is a ligand for L-selectin on neutrophils, monocytes, and CD34+ hematopoietic progenitor cells. *The Journal of cell biology* **135,** 523–531 (1996).

55. Goetz, D. J. *et al.* Isolated P-selectin glycoprotein ligand-1 dynamic adhesion to P-and E-selectin. *The Journal of cell biology* **137,** 509–519 (1997).

56. Xia, L. *et al.* N-terminal residues in murine P-selectin glycoprotein ligand-1 required for binding to murine P-selectin. *Blood, The Journal of the American Society of Hematology* **101,** 552–559 (2003).

57. Ley, K. & Kansas, G. S. Selectins in T-cell recruitment to non-lymphoid tissues and sites of inflammation. *Nature Reviews Immunology* **4,** 325–336 (2004).

58. Zarbock, A., Müller, H., Kuwano, Y. & Ley, K. PSGL-1-dependent myeloid leukocyte activation. *Journal of leukocyte biology* **86,** 1119–1124 (2009).

59. Angiari, S. *et al.* Regulatory T cells suppress the late phase of the immune response in lymph nodes through P-selectin glycoprotein ligand-1. *The Journal of Immunology* **191,** 5489–5500 (2013).

60. Estrada-Capetillo, L. *et al.* Induction of Th17 lymphocytes and Treg cells by monocyte-derived dendritic cells in patients with rheumatoid arthritis and systemic lupus erythematosus. *Journal of Immunology Research* **2013** (2013).

61. Tinoco, R. *et al.* PSGL-1 is an immune checkpoint regulator that promotes T cell exhaustion. *Immunity* **44,** 1190–1203 (2016).

62. Tinoco, R., Otero, D. C., Takahashi, A. A. & Bradley, L. M. PSGL-1: a new player in the immune checkpoint landscape. *Trends in immunology* **38,** 323–335 (2017).

63. Nowakowska, D. *et al. PSGL-1 is a novel macrophage checkpoint in immuno-oncology.* 2020.

64. Ogawa, J.-i., Inoue, H. & Koide, S. Expression of α-1, 3-fucosyltransferase type IV and VII genes is related to poor prognosis in lung cancer. *Cancer research* **56,** 325–329 (1996).

65. Raes, G. *et al.* The metastatic T-cell hybridoma antigen/P-selectin glycoprotein ligand 1 is required for hematogenous metastasis of lymphomas. *International journal of cancer* **121,** 2646–2652 (2007).

66. Hoos, A., Protsyuk, D. & Borsig, L. Metastatic growth progression caused by PSGL-1–mediated recruitment of monocytes to metastatic sites. *Cancer research* **74,** 695–704 (2014).

67. Xia, L. *et al.* P-selectin glycoprotein ligand-1–deficient mice have impaired leukocyte tethering to E-selectin under flow. *The Journal of clinical investigation* **109,** 939–950 (2002).

68. Urzainqui, A. *et al.* Functional role of P-selectin glycoprotein ligand 1/P-selectin interaction in the generation of tolerogenic dendritic cells. *The Journal of Immunology* **179,** 7457–7465 (2007).

69. Veerman, K. M. *et al.* PSGL-1 regulates the migration and proliferation of CD8+ T cells under homeostatic conditions. *The Journal of Immunology* **188,** 1638–1646 (2012).

70. Shimizu, M. & Yamauchi, K. Isolation and characterization of mucin-like glycoprotein in human milk fat globule membrane. *The Journal of Biochemistry* **91,** 515–524 (1982).

71. Peat, N., Gendler, S. J., Lalani, E.-N., Duhig, T. & Taylor-Papadimitriou, J. Tissue-specific expression of a human polymorphic epithelial mucin (MUC1) in transgenic mice. *Cancer research* **52,** 1954–1960 (1992).

72. Nath, S. & Mukherjee, P. MUC1: a multifaceted oncoprotein with a key role in cancer progression. *Trends in molecular medicine* **20,** 332–342 (2014).

73. Wesseling, J., van der Valk, S. W., Vos, H. L., Sonnenberg, A. & Hilkens, J. Episialin (MUC1) overexpression inhibits integrin-mediated cell adhesion to extracellular matrix components. *Journal of Cell Biology,* 255–265 (1995).

74. Patton, S., Gendler, S. J. & Spicer, A. P. The epithelial mucin, MUC1, of milk, mammary gland and other tissues. *Biochimica et Biophysica Acta (BBA) - Reviews on Biomembranes* (1995).

75. Agrawal, B., Krantz, M. J., Parker, J. & Longenecker, B. M. Expression of MUC1 Mucin on Activated Human T Cells: Implications for a Role of MUC1 in Normal Immune Regulation. *Cancer Research* (1998).

76. Xu, X. *et al.* MUC1 in Macrophage: Contributions to cigarette smoke–induced lung cancer. *Cancer research* **74,** 460–470 (2014).

77. Levitin, F. *et al.* The MUC1 SEA module is a self-cleaving domain. *Journal of Biological Chemistry* **280,** 33374–33386 (2005).

78. Thathiah, A. & Carson, D. D. Mt1-Mmp mediates muc1 shedding independent of tace/adam17. *Biochemical Journal* **382,** 363–373 (2004).

79. Julian, J., Dharmaraj, N. & Carson, D. D. MUC1 is a substrate for γ-secretase. *Journal of cellular biochemistry* **108,** 802–815 (2009).

80. Kinlough, C. L. *et al.* Recycling of MUC1 is dependent on its palmitoylation. *Journal of Biological Chemistry* **281,** 12112–12122 (2006).

81. Kufe, D. W. MUC1-C oncoprotein as a target in breast cancer: activation of signaling pathways and therapeutic approaches. *Oncogene* **32,** 1073–1081 (2013).

82. Lillehoj, E. P. *et al.* NEU1 Sialidase Regulates Membrane-tethered Mucin (MUC1) Ectodomain Adhesiveness for Pseudomonas aeruginosa and Decoy Receptor Release. *Journal of Biological Chemistry* **290,** 18316–18331 (2015).

83. Correa, I. *et al.* Form and pattern of MUC1 expression on T cells activated in vivo or in vitro suggests a function in T-cell migration. *Immunology* **108,** 32–41 (2003).

84. Vasir, B. *et al.* Dendritic cells induce MUC1 expression and polarization on human T cells by an IL-7-dependent mechanism. *The Journal of Immunology* **174,** 2376–2386 (2005).

85. Zhou, R. *et al.* CAR T cells targeting the tumor MUC1 glycoprotein reduce triple-negative breast cancer growth. *Frontiers in immunology* **10,** 1149 (2019).

86. Fang, J., Lai, S., Yu, H. & Ma, L. Suppression of MUC1-Overexpressing Tumors by a Novel MUC1/CD3 Bispecific Antibody. *Antibodies* **12,** 47 (2023).

87. Watt, S. M. *et al.* CD164, a novel sialomucin on CD34+ and erythroid subsets, is located on human chromosome 6q21. *Blood, The Journal of the American Society of Hematology* **92,** 849–866 (1998).

88. Rappold, I. *et al.* Functional and phenotypic characterization of cord blood and bone marrow subsets expressing FLT3 (CD135) receptor tyrosine kinase. *Blood, The Journal of the American Society of Hematology* **90,** 111–125 (1997).

89. Verfaillie, C. Adhesion receptors as regulators of the hematopoietic process. *Blood, The Journal of the American Society of Hematology* **92,** 2609–2612 (1998).

90. Zannettino, A. C. *et al.* The sialomucin CD164 (MGC-24v) is an adhesive glycoprotein expressed by human hematopoietic progenitors and bone marrow stromal cells that serves as a potent negative regulator of hematopoiesis. *Blood, The Journal of the American Society of Hematology* **92,** 2613–2628 (1998).

91. Doyonnas, R. *et al.* CD164 monoclonal antibodies that block hemopoietic progenitor cell adhesion and proliferation interact with the first mucin domain of the CD164 receptor. *The Journal of Immunology* **165,** 840–851 (2000).

92. Watt, S. M., Bühring, H.-J., Simmons, P. J. & Zannettino, A. W. The stem cell revolution: on the role of CD164 as a human stem cell marker. *NPJ Regenerative Medicine* **6,** 33 (2021).

93. Mo, D. *et al.* Apical targeting and endocytosis of the sialomucin endolyn are essential for establishment of zebrafish pronephric kidney function. *Journal of Cell Science* **125,** 5546–5554 (2012).

94. Tang, J. *et al.* Inhibiting CD164 expression in colon cancer cell line HCT116 leads to reduced cancer cell proliferation, mobility, and metastasis in vitro and in vivo. *Cancer investigation* **30,** 380–389 (2012).

95. Sundaresan, S. & Lavanya, S. Review on Bladder Cancer Diagnosis (2023).

96. Wysocka, M. *et al.* CD164 and FCRL3 are highly expressed on CD4+ CD26- T cells in Sezary syndrome patients. *Journal of Investigative Dermatology* **134,** 229–236 (2014).

97. Benoit, B. M. *et al.* CD164 identifies CD4+ T cells highly expressing genes associated with malignancy in Sézary syndrome: the Sézary signature genes, FCRL3, Tox, and miR-214. *Archives of dermatological research* **309,** 11–19 (2017).

98. Woodford-Thomas, T. & Thomas, M. *The leukocyte common antigen, CD45 and other protein tyrosine phosphatases in hematopoietic cells* in *Seminars in cell biology* **4** (1993), 409–418.

99. Hermiston, M. L., Zikherman, J. & Zhu, J. W. CD45, CD148, and Lyp/Pep: critical phosphatases regulating Src family kinase signaling networks in immune cells. *Immunological reviews* **228,** 288–311 (2009).

100. Pilling, D., Fan, T., Huang, D., Kaul, B. & Gomer, R. H. Identification of markers that distinguish monocyte-derived fibrocytes from monocytes, macrophages, and fibroblasts. *PloS one* **4,** e7475 (2009).

101. Rheinländer, A., Schraven, B. & Bommhardt, U. CD45 in human physiology and clinical medicine. *Immunology letters* **196,** 22–32 (2018).

102. Lefrancois, L., Thomas, M. L., Bevan, M. J. & Trowbridge, I. Different classes of T lymphocytes have different mRNAs for the leukocyte-common antigen, T200. *The Journal of experimental medicine* **163,** 1337–1342 (1986).

103. Oberdoerffer, S. *et al.* Regulation of CD45 alternative splicing by heterogeneous ribonucleoprotein, hnRNPLL. *Science* **321,** 686–691 (2008).

104. Desai, D. M., Sap, J., Schlessinger, J. & Weiss, A. Ligand-mediated negative regulation of a chimeric transmembrane receptor tyrosine phosphatase. *Cell* **73,** 541–554 (1993).

105. Leupin, O., Zaru, R., Laroche, T., Müller, S. & Valitutti, S. Exclusion of CD45 from the T-cell receptor signaling area in antigen-stimulated T lymphocytes. *Current Biology* **10,** 277–280 (2000).

106. Johnson, K. G., Bromley, S. K., Dustin, M. L. & Thomas, M. L. A supramolecular basis for CD45 tyrosine phosphatase regulation in sustained T cell activation. *Proceedings of the National Academy of Sciences* **97,** 10138–10143 (2000).

107. Van Der Merwe, P. A., Davis, S. J., Shaw, A. S. & Dustin, M. L. *Cytoskeletal polarization and redistribution of cell-surface molecules during T cell antigen recognition* in *Seminars in immunology* **12** (2000), 5–21.

108. Burroughs, N. J., Lazic, Z. & van der Merwe, P. A. Ligand detection and discrimination by spatial relocalization: A kinase-phosphatase segregation model of TCR activation. *Biophysical journal* **91,** 1619–1629 (2006).

109. James, J. R. & Vale, R. D. Biophysical mechanism of T-cell receptor triggering in a reconstituted system. *Nature* **487,** 64–69 (2012).

110. Byth, K. *et al.* CD45-null transgenic mice reveal a positive regulatory role for CD45 in early thymocyte development, in the selection of CD4+ CD8+ thymocytes, and B cell maturation. *The Journal of experimental medicine* **183,** 1707–1718 (1996).

111. Dhanisha, S. S., Guruvayoorappan, C., Drishya, S. & Abeesh, P. Mucins: Structural diversity, biosynthesis, its role in pathogenesis and as possible therapeutic targets. *Critical reviews in oncology/hematology* **122,** 98–122 (2018).

112. Tarp, M. A. & Clausen, H. Mucin-type O-glycosylation and its potential use in drug and vaccine development. *Biochimica et Biophysica Acta (BBA)-General Subjects* **1780,** 546–563 (2008).

113. Kasprzak, A. & Adamek, A. Mucins: the old, the new and the promising factors in hepatobiliary carcinogenesis. *International journal of molecular sciences* **20,** 1288 (2019).

114. *The Human Protein Atlas* `https://www.proteinatlas.org/ENSG00000164035-EMCN/tissue`. Accessed: 2023-09-16.

115. Pallesen, L. T., Berglund, L., Rasmussen, L. K., Petersen, T. E. & Rasmussen, J. T. Isolation and characterization of MUC15, a novel cell membrane-associated mucin. *European journal of biochemistry* **269,** 2755–2763 (2002).

116. Bardin, N. *et al.* Identification of the S-Endo 1 endothelial-associated antigen. *Biochemical and biophysical research communications* **218,** 210–216 (1996).

117. Elshal, M. F. *et al.* A unique population of effector memory lymphocytes identified by CD146 having a distinct immunophenotypic and genomic profile. *BMC immunology* **8,** 1–15 (2007).

118. Amini, A. *et al.* Mucins and tumor biology. *Utility of bromelain and n-acetylcysteine in treatment of peritoneal dissemination of gastrointestinal mucin-producing malignancies,* 43–61 (2016).

119. Choi, K.-D., Vodyanik, M. & Slukvin, I. I. Hematopoietic differentiation and production of mature myeloid cells from human pluripotent stem cells. *Nature protocols* **6,** 296–313 (2011).

120. Nakano, A., Harada, T., Morikawa, S. & Kato, Y. Expression of leukocyte common antigen (CD45) on various human leukemia/lymphoma cell lines. *Pathology International* **40,** 107–115 (1990).

121. Gottfried, E. *et al.* Expression of CD68 in non-myeloid cell types. *Scandinavian journal of immunology* **67,** 453–463 (2008).

122. Laszik, Z. *et al.* P-selectin glycoprotein ligand-1 is broadly expressed in cells of myeloid, lymphoid, and dendritic lineage and in some nonhematopoietic cells (1996).

123. Oliveira, M. *et al.* CD43 and CD49d from the B-cell chronic lymphoproliferative disorders diagnostic panel are useful to detect erythroid dysplasia. *Cytometry Part B: Clinical Cytometry* **96,** 417–425 (2019).

124. Manjunath, N., Johnson, R. S., Staunton, D. E., Pasqualini, R. & Ardman, B. Targeted disruption of CD43 gene enhances T lymphocyte adhesion. *Journal of immunology (Baltimore, Md.: 1950)* **151,** 1528–1534 (1993).

125. Walker, J. & Green, J. M. Structural requirements for CD43 function. *The Journal of Immunology* **162,** 4109–4114 (1999).

126. Tinoco, R., Neubert, E. N., Stairiker, C. J., Henriquez, M. L. & Bradley, L. M. PSGL-1 is a T cell intrinsic inhibitor that regulates effector and memory differentiation and responses during viral infection. *Frontiers in Immunology* **12,** 677824 (2021).

127. Agrawal, B., Gupta, N. & Konowalchuk, J. D. MUC1 mucin: a putative regulatory (checkpoint) molecule of T cells. *Frontiers in immunology* **9,** 2391 (2018).

128. Erick, T. K. & Mukherjee, P. Modulating MUC1 Function on T Cells. *Trends in immunology* **40,** 980–983 (2019).

129. Holmes, N. CD45: all is not yet crystal clear. *Immunology* **117,** 145–155 (2006).

130. Merzaban, J. S. *et al.* Analysis of glycoprotein E-selectin ligands on human and mouse marrow cells enriched for hematopoietic stem/progenitor cells. *Blood, The Journal of the American Society of Hematology* **118,** 1774–1783 (2011).

131. Matsumoto, M. *et al.* CD43 functions as a ligand for E-Selectin on activated T cells. *The Journal of Immunology* **175,** 8042–8050 (2005).

132. Fuhlbrigge, R. C., King, S. L., Sackstein, R. & Kupper, T. S. CD43 is a ligand for E-selectin on CLA+ human T cells. *Blood* **107,** 1421–1426 (2006).

133. Alcaide, P. *et al.* The 130-kDa glycoform of CD43 functions as an E-selectin ligand for activated Th1 cells in vitro and in delayed-type hypersensitivity reactions in vivo. *Journal of Investigative Dermatology* **127,** 1964–1972 (2007).

134. Van den Berg, T. K. *et al.* Cutting edge: CD43 functions as a T cell counterreceptor for the macrophage adhesion receptor sialoadhesin (Siglec-1). *The Journal of Immunology* **166,** 3637–3640 (2001).

135. Yamakawa, N. *et al.* Discovery of a new sialic acid binding region that regulates Siglec-7. *Scientific reports* **10,** 8647 (2020).

136. Baum, L. G. *et al.* Human thymic epithelial cells express an endogenous lectin, galectin-1, which binds to core 2 O-glycans on thymocytes and T lymphoblastoid cells. *The Journal of experimental medicine* **181,** 877–887 (1995).

137. Rosenstein, Y., Santana, A. & Pedraza-Alva, G. CD43, a molecule with multiple functions. *Immunologic research* **20,** 89–99 (1999).

138. Woodman, R. C. *et al.* The functional paradox of CD43 in leukocyte recruitment: a study using CD43-deficient mice. *The Journal of experimental medicine* **188,** 2181–2186 (1998).

139. Guyer, D. A. *et al.* P-selectin glycoprotein ligand-1 (PSGL-1) is a ligand for L-selectin in neutrophil aggregation (1996).

140. Asa, D. *et al.* The P-selectin glycoprotein ligand functions as a common human leukocyte ligand for P-and E-selectins. *Journal of biological chemistry* **270,** 11662–11670 (1995).

141. Martinez, M. *et al.* Regulation of PSGL-1 interactions with L-selectin, P-selectin, and E-selectin: role of human fucosyltransferase-IV and-VII. *Journal of Biological Chemistry* **280,** 5378–5390 (2005).

142. Sako, D. *et al.* A sulfated peptide segment at the amino terminus of PSGL-1 is critical for P-selectin binding. *Cell* **83,** 323–331 (1995).

143. Tu, L. *et al.* L-selectin binds to P-selectin glycoprotein ligand-1 on leukocytes: interactions between the lectin, epidermal growth factor, and consensus repeat domains of the

selectins determine ligand binding specificity. *Journal of immunology (Baltimore, Md.: 1950)* **157,** 3995–4004 (1996).

144. DeRogatis, J. M., Viramontes, K. M., Neubert, E. N. & Tinoco, R. PSGL-1 immune checkpoint inhibition for CD4+ T cell cancer immunotherapy. *Frontiers in Immunology* **12,** 636238 (2021).

145. Wang, L. *et al.* VISTA, a novel mouse Ig superfamily ligand that negatively regulates T cell responses. *Journal of Experimental Medicine* **208,** 577–592 (2011).

146. Johnston, R. J. *et al.* VISTA is an acidic pH-selective ligand for PSGL-1. *Nature* **574,** 565–570 (2019).

147. Koning, N. *et al.* Human milk blocks DC-SIGN–pathogen interaction via MUC1. *Frontiers in immunology* **6,** 112 (2015).

148. Tanida, S. *et al.* Binding of the sialic acid-binding lectin, Siglec-9, to the membrane mucin, MUC1, induces recruitment of β-catenin and subsequent cell growth. *Journal of Biological Chemistry* **288,** 31842–31852 (2013).

149. Smagghe, B. J. *et al.* MUC1 ligand, NM23-H1, is a novel growth factor that maintains human stem cells in a more naive state. *PloS one* **8,** e58601 (2013).

150. Yu, L.-G. *et al.* Galectin-3 interaction with Thomsen-Friedenreich disaccharide on cancer-associated MUC1 causes increased cancer cell endothelial adhesion. *Journal of Biological Chemistry* **282,** 773–781 (2007).

151. Zhao, Q. *et al.* Interaction between circulating galectin-3 and cancer-associated MUC1 enhances tumour cell homotypic aggregation and prevents anoikis. *Molecular cancer* **9,** 1–12 (2010).

152. Jorgensen-Tye, B. *et al.* Epitope recognition of antibodies that define the sialomucin, endolyn (CD164), a negative regulator of haematopoiesis. *Tissue Antigens* **65,** 220–239 (2005).

153. Van Vliet, S. J., Gringhuis, S. I., Geijtenbeek, T. B. & van Kooyk, Y. Regulation of effector T cells by antigen-presenting cells via interaction of the C-type lectin MGL with CD45. *Nature immunology* **7,** 1200–1208 (2006).

154. Walzel, H., Schulz, U., Neels, P. & Brock, J. Galectin-1, a natural ligand for the receptor-type protein tyrosine phosphatase CD45. *Immunology letters* **67,** 193–202 (1999).

155. Liu, F.-T. & Rabinovich, G. A. Galectins as modulators of tumour progression. *Nature Reviews Cancer* **5,** 29–41 (2005).

156. Crocker, P. R. *et al.* Siglecs: a family of sialic-acid binding lectins. *Glycobiology* **8,** v–vi (1998).

157. Galluzzi, L. *et al.* Molecular mechanisms of cell death: recommendations of the Nomenclature Committee on Cell Death 2018. *Cell Death & Differentiation* **25,** 486–541 (2018).

158. Fuchs, Y. & Steller, H. Programmed cell death in animal development and disease. *Cell* **147,** 742–758 (2011).

159. Conradt, B. Genetic control of programmed cell death during animal development. *Annual review of genetics* **43,** 493–523 (2009).

160. Galluzzi, L., Bravo-San Pedro, J. M., Kepp, O. & Kroemer, G. Regulated cell death and adaptive stress responses. *Cellular and Molecular Life Sciences* **73,** 2405–2410 (2016).

161. Galluzzi, L. *et al.* Essential versus accessory aspects of cell death: recommendations of the NCCD 2015. *Cell Death & Differentiation* **22,** 58–73 (2015).

162. Datta, A. *et al.* Cell death pathways in ischemic stroke and targeted pharmacotherapy. *Translational Stroke Research* **11,** 1185–1202 (2020).

163. Vogt, C. I. *Untersuchungen über die Entwicklungsgeschichte der Geburtshelferkröte (Alytes obstetricans).* (Jent, 1842).

164. Alberts, B. *et al. Essential cell biology* (Garland Science, 2015).

165. Ke, F. F. *et al.* Embryogenesis and adult life in the absence of intrinsic apoptosis effectors BAX, BAK, and BOK. *Cell* **173,** 1217–1230 (2018).

166. Honarpour, N., Gilbert, S. L., Lahn, B. T., Wang, X. & Herz, J. Apaf-1 deficiency and neural tube closure defects are found in fog mice. *Proceedings of the National Academy of Sciences* **98,** 9683–9687 (2001).

167. Knudson, C. M., Tung, K. S., Tourtellotte, W. G., Brown, G. A. & Korsmeyer, S. J. Bax-deficient mice with lymphoid hyperplasia and male germ cell death. *Science* **270,** 96–99 (1995).

168. Eischen, C. M., Roussel, M. F., Korsmeyer, S. J. & Cleveland, J. L. Bax loss impairs Myc-induced apoptosis and circumvents the selection of p53 mutations during Myc-mediated lymphomagenesis. *Molecular and cellular biology* **21,** 7653–7662 (2001).

169. Luke, J., Van De Wetering, C. & Knudson, C. Lymphoma development in Bax transgenic mice is inhibited by Bcl-2 and associated with chromosomal instability. *Cell Death & Differentiation* **10,** 740–748 (2003).

170. Gheibi Hayat, S. M., Bianconi, V., Pirro, M. & Sahebkar, A. Efferocytosis: molecular mechanisms and pathophysiological perspectives. *Immunology and cell biology* **97,** 124–133 (2019).

171. Saraste, A. & Pulkki, K. Morphologic and biochemical hallmarks of apoptosis. *Cardiovascular research* **45,** 528–537 (2000).

172. Trapani, J. A. Target cell apoptosis induced by cytotoxic T cells and natural killer cells involves synergy between the pore-forming protein, perforin, and the serine protease, granzyme B. *Australian and New Zealand journal of medicine* **25,** 793–799 (1995).

173. Nicholson, D. W. & Thornberry, N. A. Caspases: killer proteases. *Trends in biochemical sciences* **22,** 299–306 (1997).

174. Alnemri, E. S. Mammalian cell death proteases: a family of highly conserved aspartate specific cysteine proteases. *Journal of cellular biochemistry* **64,** 33–42 (1997).

175. Elmore, S. Apoptosis: a review of programmed cell death. *Toxicologic pathology* **35,** 495–516 (2007).

176. Cohen, G. M. Caspases: the executioners of apoptosis. *Biochemical Journal* **326,** 1–16 (1997).

177. Martinvalet, D., Zhu, P. & Lieberman, J. Granzyme A induces caspase-independent mitochondrial damage, a required first step for apoptosis. *Immunity* **22,** 355–370 (2005).

178. Fulda, S. & Debatin, K.-M. Extrinsic versus intrinsic apoptosis pathways in anticancer chemotherapy. *Oncogene* **25,** 4798–4811 (2006).

179. Wyllie, A. H. "Where, O death, is thy sting?" A brief review of apoptosis biology. *Molecular neurobiology* **42,** 4–9 (2010).

180. Greijer, A. & Van der Wall, E. The role of hypoxia inducible factor 1 (HIF-1) in hypoxia induced apoptosis. *Journal of clinical pathology* **57,** 1009–1014 (2004).

181. Portt, L., Norman, G., Clapp, C., Greenwood, M. & Greenwood, M. T. Anti-apoptosis and cell survival: a review. *Biochimica et Biophysica Acta (BBA)-Molecular Cell Research* **1813,** 238–259 (2011).

182. Bouillet, P. & Strasser, A. BH3-only proteins—evolutionarily conserved proapoptotic Bcl-2 family members essential for initiating programmed cell death. *Journal of cell science* **115,** 1567–1574 (2002).

183. Lalier, L. *et al.* Bax activation and mitochondrial insertion during apoptosis. *Apoptosis* **12,** 887–896 (2007).

184. Brunelle, J. K. & Letai, A. Control of mitochondrial apoptosis by the Bcl-2 family. *Journal of cell science* **122,** 437–441 (2009).

185. Wei, M. C. *et al.* Proapoptotic BAX and BAK: a requisite gateway to mitochondrial dysfunction and death. *Science* **292,** 727–730 (2001).

186. Youle, R. J. & Strasser, A. The BCL-2 protein family: opposing activities that mediate cell death. *Nature reviews Molecular cell biology* **9,** 47–59 (2008).

187. Kluck, R. M., Bossy-Wetzel, E., Green, D. R. & Newmeyer, D. D. The release of cytochrome c from mitochondria: a primary site for Bcl-2 regulation of apoptosis. *Science* **275,** 1132–1136 (1997).

188. Liu, X., Kim, C. N., Yang, J., Jemmerson, R. & Wang, X. Induction of apoptotic program in cell-free extracts: requirement for dATP and cytochrome c. *Cell* **86,** 147–157 (1996).

189. Bao, Q. & Shi, Y. Apoptosome: a platform for the activation of initiator caspases. *Cell Death & Differentiation* **14,** 56–65 (2007).

190. Slee, E. A., Adrain, C. & Martin, S. J. Executioner caspase-3,-6, and-7 perform distinct, non-redundant roles during the demolition phase of apoptosis. *Journal of biological Chemistry* **276,** 7320–7326 (2001).

191. Enari, M. *et al.* A caspase-activated DNase that degrades DNA during apoptosis, and its inhibitor ICAD. *Nature* **391,** 43–50 (1998).

192. Kischkel, F. C. *et al.* Cytotoxicity-dependent APO-1 (Fas/CD95)-associated proteins form a death-inducing signaling complex (DISC) with the receptor. *The EMBO journal* **14,** 5579–5588 (1995).

193. Thomas, L. R., Henson, A., Reed, J. C., Salsbury, F. R. & Thorburn, A. Direct binding of Fas-associated death domain (FADD) to the tumor necrosis factor-related apoptosis-inducing ligand receptor DR5 is regulated by the death effector domain of FADD. *Journal of Biological Chemistry* **279,** 32780–32785 (2004).

194. Sprick, M. R. *et al.* FADD/MORT1 and caspase-8 are recruited to TRAIL receptors 1 and 2 and are essential for apoptosis mediated by TRAIL receptor 2. *Immunity* **12,** 599–609 (2000).

195. Hirata, H. *et al.* Caspases are activated in a branched protease cascade and control distinct downstream processes in Fas-induced apoptosis. *The Journal of experimental medicine* **187,** 587–600 (1998).

196. Li, H., Zhu, H., Xu, C.-j. & Yuan, J. Cleavage of BID by caspase 8 mediates the mitochondrial damage in the Fas pathway of apoptosis. *Cell* **94,** 491–501 (1998).

197. Desagher, S. *et al.* Bid-induced conformational change of Bax is responsible for mitochondrial cytochrome c release during apoptosis. *The Journal of cell biology* **144,** 891–901 (1999).

198. Takaba, H. & Takayanagi, H. The mechanisms of T cell selection in the thymus. *Trends in immunology* **38,** 805–816 (2017).

199. Gale, R. P. in *Fetal liver transplantation* 45–56 (Springer, 1987).

200. Anderson, G. & Takahama, Y. Thymic epithelial cells: working class heroes for T cell development and repertoire selection. *Trends in immunology* **33,** 256–263 (2012).

201. Takada, K. & Takahama, Y. Positive-selection-inducing self-peptides displayed by cortical thymic epithelial cells. *Advances in immunology* **125,** 87–110 (2015).

202. Murata, S. *et al.* Regulation of CD8+ T cell development by thymus-specific proteasomes. *Science* **316,** 1349–1353 (2007).

203. Takahama, Y., Takada, K., Murata, S. & Tanaka, K. β5t-containing thymoproteasome: specific expression in thymic cortical epithelial cells and role in positive selection of CD8+ T cells. *Current opinion in immunology* **24,** 92–98 (2012).

204. Wyllie, A. H. Glucocorticoid-induced thymocyte apoptosis is associated with endogenous endonuclease activation. *Nature* **284,** 555–556 (1980).

205. Cifone, M. G. *et al.* Dexamethasone-induced thymocyte apoptosis: apoptotic signal involves the sequential activation of phosphoinositide-specific phospholipase C, acidic sphingomyelinase, and caspases. *Blood, The Journal of the American Society of Hematology* **93,** 2282–2296 (1999).

206. Veis, D. J., Sorenson, C. M., Shutter, J. R. & Korsmeyer, S. J. Bcl-2-deficient mice demonstrate fulminant lymphoid apoptosis, polycystic kidneys, and hypopigmented hair. *Cell* **75,** 229–240 (1993).

207. Rathmell, J. C., Lindsten, T., Zong, W.-X., Cinalli, R. M. & Thompson, C. B. Deficiency in Bak and Bax perturbs thymic selection and lymphoid homeostasis. *Nature immunology* **3,** 932–939 (2002).

208. Park, H. J., Ban, Y. L., Byun, D., Park, S. H. & Jung, K. C. Interaction between the mouse homologue of CD99 and its ligand PILR as a mechanism of T cell receptor-independent thymocyte apoptosis. *Experimental & Molecular Medicine* **42,** 353–365 (2010).

209. Salmena, L. *et al.* Essential role for caspase 8 in T-cell homeostasis and T-cell-mediated immunity. *Genes & development* **17,** 883–895 (2003).

210. Förster, R., Davalos-Misslitz, A. C. & Rot, A. CCR7 and its ligands: balancing immunity and tolerance. *Nature Reviews Immunology* **8,** 362–371 (2008).

211. Perry, J. S. A. Understanding the Interactions of Developing Thymocytes and Antigen Presenting Cells in the Thymic Medulla (2016).

212. Klein, L., Kyewski, B., Allen, P. M. & Hogquist, K. A. Positive and negative selection of the T cell repertoire: what thymocytes see (and don't see). *Nature Reviews Immunology* **14,** 377–391 (2014).

213. Mariathasan, S. *et al.* Duration and strength of extracellular signal-regulated kinase signals are altered during positive versus negative thymocyte selection. *The Journal of Immunology* **167,** 4966–4973 (2001).

214. Stritesky, G. L., Jameson, S. C. & Hogquist, K. A. Selection of self-reactive T cells in the thymus. *Annual review of immunology* **30,** 95–114 (2012).

215. Rincón, M., Flavell, R. A. & Davis, R. J. Signal transduction by MAP kinases in T lymphocytes. *Oncogene* **20,** 2490–2497 (2001).

216. Sabapathy, K. *et al.* c-Jun NH2-terminal kinase (JNK) 1 and JNK2 have similar and stage-dependent roles in regulating T cell apoptosis and proliferation. *The Journal of experimental medicine* **193,** 317–328 (2001).

217. Sugawara, T., Moriguchi, T., Nishida, E. & Takahama, Y. Differential roles of ERK and p38 MAP kinase pathways in positive and negative selection of T lymphocytes. *Immunity* **9,** 565–574 (1998).

218. Werlen, G., Hausmann, B., Naeher, D. & Palmer, E. Signaling life and death in the thymus: timing is everything. *Science* **299,** 1859–1863 (2003).

219. Sakaguchi, S. Regulatory T cells: key controllers of immunologic self-tolerance. *Cell* **101,** 455–458 (2000).

220. Lakhani, S. A. *et al.* Caspases 3 and 7: key mediators of mitochondrial events of apoptosis. *Science* **311,** 847–851 (2006).

221. Murakami, K. *et al.* Caspase 3 is not essential for the induction of anergy or multiple pathways of CD8+ T-cell death. *European journal of immunology* **40,** 3372–3377 (2010).

222. Joza, N. *et al.* Essential role of the mitochondrial apoptosis-inducing factor in programmed cell death. *Nature* **410,** 549–554 (2001).

223. Li, L. Y., Luo, X. & Wang, X. Endonuclease G is an apoptotic DNase when released from mitochondria. *Nature* **412,** 95–99 (2001).

224. Häcker, G., Bauer, A. & Villunger, A. Apoptosis in Activated T Cells–What Are the Triggers, and What the Signal Transducers? *Cell Cycle* **5,** 2421–2424 (2006).

225. Arakaki, R., Yamada, A., Kudo, Y., Hayashi, Y. & Ishimaru, N. Mechanism of activation-induced cell death of T cells and regulation of FasL expression. *Critical Reviews™ in Immunology* **34** (2014).

226. Chhabra, A. Mitochondria-centric activation induced cell death of cytolytic T lymphocytes and its implications for cancer immunotherapy. *Vaccine* **28,** 4566–4572 (2010).

227. Zhao, Z. *et al.* Structural design of engineered costimulation determines tumor rejection kinetics and persistence of CAR T cells. *Cancer cell* **28,** 415–428 (2015).

228. Refaeli, Y., Van Parijs, L., London, C. A., Tschopp, J. & Abbas, A. K. Biochemical mechanisms of IL-2–regulated Fas-mediated T cell apoptosis. *Immunity* **8,** 615–623 (1998).

229. Lenardo, M. J. Interleukin-2 programs mouse $\alpha\beta$ T lymphocytes for apoptosis. *Nature* **353,** 858–861 (1991).

230. Refaeli, Y., Van Parijs, L., Alexander, S. I. & Abbas, A. K. Interferon γ is required for activation-induced death of T lymphocytes. *The Journal of experimental medicine* **196,** 999–1005 (2002).

231. Brenner, D., Krammer, P. H. & Arnold, R. Concepts of activated T cell death. *Critical reviews in oncology/hematology* **66,** 52–64 (2008).

232. Li-Weber, M. & Krammer, P. H. *Function and regulation of the CD95 (APO-1/Fas) ligand in the immune system* in *Seminars in immunology* **15** (2003), 145–157.

233. Baehrecke, E. H. How death shapes life during development. *Nature reviews Molecular cell biology* **3,** 779–787 (2002).

234. Shi, C. & Pamer, E. G. Monocyte recruitment during infection and inflammation. *Nature reviews immunology* **11,** 762–774 (2011).

235. Scott, R. S. *et al.* Phagocytosis and clearance of apoptotic cells is mediated by MER. *Nature* **411,** 207–211 (2001).

236. Zent, C. S. & Elliott, M. R. Maxed out macs: physiologic cell clearance as a function of macrophage phagocytic capacity. *The FEBS journal* **284,** 1021–1039 (2017).

237. Elliott, M. R. & Ravichandran, K. S. The dynamics of apoptotic cell clearance. *Developmental cell* **38,** 147–160 (2016).

238. Ravichandran, K. S. Find-me and eat-me signals in apoptotic cell clearance: progress and conundrums. *Journal of Experimental Medicine* **207,** 1807–1817 (2010).

239. Gordon, S. Phagocytosis: an immunobiologic process. *Immunity* **44,** 463–475 (2016).

240. Underhill, D. M. & Goodridge, H. S. Information processing during phagocytosis. *Nature Reviews Immunology* **12,** 492–502 (2012).

241. Lööv, C., Mitchell, C. H., Simonsson, M. & Erlandsson, A. Slow degradation in phagocytic astrocytes can be enhanced by lysosomal acidification. *Glia* **63,** 1997–2009 (2015).

242. Monks, J., Smith-Steinhart, C., Kruk, E. R., Fadok, V. A. & Henson, P. M. Epithelial cells remove apoptotic epithelial cells during post-lactation involution of the mouse mammary gland. *Biology of reproduction* **78,** 586–594 (2008).

243. Garfield, R., Chacko, S. & Blose, S. Phagocytosis by muscle cells. *Laboratory Investigation; a Journal of Technical Methods and Pathology* **33,** 418–427 (1975).

244. Campbell, G. R., Uehara, Y., Malmfors, T. & Burnstock, G. Degeneration and regeneration of smooth muscle transplants in the anterior eye chamber: an ultrastructural study. *Zeitschrift für Zellforschung und mikroskopische Anatomie* **117,** 155–175 (1971).

245. Ichimura, T. *et al.* Kidney injury molecule–1 is a phosphatidylserine receptor that confers a phagocytic phenotype on epithelial cells. *The Journal of clinical investigation* **118,** 1657–1668 (2008).

246. Davies, S. P., Reynolds, G. M. & Stamataki, Z. Clearance of apoptotic cells by tissue epithelia: a putative role for hepatocytes in liver efferocytosis. *Frontiers in immunology* **9,** 44 (2018).

247. Henson, P. M. Cell removal: efferocytosis. *Annual review of cell and developmental biology* **33,** 127–144 (2017).

248. Birge, R. *et al.* Phosphatidylserine is a global immunosuppressive signal in efferocytosis, infectious disease, and cancer. *Cell Death & Differentiation* **23,** 962–978 (2016).

249. Martin, C. J., Peters, K. N. & Behar, S. M. Macrophages clean up: efferocytosis and microbial control. *Current opinion in microbiology* **17,** 17–23 (2014).

250. deCathelineau, A. M. & Henson, P. M. The final step in programmed cell death: phagocytes carry apoptotic cells to the grave. *Essays in biochemistry* **39,** 105–117 (2003).

251. Hoffmann, P. R. *et al.* Phosphatidylserine (PS) induces PS receptor–mediated macropinocytosis and promotes clearance of apoptotic cells. *The Journal of cell biology* **155,** 649–660 (2001).

252. Kumar, S. & Birge, R. B. Efferocytosis. *Current biology* **26,** R558–R559 (2016).

253. Fond, A. M. & Ravichandran, K. S. Clearance of dying cells by phagocytes: mechanisms and implications for disease pathogenesis. *Apoptosis in cancer pathogenesis and anti-cancer therapy: New perspectives and opportunities,* 25–49 (2016).

254. Hochreiter-Hufford, A. & Ravichandran, K. S. Clearing the dead: apoptotic cell sensing, recognition, engulfment, and digestion. *Cold Spring Harbor perspectives in biology* **5,** a008748 (2013).

255. Kroemer, G. Dying cell recognition shapes the pathophysiology of cell death. *Cell Death & Differentiation* **23,** 913–914 (2016).

256. Peter, C., Wesselborg, S. & Lauber, K. Molecular suicide notes: last call from apoptosing cells. *Journal of molecular cell biology* **2,** 78–80 (2010).

257. Segawa, K. & Nagata, S. An apoptotic 'eat me'signal: phosphatidylserine exposure. *Trends in cell biology* **25,** 639–650 (2015).

258. Li, W. Eat-me signals: Keys to molecular phagocyte biology and "Appetite" control. *Journal of cellular physiology* **227,** 1291–1297 (2012).

259. Fadok, V. A. *et al.* Exposure of phosphatidylserine on the surface of apoptotic lymphocytes triggers specific recognition and removal by macrophages. *Journal of immunology (Baltimore, Md.: 1950)* **148,** 2207–2216 (1992).

260. Fadok, V. A., De Cathelineau, A., Daleke, D. L., Henson, P. M. & Bratton, D. L. Loss of phospholipid asymmetry and surface exposure of phosphatidylserine is required for phagocytosis of apoptotic cells by macrophages and fibroblasts. *Journal of Biological Chemistry* **276,** 1071–1077 (2001).

261. Gardai, S. J., Bratton, D. L., Ogden, C. A. & Henson, P. M. Recognition ligands on apoptotic cells: a perspective. *Journal of leukocyte biology* **79,** 896–903 (2006).

262. Brown, G. C. & Neher, J. J. Eaten alive! Cell death by primary phagocytosis:'phagoptosis'. *Trends in biochemical sciences* **37,** 325–332 (2012).

263. Park, S.-Y. & Kim, I.-S. Engulfment signals and the phagocytic machinery for apoptotic cell clearance. *Experimental & molecular medicine* **49,** e331–e331 (2017).

264. Biermann, M. *et al.* Surface code—biophysical signals for apoptotic cell clearance. *Physical biology* **10,** 065007 (2013).

265. Poon, I. K., Lucas, C. D., Rossi, A. G. & Ravichandran, K. S. Apoptotic cell clearance: basic biology and therapeutic potential. *Nature Reviews Immunology* **14,** 166–180 (2014).

266. Anderson, C. L., Shen, L., Eicher, D. M., Wewers, M. D. & Gill, J. K. Phagocytosis mediated by three distinct Fc gamma receptor classes on human leukocytes. *The Journal of experimental medicine* **171,** 1333–1345 (1990).

267. Willingham, S. B. *et al.* The CD47-signal regulatory protein alpha (SIRPa) interaction is a therapeutic target for human solid tumors. *Proceedings of the National Academy of Sciences* **109,** 6662–6667 (2012).

268. Kato, K. *et al.* Membrane-tethered MUC1 mucin counter-regulates the phagocytic activity of macrophages. *American Journal of Respiratory Cell and Molecular Biology* **54,** 515–523 (2016).

269. Freeman, S. & Grinstein, S. Promoters and antagonists of phagocytosis: a plastic and tunable response. *Annual Review of Cell and Developmental Biology* **37,** 89–114 (2021).

270. Imbert, P. R. *et al.* An acquired and endogenous glycocalyx forms a bidirectional “Don’t Eat” and “Don’t Eat Me” barrier to phagocytosis. *Current Biology* **31,** 77–89 (2021).

271. Green, D., Oguin, T. H. & Martinez, J. The clearance of dying cells: table for two. *Cell Death & Differentiation* **23,** 915–926 (2016).

272. Yin, C. & Heit, B. Cellular responses to the efferocytosis of apoptotic cells. *Frontiers in Immunology* **12,** 631714 (2021).

273. Kinchen, J. M. & Ravichandran, K. S. Phagosome maturation: going through the acid test. *Nature reviews Molecular cell biology* **9,** 781–795 (2008).

274. Park, D. *et al.* BAI1 is an engulfment receptor for apoptotic cells upstream of the ELMO/Dock180/Rac module. *Nature* **450,** 430–434 (2007).

275. Kim, S.-Y. *et al.* Coordinated balance of Rac1 and RhoA plays key roles in determining phagocytic appetite. *PLoS One* **12,** e0174603 (2017).

276. Yin, C., Kim, Y., Argintaru, D. & Heit, B. Rab17 mediates differential antigen sorting following efferocytosis and phagocytosis. *Cell Death & Disease* **7,** e2529–e2529 (2016).

277. Mills, I. G., Jones, A. T. & Clague, M. J. Involvement of the endosomal autoantigen EEA1 in homotypic fusion of early endosomes. *Current Biology* **8,** 881–884 (1998).

278. Gorvel, J.-P., Chavrier, P., Zerial, M. & Gruenberg, J. rab5 controls early endosome fusion in vitro. *Cell* **64,** 915–925 (1991).

279. Harrison, R. E., Bucci, C., Vieira, O. V., Schroer, T. A. & Grinstein, S. Phagosomes fuse with late endosomes and/or lysosomes by extension of membrane protrusions along microtubules: role of Rab7 and RILP. *Molecular and cellular biology* **23,** 6494–6506 (2003).

280. Yin, C., Argintaru, D. & Heit, B. Rab17 mediates intermixing of phagocytosed apoptotic cells with recycling endosomes. *Small GTPases* **10,** 218–226 (2019).

281. Wang, Y. *et al.* Mitochondrial fission promotes the continued clearance of apoptotic cells by macrophages. *Cell* **171,** 331–345 (2017).

282. Heckmann, B. L. & Green, D. R. LC3-associated phagocytosis at a glance. *Journal of cell science* **132,** jcs222984 (2019).

283. Li, B. *et al.* The melanoma-associated transmembrane glycoprotein Gpnmb controls trafficking of cellular debris for degradation and is essential for tissue repair. *The FASEB Journal* **24,** 4767 (2010).

284. Martinez, J. *et al.* Molecular characterization of LC3-associated phagocytosis reveals distinct roles for Rubicon, NOX2 and autophagy proteins. *Nature cell biology* **17,** 893–906 (2015).

285. Wan, J. *et al.* LC3-associated phagocytosis protects against inflammation and liver fibrosis via immunoreceptor inhibitory signaling. *Science translational medicine* **12,** eaaw8523 (2020).

286. Hanayama, R. *et al.* Autoimmune disease and impaired uptake of apoptotic cells in MFG-E8-deficient mice. *Science* **304,** 1147–1150 (2004).

287. Botto, M. *et al.* Homozygous C1q deficiency causes glomerulonephritis associated with multiple apoptotic bodies. *Nature genetics* **19,** 56–59 (1998).

288. Mukundan, L. *et al.* PPAR-δ senses and orchestrates clearance of apoptotic cells to promote tolerance. *Nature medicine* **15,** 1266–1272 (2009).

289. Thorp, E. *et al.* Shedding of the Mer tyrosine kinase receptor is mediated by ADAM17 protein through a pathway involving reactive oxygen species, protein kinase Cδ, and p38 mitogen-activated protein kinase (MAPK). *Journal of Biological Chemistry* **286,** 33335–33344 (2011).

290. Sather, S. *et al.* A soluble form of the Mer receptor tyrosine kinase inhibits macrophage clearance of apoptotic cells and platelet aggregation. *Blood* **109,** 1026–1033 (2007).

291. Ait-Oufella, H. *et al.* Defective mer receptor tyrosine kinase signaling in bone marrow cells promotes apoptotic cell accumulation and accelerates atherosclerosis. *Arteriosclerosis, thrombosis, and vascular biology* **28,** 1429–1431 (2008).

292. Cai, B. *et al.* MerTK receptor cleavage promotes plaque necrosis and defective resolution in atherosclerosis. *The Journal of clinical investigation* **127,** 564–568 (2017).

293. Zhang, Y. *et al.* Angiotensin II deteriorates advanced atherosclerosis by promoting MerTK cleavage and impairing efferocytosis through the AT1R/ROS/p38 MAPK/ADAM17 pathway. *American Journal of Physiology-Cell Physiology* **317,** C776–C787 (2019).

294. Kojima, Y. *et al.* CD47-blocking antibodies restore phagocytosis and prevent atherosclerosis. *Nature* **536,** 86–90 (2016).

295. Zhang, S. *et al.* Acute CD47 blockade during ischemic myocardial reperfusion enhances phagocytosis-associated cardiac repair. *Basic to Translational Science* **2,** 386–397 (2017).

296. DeBerge, M. *et al.* MerTK cleavage on resident cardiac macrophages compromises repair after myocardial ischemia reperfusion injury. *Circulation research* **121,** 930–940 (2017).

297. Wan, E. *et al.* Enhanced efferocytosis of apoptotic cardiomyocytes through myeloid-epithelial-reproductive tyrosine kinase links acute inflammation resolution to cardiac repair after infarction. *Circulation research* **113,** 1004–1012 (2013).

298. De Couto, G. *et al.* Mechanism of enhanced MerTK-dependent macrophage efferocytosis by extracellular vesicles. *Arteriosclerosis, thrombosis, and vascular biology* **39,** 2082–2096 (2019).

299. Luo, B., Wang, Z., Zhang, Z., Shen, Z. & Zhang, Z. The deficiency of macrophage erythropoietin signaling contributes to delayed acute inflammation resolution in diet-induced obese mice. *Biochimica et Biophysica Acta (BBA)-Molecular Basis of Disease* **1865,** 339–349 (2019).

300. Li, S. *et al.* Defective phagocytosis of apoptotic cells by macrophages in atherosclerotic lesions of ob/ob mice and reversal by a fish oil diet. *Circulation research* **105,** 1072–1082 (2009).

301. Suresh Babu, S. *et al.* MicroRNA-126 overexpression rescues diabetes-induced impairment in efferocytosis of apoptotic cardiomyocytes. *Scientific reports* **6,** 36207 (2016).

302. Barkal, A. A. *et al.* CD24 signalling through macrophage Siglec-10 is a target for cancer immunotherapy. *Nature* **572,** 392–396 (2019).

303. Minson, K. A. *et al.* The MERTK/FLT3 inhibitor MRX-2843 overcomes resistance-conferring FLT3 mutations in acute myeloid leukemia. *JCI insight* **1** (2016).

304. Zeidan, A. M. *et al.* The STIMULUS program: clinical trials evaluating sabatolimab (MBG453) combination therapy in patients (Pts) with higher-risk myelodysplastic syndromes (HR-MDS) or acute myeloid leukemia (AML). *Blood* **136,** 45–46 (2020).

305. Harding, J. J. *et al.* Blocking TIM-3 in treatment-refractory advanced solid tumors: a phase Ia/b study of LY3321367 with or without an anti-PD-L1 antibody. *Clinical Cancer Research* **27,** 2168–2178 (2021).

306. Subbiah, V. *et al. Trials in progress: A phase 1, open-label, dose-escalation, pharmacokinetic, safety and tolerability study of the selective TAM kinase inhibitor PF-07265807 in patients with advanced or metastatic solid tumors.* 2021.

307. Post, S. M. *et al.* AXL/MERTK inhibitor ONO-7475 potently synergizes with venetoclax and overcomes venetoclax resistance to kill F LT 3-ITD acute myeloid leukemia. *Haematologica* **107,** 1311 (2022).

308. Pinti, M. *et al.* Circulating mitochondrial DNA increases with age and is a familiar trait: Implications for “inflamm-aging”. *European journal of immunology* **44,** 1552–1562 (2014).

309. Mehrotra, P. & Ravichandran, K. S. Drugging the efferocytosis process: concepts and opportunities. *Nature reviews Drug discovery* **21,** 601–620 (2022).

310. Rymut, N. *et al.* Resolvin D1 promotes efferocytosis in aging by limiting senescent cell-induced MerTK cleavage. *FASEB journal: official publication of the Federation of American Societies for Experimental Biology* **34,** 597 (2020).

311. Navarini, L. *et al.* Role of the specialized proresolving mediator resolvin D1 in systemic lupus erythematosus: preliminary results. *Journal of immunology research* **2018** (2018).

312. Demir, F. *et al.* Proteolysis and inflammation of the kidney glomerulus. *Cell and Tissue Research* **385,** 489–500 (2021).

313. Bond, J. S. Proteases: History, discovery, and roles in health and disease. *Journal of Biological Chemistry* **294,** 1643–1651 (2019).

314. Sterchi, E. E., Stöcker, W. & Bond, J. S. Meprins, membrane-bound and secreted astacin metalloproteinases. *Molecular aspects of medicine* **29,** 309–328 (2008).

315. Edwards, D. R., Handsley, M. M. & Pennington, C. J. The ADAM metalloproteinases. *Molecular aspects of medicine* **29,** 258–289 (2008).

316. Rosenbaum, D. & Saftig, P. New insights into the function and pathophysiology of the ectodomain sheddase A Disintegrin And Metalloproteinase 10 (ADAM10). *The FEBS Journal* (2023).

317. Weber, S. & Saftig, P. Ectodomain shedding and ADAMs in development. *Development* **139,** 3693–3709 (2012).

318. Becherer, J. D. & Blobel, C. P. Biochemical properties and functions of membrane-anchored metalloprotease-disintegrin proteins (ADAMs) (2003).

319. Brummer, T. *et al.* The metalloprotease ADAM10 (a disintegrin and metalloprotease 10) undergoes rapid, postlysis autocatalytic degradation. *The FASEB Journal* **32,** 3560 (2018).

320. Saftig, P. & Lichtenthaler, S. F. The alpha secretase ADAM10: A metalloprotease with multiple functions in the brain. *Progress in neurobiology* **135,** 1–20 (2015).

321. Blobel, C. P. ADAMs: key components in EGFR signalling and development. *Nature reviews Molecular cell biology* **6,** 32–43 (2005).

322. Arribas, J. & Massagué, J. Transforming growth factor-alpha and beta-amyloid precursor protein share a secretory mechanism. *The Journal of cell biology* **128,** 433–441 (1995).

323. De Strooper, B. & Annaert, W. Novel research horizons for presenilins and γ-secretases in cell biology and disease. *Annual review of cell and developmental biology* **26,** 235–260 (2010).

324. Zolkiewska, A. ADAM proteases: ligand processing and modulation of the Notch pathway. *Cellular and Molecular Life Sciences* **65,** 2056–2068 (2008).

325. Alabi, R. O., Farber, G. & Blobel, C. P. Intriguing roles for endothelial ADAM10/Notch signaling in the development of organ-specific vascular beds. *Physiological reviews* **98,** 2025–2061 (2018).

326. Möller-Hackbarth, K. *et al.* A disintegrin and metalloprotease (ADAM) 10 and ADAM17 are major sheddases of T cell immunoglobulin and mucin domain 3 (Tim-3). *Journal of Biological Chemistry* **288,** 34529–34544 (2013).

327. Zunke, F. & Rose-John, S. The shedding protease ADAM17: Physiology and pathophysiology. *Biochimica et Biophysica Acta (BBA)-Molecular Cell Research* **1864,** 2059–2070 (2017).

328. Hartmann, M., Herrlich, A. & Herrlich, P. Who decides when to cleave an ectodomain? *Trends in biochemical sciences* **38,** 111–120 (2013).

329. Prinzen, C., Müller, U., Endres, K., Fahrenholz, F. & Postina, R. Genomic structure and functional characterization of the human ADAM10 promoter. *The FASEB Journal* **19,** 1522–1524 (2005).

330. Corbett, G. T., Gonzalez, F. J. & Pahan, K. Activation of peroxisome proliferator-activated receptor α stimulates ADAM10-mediated proteolysis of APP. *Proceedings of the National Academy of Sciences* **112,** 8445–8450 (2015).

331. Augustin, R. *et al.* Computational identification and experimental validation of microRNAs binding to the Alzheimer-related gene ADAM10. *BMC medical genetics* **13,** 1–12 (2012).

332. Cheng, C. *et al.* MicroRNA-144 is regulated by activator protein-1 (AP-1) and decreases expression of Alzheimer disease-related a disintegrin and metalloprotease 10 (ADAM10). *Journal of Biological Chemistry* **288,** 13748–13761 (2013).

333. Anders, A., Gilbert, S., Garten, W., Postina, R. & Fahrenholz, F. Regulation of the α-secretase ADAM10 by its prodomain and proprotein convertases. *The FASEB Journal* **15,** 1837–1839 (2001).

334. Hwang, E. M. *et al.* Furin is an endogenous regulator of α-secretase associated APP processing. *Biochemical and biophysical research communications* **349,** 654–659 (2006).

335. Lopez-Perez, E. *et al.* Constitutive α-secretase cleavage of the β-amyloid precursor protein in the furin-deficient LoVo cell line: involvement of the pro-hormone convertase 7 and the disintegrin metalloprotease ADAM10. *Journal of neurochemistry* **76,** 1532–1539 (2001).

336. Seegar, T. C. *et al.* Structural basis for regulated proteolysis by the α-secretase ADAM10. *Cell* **171,** 1638–1648 (2017).

337. Lipper, C. H. *et al.* Crystal structure of the Tspan15 LEL domain reveals a conserved ADAM10 binding site. *Structure* **30,** 206–214 (2022).

338. Janes, P. W. *et al.* Adam meets Eph: an ADAM substrate recognition module acts as a molecular switch for ephrin cleavage in trans. *Cell* **123,** 291–304 (2005).

339. Lipper, C. H., Egan, E. D., Gabriel, K.-H. & Blacklow, S. C. Structural basis for membrane-proximal proteolysis of substrates by ADAM10. *Cell* **186,** 3632–3641 (2023).

340. Reiss, K. & Saftig, P. *The "a disintegrin and metalloprotease"(ADAM) family of sheddases: physiological and cellular functions* in *Seminars in cell & developmental biology* **20** (2009), 126–137.

341. Ebsen, H., Lettau, M., Kabelitz, D. & Janssen, O. Identification of SH3 domain proteins interacting with the cytoplasmic tail of the a disintegrin and metalloprotease 10 (ADAM10). *PloS one* **9,** e102899 (2014).

342. Wild-Bode, C., Fellerer, K., Kugler, J., Haass, C. & Capell, A. A basolateral sorting signal directs ADAM10 to adherens junctions and is required for its function in cell migration. *Journal of biological chemistry* **281,** 23824–23829 (2006).

343. Van Tetering, G. *et al.* Metalloprotease ADAM10 is required for Notch1 site 2 cleavage. *Journal of Biological Chemistry* **284,** 31018–31027 (2009).

344. Hundhausen, C. *et al.* Regulated shedding of transmembrane chemokines by the disintegrin and metalloproteinase 10 facilitates detachment of adherent leukocytes. *The Journal of Immunology* **178,** 8064–8072 (2007).

345. Postina, R. *et al.* A disintegrin-metalloproteinase prevents amyloid plaque formation and hippocampal defects in an Alzheimer disease mouse model. *The Journal of clinical investigation* **113,** 1456–1464 (2004).

346. Schulz, B. *et al.* ADAM10 regulates endothelial permeability and T-Cell transmigration by proteolysis of vascular endothelial cadherin. *Circulation research* **102,** 1192–1201 (2008).

347. Bender, M. *et al.* Differentially regulated GPVI ectodomain shedding by multiple platelet–expressed proteinases. *Blood, The Journal of the American Society of Hematology* **116,** 3347–3355 (2010).

348. Gardiner, E. E. & Andrews, R. K. Platelet receptor proteolysis: GPVI and ADAM10. *Chemistry Today* **25,** 8–10 (2007).

349. Altmeppen, H. C. *et al.* The sheddase ADAM10 is a potent modulator of prion disease. *Elife* **4,** e04260 (2015).

350. Yan, Y., Shirakabe, K. & Werb, Z. The metalloprotease Kuzbanian (ADAM10) mediates the transactivation of EGF receptor by G protein–coupled receptors. *The Journal of cell biology* **158,** 221–226 (2002).

351. Sahin, U. *et al.* Distinct roles for ADAM10 and ADAM17 in ectodomain shedding of six EGFR ligands. *The Journal of cell biology* **164,** 769–779 (2004).

352. Sanderson, M. P. *et al.* ADAM10 mediates ectodomain shedding of the betacellulin precursor activated by p-aminophenylmercuric acetate and extracellular calcium influx. *Journal of Biological Chemistry* **280,** 1826–1837 (2005).

353. Suzuki, J., Denning, D. P., Imanishi, E., Horvitz, H. R. & Nagata, S. Xk-related protein 8 and CED-8 promote phosphatidylserine exposure in apoptotic cells. *Science* **341,** 403–406 (2013).

354. Nagano, O. *et al.* Cell–matrix interaction via CD44 is independently regulated by different metalloproteinases activated in response to extracellular Ca2+ influx and PKC activation. *The Journal of cell biology* **165,** 893–902 (2004).

355. Reiss, K. *et al.* ADAM10 cleavage of N-cadherin and regulation of cell–cell adhesion and β-catenin nuclear signalling. *The EMBO journal* **24,** 742–752 (2005).

356. Donners, M. M. *et al.* A disintegrin and metalloprotease 10 is a novel mediator of vascular endothelial growth factor–induced endothelial cell function in angiogenesis and is associated with atherosclerosis. *Arteriosclerosis, thrombosis, and vascular biology* **30,** 2188–2195 (2010).

357. Lemieux, G. A. *et al.* The low affinity IgE receptor (CD23) is cleaved by the metalloproteinase ADAM10. *Journal of Biological Chemistry* **282,** 14836–14844 (2007).

358. Van der Vorst, E. P., Keijbeck, A. A., de Winther, M. P. & Donners, M. M. A disintegrin and metalloproteases: molecular scissors in angiogenesis, inflammation and atherosclerosis. *Atherosclerosis* **224,** 302–308 (2012).

359. Pruessmeyer, J. & Ludwig, A. *The good, the bad and the ugly substrates for ADAM10 and ADAM17 in brain pathology, inflammation and cancer* in *Seminars in cell & developmental biology* **20** (2009), 164–174.

360. Wetzel, S., Seipold, L. & Saftig, P. The metalloproteinase ADAM10: A useful therapeutic target? *Biochimica et Biophysica Acta (BBA)-Molecular Cell Research* **1864,** 2071–2081 (2017).

361. Endres, K. & Deller, T. Regulation of alpha-secretase ADAM10 in vitro and in vivo: genetic, epigenetic, and protein-based mechanisms. *Frontiers in molecular neuroscience* **10,** 56 (2017).

362. Marcello, E. *et al.* Endocytosis of synaptic ADAM10 in neuronal plasticity and Alzheimer's disease. *The Journal of clinical investigation* **123,** 2523–2538 (2013).

363. Saraceno, C. *et al.* SAP97-mediated ADAM10 trafficking from Golgi outposts depends on PKC phosphorylation. *Cell death & disease* **5,** e1547–e1547 (2014).

364. Linford, A. *et al.* Rab14 and its exchange factor FAM116 link endocytic recycling and adherens junction stability in migrating cells. *Developmental cell* **22,** 952–966 (2012).

365. Tousseyn, T. *et al.* ADAM10, the rate-limiting protease of regulated intramembrane proteolysis of Notch and other proteins, is processed by ADAMS-9, ADAMS-15, and the γ-secretase. *Journal of Biological Chemistry* **284,** 11738–11747 (2009).

366. Moss, M. L. *et al.* ADAM9 inhibition increases membrane activity of ADAM10 and controls α-secretase processing of amyloid precursor protein. *Journal of Biological Chemistry* **286,** 40443–40451 (2011).

367. Cisse, M. A. *et al.* The disintegrin ADAM9 indirectly contributes to the physiological processing of cellular prion by modulating ADAM10 activity. *Journal of Biological Chemistry* **280,** 40624–40631 (2005).

368. Murai, T. Cholesterol lowering: role in cancer prevention and treatment. *Biological chemistry* **396,** 1–11 (2015).

369. Matthews, V. *et al.* Cellular cholesterol depletion triggers shedding of the human interleukin-6 receptor by ADAM10 and ADAM17 (TACE). *Journal of biological chemistry* **278,** 38829–38839 (2003).

370. Sathya, M. *et al.* Resveratrol intervenes cholesterol-and isoprenoid-mediated amyloidogenic processing of AβPP in familial Alzheimer's disease. *Journal of Alzheimer's Disease* **60,** S3–S23 (2017).

371. Moss, M. L. *et al.* The ADAM10 prodomain is a specific inhibitor of ADAM10 proteolytic activity and inhibits cellular shedding events. *Journal of Biological Chemistry* **282,** 35712–35721 (2007).

372. Murphy, G. Tissue inhibitors of metalloproteinases. *Genome biology* **12,** 1–7 (2011).

373. Amour, A. *et al.* The in vitro activity of ADAM-10 is inhibited by TIMP-1 and TIMP-3. *FEBS letters* **473,** 275–279 (2000).

374. Facey, A. *et al.* A-disintegrin-and-metalloproteinase (ADAM) 10 activity on resting and activated platelets. *Biochemistry* **55,** 1187–1194 (2016).

375. Leitzke, S. *et al.* Influence of Anoctamin-4 and-9 on ADAM10 and ADAM17 Sheddase Function. *Membranes* **12,** 123 (2022).

376. Suzuki, J., Umeda, M., Sims, P. J. & Nagata, S. Calcium-dependent phospholipid scrambling by TMEM16F. *Nature* **468,** 834–838 (2010).

377. Bleibaum, F. *et al.* ADAM10 sheddase activation is controlled by cell membrane asymmetry. *Journal of molecular cell biology* **11,** 979–993 (2019).

378. Seipold, L. & Saftig, P. The emerging role of tetraspanins in the proteolytic processing of the amyloid precursor protein. *Frontiers in molecular neuroscience* **9,** 149 (2016).

379. Koo, C. Z. *et al.* The tetraspanin Tspan15 is an essential subunit of an ADAM10 scissor complex. *Journal of Biological Chemistry* **295,** 12822–12839 (2020).

380. Harrison, N., Koo, C. Z. & Tomlinson, M. G. Regulation of ADAM10 by the TspanC8 family of tetraspanins and their therapeutic potential. *International journal of molecular sciences* **22,** 6707 (2021).

381. Matthews, A. L., Szyroka, J., Collier, R., Noy, P. J. & Tomlinson, M. G. Scissor sisters: regulation of ADAM10 by the TspanC8 tetraspanins. *Biochemical Society Transactions* **45,** 719–730 (2017).

382. Prox, J. *et al.* Tetraspanin15 regulates cellular trafficking and activity of the ectodomain sheddase ADAM10. *Cellular and Molecular Life Sciences* **69,** 2919–2932 (2012).

383. Mullooly, M. *et al.* ADAM10: a new player in breast cancer progression? *British journal of cancer* **113,** 945–951 (2015).

384. Induruwa, I., Jung, S. M. & Warburton, E. A. Beyond antiplatelets: the role of glycoprotein VI in ischemic stroke. *International Journal of Stroke* **11,** 618–625 (2016).

385. Hartmann, D. *et al.* The disintegrin/metalloprotease ADAM 10 is essential for Notch signalling but not for α-secretase activity in fibroblasts. *Human molecular genetics* **11,** 2615–2624 (2002).

386. Meyer-Schwesinger, C., Seipold, L. & Saftig, P. Ectodomain shedding by ADAM proteases as a central regulator in kidney physiology and disease. *Biochimica et Biophysica Acta (BBA)-Molecular Cell Research* **1869,** 119165 (2022).

387. Kopan, R. & Ilagan, M. X. G. The canonical Notch signaling pathway: unfolding the activation mechanism. *Cell* **137,** 216–233 (2009).

388. Manilay, J. O., Anderson, A. C., Kang, C. & Robey, E. A. Impairment of thymocyte development by dominant-negative Kuzbanian (ADAM-10) is rescued by the Notch ligand, delta-1. *The Journal of Immunology* **174,** 6732–6741 (2005).

389. Andrews, L. P. *et al.* Resistance to PD1 blockade in the absence of metalloprotease-mediated LAG3 shedding. *Science immunology* **5,** eabc2728 (2020).

390. Woo, S.-R. *et al.* Immune inhibitory molecules LAG-3 and PD-1 synergistically regulate T-cell function to promote tumoral immune escape. *Cancer research* **72,** 917–927 (2012).

391. Yang, Y., Lee, M. & Fairn, G. D. Phospholipid subcellular localization and dynamics. *Journal of Biological Chemistry* **293,** 6230–6240 (2018).

392. Vance, J. E. Phospholipid synthesis and transport in mammalian cells. *Traffic* **16,** 1–18 (2015).

393. Gong, Y.-N. *et al.* ESCRT-III acts downstream of MLKL to regulate necroptotic cell death and its consequences. *Cell* **169,** 286–300 (2017).

394. Rühl, S. *et al.* ESCRT-dependent membrane repair negatively regulates pyroptosis downstream of GSDMD activation. *Science* **362,** 956–960 (2018).

395. Seki, M., Arashiki, N., Takakuwa, Y., Nitta, K. & Nakamura, F. Reduction in flippase activity contributes to surface presentation of phosphatidylserine in human senescent erythrocytes. *Journal of Cellular and Molecular Medicine* **24,** 13991–14000 (2020).

396. Dasgupta, S. K. *et al.* Platelet senescence and phosphatidylserine exposure. *Transfusion* **50,** 2167–2175 (2010).

397. Ball, J. B., Green-Fulgham, S. M. & Watkins, L. R. Mechanisms of microglia-mediated synapse turnover and synaptogenesis. *Progress in Neurobiology,* 102336 (2022).

398. Riedl, S. *et al.* In search of a novel target—Phosphatidylserine exposed by non-apoptotic tumor cells and metastases of malignancies with poor treatment efficacy. *Biochimica et Biophysica Acta (BBA)-Biomembranes* **1808,** 2638–2645 (2011).

399. Sahu, S. K., Gummadi, S. N., Manoj, N. & Aradhyam, G. K. Phospholipid scramblases: an overview. *Archives of biochemistry and biophysics* **462,** 103–114 (2007).

400. Leventis, P. A. & Grinstein, S. The distribution and function of phosphatidylserine in cellular membranes. *Annual review of biophysics* **39,** 407–427 (2010).

401. Bricogne, C. *et al.* TMEM16F activation by Ca2+ triggers plasma membrane expansion and directs PD-1 trafficking. *Scientific reports* **9,** 619 (2019).

402. Suzuki, J., Imanishi, E. & Nagata, S. Exposure of phosphatidylserine by Xk-related protein family members during apoptosis. *Journal of Biological Chemistry* **289,** 30257–30267 (2014).

403. Scudieri, P. *et al.* Ion channel and lipid scramblase activity associated with expression of TMEM16F/ANO6 isoforms. *The Journal of physiology* **593,** 3829–3848 (2015).

404. Gyobu, S., Ishihara, K., Suzuki, J., Segawa, K. & Nagata, S. Characterization of the scrambling domain of the TMEM16 family. *Proceedings of the National Academy of Sciences* **114,** 6274–6279 (2017).

405. Tsuji, T. *et al.* Predominant localization of phosphatidylserine at the cytoplasmic leaflet of the ER, and its TMEM16K-dependent redistribution. *Proceedings of the National Academy of Sciences* **116,** 13368–13373 (2019).

406. Fujii, T., Sakata, A., Nishimura, S., Eto, K. & Nagata, S. TMEM16F is required for phosphatidylserine exposure and microparticle release in activated mouse platelets. *Proceedings of the National Academy of Sciences* **112,** 12800–12805 (2015).

407. Bethel, N. P. & Grabe, M. Atomistic insight into lipid translocation by a TMEM16 scramblase. *Proceedings of the National Academy of Sciences* **113,** 14049–14054 (2016).

408. Kobayashi, T. & Menon, A. K. Transbilayer lipid asymmetry. *Current Biology* **28,** R386–R391 (2018).

409. Yang, H. *et al.* TMEM16F forms a Ca2+-activated cation channel required for lipid scrambling in platelets during blood coagulation. *Cell* **151,** 111–122 (2012).

410. Almaça, J. *et al.* TMEM16 proteins produce volume-regulated chloride currents that are reduced in mice lacking TMEM16A. *Journal of Biological Chemistry* **284,** 28571–28578 (2009).

411. Martins, J. R. *et al.* Anoctamin 6 is an essential component of the outwardly rectifying chloride channel. *Proceedings of the National Academy of Sciences* **108,** 18168–18172 (2011).

412. Sakuragi, T. & Nagata, S. Regulation of phospholipid distribution in the lipid bilayer by flippases and scramblases. *Nature Reviews Molecular Cell Biology,* 1–21 (2023).

413. Brunner, J. D., Lim, N. K., Schenck, S., Duerst, A. & Dutzler, R. X-ray structure of a calcium-activated TMEM16 lipid scramblase. *Nature* **516,** 207–212 (2014).

414. Veit, M. *et al.* Anoctamin-6 regulates ADAM sheddase function. *Biochimica et Biophysica Acta (BBA)-Molecular Cell Research* **1865,** 1598–1610 (2018).

415. Millington-Burgess, S. L. & Harper, M. T. Gene of the issue: ANO6 and Scott Syndrome. *Platelets* **31,** 964–967 (2020).

416. Castoldi, E., Collins, P. W., Williamson, P. L. & Bevers, E. M. Compound heterozygosity for 2 novel TMEM16F mutations in a patient with Scott syndrome. *Blood, The Journal of the American Society of Hematology* **117,** 4399–4400 (2011).

417. Boisseau, P. *et al.* A new mutation of ANO6 in two familial cases of Scott syndrome. *British journal of haematology* **180,** 750–752 (2018).

418. Nagata, S., Sakuragi, T. & Segawa, K. Flippase and scramblase for phosphatidylserine exposure. *Current Opinion in Immunology* **62,** 31–38 (2020).

419. Pervaiz, N. *et al.* Evolutionary history of the human multigene families reveals widespread gene duplications throughout the history of animals. *BMC Evolutionary Biology* **19,** 1–11 (2019).

420. Suzuki, J., Imanishi, E. & Nagata, S. Xkr8 phospholipid scrambling complex in apoptotic phosphatidylserine exposure. *Proceedings of the National Academy of Sciences* **113,** 9509–9514 (2016).

421. Sakuragi, T., Kosako, H. & Nagata, S. Phosphorylation-mediated activation of mouse Xkr8 scramblase for phosphatidylserine exposure. *Proceedings of the National Academy of Sciences* **116,** 2907–2912 (2019).

422. Kawano, M. & Nagata, S. Lupus-like autoimmune disease caused by a lack of Xkr8, a caspase-dependent phospholipid scramblase. *Proceedings of the National Academy of Sciences* **115,** 2132–2137 (2018).

423. Yamashita, Y., Suzuki, C., Uchiyama, Y. & Nagata, S. Infertility caused by inefficient apoptotic germ cell clearance in Xkr8-deficient male mice. *Molecular and cellular biology* **40,** e00402–19 (2020).

424. Delon, J., Kaibuchi, K. & Germain, R. N. Exclusion of CD43 from the immunological synapse is mediated by phosphorylation-regulated relocation of the cytoskeletal adaptor moesin. *Immunity* **15,** 691–701 (2001).

425. Schmid, E. M. *et al.* Size-dependent protein segregation at membrane interfaces. *Nature physics* **12,** 704–711 (2016).

426. Van Heesch, S. *et al.* The translational landscape of the human heart. *Cell* **178,** 242–260 (2019).

427. Fuchs, S. *et al.* Defining the landscape of circular RNAs in neuroblastoma unveils a global suppressive function of MYCN. *Nature Communications* **14,** 3936 (2023).

428. Ritchie, M. E. *et al.* limma powers differential expression analyses for RNA-sequencing and microarray studies. *Nucleic acids research* **43,** e47–e47 (2015).

429. Pettmann, J. *et al.* The discriminatory power of the T cell receptor. *Elife* **10,** e67092 (2021).

430. Chen, J.-L. *et al.* Structural and kinetic basis for heightened immunogenicity of T cell vaccines. *The Journal of experimental medicine* **201,** 1243–1255 (2005).

431. Shon, D. J., Kuo, A., Ferracane, M. J. & Malaker, S. A. Classification, structural biology, and applications of mucin domain-targeting proteases. *Biochemical Journal* **478,** 1585–1603 (2021).

432. Rangel-Angarita, V., Mahoney, K. E., Ince, D. & Malaker, S. A. A systematic comparison of current bioinformatic tools for glycoproteomics data. *bioRxiv,* 2022–03 (2022).

433. Symons, A., Willis, A. C. & Barclay, A. N. Domain organization of the extracellular region of CD45. *Protein engineering* **12,** 885–892 (1999).

434. Angiari, S. *et al.* TIM-1 glycoprotein binds the adhesion receptor P-selectin and mediates T cell trafficking during inflammation and autoimmunity. *Immunity* **40,** 542–553 (2014).

435. Tuccillo, F. M. *et al.* Aberrant glycosylation as biomarker for cancer: focus on CD43. *BioMed research international* **2014** (2014).

436. Zhang, X.-G., Zhang, T., Li, C.-Y., Zhang, M.-H. & Chen, F.-M. CD 164 promotes tumor progression and predicts the poor prognosis of bladder cancer. *Cancer medicine* **7,** 3763–3772 (2018).

437. Spertini, C. *et al.* Acute myeloid and lymphoblastic leukemia cell interactions with endothelial selectins: critical role of PSGL-1, CD44 and CD43. *Cancers* **11,** 1253 (2019).

438. Ye, N. *et al.* A multi-omic approach reveals utility of CD45 expression in prognosis and novel target discovery. *Frontiers in Genetics* **13,** 928328 (2022).

439. Peixoto, A., Relvas-Santos, M., Azevedo, R., Santos, L. L. & Ferreira, J. A. Protein glycosylation and tumor microenvironment alterations driving cancer hallmarks. *Frontiers in oncology* **9,** 380 (2019).

440. Foley, G. E. *et al.* Continuous culture of human lymphoblasts from peripheral blood of a child with acute leukemia. *Cancer* **18,** 522–529 (1965).

441. Schneider, U., Schwenk, H.-U. & Bornkamm, G. Characterization of EBV-genome negative "null" and "T" cell lines derived from children with acute lymphoblastic leukemia and leukemic transformed non-Hodgkin lymphoma. *International journal of cancer* **19,** 621–626 (1977).

442. Hurwitz, R. *et al.* Characterization of a leukemic cell line of the pre-B phenotype. *International Journal of Cancer* **23,** 174–180 (1979).

443. Koren, H. S., Anderson, S. J. & Larrick, J. W. In vitro activation of a human macrophage-like cell line. *Nature* **279,** 328–331 (1979).

444. Manjunath, N., Correa, M., Ardman, M. & Ardman, B. Negative regulation of T-cell adhesion and activation by CD43. *Nature* **377,** 535–539 (1995).

445. Dabbagh, D. *et al.* Identification of the SHREK family of proteins as broad-spectrum host antiviral factors. *Viruses* **13,** 832 (2021).

446. Fu, Y. *et al.* PSGL-1 restricts HIV-1 infectivity by blocking virus particle attachment to target cells. *Proceedings of the National Academy of Sciences* **117,** 9537–9545 (2020).

447. Burnie, J. *et al.* P-selectin glycoprotein ligand-1 (PSGL-1/CD162) is incorporated into clinical HIV-1 isolates and can mediate virus capture and subsequent transfer to permissive cells. *Retrovirology* **19,** 9 (2022).

448. Mazurov, D., Ilinskaya, A., Heidecker, G. & Filatov, A. Role of O-glycosylation and expression of CD43 and CD45 on the surfaces of effector T cells in human T cell leukemia virus type 1 cell-to-cell infection. *Journal of virology* **86,** 2447–2458 (2012).

449. *The Human Protein Atlas* `https://www.proteinatlas.org`. Accessed: 2023-06-15.

450. Bian, H.-T. *et al.* CD47: Beyond an immune checkpoint in cancer treatment. *Biochimica et Biophysica Acta (BBA)-Reviews on Cancer,* 188771 (2022).

451. *Fluorchrome Brightness Chart* `https://www.bu.edu/flow-cytometry/files/2013/06/Fluorochromes-Brightness-Chart.pdf`. Accessed: 2023-06-06.

452. Dzwonek, J. & Wilczynski, G. M. CD44: molecular interactions, signaling and functions in the nervous system. *Frontiers in cellular neuroscience* **9,** 175 (2015).

453. Omura, S. *et al.* A new alkaloid AM-2282 of Streptomyces origin taxonomy, fermentation, isolation and preliminary characterization. *The Journal of antibiotics* **30,** 275–282 (1977).

454. Stepczynska, A. *et al.* Staurosporine and conventional anticancer drugs induce overlapping, yet distinct pathways of apoptosis and caspase activation. *Oncogene* **20,** 1193–1202 (2001).

455. Herold, M., McPherson, K. & Reichardt, H. Glucocorticoids in T cell apoptosis and function. *Cellular and molecular life sciences* **63,** 60–72 (2006).

456. Rocamora-Reverte, L., Reichardt, H. M., Villunger, A. & Wiegers, G. T-cell autonomous death induced by regeneration of inert glucocorticoid metabolites. *Cell death & disease* **8,** e2948–e2948 (2017).

457. Talabér, G. *et al.* Mitochondrial translocation of the glucocorticoid receptor in double-positive thymocytes correlates with their sensitivity to glucocorticoid-induced apoptosis. *International immunology* **21,** 1269–1276 (2009).

458. Chao, M. P., Weissman, I. L. & Majeti, R. The CD47–SIRPα pathway in cancer immune evasion and potential therapeutic implications. *Current opinion in immunology* **24,** 225–232 (2012).

459. Pereira, J. L. *et al.* P-selectin glycoprotein ligand 1 promotes T cell lymphoma development and dissemination. *Translational Oncology* **14,** 101125 (2021).

460. Pelaseyed, T. *et al.* Unfolding dynamics of the mucin SEA domain probed by force spectroscopy suggest that it acts as a cell-protective device. *The FEBS journal* **280,** 1491–1501 (2013).

461. Nusbaum, P., Laine, C., Seveau, S., Lesavre, P. & Halbwachs-Mecarelli, L. Early membrane events in polymorphonuclear cell (PMN) apoptosis: membrane blebbing and vesicle release, CD43 and CD16 down-regulation and phosphatidylserine externalization. *Biochemical Society Transactions* **32,** 477–479 (2004).

462. Stampfuss, J.-J. *et al.* Complete downmodulation of P-selectin glycoprotein ligand in monocytes undergoing apoptosis. *Arteriosclerosis, thrombosis, and vascular biology* **28,** 1375–1378 (2008).

463. Thathiah, A., Blobel, C. P. & Carson, D. D. Tumor necrosis factor-α converting enzyme/ADAM 17 mediates MUC1 shedding. *Journal of Biological Chemistry* **278,** 3386–3394 (2003).

464. Foot, N., Henshall, T. & Kumar, S. Ubiquitination and the regulation of membrane proteins. *Physiological reviews* **97,** 253–281 (2017).

465. Bareford, L. M. & Swaan, P. W. Endocytic mechanisms for targeted drug delivery. *Advanced drug delivery reviews* **59,** 748–758 (2007).

466. McMahon, H. T. & Boucrot, E. Molecular mechanism and physiological functions of clathrin-mediated endocytosis. *Nature reviews Molecular cell biology* **12,** 517–533 (2011).

467. Litvinov, S. & Hilkens, J. The epithelial sialomucin, episialin, is sialylated during recycling. *Journal of Biological Chemistry* **268,** 21364–21371 (1993).

468. Altschuler, Y. *et al.* Clathrin-mediated endocytosis of MUC1 is modulated by its glycosylation state. *Molecular biology of the cell* **11,** 819–831 (2000).

469. Brayman, M., Thathiah, A. & Carson, D. D. MUC1: a multifunctional cell surface component of reproductive tissue epithelia. *Reproductive Biology and Endocrinology* **2,** 1–9 (2004).

470. Xu, Y. *et al.* Endocytosis and membrane receptor internalization: Implication of F-BAR protein Carom. *Frontiers in bioscience (Landmark edition)* **22,** 1439 (2017).

471. Jin, Y., Deng, Z. & Zhu, T. Membrane protein trafficking in the anti-tumor immune response: work of endosomal-lysosomal system. *Cancer Cell International* **22,** 413 (2022).

472. Agrawal, B. & Longenecker, B. M. MUC1 mucin-mediated regulation of human T cells. *International immunology* **17,** 391–399 (2005).

473. Clark, M. C. & Baum, L. G. T cells modulate glycans on CD43 and CD45 during development and activation, signal regulation, and survival. *Annals of the New York Academy of Sciences* **1253,** 58–67 (2012).

474. Meesmann, H. M. *et al.* Decrease of sialic acid residues as an eat-me signal on the surface of apoptotic lymphocytes. *Journal of cell science* **123,** 3347–3356 (2010).

475. Houde, D., Peng, Y., Berkowitz, S. A. & Engen, J. R. Post-translational modifications differentially affect IgG1 conformation and receptor binding. *Molecular & Cellular Proteomics* **9,** 1716–1728 (2010).

476. Michielssens, S., de Groot, B. L. & Grubmüller, H. Binding affinities controlled by shifting conformational equilibria: opportunities and limitations. *Biophysical Journal* **108,** 2585–2590 (2015).

477. Ha, J.-H. & Loh, S. N. Protein conformational switches: from nature to design. *Chemistry–A European Journal* **18,** 7984–7999 (2012).

478. Keskin, O. Binding induced conformational changes of proteins correlate with their intrinsic fluctuations: a case study of antibodies. *BMC structural biology* **7,** 1–11 (2007).

479. Yanaba, K., Takehara, K. & Sato, S. Serum concentrations of soluble P-selectin glycoprotein ligand-1 are increased in patients with systemic sclerosis: association with lower frequency of pulmonary fibrosis. *Annals of the rheumatic diseases* **63,** 583–587 (2004).

480. Burchell, J., Wang, D. & Taylor-Papadimitriou, J. Detection of the tumour-associated antigens recognized by the monoclonal antibodies hmfg-1 and 2 in serum from patients with breast cancer. *International journal of cancer* **34,** 763–768 (1984).

481. Bazil, V. & Strominger, J. L. Metalloprotease and serine protease are involved in cleavage of CD43, CD44, and CD16 from stimulated human granulocytes. Induction of cleavage of L-selectin via CD16. *Journal of immunology (Baltimore, Md.: 1950)* **152,** 1314–1322 (1994).

482. Rieu, P., Porteu, F., Bessou, G., Lesavre, P. & Halbwachs-Mecarelli, L. Human neutrophils release their major membrane sialoprotein, leukosialin (CD43), during cell activation. *European journal of immunology* **22,** 3021–3026 (1992).

483. Remold-O'Donnell, E. & Parent, D. Two proteolytic pathways for down-regulation of the barrier molecule CD43 of human neutrophils. *Journal of immunology (Baltimore, Md.: 1950)* **152,** 3595–3605 (1994).

484. Weber, S., Babina, M., Hermann, B. & Henz, B. M. Leukosialin (CD43) is proteolytically cleaved from stimulated HMC-1 cells. *Immunobiology* **197,** 82–96 (1997).

485. Choi, K.-S., Garyu, J., Park, J. & Dumler, J. S. Diminished adhesion of Anaplasma phagocytophilum-infected neutrophils to endothelial cells is associated with reduced expression of leukocyte surface selectin. *Infection and immunity* **71,** 4586–4594 (2003).

486. Domıénguez-Luis, M. *et al.* The metalloprotease ADAM8 is associated with and regulates the function of the adhesion receptor PSGL-1 through ERM proteins. *European journal of immunology* **41,** 3436–3442 (2011).

487. Lichtenthaler, S. F. *et al.* The cell adhesion protein P-selectin glycoprotein ligand-1 is a substrate for the aspartyl protease BACE1. *Journal of Biological Chemistry* **278,** 48713–48719 (2003).

488. Hashizume, M., Higuchi, Y., Uchiyama, Y. & Mihara, M. IL-6 plays an essential role in neutrophilia under inflammation. *Cytokine* **54,** 92–99 (2011).

489. Fang, Y. *et al.* Higher-order oligomerization targets plasma membrane proteins and HIV gag to exosomes. *PLoS biology* **5,** e158 (2007).

490. Del Conde, I., Shrimpton, C. N., Thiagarajan, P. & López, J. A. Tissue-factor–bearing microvesicles arise from lipid rafts and fuse with activated platelets to initiate coagulation. *Blood* **106,** 1604–1611 (2005).

491. Razawi. Die Rolle der Rezyklisierung in der O-Glykosylierung des transmembranären Glykoproteins MUC1, 176 (2013).

492. Schneider, A. & Simons, M. Exosomes: vesicular carriers for intercellular communication in neurodegenerative disorders. *Cell and tissue research* **352,** 33–47 (2013).

493. Bork, P. & Patthy, L. The SEA module: a new extracellular domain associated with O-glycosylation. *Protein Science* **4,** 1421–1425 (1995).

494. *Simon Davis Lab* `https://davislab-oxford.org`. Accessed: 2023-06-28.

495. Sulis, M. L., Saftig, P. & Ferrando, A. Redundancy and specificity of the metalloprotease system mediating oncogenic NOTCH1 activation in T-ALL. *Leukemia* **25,** 1564–1569 (2011).

496. Malemud, C. J. Inhibition of MMPs and ADAM/ADAMTS. *Biochemical pharmacology* **165,** 33–40 (2019).

497. King, L. B. & Ashwell, J. D. Signaling for death of lymphoid cells. *Current opinion in immunology* **5,** 368–373 (1993).

498. Ramsey, K. A., Rushton, Z. L. & Ehre, C. Mucin agarose gel electrophoresis: Western blotting for high-molecular-weight glycoproteins. *JoVE (Journal of Visualized Experiments),* e54153 (2016).

499. Serrano-Heras, G. *et al.* Isolation and quantification of blood apoptotic bodies, a non-invasive tool to evaluate apoptosis in patients with ischemic stroke and neurodegenerative diseases. *Biological Procedures Online* **22,** 1–17 (2020).

500. Drexhage, L. Z. *et al.* Apoptosis-mediated ADAM10 activation removes a mucin barrier promoting T cell efferocytosis. *bioRxiv,* 2023–08 (2023).

501. Eschenbrenner, E. *et al.* TspanC8 tetraspanins differentially regulate ADAM10 endocytosis and half-life. *Life Science Alliance* **3** (2020).

502. Jouannet, S. *et al.* TspanC8 tetraspanins differentially regulate the cleavage of ADAM10 substrates, Notch activation and ADAM10 membrane compartmentalization. *Cellular and Molecular Life Sciences* **73,** 1895–1915 (2016).

503. Matthews, A. L., Noy, P. J., Reyat, J. S. & Tomlinson, M. G. Regulation of A disintegrin and metalloproteinase (ADAM) family sheddases ADAM10 and ADAM17: The emerging role of tetraspanins and rhomboids. *Platelets* **28,** 333–341 (2017).

504. Noy, P. J. *et al.* TspanC8 tetraspanins and a disintegrin and metalloprotease 10 (ADAM10) interact via their extracellular regions: evidence for distinct binding mechanisms for different TspanC8 proteins. *Journal of Biological Chemistry* **291,** 3145–3157 (2016).

505. Zhou, J., Fujiwara, T., Ye, S., Li, X. & Zhao, H. Downregulation of Notch modulators, tetraspanin 5 and 10, inhibits osteoclastogenesis in vitro. *Calcified tissue international* **95,** 209–217 (2014).

506. *UniProt* `https://www.uniprot.org/uniprotkb/Q14242`. Accessed: 2023-08-9.

507. Nam, H.-J., Poy, F., Saito, H. & Frederick, C. A. Structural basis for the function and regulation of the receptor protein tyrosine phosphatase CD45. *The Journal of experimental medicine* **201,** 441–452 (2005).

508. Davenpeck, K. L., Brummet, M. E., Hudson, S. A., Mayer, R. J. & Bochner, B. S. Activation of human leukocytes reduces surface P-selectin glycoprotein ligand-1 (PSGL-1, CD162) and adhesion to P-selectin in vitro. *The Journal of Immunology* **165,** 2764–2772 (2000).

509. Andersson, C. X. *et al.* Shedding and γ-secretase-mediated intramembrane proteolysis of the mucin-type molecule CD43. *Biochemical Journal* **387,** 377–384 (2005).

510. Kuhn, P.-H. *et al.* Systematic substrate identification indicates a central role for the metalloprotease ADAM10 in axon targeting and synapse function. *Elife* **5,** e12748 (2016).

511. Bahrami, E. *et al.* Combined proteomics and CRISPR–Cas9 screens in PDX identify ADAM10 as essential for leukemia in vivo. *Molecular Cancer* **22,** 107 (2023).

512. Scharfenberg, F. *et al.* Degradome of soluble ADAM10 and ADAM17 metalloproteases. *Cellular and Molecular Life Sciences* **77,** 331–350 (2020).

513. Hu, Y. *et al.* Scramblase TMEM16F terminates T cell receptor signaling to restrict T cell exhaustion. *Journal of Experimental Medicine* **213,** 2759–2772 (2016).

514. Hampton, M. B., Vanags, D. M., Pörn-Ares, M. I. & Orrenius, S. Involvement of extracellular calcium in phosphatidylserine exposure during apoptosis. *FEBS letters* **399,** 277–282 (1996).

515. Bratton, D. L. *et al.* Appearance of phosphatidylserine on apoptotic cells requires calcium-mediated nonspecific flip-flop and is enhanced by loss of the aminophospholipid translocase. *Journal of Biological Chemistry* **272,** 26159–26165 (1997).

516. Song, W. *et al.* Synergistic and low adverse effect cancer immunotherapy by immunogenic chemotherapy and locally expressed PD-L1 trap. *Nature communications* **9,** 2237 (2018).

517. Chen, Y. *et al.* Targeting Xkr8 via nanoparticle-mediated in situ co-delivery of siRNA and chemotherapy drugs for cancer immunochemotherapy. *Nature Nanotechnology* **18,** 193–204 (2023).

518. Acciani, M. D. *et al.* Ebola virus requires phosphatidylserine scrambling activity for efficient budding and optimal infectivity. *Journal of Virology* **95,** 10–1128 (2021).

519. Maderna, P. & Godson, C. Phagocytosis of apoptotic cells and the resolution of inflammation. *Biochimica et Biophysica Acta (BBA)-Molecular Basis of Disease* **1639,** 141–151 (2003).

520. Savill, J. & Fadok, V. Corpse clearance defines the meaning of cell death. *Nature* **407,** 784–788 (2000).

521. Arandjelovic, S. & Ravichandran, K. S. Phagocytosis of apoptotic cells in homeostasis. *Nature immunology* **16,** 907–917 (2015).

522. Berghe, T. V., Linkermann, A., Jouan-Lanhouet, S., Walczak, H. & Vandenabeele, P. Regulated necrosis: the expanding network of non-apoptotic cell death pathways. *Nature reviews Molecular cell biology* **15,** 135–147 (2014).

523. SVENSSON, B. O. Serum factors causing impaired macrophage function in systemic lupus erythematosus. *Scandinavian journal of immunology* **4,** 145–150 (1975).

524. Mahajan, A., Herrmann, M. & Muñoz, L. E. Clearance deficiency and cell death pathways: a model for the pathogenesis of SLE. *Frontiers in immunology* **7,** 35 (2016).

525. Wesseling, J., van der Valk, S. W. & Hilkens, J. A mechanism for inhibition of E-cadherin-mediated cell-cell adhesion by the membrane-associated mucin episialin/MUC1. *Molecular biology of the cell* **7,** 565–577 (1996).

526. Malette, B., Paquette, Y., Merlen, Y. & Bleau, G. Oviductins possess chitinase-and mucin-like domains: A lead in the search for the biological function of these oviduct-specific ZP-associating glycoproteins. *Molecular Reproduction and Development* **41,** 384–397 (1995).

527. Ardman, B., Sikorski, M. A. & Staunton, D. E. CD43 interferes with T-lymphocyte adhesion. *Proceedings of the National Academy of Sciences* **89,** 5001–5005 (1992).

528. Ostberg, J. R. *et al.* Disregulated expression of CD43 (leukosialin, sialophorin) in the B cell lineage leads to immunodeficiency. *Journal of immunology (Baltimore, Md.: 1950)* **157,** 4876–4884 (1996).

529. Zadeh, A. D., Seveau, S., Halbwachs-Mecarelli, L. & Keller, H. Chemotactically-induced redistribution of CD43 as related to polarity and locomotion of human polymorphonuclear leucocytes. *Biology of the Cell* **95,** 265–273 (2003).

530. Gubina, E., Chen, T., Zhang, L., Lizzio, E. F. & Kozlowski, S. CD43 polarization in unprimed T cells can be dissociated from raft coalescence by inhibition of HMG CoA reductase. *Blood, The Journal of the American Society of Hematology* **99,** 2518–2525 (2002).

531. Sako, D. *et al.* Expression cloning of a functional glycoprotein ligand for P-selectin. *Cell* **75,** 1179–1186 (1993).

532. Matsumoto, M., Miyasaka, M. & Hirata, T. P-selectin glycoprotein ligand-1 negatively regulates T-cell immune responses. *The Journal of Immunology* **183,** 7204–7211 (2009).

533. Aplin, J. *et al. MUCI, glycans and the cell-surface barrier to embryo implantation* 2001.

534. Huang, H. *et al.* CD5 and CD43 expression are associate with poor prognosis in DLBCL patients. *Open Medicine* **13,** 605–609 (2018).

535. Jing, X., Liang, H., Hao, C., Yang, X. & Cui, X. Overexpression of MUC1 predicts poor prognosis in patients with breast cancer. *Oncology reports* **41,** 801–810 (2019).

536. Lin, Y. *et al.* PSGL-1 is a novel tumor microenvironment prognostic biomarker with cervical high-grade squamous lesions and more. *Frontiers in Oncology* **13,** 1052201 (2023).

537. Baxter, A. E. *et al.* Macrophage infection via selective capture of HIV-1-infected CD4+ T cells. *Cell host & microbe* **16,** 711–721 (2014).

538. Zhou, Z.-h. *et al.* Polyreactive antibodies plus complement enhance the phagocytosis of cells made apoptotic by UV-light or HIV. *Scientific reports* **3,** 2271 (2013).

539. Szabady, R. L., Lokuta, M. A., Walters, K. B., Huttenlocher, A. & Welch, R. A. Modulation of neutrophil function by a secreted mucinase of Escherichia coli O157 H7. *PLoS Pathogens* **5,** e1000320 (2009).

540. Malaker, S. A. *et al.* The mucin-selective protease StcE enables molecular and functional analysis of human cancer-associated mucins. *Proceedings of the National Academy of Sciences* **116,** 7278–7287 (2019).

541. Raymond, M. H. *et al.* Live cell tracking of macrophage efferocytosis during Drosophila embryo development in vivo. *Science* **375,** 1182–1187 (2022).

542. Kim, H., Terazono, H., Takei, H. & Yasuda, K. Cup-shaped superparamagnetic hemispheres for size-selective cell filtration. *Scientific reports* **4,** 6362 (2014).

543. Pedram, K. *et al.* Design of a mucin-selective protease for targeted degradation of cancer-associated mucins. *Nature Biotechnology,* 1–11 (2023).

544. Chatterjee, M. *et al.* The glycosylated extracellular domain of MUC1 protects against SARS-CoV-2 infection at the respiratory surface (preprint) (2021).

545. Goh, J. B. & Ng, S. K. Impact of host cell line choice on glycan profile. *Critical Reviews in Biotechnology* **38,** 851–867 (2018).

546. Hart, S., Ross, J., Ross, K., Haslett, C. & Dransfield, I. Molecular characterization of the surface of apoptotic neutrophils: implications for functional downregulation and recognition by phagocytes. *Cell Death & Differentiation* **7,** 493–503 (2000).

547. Vorselen, D. Dynamics of phagocytosis mediated by phosphatidylserine. *Biochemical Society Transactions* **50,** 1281–1291 (2022).

548. Park, S. *et al.* Mucins form a nanoscale material barrier against immune cell attack. *bioRxiv,* 2022–01 (2022).

549. Dias-Baruffi, M. *et al.* Dimeric galectin-1 induces surface exposure of phosphatidylserine and phagocytic recognition of leukocytes without inducing apoptosis. *Journal of Biological Chemistry* **278,** 41282–41293 (2003).

550. Li, Y.-y. *et al.* Targeting CD43 optimizes cancer immunotherapy through reinvigorating antitumor immune response in colorectal cancer. *Cellular Oncology* **46,** 777–791 (2023).

551. Lv, Z. *et al.* Loss of cell surface CD47 clustering formation and binding avidity to SIRPα facilitate apoptotic cell clearance by macrophages. *The Journal of Immunology* **195,** 661–671 (2015).

552. Freeman, S. A. *et al.* Integrins form an expanding diffusional barrier that coordinates phagocytosis. *Cell* **164,** 128–140 (2016).

553. Bollinger, A.-L. *et al.* Annexin V expression on CD4+ T cells with regulatory function. *Immunology* **159,** 205–220 (2020).

554. Mao, C.-P. *et al.* Programmed self-assembly of peptide–major histocompatibility complex for antigen-specific immune modulation. *Proceedings of the National Academy of Sciences* **115,** E4032–E4040 (2018).

555. Fierro, N. A., Pedraza-Alva, G. & Rosenstein, Y. TCR-dependent cell response is modulated by the timing of CD43 engagement. *The Journal of Immunology* **176,** 7346–7353 (2006).

556. Pedraza-Alva, G. *et al.* CD43 regulates the threshold for T cell activation by targeting Cbl functions. *IUBMB life* **63,** 940–948 (2011).

557. Hope, J. L. *et al.* PSGL-1 attenuates early TCR signaling to suppress CD8+ T cell progenitor differentiation and elicit terminal CD8+ T cell exhaustion. *Cell Reports* **42** (2023).

558. Barrow, A. D. & Trowsdale, J. You say ITAM and I say ITIM, let's call the whole thing off: the ambiguity of immunoreceptor signalling. *European journal of immunology* **36,** 1646–1653 (2006).

559. Yuan, L., Tatineni, J., Mahoney, K. M. & Freeman, G. J. VISTA: a mediator of quiescence and a promising target in cancer immunotherapy. *Trends in immunology* **42,** 209–227 (2021).

560. Alexander, D. R. *The CD45 tyrosine phosphatase: a positive and negative regulator of immune cell function* in *Seminars in immunology* **12** (2000), 349–359.

561. Courtney, A. H. *et al.* A phosphosite within the SH2 domain of Lck regulates its activation by CD45. *Molecular cell* **67,** 498–511 (2017).

562. Courtney, A. H. *et al.* CD45 functions as a signaling gatekeeper in T cells. *Science signaling* **12,** eaaw8151 (2019).

563. Arroyo, A. G. *et al.* Induction of tyrosine phosphorylation during ICAM-3 and LFA-1-mediated intercellular adhesion, and its regulation by the CD45 tyrosine phosphatase. *The Journal of cell biology* **126,** 1277–1286 (1994).

564. Shenoi, H., Seavitt, J., Zheleznyak, A., Thomas, M. L. & Brown, E. J. Regulation of integrin-mediated T cell adhesion by the transmembrane protein tyrosine phosphatase CD45. *The Journal of Immunology* **162,** 7120–7127 (1999).

565. Li, R., Wong, N., Jabali, M. D. & Johnson, P. CD44-initiated cell spreading induces Pyk2 phosphorylation, is mediated by Src family kinases, and is negatively regulated by CD45. *Journal of Biological Chemistry* **276,** 28767–28773 (2001).

566. Serrador, J. M. *et al.* A juxta-membrane amino acid sequence of P-selectin glycoprotein ligand-1 is involved in moesin binding and ezrin/radixin/moesin-directed targeting at the trailing edge of migrating lymphocytes. *European journal of immunology* **32,** 1560–1566 (2002).

567. Tong, J. *et al.* CD43 regulation of T cell activation is not through steric inhibition of T cell–APC interactions but through an intracellular mechanism. *The Journal of experimental medicine* **199,** 1277–1283 (2004).

568. Allenspach, E. J. *et al.* ERM-dependent movement of CD43 defines a novel protein complex distal to the immunological synapse. *Immunity* **15,** 739–750 (2001).

569. Shaffer, M. H. *et al.* Ezrin and moesin function together to promote T cell activation. *The Journal of Immunology* **182,** 1021–1032 (2009).

570. Jung, Y., Wen, L., Altman, A. & Ley, K. CD45 pre-exclusion from the tips of T cell microvilli prior to antigen recognition. *Nature communications* **12,** 3872 (2021).

571. Chatila, T., Silverman, L., Miller, R. & Geha, R. Mechanisms of T cell activation by the calcium ionophore ionomycin. *Journal of immunology (Baltimore, Md.: 1950)* **143,** 1283–1289 (1989).

572. Lavin, M. & Watters, D. *Programmed cell death* (CRC Press, 1993).

573. Zhao, Y., Tozawa, Y., Iseki, R., Mukai, M. & Iwata, M. Calcineurin activation protects T cells from glucocorticoid-induced apoptosis. *Journal of immunology (Baltimore, Md.: 1950)* **154,** 6346–6354 (1995).

574. Vääräniemi, J., Huotari, V., Lehto, V.-P. & Eskelinen, S. The effects of PMA and TFP and alterations in intracellular pH and calcium concentration on the membrane associations of phospholipid-binding proteins fodrin, protein kinase C and annexin II in cultured MDCK cells. *Biochimica et Biophysica Acta (BBA)-Biomembranes* **1189,** 21–30 (1994).

575. Imboden, J. B., Weiss, A. & Stobo, J. D. The antigen receptor on a human T cell line initiates activation by increasing cytoplasmic free calcium. *Journal of immunology (Baltimore, Md.: 1950)* **134,** 663–665 (1985).

576. Kao, J., Alderton, J. M., Tsien, R. Y. & Steinhardt, R. A. Active involvement of Ca2+ in mitotic progression of Swiss 3T3 fibroblasts. *The Journal of cell biology* **111,** 183–196 (1990).

577. Kunzelmann, K. *et al.* Molecular functions of anoctamin 6 (TMEM16F): a chloride channel, cation channel, or phospholipid scramblase? *Pflügers Archiv-European Journal of Physiology* **466,** 407–414 (2014).

578. Whitlock, J. M. & Hartzell, H. C. Anoctamins/TMEM16 proteins: chloride channels flirting with lipids and extracellular vesicles. *Annual review of physiology* **79,** 119–143 (2017).

579. Abraham, R. T. & Weiss, A. Jurkat T cells and development of the T-cell receptor signalling paradigm. *Nature reviews immunology* **4,** 301–308 (2004).

580. Penheiter, S. G. *et al.* Internalization-dependent and-independent requirements for transforming growth factor β receptor signaling via the Smad pathway. *Molecular and cellular biology* **22,** 4750–4759 (2002).

581. Cibrián, D. & Sánchez-Madrid, F. CD69: from activation marker to metabolic gatekeeper. *European journal of immunology* **47,** 946–953 (2017).

582. Laronha, H. *et al.* Challenges in matrix metalloproteinases inhibition. *Biomolecules* **10,** 717 (2020).

583. Elkin, S. R. *et al.* Ikarugamycin: a natural product inhibitor of clathrin-mediated endocytosis. *Traffic* **17,** 1139–1149 (2016).

584. PontÉN, J. & Macintyre, E. H. Long term culture of normal and neoplastic human glia. *Acta Pathologica Microbiologica Scandinavica* **74,** 465–486 (1968).

585. Kwon, B. S. & Weissman, S. M. cDNA sequences of two inducible T-cell genes. *Proceedings of the National Academy of Sciences* **86,** 1963–1967 (1989).

586. Wölfl, M., Kuball, J., Eyrich, M., Schlegel, P. G. & Greenberg, P. D. Use of CD137 to study the full repertoire of CD8+ T cells without the need to know epitope specificities. *Cytometry Part A* **73,** 1043–1049 (2008).

587. Bacher, P. *et al.* Antigen-specific expansion of human regulatory T cells as a major tolerance mechanism against mucosal fungi. *Mucosal immunology* **7,** 916–928 (2014).

588. Nowak, A. *et al.* CD137+ CD154- expression as a regulatory T cell (Treg)-specific activation signature for identification and sorting of stable human tregs from in vitro expansion cultures. *Frontiers in immunology* **9,** 199 (2018).

589. Cimo, A.-M., Ahmed, Z., McIntyre, B. W., Lewis, D. E. & Ladbury, J. E. CD25 and CD69 induction by $\alpha 4\beta 1$ outside-in signalling requires TCR early signalling complex proteins. *Biochemical Journal* **454,** 109–121 (2013).

590. Wu, H., Witzl, A. & Ueno, H. Assessment of TCR signal strength of antigen-specific memory CD8+ T cells in human blood. *Blood Advances* **3,** 2153–2163 (2019).

591. Poloni, C. *et al.* T-cell activation–induced marker assays in health and disease. *Immunology and Cell Biology* (2023).

592. Catala-Rabasa, A. *et al.* High ACSL5 transcript levels associate with systemic lupus erythematosus and apoptosis in Jurkat T lymphocytes and peripheral blood cells. *PloS one* **6,** e28591 (2011).

593. Ruiz-Ruiz, M. D. C., Oliver, F. J., Izquierdo, M. & López-Rivas, A. Activation-induced apoptosis in Jurkat cells through a myc-independent mechanism. *Molecular immunology* **32,** 947–955 (1995).

594. Holler, N. *et al.* Fas triggers an alternative, caspase-8–independent cell death pathway using the kinase RIP as effector molecule. *Nature immunology* **1,** 489–495 (2000).

595. Ch'en, I. L., Tsau, J. S., Molkentin, J. D., Komatsu, M. & Hedrick, S. M. Mechanisms of necroptosis in T cells. *Journal of Experimental Medicine* **208,** 633–641 (2011).

596. Le, T. *et al.* An inner activation gate controls TMEM16F phospholipid scrambling. *Nature communications* **10,** 1846 (2019).

597. Da Silva, T. A., Oliveira-Brito, P. K. M., Gonçalves, T. E., Vendruscolo, P. E. & Roque-Barreira, M. C. ArtinM mediates murine T cell activation and induces cell death in Jurkat human leukemic T cells. *International Journal of Molecular Sciences* **18,** 1400 (2017).

598. Ho, C.-H. & Tsai, S.-F. Functional and biochemical characterization of a T cell-associated anti-apoptotic protein, GIMAP6. *Journal of Biological Chemistry* **292,** 9305–9319 (2017).

599. Wang, Y. *et al.* Ionomycin inhibits Jurkat T cell behaviors in the presence of phorbol-12, 13-dibutyrate. *Annals of hematology* **93,** 735–746 (2014).

600. Yue, C., Soboloff, J. & Gamero, A. M. Control of type I interferon-induced cell death by Orai1-mediated calcium entry in T cells. *Journal of Biological Chemistry* **287,** 3207–3216 (2012).

601. Chwae, Y.-J. *et al.* Molecular mechanism of the activation-induced cell death inhibition mediated by a p70 inhibitory killer cell Ig-like receptor in Jurkat T cells. *The Journal of Immunology* **169,** 3726–3735 (2002).

602. Goda, C. *et al.* Involvement of IL-32 in activation-induced cell death in T cells. *International immunology* **18,** 233–240 (2006).

603. MacDonald, A. *et al.* Delivery of IL-2 to the T cell surface through phosphatidylserine permits robust expansion of CD8 T cells. *Frontiers in immunology* **12,** 755995 (2021).

604. Jelley-Gibbs, D. M. *et al.* Repeated stimulation of CD4 effector T cells can limit their protective function. *The Journal of experimental medicine* **201,** 1101–1112 (2005).

605. Hope, J. L. *et al.* Abstract PO014: PSGL-1 is an early T cell signaling regulator that drives immunometabolism and terminal differentiation in tumor-specific CD8 T cells. *Cancer Immunology Research* **9,** PO014–PO014 (2021).

606. Sibener, L. V. *et al.* Isolation of a structural mechanism for uncoupling T cell receptor signaling from peptide-MHC binding. *Cell* **174,** 672–687 (2018).

607. Bennett Jr, R. *et al.* Mucin MUC1 is seen in cell surface protrusions together with ezrin in immunoelectron tomography and is concentrated at tips of filopodial protrusions in

MCF-7 breast carcinoma cells. *Journal of Histochemistry & Cytochemistry* **49,** 67–77 (2001).

608. Tucher, J. *et al.* LC–MS Based Cleavage Site Profiling of the Proteases ADAM10 and ADAM17 Using Proteome-Derived Peptide Libraries. *Journal of proteome research* **13,** 2205–2214 (2014).

609. Hershkovits, A. S. *et al.* Shifting the balance: soluble ADAM10 as a potential treatment for Alzheimer's disease. *Frontiers in Aging Neuroscience* **15,** 1171123 (2023).